Examining the Mechanism of Action of Small-molecule Negative Allosteric Modulators of the Human Chemokine Receptor CXCR2

Desislava Nikolaeva Nesheva, BSc (Hons)

Thesis submitted to the University of Nottingham for the degree of Doctor of Philosophy

January 2022

This thesis is entirely the candidate's own work. The experiments described in this thesis were performed by the author between May 2018 and September 2021 in the Cell Signalling Research Group at the Centre of Membrane Proteins and Receptors, University of Nottingham, UK. No part of this material has been submitted previously for a degree or any other qualification at any University.

i. Acknowledgments

Firstly, I would like to thank my PhD supervisors – Dr Nicholas Holliday, Prof Steven Charlton, and Dr Shailesh Mistry for coming up with the idea of a CXCR2 focused project that inspired me to continue working in the field of chemokine drug discovery, for their support and brilliant ideas.

I would like to focus on thanking Nick for pushing me to always do better and believing in me when I didn't quite believe in myself. He really was an ongoing support for me in these very dynamic four years and I would always value I had the opportunity to be his student.

I would next like to thank Dr Liciane Medeiros for her patience in teaching me the vary basics of pipetting and diluting drugs, for being patient and supportive.

I would of course like to thank my parents and Ivan and especially my mother for being the most caring person in my life. Your resilience never ceases to amaze me.

Thank you, Bianca, for working hard on the chemistry side of the project and not giving up on the challenging fluorescent probe preparation. Thank you for being so kind and supportive as a friend too.

Thank you, Marleen, June and Jackie, for not only helping us around the lab but also for being welcoming to me when I was too shy to speak to the older PhD students; and Rick – thank you for the daily savage humour.

I would further like to thank the SLIM team and especially Tim Self for always being so nice and friendly and for teaching me obscure Midlands expressions.

And the list of the ICS members I would like to thank is maybe a bit too long, but I have been lucky to make many friends in this group who also served a family in these 4 years. Thank you, Chloe, Nikki, Jack, Al and Brad, Laura H. for making me worry I am having too much fun for a PhD student. Thank you for your friendship and open conversations. Thank you, Lydia, Eddy, Charlie, Sean, Clare, Simon, George, Noemi, James and everyone else for making me cry with laughter on everyday basis, for just being there and being you.

ii. Abstract

The CXC chemokine receptor 2 (CXCR2) is a G protein-coupled receptor (GPCR) with key functions in neutrophil trafficking and activation both during normal homeostasis, and in acute and chronic inflammation. In addition, CXCR2 signalling promotes tumour survival through the mediation of cell proliferation and metastasis, angiogenesis and immune suppression. Despite the therapeutic potential of inhibiting CXCR2 for the treatment of inflammatory conditions and cancer, there is currently not an approved treatment at the receptor. This is largely due to the challenging task of balancing the successful treatment of inflammation or cancer suppression whilst maintaining the homeostatic function of the immune system intact when blocking CXCR2 (Cheng et al., 2019a).

There are a range of structurally distinct negative allosteric modulators (NAMs) of CXCR2 compounds that bind to the receptor at an intracellular pocket overlapping with the site of G protein coupling. Two compounds – navarixin and AZD5069 remain in clinical trials as combination therapies for the treatment of cancer. These compounds, in particular, have been reported to have slow dissociation kinetics at CXCR2.

This thesis generated new approaches to explore the in vitro pharmacology of candidate CXCR2 NAMs, in particular to understand their mechanism of action in more depth. A number of key questions were identified to address – first, the ability of NAMs to regulate CXCR2 signalling through different effector proteins (e.g. arrestins as well as G proteins); second, the extent to which different NAMs can regulate CXCR2 conformation and modulate chemokine binding, as well as blocking effector coupling; and third, the extent to which NAM binding kinetics at the intracellular site, as well as the allosteric nature of the mechanism, influenced the functional profile of their antagonism over time.

First, we co-expressed the human CXCR2 receptor tagged C- terminally with the LgBiT fragment, and β-arrestin2 and mini Gαo effectors with the SmBit

fragment of the Nanoluciferase enzyme to generate a luciferase complementation assay (NanoBiT) for CXCR2-effector interactions in stably transfected HEK293 cells. These assays provided live-cell real time readouts of the agonist chemokine CXCL8 activation, and the effects over time of NAM inhibition. For the range of NAM pharmacophores explored, these approaches demonstrated their equivalent inhibition of both mini G protein and arrestin receptor interactions. We also identified differences among the NAMs in their ability to supress the basal receptor activation and in the surmountability of their effects. Using mathematical modelling approaches and comparison of close homologues (enantiomers) of navarixin, NAMs functional effects were attributed to their binding kinetics properties showing that slow koff NAMs insurmountably supress receptor-effector interactions, due to the insufficient time of binding equilibrium to be established. In contrast, fast koff NAMs promoted rightward shifts in the CXCL8 concentration-response curves likely due to negative binding cooperativity between the NAM and the orthosteric agonist.

Next, a commercially available AF647 labelled CXCL8 peptide was used to establish a non-radiolabelled CXCR2 binding assay format via both imaging and TR-FRET methodologies, applicable in whole-cells and in membrane preparations. NAMs fully inhibited tracer binding at CXCR2 in high sodium-conditions suggesting stabilisation of the inactive receptor conformation and apparently mutually exclusive binding of the NAM and chemokine, despite the difference in their topography of binding sites. Under conditions in which receptor transition to an active conformation would be better promoted (low sodium), an allosteric effect of NAM inhibition was demonstrated, and an influence on labelled chemokine dissociation kinetics measured in the real time homogeneous TR-FRET assay.

In developing novel receptor-effector interaction and fluorescent ligand approaches applicable to real time studies of binding and signalling, these results provide new information on the action of intracellular NAMs at the CXCR2 receptor. Key findings include the ability of NAMs to prevent CXCR2 coupling with multiple effectors, and a role for NAMs in allosteric modulation

6

of chemokine affinity through conformational selection (supported by recent structural studies) – as well as steric blockade of effector interaction.

Finally, our data reveal the importance of slow binding kinetics, as well as non-competitive interactions in generating insurmountable inhibition – a feature of CXCR2 antagonism which may be beneficial under inflammatory conditions involving a cytokine storm. This increased understanding may aid future in vitro optimisation of CXCR2 NAM compounds, to titrate the desire for blockade that is therapeutically effective while managing the risk of side effects.

iii. Abbreviations

AC – Adenylyl cyclase

ACKR – Atypical Chemokine Receptor

ATCM- Allosteric Ternary Complex Model

B_{max} – Maximal Binding

BRET – Bioluminescence

BSA – Bovine Serum Albumin

cAMP – cyclic Adenosine Monophosphate

CFP – Cyan Fluorescent Protein

CKR – Chemokine Receptor

CNS – Central Nervous System

COPD – Chronic Obstructive Pulmonary Disease

CRS – Chemokine Receptor Site

Cryo-EM – Cryogenic Electron Microscopy

CS – Chemokine Site

DC – Dendritic Cell

EC_{50} – Half Maximal Effective Concentration

ECL – Extracellular Loop

ER – Endoplasmic Reticulum

ETCM – Extended Ternary Complex Model

FRET – Förster Resonance Energy Transfer

GAG – Glycosaminoglycan

GDP – Guanosine Diphosphate

GFP – Green Fluorescent Protein

GPCR – G-protein coupled Receptor

GRK – G- protein coupled Receptor Kinase

GTP – Guanosine Triphosphate

IC_{50} – Half-maximal Inhibitory Concentration

ICL – Intracellular Loop

IP3 – Inositol 1,4,5-Trisphosphate

k_{ob} – Observed Rate Constant

k_{on} – Association Rate Constant

k_{off} – Dissociation Rate Constant

MCS – Multiple Cloning Site

MDSC – Myeloid Derived Suppressor Cell

MMP – Matric Metalloprotease

NAM – Negative Allosteric Modulator

NK – Natural Killer cell

Nluc – Nanoluciferase

PAM – Positive Allosteric Modulator

PBS – Phosphate-buffer saline

PCR – Polymerase Chain Reaction

PI3K – Phosphoinositide 3-kinase

PKB – Protein Kinase B (AKT)

PKC – Protein Kinase C

Rmax – Maximal Response

SAP – Shrimp alkaline phosphatase

SMALP – Styrene Maleic Acid-Lipid Particle

Tb – Terbium

TGF – Tumour Growth Factor

TM – Transmembrane

WT – Wild Type

YFP – Yellow Fluorescent Protein

Chapter One: General Introduction

1. Chapter one: General Introduction

1.1 Introduction to G-protein coupled receptors (GPCRs)

G protein coupled receptors (GPCRs) represent the largest protein superfamily among mammals with approximately 800 identified in the human genome (Fredriksson et al., 2003). GPCRs transduce extracellular stimuli into biological responses through the mediation of intracellular signalling cascades (Rosenbaum et al., 2014) and are a major drug target with 35% of the approved drugs acting on this class of proteins (Sriram and Insel, 2018).

Based on phylogenetics, GPCRs are classified into five main families following the GRAFS system: Glutamate (G), Rhodopsin (R), Adhesion (A), Frizzled/Taste2 (F), and Secretin (S) (Fredriksson, 2003). They share certain structural features but are also characterised by family-specific motifs. Insights into GPCR structures were gained through pioneering studies of the structure of rhodopsin, firstly through analysis of the amino-acid sequence (Baldwin, 1993), and later solved in two- (Schertler, 1998) and three- (Palczewski et al., 2000) dimensions. Later on, the resolution of the 3D structures of many more GPCR representatives provided further details of their tertiary organisation in space (Rasmussen et al., 2007), (Underwood et al., 2008), (Thal et al., 2016), (Liu et al., 2020), (Zhang et al., 2017), (Wang et al., 2021), (García-Nafría et al., 2018a) and so on.

All GPCRs are comprised of seven membrane spanning α helices (TM1-TM7), connected via 6 alternating intracellular and extracellular loops (1-3 ECLs, 1-3 ICLs). Each GPCR is characterised by an extracellular N and intracellular C terminus which, along with the loops, can differ greatly in size between members of the family, even within rhodopsin-like receptors. The extracellular loops contain two conserved cysteines that form a disulphide bond.

The Rhodopsin family, also known as *class A* GPCRs, is the largest and most diverse family among vertebrates comprised of 388 olfactory (Spehr and Munger, 2009) and 286 non-olfactory receptors (Munk et al., 2019). Class A GPCRs respond to a vast variety of extracellular stimuli ranging from small

molecules to peptides, proteins, and lipids which is facilitated by the presence of diverse transmembrane and extracellular ligand binding pockets varying in the length of the N termini as well as the amino acid sequence in the transmembrane regions (Venkatakrishnan et al., 2013). Equally, the intracellular residues GPCRs use to interact with G proteins are also variable not only between receptors interacting with distinct Gα subunit members (section 1.3 / section 3), but also between ones interacting with the same subtype (Flock et al., 2017). Residues, however, that connect the agonist binding pocket to G protein coupling on activation are highly conserved and reflected in the presence of common amino acid motifs amongst Class A receptor members, such as the tryptophan residue in CWxP motif in TM6, the NPxxY motif in the cytoplasmic end of TM7, the E/DRY motif within TM3, and Na$^+$ binding pocket (Barak et al., 1995), (Favre *et al.*, 2005) (Zhou *et al.*, 2019), (Filipek, 2019). The way these residues are involved in the process of GPCRs switching from inactive to active conformations is described in section 1.2.

Agonists bind GPCRs at the endogenous ligand binding pocket, referred to as the 'orthosteric' binding site. It has also become apparent that GPCRs can be modulated by allosteric molecules binding elsewhere within the protein. Sometimes, distinct but overlapping binding sites may be present making the orthosteric/allosteric classification of ligands more complex (Christopoulos and Kenakin, 2002). GPCR allosteric modulation is discussed in more detail in section 1.5.

Pharmacological theory proposes the characterisation of ligands according to the functional response elicited by their interaction with cognate GPCRs. This is defined first by the goodness of the fit between the ligand and receptor binding referred to as *affinity* at equilibrium, and as more recently discovered – the kinetics of binding interactions (see chapter 4.1). Second, *efficacy* is the ability of the ligand once bound, to produce a response (Kenakin, 2004). The classification is importantly driven by the term 'intrinsic efficacy' which measures the stimulus imposed per receptor molecule by a ligand (Ariens, 1954). Ligands with high intrinsic efficacy, able to stimulate maximum cellular responses, are defined as full agonists according, and those with low intrinsic

16

efficacy – as partial agonists. As most GPCRs exhibit a certain level of basal activity in the absence of stimulating ligands, ligand efficacy can also be defined by the ability of the ligand to inhibit activity below the basal signalling of the receptor. Thus, while full/partial agonists stimulate GPCR signalling above the basal levels, inverse agonists reduce the constitutive receptor activity. Neutral antagonists, on the other hand, inhibit agonist stimulated receptor activation without affecting the basal receptor activity (Weis and Kobilka, 2018), but their pharmacological effect becomes apparent in their ability to inhibit agonist or inverse agonist effects.

The binding of ligands and their behaviour once bound, however, is insufficient to describe the pharmacological response observed. In reality, the system used for testing the ligands of interest influences the response through the phenomenon of receptor reserve and signal amplification (Kenakin, 2017). For example, increasing receptor number in a cellular system enables an agonist maximal response to be obtained without full occupancy of the receptors. In this instance, agonists are more potent in eliciting the response than would be predicted by their equilibrium dissociation constant Kd (the standard measure of affinity: ligand concentration to occupy 50 % of the receptor population). Mathematical models have been developed to account for such system factors when quantifying ligand efficacies (Kenakin, 2017), (Black et al., 1985), (Stott et al., 2016).

1.2 Class A GPCRs: activation and signalling

Upon binding to GPCRs, ligands induce conformational changes within the receptor which, in the case of agonists, leads to receptor activation. Based on studies in rhodopsin reviewed elsewhere (Hubbell et al., 2003), and later confirmed through the identification of GPCR crystal structures, a number of structural rearrangements in the transmembrane and cytoplasmic domains associated with receptor activation have been identified (García-Nafría et al., 2018a), (Rasmussen et al., 2007), (Manglik et al., 2015), (Liu et al., 2020), (Zhang et al., 2017).

The binding of the agonist promotes the reorganisation of residues in TM3,5,6 including the switch of $W^{6.48}$ in the conserved microswitch motif CWxP to its active rotamer conformation, and conformational rearrangements in the PIF motif and Na^+ pocket. These events cause the initial rotation of the cytoplasmic end of TM6. Following more structural rearrangements in residues in TM3,5, and 6, a larger outward movement of TM6 is facilitated and a movement of TM7 towards TM3 marking receptor activation. This leads to the switch of contacts of $Y^{7.53}$ from the NPxxY sequence strengthening TM7-3 packing and further facilitates the TM6 outer movement. The final step is facilitated by the DRY motif where $R^{3.50}$ is released from its interactions with $D^{3x49}/^{6.30}$ breaking the remaining contacts between TM3 and TM6 in the cytoplasmic areas, driving TM6 to move outward even further (Zhou *et al.*, 2019), (Rasmussen et al., 2011c), (Rosenbaum et al., 2014). Receptor activation is importantly facilitated by the influx of water molecules that remove the hydrophobic barrier and help rearrange the hydrogen network inside the receptor (Venkatakrishnan et al., 2019). The overall result of these harmonious rearrangements of residues in the TM helices is the opening of a binding crevice to accommodate the binding of G protein effectors that GPCRs canonically signal through (Rasmussen *et al.*, 2011).

G proteins are composed of the guanine nucleotide binding subunit Gα, and the dimer Gβγ. The Gα protein contains a nucleotide binding domain GαRas (evolutionary connected to the RAS family of proteins), connected to an N-terminal helix (αN) and an alpha helical domain GαAH (Chung et al., 2011) (Figure 1.1). The Ras domain contains the essential residues for nucleotide catalysis and provides the βγ and GPCR binding surfaces. The structures within the Ras region change conformations depending on the nature of the nucleotide bound (Sprang, 2003).

In their inactive state, Gα proteins are bound to GDP and associated with the βγ dimer. Receptor activation causes structural changes within the Gα subunit leading to the dissociation of GDP leaving the G protein in a nucleotide-free state (Bos et al., 2007). The nucleotide-free state is short lasting due to the quick binding of GTP which is highly concentrated in the cytosol (Higashijima et

18

al., 1987). The binding of GTP, associated with further structural rearrangements within the Gα subunit, leads to its dissociation from the βγ dimer and the mediation of cellular functions through the individual subunits' interaction with effector proteins. GTP hydrolysis into GDP and inorganic phosphate (Pi) closes the G protein activation cycle and leads to restoration of the G protein heterotrimer (Figure 1.2), (Rasmussen *et al.*, 2011).
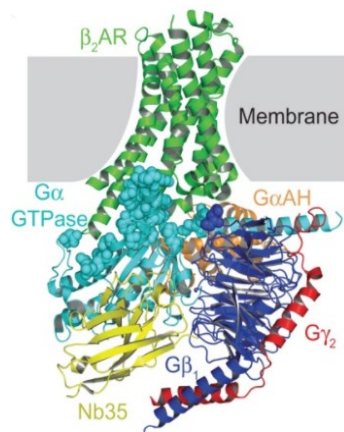
Figure 1.1 Structure of a heterotrimeric G protein engaged with a GPCR. The B2AR in green bound by the heterotrimeric G protein consisting of Gαs GTPase domain (cyan), Gαs AH domain (orange), Gβ (purple), Gγ (red) and stabilised by a crystallising nanobody Nb35 (yellow). Image taken from (Carpenter and Tate, 2016).
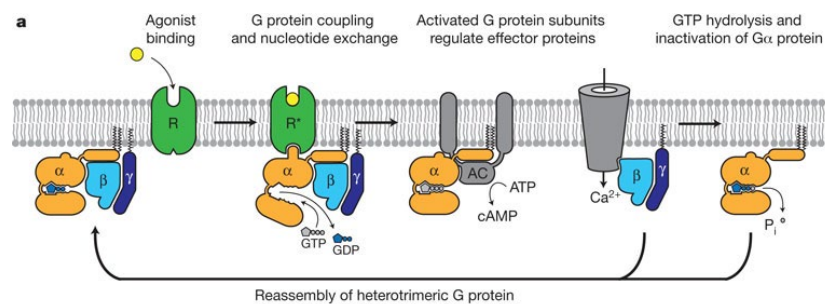
Figure 1.2 Activation of G proteins. The binding of agonist leads to the recruitment of heterotrimeric G proteins bound to GDP followed by the exchange of GDP by GTP and the separation of the Gα and Gβγ subunits. The Gα and Gβγ subunits then interact with various effectors including adenylyl cyclase (AC) and ion channels, modulating second messenger molecules (cAMP, Ca^{2+}) to mediate cellular responses. Image taken from (Rasmussen *et al.,* 2011).

Based on homology between Gα isotypes, G proteins have been grouped into four major families - $Gα_s$, $Gα_{i/o}$, $Gα_{q/11}$, $Gα_{12/13}$ (Downes and Gautam, 1999). There are 5 Gβ and 12 Gγ subunits with different tissue distribution but similar biochemical profiles and signalling properties in in vitro assays (Syrovatkina et al., 2016). Nevertheless, knockouts of individual β and γ subunits have detrimental effects in vivo (Schwindinger et al., 2004), (Masuho et al., 2021) suggesting that the different subunits are essential in cellular signalling, and their roles are not redundant.

On the other hand, the subtype dependent signalling effectors and/or their modulation by the activation of different Gα subunits is well defined. Both $Gα_s$ and $Gα_{i/o,}$ interact with the second messenger adenylyl cyclase (AC) to upregulate or downregulate respectively the production of cyclic adenosine monophosphate (cAMP). cAMP in turn regulates downstream signalling events via its interaction with protein kinase A, ion channels and transcription factors (Wright et al., 2015). Gαq activation is primarily associated with the activation of phospholipase Cβ (PLCβ) and the increase in the cytosolic calcium levels via the action of inositol trisphosphate (IP_3) via its endoplasmic reticulum (ER) receptors (Rhee and Bae, 1997). The second PLCβ product, diacylglycerol, activates protein kinase C (PKC). Finally, there is reported cross talk between the signalling of $Gα_{12/13}$ and other Gα subunits, but specific $Gα_{12/13}$ signalling is likely involved in the control of proteins associated with cytoskeletal rearrangements within the cell, including monomeric G proteins such as Rho (Suzuki et al., 2009).

The kinetics of ligand binding to GPCRs and the subsequent G protein activation has been investigated more recently through the use of biosensors measuring signalling events in real time (Stumpf and Hoffmann, 2016). The conformational changes in GPCRs caused by agonist binding differ between receptors depending on the nature and size of endogenous agonists. For example, the activation kinetics of the parathyroid hormone receptor (PTHR) by large hormone ligands is ~1 s compared to the fast kinetics of the adrenoceptor $α_{2A}$ ($α_{2A}AR$) (~40 ms) stimulated by small molecule monoamine neurotransmitters (Vilardaga et al., 2003). The activation kinetics may also be

affected by receptor dimer formation or the ligand multi-step binding events as shown for the chemokine receptor CXCR4 (Perpina-Viciano et al., 2020). The subsequent coupling of G proteins is a rapid step (30-50 ms) which may overlap with receptor activation (Hein et al., 2006) whilst guanine nucleotide exchange acts as the rate limiting process of G protein mediated signalling. This takes place over 300-500 ms and so introduces a delay between agonist activation of the receptor and the activation of the G protein (Bünemann et al., 2001), (Hein et al., 2006).

1.3 Termination of GPCR signalling and receptor trafficking

GPCRs also interact with G protein-coupled receptor kinases (GRKs) and arrestin proteins. These generally serve to terminate receptor activation but can also initiate separate signalling cascades (Shenoy and Lefkowitz, 2011). The GRK interacting with Rhodopsin was identified first, followed by the one interacting with the β2AR, now named GRK1 and GRK2 respectively (Shichi and Somers, 1978), (Benovic et al., 1989). Following the cloning of GRK2, five more kinases have been identified (GRK3-7) which preferentially bind different GPCRs (Pitcher et al., 2003), (Benovic, 2021). The activation of G proteins serves to guide the GRK2 and GRK3 to activated GPCRs to shut off or reduce signalling (Gurevich and Gurevich, 2019). GRK2/3 bind the Gβγ subunit via their pleckstrin homology (PH) domain which facilitates their recruitment from the cytosol to the plasma membrane (Koch et al., 1993). GRK2 has even been crystallised in complex with the Gβγ subunit (Lodowski et al., 2006). On the other hand, the visual GRK1 and GRK7 are constitutively localised at the plasma membrane via a C terminal prenylation, whereas GRK4/5/6 lack the PH domain and the C-terminal prenylation but associate with the plasma membrane via C terminal cysteine palmitoylation and via an amphipathic helix interacting with the membrane phospholipids (Gurevich et al., 2012).

In the process of homologous desensitisation GRKs phosphorylate serine and threonine residues of the intracellular loops and C termini of agonist-occupied active GPCRs. This leads to to their desensitisation associated with reduced G protein binding (Benovic et al., 1987). Target GPCRs can also be

21

phosphorylated without agonist activation but by second messenger associated protein kinases activated through the signalling of the same- or different- ligand GPCRs, and this event is referred to as heterologous desensitisation (Lefkowitz, 1993).

Once phosphorylated by GRKs, GPCRs are preferentially bound by the ubiquitous regulator proteins – arrestins. So far four functional arrestins have been identified – visual (arrestin1 and arrestin4) and non-visual ones (arrestin2/β-arrestin1, arrestin3/β-arrestin2) (Gurevich and Gurevich, 2006), Arrestins bind cytoplasmic GPCR residues upon receptor activation and serve to provide a rapid signal turnoff (Carman and Benovic, 1998). This is based on competition with the G protein shown for visual arrestins very early on (Wilden et al., 1986), and through more recent structural studies (Szczepek et al., 2014a). The arrestin/G protein GPCR binding interface will be discussed in more detail in chapter 3. Arrestins also terminate GPCR signalling partly through mediating receptor internalisation upon prolonged (minutes) agonist exposure (Cahill et al., 2017). Certain GPCRs, however, undergo this process in an arrestin-independent manner (Van Koppen and Jakobs, 2004). GPCRs internalise into intracellular compartments – endosomes - through clathrin-coated vesicles and adaptor proteins such as AP2, although clathrin-independent mechanisms are also present (Komolov and Benovic, 2018), (Hansen and Nichols, 2003). The internalisation and trafficking patterns can vary greatly between distinct GPCRs. Whilst the β_2 adrenoceptor (β_2AR) and the V_{1A} vasopressin receptor (V_{1A}R) are readily recycled back to the plasma membrane (Morrison et al., 1996; Innamorati et al., 2001), the V_2 vasopressin receptor (V_2R) engages a long recycling pathway where it is confined to perinuclear compartments. These differences are strongly attributed to the dynamics of receptor-arrestin interactions which in turn regulates the dephosphorylation of the C-terminal tail of the receptor (Palczewski et al., 1989; Pippig et al., 1995; Bremnes et al., 2000). For example, the β_2AR recruits arrestin proteins transiently allowing for the receptor C-terminal domain to undergo dephosphorylation and to be trafficked back to the plasma membrane. On the other hand, the V_2R forms a stable complex with arrestin

22

proteins which may protect the C-terminal tail from being dephosphorylated and thus, is not readily trafficked back to the cell surface (Oakley et al., 1999).

1.4 GPCRs as drug targets

GPCRs are the most heavily studied and exploited proteins as drug targets, underlined by their expression in multiple tissues and their involvement in the modulation of a vast range of physiological and pathophysiological responses. Most recent data suggest that around 700 approved drugs target GPCRs meaning that GPCRs account for 35% of the approved drug targets (Sriram and Insel, 2018). Generally, most drugs acting at GPCRs are orthosteric agonists or antagonists. The development of techniques to obtain structural details of GPCR binding pockets and organisation in space has enabled drug discovery efforts to expand to targeting GPCRs allosterically (Christopoulos, 2002).

1.4.1 GPCR antagonism

GPCR-targeted drugs can act directly as agonists at the receptors or indirectly, by modifying the physiological stimulus. Antagonism describes the inhibitory modification of GPCR stimuli, and it is analysed in terms of the effects of antagonist on the endogenous agonist concentration-response curves or in terms of its molecular interactions with the target protein (Kenakin, 2006).

Antagonist effects on agonist concentration-response curves can be saturable reaching a maximal limit despite increasing antagonist concentration, or unsaturable with infinite inhibition on agonist response; the latter, however, may be affected by solubility issues or secondary effects of the antagonists e.g. non-specific effects underlined by its interaction with other protein targets at high concentrations. Second, the effect of increasing antagonist concentration can be surmountable by the agonist manifesting as parallel rightward shifts in the concentration-response curves without a reduction in the maximal response, or insurmountable characterised by a decrease in the maxima (Figure 1.3), (Kenakin, 2006).

The patterns of changes in the concentration-response curves as a results of antagonist treatment are varied, nevertheless, they are often also affected by the assay set-up and experimental model system. Therefore, when identifying the molecular mechanism underlying antagonist profiles, system effects must be considered.

Based on the molecular mechanism of action, antagonism can also be subdivided into orthosteric and allosteric binding modes.

1.4.2 Orthosteric antagonism

Drugs lacking efficacy in causing receptor activation and binding to the same pocket, and thus occluding the binding site of the endogenous agonist, are defined as orthosteric antagonists. Orthosteric antagonism is competitive provided the binding of the orthosteric antagonist is reversible, allowing for the dynamic equilibrium between an agonist and antagonist to be established. This typically manifests as surmountable antagonist behaviour. Irreversible binding of the antagonist, on the other hand, does not allow for the agonist to surmount the antagonism and the maxima of the response would be reduced. There are examples of cases in between these two situations, where antagonists with slow binding kinetics manifest as non-surmountable due to the lack of equilibrium achieved in the system; this is often observed for antagonists with significantly slower dissociation constant (k_{off}) relative to the agonist (Figure 1.3) (Sum et al., 2004), (Kenakin et al., 2006), (Kenakin, 2006).
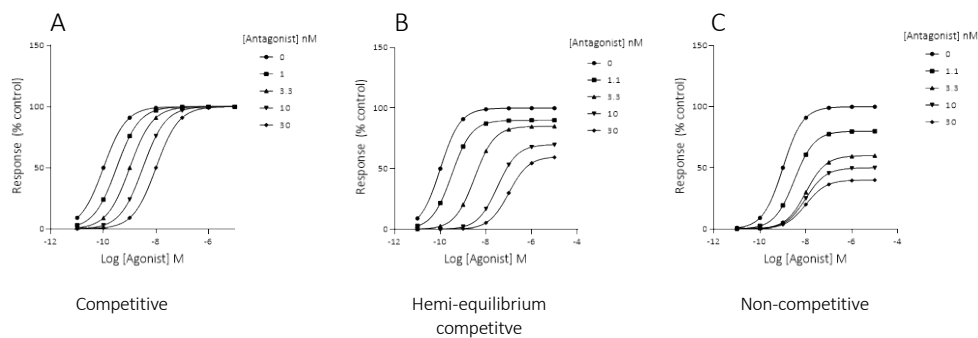
Figure 1.3 Antagonist effects on agonist concentration-response relationships. (A) Surmountable antagonism characterised by rightward shifts of agonist potency and no reduction in the maximal response. (B) A combined effect of the antagonist on both agonist potency and maximal response observed in conditions of lack of binding equilibrium between agonist, antagonist and receptor target. (C) Insurmountable antagonism characterised by reduced agonist maximal response. Graphs represent simulated data following Kenakin (2006) pharmacological theory.

1.5 Allosteric modulation of GPCRs
1.5.1 Introduction to allosteric drug effects

GPCRs can be defined as naturally allosteric proteins based on their possession of distinct interaction sites for the activating ligands and for effector molecules such as G proteins and arrestins (Christopoulos and Kenakin, 2002). Similarly, drugs that bind GPCRs at sites distinct from the orthosteric pocket for the endogenous ligand and modulate receptor function are defined as allosteric molecules. Allosteric drugs that potentiate the action of the endogenous agonist supporting GPCR activation are referred to as positive allosteric modulators (PAMs), and those that negatively modulate receptor function, as negative allosteric modulators (NAMs) (May *et al.*, 2007).

An important feature of allosterism is the reciprocity of the effects – the effects of the allosteric ligand on the orthosteric ligand behaviour should be reciprocated by the effects of the orthosteric ligand on the allosteric ligand behaviour. Considering effects on binding (affinity), this allows for the relationship of allosteric and orthosteric ligand to be described by the mutual cooperativity term α, describing the influence of one drug binding on the other. However allosteric ligands also have potential to modulate the efficacy of the orthosteric ligand, defined by the cooperativity term β. Finally, it is

possible for allosteric ligands to have their own efficacy in activating the receptor in the absence of orthosteric ligands – i.e. acting as agonists. In operational models of allosterism for example, this is represented by an allosteric efficacy term τ_B (Kenakin, 2013).

1.5.2 Allosteric effects on affinity

GPCRs exist in thermal equilibrium switching between a selection of conformations with various energy demands (Weis and Kobilka, 2018). Each step in the receptor activation, alongside interactions with effector molecules, would ultimately affect the behaviour of the receptor through changes in its conformation. The binding of allosteric ligands adds an additional layer of complexity as they could shift the receptor to distinct conformations when free or bound to the orthosteric ligand (May *et al.*, 2007). The affinity of ligands is generally defined by the equilibrium dissociation constant Kd, but this is also the ratio of the dissociation and association rate constants $(Kd = \frac{koff}{kon})$ (more details in chapters 2 and 4). Therefore, allosteric drug effects which modulate affinity (α co-operativity) are also likely to involve changes in the binding kinetics rates of the orthosteric ligand (May *et al.*, 2007), (May *et al.*, 2010). For example, positive allosteric modulation can arise from an increase in ligand association rate (kon) and decrease in its dissociation rate (koff), and negative allosteric modulation from the opposite changes. Such changes in the orthosteric ligand binding kinetics rates are attributed to changes in receptor conformation as a result of the allosteric ligand interaction with its separate site.

The equilibrium effects of allosteric drugs on agonist affinity have been commonly described by the allosteric ternary complex model (ATCM) (Christopoulos and Mitchelson, 1997), (May et al., 2007b) (Figure 1.4). The model quantifies the reversible and saturable binding of an allosteric and an orthosteric ligand driven by their concentrations, equilibrium dissociation constants and the factor of cooperativity. As discussed above α cooperativity describes the reciprocal effects of orthosteric and allosteric ligand to each

26

other's interaction with the target protein (Ehlert, 1988). Allosteric ligands with negative cooperativity are therefore described by a $\alpha < 1$ cooperativity factor (reduce orthosteric ligand binding affinity); those with positive cooperativity by $\alpha > 1$ (potentiate orthosteric ligand binding), and those with no net effect of orthosteric ligand binding affinity, by $\alpha = 1$.

1.5.3 Allosteric effects on efficacy

The ATCM could be easily applied for studying the effects of allosteric ligands in binding assays, nevertheless, its application may be limited when it comes to functional data, because of additional β co-operativity effects on receptor activation.

The effect of allosterically binding drugs on orthosteric ligand behaviour vary from no effect on binding but signalling inhibition (Litschig et al., 1993) or enhancement of ligand efficacy (Urwyler et al., 2001), to a combined inhibition of signalling with simultaneous enhancement of binding of the orthosteric ligand (Price et al., 2005). Therefore, the ATCM model cannot adequately quantify the range of effects allosteric drugs may exert on orthosteric ligands. To describe changes in receptor activation and signalling, the β term is introduced to represent the effect of the allosteric molecule on the intrinsic efficacy of the orthosteric ligand (ε). With this extension, the extended model describes the way the allosteric and orthosteric ligands interact both through binding and functional regulation of the receptor (May *et al.*, 2007) (Figure 1.4).

Alternative models to interpret allosterism have been proposed. For example, one representation of orthosteric agonism, applicable to GPCRs, is the two state model. This describes the promotion of an active receptor conformation (R*) from the inactive state (R) by agonist binding. The allosteric two-state model (ATSM) (Hall, 2000) allows for the ability of allosteric as well as orthosteric ligands to discriminate between the R and R* receptor states in terms of their binding affinity. Here the cooperativity factor α then describes the ability of the orthosteric ligand to promote an active state, and β – the

ability of the allosteric one to promote one. The affinity effects of each ligand on each other is described by γ, whereas the factor δ describes the activation cooperativity between the ligands (Hall, 2000), (May *et al.*, 2007).

$$
\begin{array}{ccc}
R & \xrightarrow{\quad K_A \quad} & AR \quad\dashrightarrow\quad \text{Stimulus (S)} \\[2em]
\Big\updownarrow K_B & & \Big\updownarrow K_B/\alpha \\[2em]
BR & \xrightarrow{\quad K_A/\alpha \quad} & ABR \quad\dashrightarrow\quad \text{Modified stimulus } (\beta \times S)
\end{array}
$$
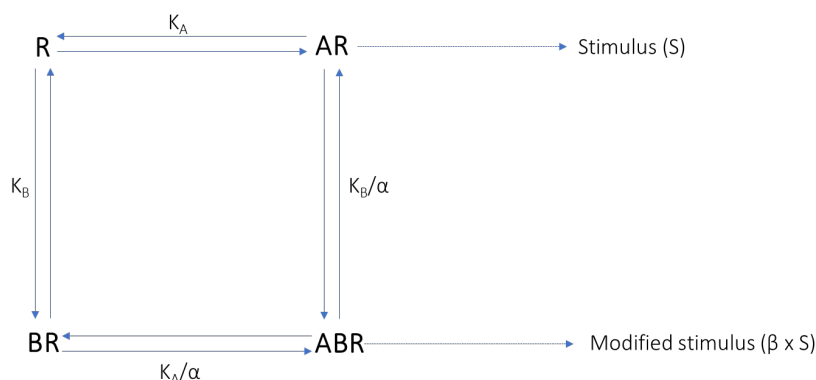
Figure 1.4 Simple allosteric ternary complex model (ATCM). The binding of the orthosteric ligand (A) to receptors (R) to form AR is governed by the orthosteric ligand affinity K_A. The binding of the allosteric ligand (B) to R to form BR is governed by the allosteric ligand affinity (K_B). The binding of B to AR or A to BR to form ABR is governed by the cooperativity factor $-\alpha$. The stimulus exhibited by the effect of A on R is either unmodified or modified as describe by the proportionality factor β. Image adapted from (May *et al.,* 2007).

1.5.4 Importance of allosteric ligands in drug discovery

There are a number of advantages associated with the use of allosteric molecules in targeting GPCRs.   Firstly, the effect of allosteric compounds on the orthosteric agonist response (e.g. a neurotransmitter) should be saturable once the allosteric site has been fully occupied. Therefore, there is a ceiling of the receptor modulation retained even at high drug concentrations, potentially making allosteric treatment safer in terms of their therapeutic window. The use of allosteric drugs allows for the fine tuning of receptors' functional responses without causing a blanket activation of targets or completely abolishing their function. This is particularly important in the CNS where complex neuronal signalling pathways need to be finely modulated for a balance between a therapeutic effect and preservation of other functions to be established (Foster and Conn, 2017).   For example, the effect of a true allosteric ligand depends on the presence of the orthosteric agonist, giving rise to the phenomenon of use dependence in the CNS, in which the most active

28

neuronal synapses releasing orthosteric neurotransmitter are preferentially modulated.

A further behaviour of allosteric compounds is their probe dependence underlying their selective enhancement or inhibition of the effect of some endogenous ligands over others. This feature of allosterism can be exploited in physiological systems where one receptor mediates numerous functions through its activation by multiple endogenous ligands; such promiscuity is common for some chemokine receptors such as representatives of the CXC-family (Rajagopalan and Rajarathnam, 2006), (Raport and Gray, 2010). The probe dependence of NAMs acting in the chemokine signalling system has been exploited for the modulation of the pathophysiological signalling of the CCR5 receptor allowing the entry of HIV virus into cells, without inhibiting the binding other CCR5 endogenous agonists that promote beneficial signalling (Watson et al., 2005),(Xu et al., 2014).

In fact, the use of allosteric drugs allows for the introduction of a texture of receptor structures supposed by modulators different from each other by only minor chemical modifications. For example, an allosteric modulator of CCR5 with minor modifications to the approved maraviroc, may be sufficient to cause CCR5 to obtain another conformation not permissive to viral entry, but unfamiliar to the readily adapting virus overcoming the effects of maraviroc.

Finally, due to the lesser conservation of allosteric sites, allosteric drugs may allow for better receptor subtype selectivity. Targeting the muscarinic receptors allosterically, has been the preferred strategy compared to orthosteric drugs due to the high conservation of the orthosteric pocket leading to non-specific effects (Korczynska et al., 2018).

Muscarinic receptors (M1-M5 types) are a good example of differential tissue distribution and function (Abrams et al., 2006) and a conserved orthosteric binding pocket accommodating the endogenous ligand Acetylcholine (Ach). The targeting of the receptors for neurodegenerative conditions has therefore, been challenging due to the lack of selective orthosteric compounds. Xanomeline, for instance, a muscarinic nonselective orthosteric agonist, showed promising behavioural improvement in patients with Alzheimer's

disease due to the functions of the muscarinic receptors M1 and M4 in neuroprotection (Felder et al., 2018). The drug, nevertheless, additionally produced GI tract disturbances due to its action on smooth muscle muscarinic receptor subtypes which led to its failure in trials. (Bender et al., 2017), (Moran et al., 2019). Efforts in the field, have therefore focused on the development of allosteric modulators for M1 and M4 receptors, devoid of activity on the peripheral M2 and M3 ones (Conn et al., 2009), (Yohn and Conn, 2018).

1.6 Introduction to the chemokine signalling system

1.6.1 Chemokines

The chemokine signalling system is comprised of chemokine ligands and their rhodopsin family 7-transmembrane domain (7TM) cognate receptors. Chemokines represent a family of small (8-12 kDa) soluble proteins defined by four N-terminal conserved cysteine residues. They are classfied into four subfamilies according to the number and position of the conserved cysteine residues – the CXC, CC, CX3C, and C families (Zlotnik and Yoshie, 2000). The largest families are the CXC and CC chemokines, both containing four N-terminal cysteines. The first two cysteines in the CXC sub-family are separated by another amino acid (X), and are adjacent for the CC- group (Figure 1.5).


```
CXC:      .....CX__C.........C...........C...
CC:       .....C___C.........C...........C...
CX3C:     .....CXXXC.........C...........C...
C:        .............C......................C...
```
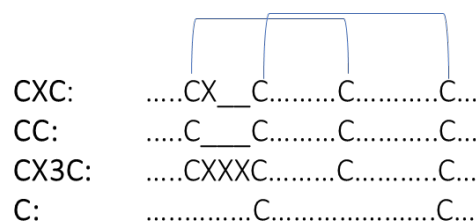
Figure 1.5 Primary structure of chemokines. Chemokines are classified according to the position and number of the conserved cysteine residues. Three chemokine classes contain four conserved cysteines (CXC, CC, and CX3C) and one – two cysteines (C); the position of disulphide bond formation is shown with blue brackets. (Diagram adapted from Bachelerie *et al.*, 2014).

All chemokines share a similar tertiary structure stabilised by disulphide bonds formed between the N-terminal cysteines - two for the CX3C, CXC, and CC chemokines, and one for the C chemokines (Bachelerie et al., 2014). The N terminus of chemokines is flexible and the first two cysteines are located very close to it followed by a coil region termed the N-loop. The N-loop region is important for interactions with receptor's N terminus upon binding (Scholten *et al.*, 2012). The core domain of chemokines is highly structured consisting of three antiparellel β strands, and the C terminus consists of an α helix (Scholten *et al.*, 2012), (Miller and Mayo, 2017) (Clore et al., 2002), (Booth et al., 2004) (Figure 1.6).

The CXC chemokine family is further subdivided into ELR+ or ELR- chemokines depending on the presence or absence of the N-terminal glutamic acid-leucine-arginine amino acid motif prior to the CXC one. The ELR+ chemokines tend to manifest as angiostatic and inflammatory, nevertheless they also exhibit homeostatic functions, therefore relating overall structural motifs to function is not a straightforward strategy for chemokine classification (Kiefer and Siekmann, 2011), (Zlotnik and Yoshie, 2000).
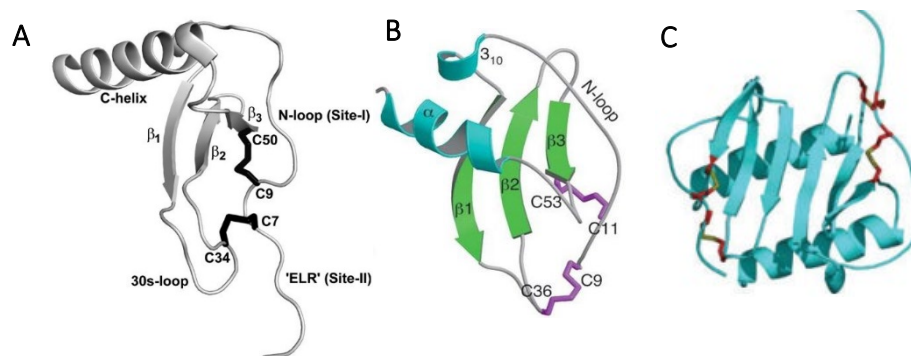
Figure 1.6 Tertiary structure of the chemokines CXCL8 and CXCL11. A) The NMR structure of monomeric CXCL8 chemokine; (Clore *et al.,* 2002); (Joseph *et al.,* 2010); The CXCL8 structure diagram showing sites 1 and 2 discussed later in the chapter. B) monomeric CXCL1 (Booth *et al.,* 2004). C) Generic structure of a CXC dimer chemokine (Allen, Crown, and Handel, 2003).

Following the cleavage of the signal sequence prior to the secretion of the mature proteins, chemokines undrego further posttranslational modifications such as N- and C-terminal truncations (Mortier et al., 2008). The naturally occuring N-terminal truncation can modify chemokine acticity at cognate receptors or alter receptor selectivity. This is true for CXCL8 that undergoes multiple cleavage steps and can exist as a peptide of different lengths of which the shorter versions, including $CXCL8_{28-99}$ are more potent at activating receptors and inducing chemotaxis (Mortier et al., 2011).

C terminal chemokine truncations do not affect receptor interactions, but may affect binding to extracellular matrix glycosaminoglycan molceules (GAGs) as demonstrated by SDF-1α (CXCL12 splice variant) reduced binding to the GAG heparin as a result of a C-terminal residue deletion (Eckhard et al., 2016). Apart from proteolytic modifications, CXCL8 undergoes citrullination (deamination of arginine residues to yield citruline), but the effect of this modification on ligand properties is controversial l (Stone et al., 2017). For other chemokine ligands such as CXCL5, CXCL10, CXCL11, CXCL12, citrullination generally leads to a lower receptor binding affinity (Stone et al., 2017).

Many chemokines dimerise or oligomerise on their own in solution or upon interaction with cell surface / extracellular matrix GAGs (Johnson et al., 2005), (Allen et al., 2007). The dimer / oligomer formation is essential for non-receptor mediated functions of chemokines such as the formation of chemotactic gradients based on GAG interactions (Proudfoot et al., 2003). The role of dimer / oligomer formation on chemokine – chemokine receptor interactions is less clear but most evidence supports the ability of CXC chemokines to interact with receptors both as dimers and monomers (Liu et al., 2020), (Drury et al., 2011), (Sawant et al., 2016), (Das et al., 2010) with some studies suggesting differential downstream effects caused by monomers or dimers (Nasser et al., 2009b). Dimer formation may negatively impact receptor interaction for CC chemokines, however, as they form dimers via the N terminal region essential for receptor binding. For example, the CC chemokine MIP-1β can bind the CCR5 receptor as a monomer but not as a dimer (Jin et al., 2007).

1.6.2 Chemokine receptors

Chemokines interact with chemokine receptors (CKRs) that belong to the class A GPCRs and thus, share the structural motifs typical for this family (Bachelerie et al., 2014) discussed in section 1.1 and 1.2. Based on their signalling behaviours, chemokine receptors can be subdivided into two groups: G protein- coupled chemokine receptors which signal via pertussis toxin sensitive Gi proteins, and atypical chemokine receptors which interact with arrestin but not G protein effectors. To date 23 CKRs, both typical and atypical, have been identified (Alexander et al., 2019). The two groups of chemokine receptors differ structurally in a key sequence DRYLAIV located at the intracellular end of TM3, including the previously mentioned DRY motif (section 1.2), which is conserved only among the 'typical' G-protein coupled chemokine receptors (Bachelerie et al., 2014). The atypical chemokine receptors (ACKR1 (DARC), ACKR2 (D6), ACKR3 (CXCR7), ACKR4) recruit β arrestin effectors leading to receptor internalisation and chemokine scavenging (Ulvmar et al., 2011).

Chemokine receptors are further divided into 4 groups according to the subfamily of their major chemokine ligands CC, CXC, CX3C, C (Zlotnik and Yoshie, 2000) (table 1.1). Chemokine ligands can be shared between different receptors and a number of CKRs are promiscuous to multiple ligands (Dyer et al., 2019). Furthermore, chemokine agonist ligands of some CKRs, may serve as antagonists for others. For example, chemokine agonists for CCR3 and CXCR3 act as antagonists to the reciprocal receptor (Loetscher et al., 2001).

Not all endogenous ligands for CKRs are chemokines. An example is the pro-inflammatory cytokine Macrophage migration inhibitory factor (MIF) that is a non-canonical ligand for CXCR4 (Bernhagen et al., 2007) as well as an extracellular ubiquitin with anti-inflammatory properties (Saini et al., 2010). Another non-canonical chemokine agonist is the extracellular matrix product N-acetyl Pro-Gly-Pro (acPGP) suggested to activate the CXCR1 and CXCR2 receptors (Patel and Snelgrove, 2018).

Chemokine binding to chemokine receptors is a complex process consisting of the multi-step, multi-site interactions established between the ligand and the CKR. The first interaction occurs between the N loop and β3 strand of the

chemokine (CS1) and the N-terminal residues of the receptor (CRS1) (figure 1.7). This is followed by ligand N terminal domains including the ELR motif (for ELR chemokines) and the 30s loops (CS2) binding at a transmembrane receptor pocket formed by TM4,5,6 and ECL2 (CRS2) (Burg et al., 2015a), (Kufareva et al., 2014), (Zheng et al., 2017), (Liu et al., 2020). This sequential two-site binding model proposed that the affinity of chemokine ligands is based on their initial interaction with receptor's N-terminus and that the second interaction mediates receptor activation and signalling. Nevertheless, more recently it has been demonstrated that both CRS1 and CRS2 domains contribute to binding interactions underlying high chemokine affinity (Sanchez et al., 2019).

There are also reports for the formation of dimers between the same (homodimers) or different (heterodimers) chemokine receptors, but this has not in all cases been matched to functional consequences (Springael et al., 2005). The formation of homodimers has been extensively studied for the CXCR4 receptor (Işbilir et al., 2020), (Wu et al., 2010). There are also reports for the formation of CXCR2 homodimers and CXCR2 / CXCR1 heterodimers (Trettel et al., 2003), (Papers et al., 2005) as well as CCR5 receptor oligomerisation (Issafras et al., 2002). The formation of dimers /oligomers as well as the presence of a complex multi domain orthosteric site further complicates the matter of chemokine-CKR interactions (Perpina-Viciano et al., 2020), (Kufareva et al., 2014).

Table 1.1 Human chemokine-chemokine receptor signalling system; orange: agonist; blue: antagonist; grey: undefined. CXCL8-CXCR2 (bold) is the chemokine-chemokine receptor pair studied in this work. Adapted from (Stone et al., 2017)

Cell fill legend: O = orange (agonist), B = blue (antagonist), G = grey (undefined); blank = no interaction.

Ligand	CCR1	CCR2	CCR3	CCR4	CCR5	CCR6	CCR7	CCR8	CCR9	CCR10	CXCR1	**CXCR2**	CXCR3	CXCR4	CXCR5	CXCR6	CX3CR1	XCR1	ACKR1	ACKR2	ACKR3	ACKR4	CCRL2
CCL1								O															
CCL2		O	O		O														G	G			
CCL3	O				O															G			
CCL4	B				O															G			
CCL5			O		O														G	G			
CCL7	O	O	O		B														G	G			
CCL8	O	O	O		O															G			
CCL11		O	O		O															G			
CCL13	O	O	O		O															G			
CCL14	O				O														G	G			
CCL15	O		O																				
CCL16	O	O			O																		
CCL17				O															G	G			
CCL18	B		B																				
CCL19							O															O	G
CCL20						O																	
CCL21							O															O	
CCL22			O																	G			
CCL23	O																						
CCL24		B	O																				
CCL25									O													O	
CCL26		B	O																				
CCL27										O													
CCL28			O							O													
CXCL1											G	O											
CXCL2												O											
CXCL3												O											
CXCL4																							
CXCL5												O							G				
CXCL6											O	O							G				
CXCL7												O											
CXCL8											O	O							G				
CXCL9			B										O										
CXCL10			B										O										
CXCL11			B										O						G		O		
CXCL12													O	O							O		
CXCL13															O								
CXCL14																							
CXCL16																O							
CXCL17																							
CX3CL1																	O						
XCL1																		O					
XCL2																							

1.7 Functions of the chemokine signalling system

1.7.1 Maintenance of immune cell homeostasis

Chemokines are chemotactic cytokines that mediate the migration (chemotaxis) of immune cells between the immune organs, blood and peripheral tissues. Their roles in controlling immune cell migratory patterns are essential both for the development of immune cells and normal homeostasis, and for the mediation of primary immune defence through the process of inflammation (Griffith et al., 2014a).

The development and differentiation of immune cell precursors start in the primary immune organs – the bone marrow and thymus, and it is under the fine control of chemokines and their cognate receptors. T cell development in the thymus is controlled by the interactions of CCL21, CCL19, CXCL12 with CCR7, CCR9, and CXCR4 respectively expressed on progenitor T cells (Love and Bhandoola, 2011). The homeostatic retention of immune cells and the development of B cells, macrophages, monocytes, neutrophils, plasmacytoid dendritic cells (pDCs), and natural killer (NK) cells takes place in the bone marrow and is largely regulated by the CXCL12-CXCR4 axis (Broxmeyer et al., 2005). Other CKRs such as CCR7 and CXCR2 (Mcheik et al., 2019), (Eash et al., 2010) contribute to the roles of CXCR4 in bone marrow cell retention by a potential negative regulation of CXCR4.

The migration to and localisation of immune cells into secondary immune organs (lymph nodes, spleen, Peyer's patches) is also controlled by the formation of chemokine gradients with highlighted roles of CXCR7 for the homeostatic positioning of B cells in the spleen and CXCR4 and CCR7 regulating T cells and dendritic cells respectively (Griffith, Sokol and Luster, 2014).

Adequate defence against pathogen infection is dependent on the localisation of immune cells at peripheral sites in the body which is also largely dependent on the presence and appropriate activity of the chemokine signalling system. Mature neutrophils migrate from the bone marrow to the blood where they wait for inflammatory stimulation to promote their localisation in peripheral

tissues. The retention of neutrophils in the bone marrow is mediated by SDF-1α acting via CXCR4 which also cross regulates CXCR2. The release of neutrophils from the bone marrow is stimulated by either blocking CXCR4 or activating CXCR2 (Martin et al., 2003).

Eosinophils are largely found in the peripheral tissues and particularly – in the gastrointestinal tract (Loktionov, 2019). Their baseline migration to the periphery is strongly mediated by the release of CCL11 by stromal and immune cells and its action on the CCR3 receptor (Griffith et al., 2014b). The CCR7 receptor is important for the guidance of dendritic cells (DC) to T-cell rich areas where they link the innate and adaptive immune response by the process of antigen presentation (Sánchez-Sánchez et al., 2006).

The constant circulation of lymphocytes (T cells, natural killer cells (NKs), B cells) between the blood and secondary immune organs is mediated largely by CCL19-CCR7 interactions for T cell migration, and a combination of signals mediated by CCR7, CXCR4, and CXCR5 for B cells (Stein and Nombela-Arrieta, 2005).

This homeostatic movement of immune cells ultimately serves to provide defence against pathogens which starts with the event of acute inflammation.

1.7.2 Inflammation and the roles of the CXCL8 - CXCR2 / CXCR1 axis

The acute inflammatory response is initiated when resident immune cells (mast cells, dendritic cells (DC), pro-inflammatory macrophages etc.) detect foreign or host derived signals with their pattern recognition receptors (PRRs) and release pro-inflammatory mediators such as CXCL1, CXCL2, CXCL8, Leukotriene B4,TNF etc (Chen et al., 2018a), (Griffith et al., 2014a). These serve to attract more immune cells and activate the blood vessel epithelium to allow for these cells to transmigrate. The interaction of chemokines with GAGs allows for their accumulation at the blood vessel endothelium where they form gradients that facilitate the migration of other immune cells (Kufareva et al., 2015b).

Some of the earliest cells to follow these gradients and migrate from the peripheral blood to areas of acute inflammation are neutrophils. Neutrophils

transmigrate through the activated blood epithelium (Hughes and Nibbs, 2018) following the CXCL8 and other chemokine created gradients through their surface CXCR2 / CXCR1 receptors. Neutrophils act to clear the infection by direct phagocytosis but also through the release of effector molecules that attract further immune cells (Nathan, 2006).

Indeed, the CXCL8 − CXCR2 / CXCR1 axis is essential in mediating the inflammatory response through the recruitment and activation on neutrophils (Ha et al., 2017). CXCL8 gene knockout attenuates wound healing and neutrophil recruitment in zebrafish (Oliveira et al., 2013). Furthermore, CXCR2 knockout mice exhibit delayed wound healing and compromised neutrophil chemotaxis (Devalaraja et al., 2000), (Rio et al., 2001). Gene targeting in mice has further demonstrated that CXCR2 regulates neutrophil-mediated immune response in bacterial and parasitic infections, as well in the process of wound healing (Frendéus et al., 2000). A CXCR2 mediated inflammatory response is also necessary for the clearance of E.Coli urinary tract infections (Olszyna et al., 2001).

The activation of Gi/o proteins following CXCR2 agonist stimulation leads to canonical separation of αi and βγ subunits (Ha et al., 2017). The roles of the Gαi in mediating cell chemotaxis are controversial as studies have shown both inhibition and lack of effect of pertussis toxin on this process (Im et al., 1989), (Neptune et al., 1999). It is clear, however, that Gβγ needs to be released from Gαi coupled receptors and not Gαs or Gαq in order to mediate cell migration (Neptune and Bourne, 1997), (Thelen, 2001). The βγ subunit is suggested as the major player in mediating neutrophil function. It activates phospholipase C (PLCβ) which results in the mobilisation of calcium from the endoplasmic reticulum through IP3 generation, and protein kinase C (PKC) activation via diacylglycerol (DAG) (Stadtmann and Zarbock, 2012). PKC is suggested as an essential molecule in mediating neutrophil cytotoxic functions (Bertram and Ley, 2011). The downstream effectors mediating the motility and chemotaxis of neutrophils, however, are less clear. The polarised membrane redistribution of CKRs or other GPCRs mediating chemotaxis does not underlie the directional movement of cells (Xiao et al., 1997), (Servant et al., 2000). However, the

activation of the small GTPase Ras through βγ release binds class IB phosphoinositide 3-kinase (PI3K/ PI3Kγ) which ultimately leads to phosphatidylinositol 3,4,5-trisphosphate (PIP3) generation. PIP3 then recruits Pleckstrin homology (PH)-domain proteins at the leading edge of plasma membrane that leads to actin polarisation and drives the cells forward (Jin et al., 2008).

While CXCR2 is an important part of the immune defence for the clearance of pathogens, its overactivity / overexpression contributes to the pathophysiology of other conditions such as sepsis. Cell-penetrating peptides blocking CXCR2 / CXCR1 have been shown to reverse multi-organ failure disseminated intravascular coagulation as well as mortality in murine models of sepsis (Kaneider et al., 2005), (Ness et al., 2003). Furthermore, neutrophil migration mediated by CXCR2 promotes lung inflammation, certain types of inflammatory arthritis and experimentally induced colitis (Buanne et al., 2007). CXCR2 is upregulated in patients suffering from chronic obstructive pulmonary disease (COPD) and airway inflammation, associated with excessive recruitment of neutrophils (Qiu et al., 2003). In addition, CXCR2 is expressed by neurones, oligodendrocyte progenitor cells and astrocytes in pathologies such as multiple sclerosis and experimental autoimmune encephalomyelitis (Semple et al., 2010); however, it is unknown whether and how it contributes to the development of these conditions.

1.7.3 CXCR2 roles in cancer

Malignant cells create a microenvironment that supports their growth and simultaneously protects them from the host's immune response. Chemokines and chemokine receptors have important roles in shaping the tumour immunity and cancer microenvironment (Nagarsheth et al., 2017). Whilst some chemokine and CKRs such as CXCL9, CXCL10 and CXCR3 mediate the recruitment of CD8+ cytotoxic T cells that have anti-tumorigenic activities, the activity of CXCR2 in the context of cancer is largely tumorigenic (Nagarsheth et al., 2017).

CXCR2 expression is associated with poor prognosis in gastric cancer as it mediates cancer cell metastasis (Zhou *et al.*, 2019). CXCR2 expression and signalling is implicated in the progression of various other cancers such as pancreatic, prostate, and breast cancer (Wente et al., 2006), (Murphy et al., 2005),(Xu et al., 2018). CXCR2 exhibits tumorigenesis by directly promoting tumour cell growth and survival but also by shaping the tumour microenvironment through the regulation of angiogenesis and immunosuppression (Cheng et al., 2019a).

An important step in tumour progression is the 'angiogenic switch' resulting in the heavy vascularisation of tumours supporting their survival (Baeriswyl and Christofori, 2009). Tumour cells deprived of vasculature become necrotic and undergo apoptosis (Kiefer and Siekmann, 2011). ELR+ chemokines including CXCL8 are potent angiogenic factors and CXCR2, largely mediates this function. CXCR2 activation stimulates the migration of microvascular endothelial cells expressing the receptor through a pertussis sensitive mechanism mediated by G protein activation (Addison et al., 2000). CXCL8 mediated CXCR2 activation promotes angiogenesis also by stimulating endothelial cell survival and proliferation and the breakage of the extracellular matrix (ECM) via the release of matrix metalloproteinases (MMPs) (Li et al., 2003). CXCR2 signalling via the Gβγ dimer leads to the activation of PI3K and protein kinase B (PKB / AKT) – a pathway which alteration is very common in human malignancy as it mediates cell survival, angiogenesis and motility (Wang et al., 2008). CXCR2 further supports cancer progression by mediating chemotherapy resistance as knockdown of the receptor enhances responsiveness to paclitaxel and doxorubicin chemotherapy agents in mammary cancer cells (Sharma et al., 2013).

The formation of the tumour microenvironment is associated with the infiltration of immunosuppressive cells generally referred to as myeloid derived suppressor cells (MDSCs) (Veglia et al., 2021). MDSCs could be granulocytic such as the tumour-derived neutrophils (TAN) also known as N2, or monocytic macrophages in different maturation stages (Nagarsheth et al., 2017). Tumour cells release various chemokines, and neutrophils expressing

CXCR2 migrate to the cancer locations. In response to other mediators released by cancer cells such as transforming growth factor beta (TGFβ), the migrated neutrophils undergo polarisation to their immunosuppressive phenotype - N2 (Powell and Huttenlocher, 2016). In response to CXCL8, the TANs release arginase 1 which inhibits T cell mediated immune defence and CXCR2 genetic deletion leads to a reduction in TAN accumulation and T cell mediated tumour suppression in pancreatic cancer (Rotondo et al., 2009), (Chao et al., 2016). CXCR2 mediated MDSC accumulation is also observed in the colonic mucosa in colitis-associated tumours (Katoh et al., 2013). A recent study examined the effects of targeted deletion of CXCR2 in myeloid cells in the context of the progression and tumour immunity in breast cancer, lung cancer and melanoma (Yang et al., 2021). The study showed that receptor deletion and inhibition with a small-molecule drug SX-682 enhances the cytotoxic T cell anti-tumour activity and reduces MDSC cells in the tumour niche.

Overall, there are multiple reports of the upregulation of CXCR2 in various cancers and its correlation with poor prognosis with less of mechanistical explanation of how the receptor executes these functions. Most supported functions with evidence for the mediation of immunosuppressive cell infiltration and angiogenesis. The receptor therefore represents a potential target for antagonists (NAMs, biologicals etc.) in cancer therapies.

1.8 CXCL8 and CXCR2 from a structural perspective

The cryo-electron microscopy (cryo-EM) structure of CXCR2 was solved and published by Liu et *al.* in 2020 (Liu et al., 2020) and provides structural insights into CXCL8-CXCR2 interactions, an active receptor conformation supported by a bound Gi protein, as well an inactive conformation supported by a bound intracellular small molecule NAM.

As predicted prior to the structural study, the interaction of CXCL8 with the receptor is composed of separate binding surfaces. Firstly, the N loop and β3 strand of CXCL8 interact with N-terminal residues of CXCR2 causing the Pro-Cys motif in the receptor to obtain a bent conformation. The N terminus of

CXCR2 is further accommodated in the binding groove of CXCL8 via the Cys39-Cys286 disulphide bond. The second chemokine-CKR interaction is facilitated by the ELR motif in the N terminus of CXCL8 and the Gly-Pro motif in the 30s loop (connecting β2 and β3), and the ECL2 and TM domains of CXCR2. Important contacts to be highlighted are the charged interactions between Glu4 in ELR and positively charged arginine residues Arg278, Arg208, and Arg212 in TM6 and TM7 and the hydrophobic connection with Tyr197 in ECL2 (Figure 1.7).

The structure also shows that CXCL8 can bind CXCR2 both as a monomer and as a dimer and that the first subunit (CXCL8 A) of the dimer interacts with the receptor in the same way as a CXCL8 monomer.

In comparison with the interactions of other chemokine-CKRs with available structures, the N terminus of CXCL8 seems to form a more shallow interaction with the TM agonist pocket, and does not to interact with a potential minor transmembrane subpocket, evident for example in the viral chemokine vMIP-II - CXCR4 interaction (Qin et al., 2015). This is likely a result of the presence of large side chains of the receptor Lys108 and Arg184 occluding the access for the N terminus of the chemokine.

Compared to less ligand promiscuous CXCR1 receptor (77% homology), the CXCR2 N terminal region between the Pro-Pro and Pro-Cys consists primarily of hydrophobic residues. In contrast, these residues in CXCR1 are charged allowing interaction with charged N-loops specific to CXCL8 and CXCL6 chemokines (Park et al., 2012) explaining the different degrees of ligand selectivity for CXCR2 and CXCR1.

In terms of activation, the biggest driver for CXCR2 active conformation is the inward movement of TM5 followed by structural rearrangements in TM3 and TM6 allowing for the outward swing of the cytosolic part of TM6. Rearrangements of residues part of class A signature motifs NPxxY and DRY participate in CXCR2 activation, as discussed in section 1.2.

The CXCR2 Gi interaction surface is composed of residues in TM3, TM5, TM6 and ICL3 of the receptor and the α5 helix, αN helix and αN–β1 loop of the Gαi subunit. The hydrophobic receptor pocket accommodating the C terminal G

42

protein α5 helix is composed of Ile148, Leu238, Val252, Ile253 and Ile317 from the cytosolic ends of TM3, TM5, TM6 and TM7 (Figure 1.8).
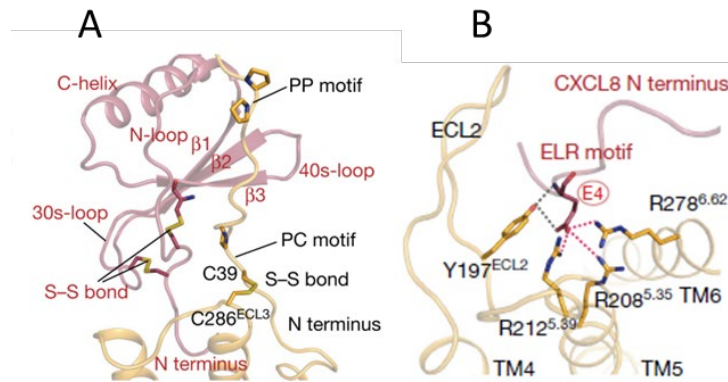
Figure 1.7 The interaction of CXCL8 with CXCR2. A) The first step of CXCL8-CXCR2 interaction is the formed between the chemokine N loop and β3 strand interact with CXCR2 N terminus. B) This is followed by the interaction between CXCL8 N terminus and transmembrane pocket at CXCR2. The images represent cryo-EM structures by Liu *et al.,* (2020).
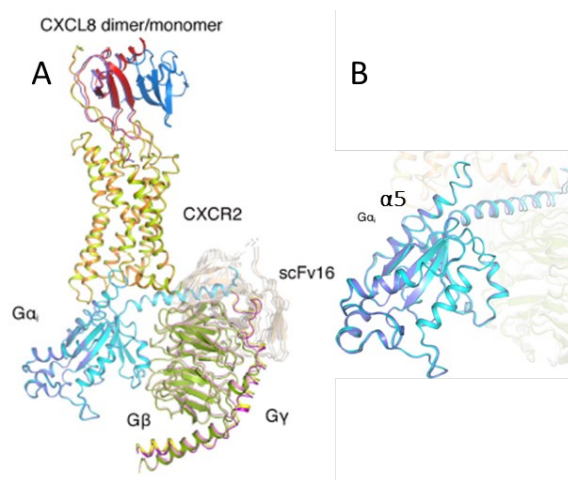
Figure 1.8 The interaction of CXCR2 with heterotrimeric Gi protein. A) CXCR2 bound by CXCL8 shown both as a monomer and dimer and the heterotrimer Gi protein consisting of Gα, Gβ and Gγ subunits. B) Closer look into the insertion of the Gα5 helix into the transmembrane crevice of CXCR2. The images represent cryo-EM structures by Liu *et al.,* (2020).

The study confirmed the presence of an intracellular allosteric pocket that overlaps with the α5 insertion cavity, hence small-molecule drugs binding there sterically hinder G protein coupling (section 1.9). The inactive

43

conformation of CXCR2 bound to one such intracellular NAM (an analogue of navarixin) is characterised by a less compact extracellular surface due to differences in TM5 residue conformations, together with differences in the cytosolic residue contacts of TM6, TM3, and TM5 responsible for the formation of the G protein binding crevice. These findings provide structural evidence for the potential mechanism of NAM CXCR2 inhibition suggesting both G protein competition, but also changes in receptor conformation that may affect agonist binding affinity.

1.9 Pharmacological modulation of CXCR2

There are multiple small-molecule inhibitors or biologics interacting with growth factors and their receptors such as VEGF and EGF (Roland et al., 2009), (Bolitho et al., 2010) as well as inhibitors of intracellular kinases (Bhat et al., 2017), that have been developed as potential cancer therapies, and that indirectly affect the secretion of the CXCL1 and other CXC- chemokines activating CXCR2. Targeting CXC- ligands directly has been attempted through the development of antibodies against CXCL7 (Zhang et al., 2018), CXCL6 (Besnard et al., 2013), CXCL2 (Kollmar et al., 2008), CXCL5 (Hsu et al., 2013), and CXCL8 (Yang et al., 1999) for treating conditions such as glomerular endothelial dysfunction, respiratory failure in chronic pulmonary disease, breast cancer, and inflammatory conditions respectively. The blocking of these and other CXC ligands has been thoroughly reviewed by Chen et al (Cheng et al., 2019b).

The inhibitors of CXC chemokines represent a useful tool for potential combination therapies for the treatment of cancer or inflammatory conditions. Nevertheless, specific CXCR2 blockage cannot be achieved through this route, due in part to the receptor's promiscuous interaction with all pro-inflammatory chemokines.

Direct CXCR2 inhibition has been achieved through the use of biologics such as biparatopic nanobodies (Bradley et al., 2015), as well as receptor-targeted monoclonal antibodies shown to inhibit angiogenesis mediated via CXCR2 activation (Matsuo et al., 2009). However, the use of orthosteric small

molecule antagonists has not been applied as a strategy to target CXCR2 due to the multiple areas at the receptor involved in chemokine binding and the complexity of this process. Nevertheless, the presence of potential binding sites topographically distinct from the chemokine binding area has underlined the development of small-molecule negative allosteric modulators (NAMs) that interact with them and block CXCR2.

Based on their chemical properties CXCR2 NAMs can be generally classified into – N, N'-diarylureas and derivatives, and aromatic ring derivatives (Table 1.2). The diarylurea- skeleton for the basis of CXCR2 antagonists was established with the development of the first non-peptidergic CXCR2 selective antagonist – SB225002 (White et al., 1998) followed by others (Widdowson et al., 2004) such as SB265610 (Bradley et al., 2009), GSK1325756 (danirixin) (Miller et al., 2015), SB656933 (elubrixin) (Lazaar et al., 2011). Elubrixin and danirixin are representatives of the diarylurea compounds that entered clinical trials but failed due to lack of efficacy in the treatment of COPD, colitis and cystic fibrosis (Lazaar et al., 2020), (Mozaffari et al., 2015). The diarylureas were the basis for the synthesis of the N, N'-diarylsquaramides and analogues. One such compound navarixin (Sch527123, MK-7123) was identified by Dwyer *et al.* (2006) and entered clinical trials for the treatment of chronic inflammatory conditions, however, it was discontinued for causing neutropenia in healthy patients (Holz et al., 2010), an on target effect due to the role of CXCR2 in immune cell migration in bone marrow. Navarixin is currently in clinical trials as a combination therapy along with an immune checkpoint inhibitor antibody for the treatment of solid metastatic tumours. Other compounds developed to block CXCR2 allosterically are the aromatic ring derivative compounds including AZD5069 (Nicholls et al., 2015a) and AZ10397767. AZD5069 entered clinical trials for the treatment of airway inflammatory conditions but similarly to navarixin, was terminated due to causing neutropenia (Jurcevic et al., 2015). Nevertheless, it is currently in clinical trials in combination with an antiandrogenic drug for the treatment of prostate cancer. The fine balance between obtaining an effective therapy through sufficient CXCR2 inhibition, and on target side effects, illustrates the

45

need to understand fully and titrate the pharmacological modulation of individual NAMs at the receptor to the desired outcome.

CXCR2 is also negatively modulated by a dual CXCR1/CXCR2 NAM binding within the transmembrane domains – reparixin, which was synthesised on the basis of ibuprofen (Bertini et al., 2012). Reparixin has successfully completed phase 3 clinical trials as an anti-inflammatory drug in islet transplant surgeries in diabetes (Citro et al., 2013).

These NAMs interact with and block CXCR2 at allosteric binding pockets distinct from the chemokine binding area. The first allosteric pocket was identified in CXCR1 (77 % homology with CXCR2) and comprises of residues in the outer regions of the helices 1,2,3,6, and 7. The binding of reparixin at this pocket was detected in CXCR2 using modelling techniques and was found to share similar features with the binding of ketoprofen at cyclo-oxygenase COX1 (Bertini et al., 2004). CXCR2 binding of reparixin was later demonstrated but with lower affinity compared to CXCR1, likely attributed to some non-conserved residues in the pocket (Moriconi et al., 2007), (Allegretti et al., 2005).

Through site-directed mutagenesis and molecular modelling approaches, a site in the outer transmembrane domains of CXCR2 was later on identified (Kruijf et al., 2011) and shown to be the binding pocket of non-peptidergic NAMs belonging to the imidazolylpyrimidines chemical class. The study suggested that the binding of this class of NAMs is via the major orthosteric subpocket and the site is distinct from the reparixin area. Nevertheless, there have been no competition binding studies with labelled reparixin or structural studies so far to confirm the distinction of these binding pocket within CXCR2.

The existence of an intracellular allosteric pocket at CXCR2, described in the structural study above (Figure 1.8) was identified as early as 2008 (Nicholls et al., 2008) using mutagenesis and molecular modelling tools and shown to be the binding area for the diarylureas (SB265610, danirixin etc) , diarylsquaramides (navarixin), and some of the aromatic ring derivative compounds (AZ10397767, AZD506) (Salchow et al., 2010), (Kruijf et al., 2009), (Nicholls et al., 2008). The overlap of this site with the effector coupling

surface immediately suggested a mechanism of action of the intracellular NAMs at CXCR2, through competition with G proteins and/or changes in receptor conformation as seen in classic GPCR allosterism (Bradley et al., 2009). The Cryo-EM structure of CXCR2 bound by a diarylsquaramide NAM – 00767013 (navarixin structural analogue) details the intracellular NAM binding pocket formed by the cytosolic ends of TM1,2,3,6 and 7 with participating residues from the DRY motif (Arg144) and NPxxY motif (Tyr134) involved in its formation (Figure 1.9). The study showed the pocket overlaps with the $\alpha 5$ helix binding crevice at the receptor and residues participating in the formation of the receptor-Gα complex (Liu et al., 2020), but also that NAM binding at the intracellular site promotes broader changes in the extracellular and transmembrane CXCR2 domains characteristic of the inactive conformation.

Such intracellular binding pockets have been identified in a range of GPCRs such as the $\beta 2$-adrenergic receptor (Ahn et al., 2017), the muscarinic receptor M2 (Miao et al., 2014), as well as the chemokine receptor representatives CCR2, CCR7, and CCR9 (Zweemer et al., 2014), (Jaeger et al., 2019),(Oswald et al., 2016) suggesting the Gi / Gs protein interaction site could be more broadly targeted. Modulation of GPCRs intracellularly, therefore, represents an exciting venue to be explored in terms of selectivity of the intracellular small molecules as well as their precise mechanism of action.
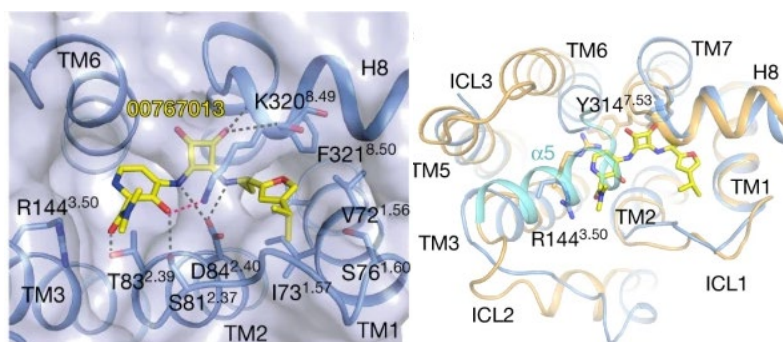
Figure 1.9 The interaction of CXCR2 with small-molecule intracellular NAM. The CXCR2 receptor structure bound by the structural equivalent of navarixin 00767013 showing the insertion of the NAM in the intrahelical receptor cavity that also accommodates Gα α5 helix. The images represent cryo-EM structures by Liu *et al.,* (2020).

1.10 Aims

As a mediator of important pathophysiological functions in inflammatory pathologies and cancer, the chemokine receptor CXCR2 represents a relevant druggable target. Within the development of a range of therapies against the receptor and chemokine, small-molecule intracellular NAMs have provided the most widespread opportunity to develop orally bioavailable and effective CXCR2 selective inhibition. However, clinical trials to date have been limited by the degree of therapeutic efficacy and also the potential for on target CXCR2 related side effects, such as neutropenia. Better characterisation of the allosteric mechanism of action of CXCR2 NAMs may lead to an improved understanding of how to fine tune their pharmacological properties at the receptor, and ultimately deliver more therapeutically effective molecules.

This work aimed to provide detailed pharmacological characterisation of structurally distinct intracellular CXCR2 NAMs to decipher the key aspects of their mechanism of action at the receptor. The example NAMs chosen are SB265610, danirixin, AZ10397767, AZD5069, R-navarixin, and S-navarixin (table 1.2).

Chapter three explores the effect of NAMs on CXCR2 activation as a function of intracellular effector recuitment measured in real-time, in living cells using the Split luciferase complementation technology (NanoBiT). NAMs are applied

both prior and following agonist treatment and are compared in their ability to inhibit receptor-effector interactions. The real time assay format enabled the affinities and binding kinetics of NAMs to be estimated by means of mathematical model fitting, and their binding reversibility is further assessed through the use of wash-out assay. The chapter also compared the ability of NAMs to affect CXCR2 interaction with different effectors (mini G proteins compared to arrestins) to analyse whether the nature of the receptor-effector binding surface altered the pharmacological action of the NAM.

Chapter four further assesses NAMs through their ability to affect the binding of a fluorescent chemokine agonist to CXCR2 receptors, through development of a TR-FRET based homogeneous and real time binding assay The first chapter explores the characterisation of the chemokine tracer binding in both whole cells and in membrane preparations under different buffer conditions using high-content confocal imaging and TR FRET. NAMs are then compared in their abilities compete for binding with the tracer and also to mdulate chemokine dissociation kinetics. This chapter provides important evidence to support the existance of negative binding cooperativity between CXCR2 NAMs and the chemokine agonist and so suggests a strong effect of NAMs on receptor conformation, in addition to direct inhibition of G protein interaction.
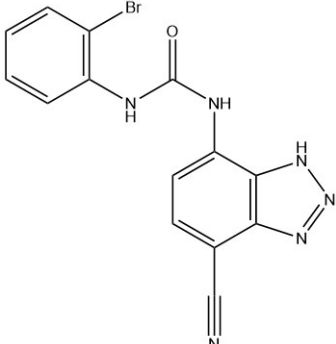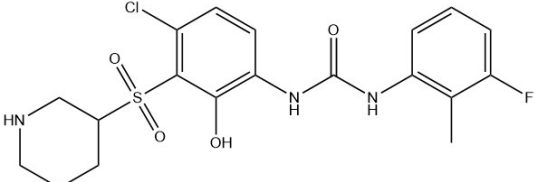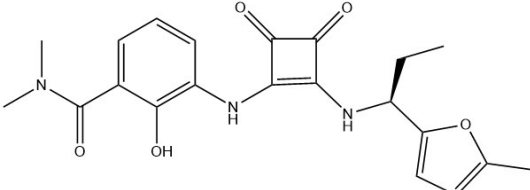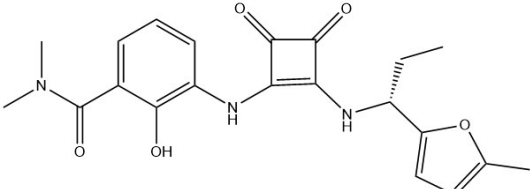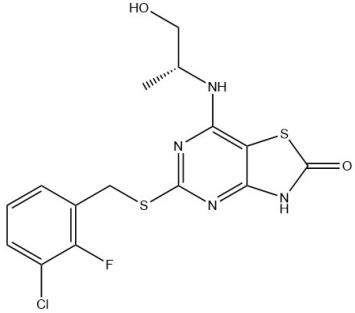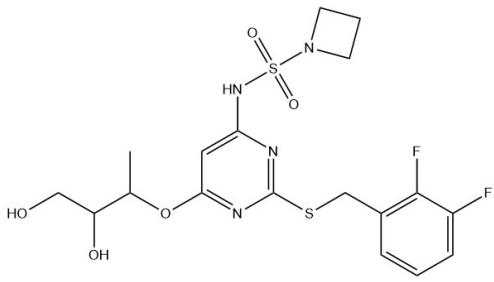
	SB265610
	Danirixin
	S-navarixin
	R-navarixin
	AZ10397767
	AZD5069

Table 1.2. CXCR2 negative allosteric modulators used in this work.
Structures drawn on using ChemDraw Professional software.

Chapter 2. Materials and Methods

2. Chapter Two: Materials and Methods

2.1 Materials

2.1.1 Molecular Biology and cell culture

DNA was isolated and purified using commercially available kits including PCR Cleanup Kit, Gel Extraction Kit, and Miniprep kit purchased from Sigma-Aldrich LDT (Poole, UK), and Maxiprep Kit from Qiagen (Hilden, Germany). Bacterial growth media (Luria Bertani broth / LB broth), and LB Agar as well as compounds for other working buffers, and Ampicillin (used at 50 mg.mL^{-1}) were also purchased from Signa-Aldrich.

The FastDigest buffers used for restriction digestion, the alkaline phosphatase (FastAP) and the T4 DNA ligase and the associated buffers were obtained from Thermo Fisher Scientific (Waltham, MA, USA).

All primers for DNA amplification and modification were designed in house.

The pcDNA3.1(+) neomycin (neo) or zeocin (zeo) vectors containing an N terminal 5HT3 signal sequence and SNAP tag (between Kpn1 and BamH1 sites) were made in house by members of the lab of Dr Nicholas Holliday.

The vector containing the human CXCR2 sequence (NM_001557.3) - pCMV6-AC neo, was purchased from Origene (Maryland, US). The pcDNA3.1 neo SNAP-6xHis vector was synthesised by GeneArt (Invitrogen; Paisley, UK). The mini Gαo protein sequence was synthesised by GeneArt according to Tate's lab study (Nehmé et al., 2017a) and cloned into a pcDNA3.1 zeo vector in house. The β-arrestin2 (NC_000017.1) sequence was cloned into a pcDNA3.1 zeo vector in house prior to the start of this project.

The SmBiT and LgBiT sequences for the NanoBiT assay constructs were obtained from Promega corporation (Madison, US).

HEK293T cells were obtained from Invitrogen and cultured in media containing DMEM high glucose with 10% foetal calf serum (FCS) purchased from Sigma Aldrich and GE Healthcare Life Sciences (Buckinghamshire, UK) respectively. Mammalian expression antibiotics zeocin (used at 20μg.mL^{-1}) and Geneticin (used at 0.2 mg.ml^{-1}) were provided by Thermo Fisher Scientific and Invitrogen

respectively. Lipofectamine and Lipofectamine 3000 chemotransfection agents were obtained from Invitrogen.

2.1.2 Compounds and assay reagents

The unlabelled CXCL8 (28-99) chemokine was purchased from Stratech Scientific (Cambridge, UK), and the labelled chemokine probe CXCL8-AF647 – from Almac (NI, UK).

SB265610 and AZ10397767 were obtained from Tocris Bioscience (Bristol, UK), danirixin and AZD5069 - from Cayman Chemical / Cambridge Bioscience (Michigan, US / Cambridge, UK), and R- navarixin and S-navarixin were synthesised in house by Bianca Casella (Shailesh Mistry group).

The non-hydrolysable GTP analogue GppNHp was obtained from Abcam (Cambridge, UK). The NanoGlo furimazine substrate for the NanoBit assays was provided by Promega corporation. SNAP-Lumi4-Tb and LabMed buffer were obtained from Cisbio (Codolet, France).

White and black 96 well plates were purchased from Greiner Bio-One (Stonehouse, UK), and white 384 well Optiplates – from PerkinElmer Beaconsfield, UK. Bovine Serum Albumin (BSA) was purchased from Sigma Aldrich.

2.2 Molecular Biology
2.2.1 Overview of construct preparation
2.2.1.1 CXCR2 cloning by polymerase chain reaction (PCR)

Polymerase chain reaction (PCR) (Figure 1) was used to clone and modify the human CXCR2 receptor cDNA (Genbank NM_001557.3). PCR permits the exponential amplification of a desired sequence by using short oligonucleotide sequences (primers) complementary to the sequence of interest. The PCR process involves heating the reaction to 95°C causing denaturation of the double-stranded DNA template into two single-stranded DNA molecules. The second step is the annealing of forward and reverse primers to each of the single stranded DNA fragments allowed by the rapid reduction of temperature down to 58°C. The reaction is then heated to the optimal activity temperature of the DNA polymerase (72 °C for Q5 DNA polymerase) which extends the DNA sequence from the point of primer attachment to the template. The thermal steps of denaturation, annealing and primer extension are repeated 25 times leading to an exponential increase in the amount of product.

Forward and reverse primers (18-30 base-pair length) were designed to recognise and anneal to the receptor sequence and to modify it by introducing restrictions sites at the 5' and 3' prime ends recognisable by restriction nucleases used to digest the DNA and clone it into vectors of interest. For constructs requiring further N- or C-terminal modifications, the primers were designed to remove the start or stop codons of the template to create an in-frame fusion protein (Table 2.1).

The PCR reactions were carried out using Q5 High Fidelity DNA Polymerase, an enzyme with proof-reading activity ensuring the correct DNA sequence is replicated. A typical PCR reaction contained 50 ng DNA template, 10 μM reverse and forward primers, 200 uM dNTPs, 1x buffer Q5 containing 2 mM Mg^{2+}buffer Q5 and double distilled water (ddH$_2$0) to a final volume of 50 μl. The Q5 DNA polymerase enzyme was added following heating up the reaction to 95°C.
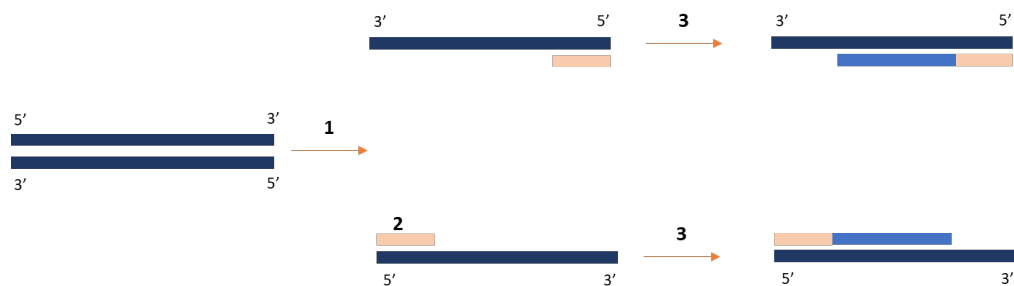
Figure 2. 1 Principles of the polymerase chain reaction. 1) The double stranded DNA template is denatured into two single stranded DNA strains. 2) The primers recognise and anneal to each single stranded DNA-molecule and 3) extend them from the 5' end.

Construct	Primer	Sequence
EcoRI CXCR2 XhoI No start codon	Forward	5' AAATAT <u>G AAT TCT</u> gaagatttt aacatggaga gtgacagc
	Reverse	5' AAATAT <u>CTC GAG</u> ttagagagtagtggaagtgtgc
HindIII CXCR2 XhoI No stop codon	Forward	5' AAATAT <u>AAGCTT</u> gccacc atg gaa gat ttt aac atg gag
	Reverse	5' AAATAT <u>CTCGAG</u> gagagtagtggaagtgtgc

Table 2.1 Primers used in the construct preparation.
In EcoR1 forward primer the restriction site GAA TTC is not in frame with the start of the CXCR2 sequence. Therefore, additional T bases were added to adjust the reading frame to that of the SNAP coding sequence in the vector. In the other three primers, the 5' restriction sites are in frame with the receptor sequence. The restriction site sequences are underlined

2.2.1.2 N-terminally SNAP-tagged CXCR2 constructs

The PCR amplified CXCR2 sequence cloned between EcoRI and XhoI and lacking a stop codon was placed in a pcDNA3.1 (+) zeo vector (made by Dr Nicholas Holliday, University of Nottingham) downstream from the SNAP coding region (NEB). The pcDNA3.1 (+) neo vector contains a human cytomegalovirus immediate-early (CMV) promoter which gives high protein expression in mammalian cells, and a bovine growth hormone (BGH) polyadenylation signal for transcription termination and polyadenylation of mRNA. The vector also contains resistance genes for the antibiotics ampicillin and neomycin for selection in *E.coli* and in mammalian cells respectively, and T7 and BGH reverse promoters for sequencing. The SNAP tag in the vector was

placed into the multiple cloning site (MCS) between KpnI and BamHI restriction sites with the 5-HT3 receptor signal sequence (amino acids MRLCIPQVLLALFLSMLTGPGEGSRK) placed upstream to facilitate membrane integration.

2.2.1.3 C-terminally modified CXCR2 constructs

The SNAP-tagged CXCR2 receptor lacking a stop codon was the basis of other DNA constructs. The SNAP-CXCR2 sequence with the restriction sites described above lacking a stop codon was cloned into a pcDNA3.1 vector upstream from a LgBiT sequence (containing no start but including a stop codon) placed between XhoI and XbaI restriction sites (provided by Dr Nicholas Holliday, University of Nottingham) (Figure 2.2).

The SNAP-tagged CXCR2 sequence lacking a stop-codon was digested with the appropriate restriction enzymes and inserted into a pcDNA3.1 (+) zeo upstream from a double 6x Histidine tag sequence (from Holliday group, University of Nottingham) with a stop codon, located between XhoI and XbaI. This vector encodes mammalian cell resistance to zeocin (zeo) rather than neomycin.

The vector containing SNAP-CXCR2-LgBiT construct was digested with the appropriate restriction enzymes and the LgBiT fragment replaced with a complemented thermostable Nanoluciferase (tsNluc) (made by Nicola Dijon, University of Nottingham) containing flanked as before by XhoI / XbaI restriction sites. tsNluc contains NanoBiT amino acid substitutions in the luciferase protein to enhance thermal stability ((Dixon et al., 2016), (Hoare *et al.,* 2020; manuscript submitted).
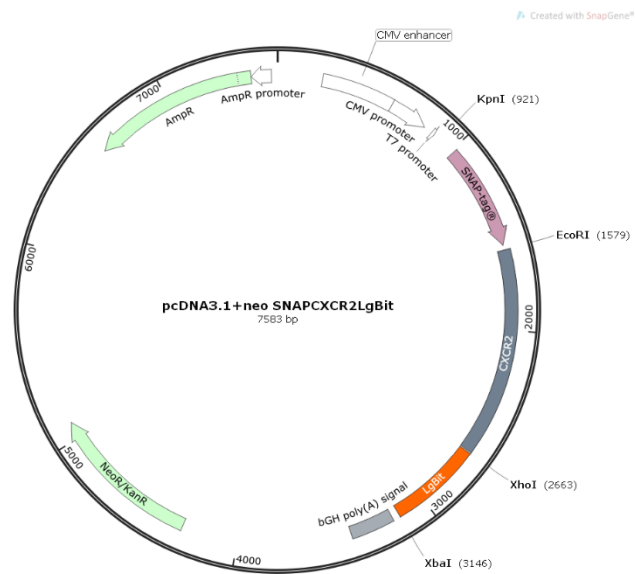
Figure 2.2 Vector map of the SNAP-CXCR2-LgBit construct. The map shows pcDNA 3.1 vector containing neomycin and ampicillin resistance (green), CMV promoter (white), T7 and BGHrev sequencing primer sites, and a CXCR2 sequence with a SNAP tag sequence upstream and LgBit sequence – downstream. The map was made using SnapGene.

2.2.1.4. C-terminally SNAP-tagged CXCR2 construct

The human CXCR2 gene was PCR amplified and HindIII and XhoI restriction sites were introduced at the 5' end and XhoI site at the 3' end. The forward primer used introduced a start codon and a Kozak sequence to ensure successful transcription and ribosomal translation of the gene and the reverse primer removed the stop codon of the CXCR2 sequence. The created construct was cloned into a pcDNA3.1 (+) neo vector.

A pcDNA3.1 vector containing the SNAP tag sequence in frame, without start codon and adding a stop codon (Holliday group, University of Nottingham) was digested with XhoI and XbaI to excise this insert, which was then cloned into the pcDNA3.1 (+) neo vector described above downstream from the CXCR2 sequence.

2.2.1.5 Generation of mini GαoA and β-arrestin2 constructs

A vector containing the sequence of the mini GαoA protein (Nehmé et al.,

57

2017a), original sequence synthesised by GeneArt, Invitrogen) was digested with BamHI and XbaI restriction enzymes and inserted into a pcDNA3.1(+) zeo vector downstream from the SmBit fragment sequence using a 5 amino-acid linker.

Similarly, the human β-arrestin2 sequence (GenBank NC_000017.1) from an existing fluorescence complementation lab construct (Kilpatrick et al., 2012) was digested with BamHI and XbaI and inserted in frame into a pcDNA3.1 (+) zeo vector downstream from a SmBiT sequence, eliminating the start codon.

DNA Construct	Source
pcDNA3.1 neo Kpn1 SNAP BamHI	Obtained from the Holliday group
pcDNA3.1 neo Kpn1 SNAP BamHI EcoRI CXCR2 XhoI	Made by author
pcDNA3.1 neo Kpn1 SNAP BamHI EcoRI CXCR2 XhoI LgBit XbaI	Made by author
pcDNA3.1 zeo Kpn1 SNAP BamHI EcoRI CXCR2 XhoI 6xHis	Made by author
pcDNA3.1 neo HindIII CXCR2 XhoI SNAP XbaI 6xHis	Made by author
pcDNA3.1 zeo HindIII SmBiT BamHI β-arrestin2 XbaI	Made by Nicola Dijon
pcDNA3.1 zeo HindIII SmBiT BamHI mini Go XbaI	Made by author
pcDNA3.1 neo SNAP EcoRI CXCR2 XhoI tsNluc XbaI	Made by author
pcDNA3.1 neo XhoI tsNluc XbaI	Made by Nicola Dijon

Table 2.2 List of DNA constructs used in this project and their sources. The restriction sites are shown in blue upstream or downstream of the sequence of interest.

2.2.2 DNA processing and preparation

2.2.2.1 Restriction Digestion

The preparation of desired DNA constructs requires the joining of DNA fragments (referred to as an insert and a vector) through a reaction called ligation (described in section 2.2.3. below). To be able to clone a DNA insert into a vector of interest, the insert and vector must first be treated with restriction endonucleases, enzymes which recognise and cut at specific nucleotide sequences, and can create compatible overhanging ends. The generation of different restriction sites at the 3' and 5' ends of the PCR-amplified DNA sequences allow the use of different restriction enzymes that leave different overhangs on each end. This ensures correct orientation of the insert when cloned into the vector.

58

A typical restriction digestion reaction of the vector DNA contained 2 µg DNA plasmid, 2 µl 10x clear Fast Digest Clear Buffer, 1 µl of each Fast Digest restriction enzyme and ddH$_2$0 to a final volume of 20 µl. The digestion was carried out at 37°C for 1-3 hours depending on the size of the DNA fragment; the restriction endonucleases were inactivated by heating the reaction to 65-75°C for 10-20-minutes. Digestion of PCR products (100 – 200 ng DNA) was carried out at longer incubation times in order to maximise the extent of cleavage close to the ends of the DNA fragment. This was also facilitated by the addition of additional bases (~6) flanking the restriction endonuclease site and enzymes less inhibited by positioning at the end of DNA fragments were chosen.

2.2.2.2 Agarose Gel Electrophoresis

Agarose gel electrophoresis is a technique used to separate DNA molecules based on their molecular weights by applying an electric field through an agarose gel matrix. The negatively charged DNA fragments migrate towards a positively charged anode with smaller fragments migrating faster than larger ones. A gel consisting of 1% agarose (Sigma Aldrich) in TBE buffer (89 mM Tris HCl, 89 mM Boric acid, 2 mM EDTA (ethylenediaminetetraacetic acid); pH 7.6 was prepared. The solution was microwaved to dissolve the agarose and after sufficient cooling 0.1 µg.ml-1 ethidium bromide was added to allow DNA isolation under ultraviolet light. The gel was left to set prior to being placed into an electrophoresis tank and covered with TBE buffer. Clear DNA samples such as PCR products were mixed with 6x Gel Loading dye / glycerol for loading. Samples were run against 1kb DNA ladder (Promega, Madison, US) to serve as a molecular weight marker. The gel was run at 80 V for 30-45 minutes and then visualised using UV irradiation using the GeneFlash gel documentation system (Syngene Bioimaging, Cambridge, UK) and a PULNiX TM-300 CCD camera.

2.2.2.3 Isolation and purification of insert DNA

After restriction digestion and gel electrophoresis, the gel slice containing the DNA band was excised from the gel and extracted using gel extraction kit (Sigma Aldrich). The kit uses silica gel-based column purification to isolate the DNA from the gel. For a 100 mg of excised gel fragment 300 µl of gel solubilisation solution was added and heated at 65 °C for 15 minutes. 100 µl isopropanol (1 volume) was added to the fully solubilised gel and the solution was loaded into the purification column previously prepared by the addition of 500 µl column preparation solution and centrifugation for 30 seconds at 14 000 rpm. The column containing the gel solution was centrifuged for 30 seconds at 14 000 rpm and the flow-through discarded – the DNA bound the column under these conditions due to the presence of a chaotropic salt. The column was then washed by adding 500 µl wash solution containing 80% v/v EtOH and centrifuged for 30 seconds at 14 000 rpm. After the eluate was discarded, the column for centrifuged for a minute at the same conditions allowing any excess ethanol to be removed. After transferring the column to a new collection tube, DNA was unbound from the silica by the addition of 50 µl ddH$_2$0 and centrifuging it for 1 minute at 14 000 rpm.

2.2.2.4 Alkaline phosphatase treatment of vector DNA

Following restriction digestion, the vector DNA was treated with shrimp alkaline phosphatase (SAP) (2 µl SAP, 2 µl SAP buffer supplied with the enzyme; 5x final concentration 50 mM Tris HCl, 25 mM MgCl$_2$, 0.5 M KCl, 0.1% Triton-X-100; 100mM Tris-HCl, 50mM MgCl$_2$, 1M KCl, 0.2% Triton-X-100, 1; pH 8.0).
 The reaction as carried out at 37°C for 90 minutes followed by 10 minutes at 75°C allowing SAP inactivation. The SAP treatment removes phosphate groups from terminal nucleotides which prevents self-ligation of the vector, allowing preferential ligation with the digested insert DNA.   This also avoided the need to gel purify the vector DNA prior to ligation.

2.2.2.5 Isolation and purification of vector DNA

Digested and SAP treated vector DNA was purified using a PCR clean-up kit (Sigma Aldrich, according to the manufacturer's instructions) which similarly to the gel extraction kit uses a silica spin column to remove contaminants in the DNA sample, after first allowing it to bind in a solution containing a chaotropic salt. The final step was eluting the DNA from the column in 40 µl ddH$_2$0.

2.2.3 Ligations

2.2.3.1 Ligation of DNA fragments with cohesive ends

Ligation is the joining of two DNA fragments through the formation of a phosphodiester bond which is catalysed by DNA ligase enzymes. Ligations of DNA fragments with compatible cohesive ends generated through restriction digestion were carried out to generate the desired molecular constructs.

Two ligation reactions were set up for each plasmid – one containing the DNA to be inserted in the desired plasmid (positive), and another one – without it (negative), serving as a control. Both reactions contained 50 ng of digested, purified and alkaline phosphatase-treated DNA serving as a vector, 1 µl 10x DNA ligase buffer (40 mM Tris-HCl, 10 mM MgCl2, 10 mM dithiothreitol, 0.5 mM ATP; pH 7.8), 1 µl DNA ligase enzyme and ddH$_2$0 to a final volume of 10 µl. The positive ligation reaction contained the DNA fragment serving as an insert in a 3:1 molar ratio with the vector DNA. The amount of DNA added to the reactions was calculated assuming 80% yield from the previous DNA processing ancestor initial DNA added in the restriction digestion reaction (2 µg) for the vector DNA. For PCR products or the insert DNA, the amount was estimated according to the intensity of the band on the agarose gel. Equation 1 shows the calculation for the amount of insert DNA required, adjusting for the relative sizes of the fragments in base pairs and assuming a 1:3 ratio. The ligations were incubated at 16°C for 16hr.

Equation 2.1:

$$\text{Insert DNA (ug)} = \text{Vector DNA (μg)} \quad \times \quad \frac{\text{Insert Size}}{\text{Vector Size}} \quad \times \, 3$$

2.2.4 Bacterial Transformation

Transformation is the process of introducing DNA into a host cell through electroporation or through chemical treatment of the host cells to facilitate the uptake of plasmid DNA. Chemically treated cells primed for DNA transformation are referred to as 'competent' cells. In this study, plasmids were transformed into TOP10F *Escherichia coli* competent cells (Thermofisher Scientific, Paisley, UK). These cells yield high transformation efficiency (> 1 x 10^9 cfu/μg) and contain an F' episome that carries tetracycline resistance. Transformation of the ligation products was carried out following manufacturer's instructions.

Transformations were normally carried out the day following the overnight (16 h) incubation of the ligation reactions. Competent cells were defrosted on ice and 1-2.5 μl of ligation reaction was added to 17.5 – 25 μl competent cells and incubated for 30 minutes on ice. This was followed by heat shocking the bacteria (42 °C for 30 seconds) causing the perforation of the cell wall and membranes which allows for the plasmid DNA to enter. The cells were immediately returned to ice for another 2 minutes before the addition of 175 μl of rich medium supporting bacterial growth (Luria-Bertani (LB) broth, Sigma Aldrich, Poole, UK) under sterile conditions and 1-hour incubation at 37°C on a shaking plate (225 rpm).

Following the shaking incubation, competent cells were spread onto previously prepared agar plates containing the correct selection antibiotic (e.g. 75 μg.ml^{-1} ampicillin) and were incubated overnight at 37 °C. The ligation/transformation were considered successful if the plates containing bacteria transformed the positive ligation reactions produced more colonies that those transformed with the control ligation reaction, in which case minipreps were generated for plasmid screening by restriction digest (described in the next section).

2.2.5 Small scale isolation and purification of DNA (mini prep)

Resistant colonies were picked using a 200 μl sterile pipette tip and incubated in LB broth containing ampicillin (5 ml LB, 75 μg.ml^{-1} ampicillin) overnight at 37°C on a shaking plate (225 rpm) to allow the bacteria to grow. Following the overnight colony incubation, small-scale DNA isolation (Miniprep) was carried out for diagnostic purposes using GenElute™ Plasmid Miniprep Kit (Sigma-Aldrich) according to the manufacturer's instructions. 3 ml of the overnight LB broth containing resistance colonies was centrifuged at 4000 rpm for 5 minutes twice, discarding the supernatant. The pellet containing the bacteria was then resuspended completely with 200 μl Resuspension solution which contains sucrose TE and RNAse removing any present RNAs. Next, 200 μl Lysis solution was added and the preparations were gently inverted up and down. The Lysis solution contains sodium dodecyl sulphate (SDS) which is a strong detergent used to solubilise proteins, and sodium hydroxide which degrades bacterial cell walls and denatures proteins and genomic DNA, allowing plasmid DNA release. The following addition of neutralisation solution containing potassium acetate precipitates cell debris and genomic DNA allowing for the plasmid DNA (which remains soluble) to be separated by 10 minutes centrifugation at 14 000 rpm. Meanwhile, a binding column was prepared by the addition of 500 μl Column preparation solution and 30-second centrifugation at 14 000 rpm. The clear lysate resulting from the neutralisation step was added to the binding column and centrifuged for 30 seconds at 14 000 rpm. The supernatant was removed and 750 μl Wash solution (80% v/v ethanol) was added followed by another 30-second centrifugation at 14 000 rpm. The supernatant was removed and after an empty centrifugation to remove residual ethanol, the column was placed in a tube collection tube and the DNA was eluted with 100 μl ddH$_2$0. The DNA product was digested with the appropriate restriction enzymes and loaded on agarose gel to check if the DNA fragment is of the expected size for the required insert. In some cases, miniprep DNA was also sequenced using T7 promoter and BGH reverse primers to check if the construct of interest was present.

2.2.6 Large scale isolation and purification of DNA (maxi prep)

Large scale DNA isolation (Maxiprep) was carried out in order to amplify the amount of desired DNA for further transfection into mammalian cells. The day before the Maxiprep, 50 μl of the desired DNA plasmid colonies (previously picked and grown in LB broth) was added to 5 ml of LB broth containing ampicillin (75 μl.ml^{-1}). The culture was incubated at 37°C on a shaking plate (225 rpm) for roughly 6 hours to initiate exponential phase bacterial growth. The culture was then added to a conical flask containing 120 ml LB broth and ampicillin (75 μl.ml^{-1}) which was incubated at 37°C on a shaking plate (225 rpm) overnight.

The following day bacteria were pelleted by 15-minute centrifugation at 3900 rpm and the supernatant discarded. The DNA was then extracted using Qiagen Maxiprep Kit (Qiagen, location) following manufacturer's instructions. The principles of the techniques are the same as described for Miniprep but the Qiagen resins operate by gravity flow, which eliminates the requirement for centrifugation steps.

The bacterial pellet was fully resuspended with 10 ml Resuspension solution containing RNAse. Next, Lysis solution was added to break up bacterial cell walls and allow plasmid extraction; the contents were mixed and incubated for 2-3 minutes at room temperature. The lysed cells were neutralised with the addition of 10 ml Neutralisation solution and poured into QIAfilter cartridge provided in the kit and incubated for 10 minutes at room temperature. Meanwhile, a DNA binding column (Qiagen Tip) was prepared by the addition of 10 ml QBT equilibration buffer and allowed to pass through gravity flow. Following the 10-minute incubation step, the clear bacterial lysate separated through neutralisation was transferred into the Qiagen Tip and allowed to empty. The column was then washed twice with 30 ml QC buffer to remove impurities from the column. The DNA was eluted from the column by the addition of 15 ml QF buffer and precipitated with the addition of 10.5 ml isopropanol followed by a 60-minute centrifugation at 3900 rpm. The pellet resulting from the centrifugation was resuspended in 300 μl Tris-EDTA buffer (10mM Tris-HCl, 1mM disodium EDTA, pH 8.0), which provides slightly alkaline

64

pH conditions along with the presence of cation chelator EDTA to inactivate nucleases and thus, prevent DNA from degradation. This was followed by further DNA precipitation with the addition of 0.1 volume (30 µl) 3M NaOAC (pH 5.2) and 2 volumes (660 µl) 100% ethanol, and 10-minute centrifugation at 14000 rpm. The pellet was washed with the addition of 200 µl 70% ethanol and the sample was centrifuged for another 5 minutes at 14000 rpm. The supernatant was discarded the pellet was left to air dry sufficiently before its resuspension with 300 µl TE buffer. DNA concentration and purity were defined using a UV spectrophotometer (Eppendorf Biophotometer; Eppendorf UK). This technique is based on the intrinsic property of DNA to absorb light with a characteristic peak of 260 nm. The DNA concentration was calculated through the conversion of absorbance such as at 260 nm the absorbance of 50 ng. mL-1 DNA will equal 1 AU. Protein peak absorption was measured at 280 nm and the ratio 260/280 nm was used to determine DNA purity with a desired ratio of 1.8 (1.7-1.9). The concentration of the DNA was then adjusted to 1 µg. ml^{-1} (if higher than that) by diluting the sample in TE buffer.

Maxi-prepped DNA was fully sequenced using T7 promoter and BGH reverse primers before transfecting it into cells.

2.3 Cell Culture
2.3.1 Cell passaging

The cell line used for all cell-based assays, as well as for the preparation of membranes was human embryonic kidney (HEK293T). Cells were grown in Media (Dulbecco's Modified Eagle's Medium with high glucose, L-glutamine, sodium pyruvate and 10 % foetal calf serum added (FCS)), in flasks with surface area of 25 cm^2, 75 cm^2, or 175 cm^2 and kept at 37°C under the conditions of 95% air/5% CO_2. Cells were passaged at 70-80% confluency with split ratios varying from 1:2 to 1:20 depending on the day required for experiments or next passage (1 − 6 days). The media was removed, and cells were washed with 5 ml sterile phosphate buffered saline (PBS). 1-3 ml of trypsin-EDTA solution was added and cells were incubated for 5 minutes at 37° which allowed for their detachment from the plastic. The flask surface was washed

with 10 ml of media, transferred to a 30 ml universal container and centrifuged for 5 minutes at 1000 rpm. The supernatant was discarded, and the cell pellet resuspended in 10 ml of media and this solution was used to either count and plate the cells or passage them.

2.3.2 Seeding cells

Cells were seeded 24-hours prior to conducting the assay they were used for. Following the final step described in the previous section, a sample of the resuspended cell pellet was loaded into a haemocytometer 5x5 1 mm^2 grid and the number of cells was counted. The cell count in the sample volume (0.1 µl) was multiplied by 10^4 to derive the number of cells per ml. The volume of cell solution required for the desired cell density was calculated using the equation below:

Equation 2.2:

$$Volume\ cell\ suspension\ required\ (ml) = \frac{Number\ of\ cells\ required\ /m\ l\ \times Volume\ (ml)\ required}{Number\ of\ cell\ counted/ml}$$

The calculated cell suspension was then diluted with media to the required volume to give the correct concentration of cells required for the relevant experiment. 100 µl of cell suspension was added per well in a 96-well plate, pre-coated with poly-D-lysine (10 µg/ml in PBS, filter sterilised; Sigma P6407) for 30 minutes at room temperature prior to seeding.

2.3.3 Cell freezing and defrosting

Cell were grown to 90-100% confluency prior to freezing. To freeze down cells grown in T75 flasks, cells were removed for the flasks and centrifuged as described in section 2.3.1. The supernatant was discarded, and the cell pellet was resuspended in 2 ml freezing media (FCS containing 10% (v/v) DMSO). The resuspended cells were aliquoted in cryovials (1 ml/cryovial) and transferred to a freezing container (Nalgene® Mr. Frosty) containing isopropanol and placed in a -80 freezer for 24 hours allowing for the slow cooling down of cells to

ensure their preservation. Cells were then transferred to liquid nitrogen storage.

Cell were defrosted by adding the cryovial suspension, once defrosted at room temperature, to 10 ml media and centrifugation for 5 minutes at 1000 rpm. The supernatant was discarded, and the cell pellet was resuspended with 10 ml of media and placed in a flask. The media was replaced 24 h later, adding the relevant antibiotic as required.

2.3.4 Generation of cell lines

Transfection is the process of introducing genetic material (DNA or RNA) into a host eukaryotic cell which could be either transiently, when the transfected material is not introduced into the cell genome, or stably when the DNA/RNA introduced in integrated in the host cell's genome and passed the daughter cell upon division. For stable transfection, it is essential that the introduced genetic material has a resistance gene allowing selection of the transfected cells with the appropriate antibiotic.

2.3.4.1 Transfection of HEK293T cells

HEK293T cells were stably transfected with the DNA construct of interest using lipofectamine 3000 (Invitrogen, Paisley, UK). Lipofectamine is a cationic lipid reagent designed to form liposomes which interact with the negatively charged phosphate backbone of nucleic acids. The liposome-DNA complexes fuse with cells' plasma membranes and are integrated into the cells through endocytosis. Once inside the cells the complex is suggested to escape the endocytic machinery and enter the nucleus. Successful lipofectamine transfection requires the use of serum-reduced media such as OptiMEM (Invitrogen) because the serum interferes with the liposome-DNA complex formation. Lipofectamine 3000 is an improved version of lipofectamine for higher transfection efficiency and reduce cell toxicity. The stable transfection of HEK293T with DNA constructs of interest was performed under sterile conditions following lipofectamine 3000 manufacturer's instructions. The media of cells grown to 70% confluency in T25 flasks was removed and replaced with 1.2 ml OptiMEM. Two transfection mixes were prepared

separately (i) 5 μg DNA, 250 μl OptiMEM, and 10 μl p3000 reagent and (ii) 7.5 μl lipofectamine 3000 in 250 μl OptiMEM. The mixes were then combined by gentle pipetting and incubated for 5 minutes at room temperature to allow the formation of lipofectamine/DNA complexes. After the end of the incubation, 700 μl of OptiMEM was added to the lipofectamine/DNA reaction and the whole mixture was added to the previously prepared flask. The transfected cells were incubated overnight and then split at 1:5 – 1:10 ratio on the following day. The relevant selection antibiotic treatment was introduced on day 3 after the transfection, and selection was carried out for 14 days (G418 0.8 mg.ml^{-1}; zeocin 200 μg.ml^{-1}) to obtain the stable mixed population cell lines used in this study.

Stable transfected cells were treated with geneticin G418 (0.2 mg.ml^{-1}) or/and zeocin (50 μg.ml^{-1}) as part of their normal maintenance to maintain selection pressure.

For transient transfections, cells were seeded in poly-D-lysine 6-well plates (see cell seeding section) at density of 500 000 cells / well and grown to a confluency of 80%. DMEM was aspirated from the wells and after an OptiMEM wash, 1.5 ml of OptiMEM was added per well. 2.5 μg of DNA was mixed with 125 μl of OptiMEM and 5 μl p3000 reagent and separately, 3.75 μl lipofectamine 3000 was mixed with 125 μl OptiMEM. The DNA and lipofectamine preparations were mixed and incubated for 6 minutes at room temperature. After the end of the incubation, the DNA/lipofectamine reaction was added to the well plate (250 μl per well) and incubated for 24 hours in a 37°C incubator. After 24 hours the cells were plated into 96-well plates for the appropriate experiment following standard cell splitting/seeding procedures.

2.4 Membrane preparations and labelling
2.4.1 Membrane preparations

Cells were grown in T175 flasks to 90-100% confluency. Media was aspirated and cells were washed with 50 ml PBS, followed by a 5-minute incubation with trypsin-EDTA at 37°C. The cells were further detached from the flask through a 10 ml media wash and centrifuged for 10 minutes at 2000 rpm. The

supernatant was discarded, and the pellet was used to prepare membranes. The pellets were resuspended in 20 ml pre-chilled membrane preparation buffer (10 mM HEPES, 10 mM EDTA, pH7.4), homogenised using a polytron tissue homogeniser (Ultra-Turrax) in 8x 2-second bursts and centrifuged at 48 000xg at 4°C (Beckman Avanti J-251 Ultracentrifuge; Beckman Coulter, Fullerton, CA) for 30 minutes. The supernatant was removed, and the pellets resuspended in 20 ml of the same buffer followed by another centrifugation under the same conditions. After the second centrifugation step, the pellets were resuspended in membrane storage buffer (10 mM HEPES, 0.1 mM EDTA, pH7.4). The cell pellets were kept on ice throughout the whole membrane preparation in order to preserve protein integrity.

The protein concentration of the membrane preparation was determined by a Pierce^{TM} BCA (Bicinchoninic acid) assay (Pierce, Thermofisher Scientific). The assay is based on the reduction of Cu^{2+} to Cu^{+} by proteins in an alkaline medium with the colorimetric detection of Cu^{2+} by bicinchoninic acid (BCA). The complex formed between BCA and copper ions exhibits a strong linear absorbance at 562 nm in a protein concentration-dependent manner. A standard curve for the assay was generated by serial dilution of known concentrations of purified bovine serum albumin (BSA). The BSA standards were added to a white clear-bottom 96-well plate, along with the unknown samples from the membrane preparation diluted 1:10. The BCA working reagent was prepared by mixing 50 parts of bicinchoninic acid and 1 part 4% $CuSO_4$ solution until the mixture changes colour to light green. 200 µl per well was then added to each to the well containing the range of BSA concentrations or the membrane preparation samples. The reaction was incubated for 30 minutes at room temperature and absorbance was measured at 562 nm using a CLARIOstar (BMG Labtech, Offenburg, Germany). The absorbance values for the BSA absorbance were plotted to produce a standard curve used to extract the concentrations of the samples of interest. The membrane preparation solution was then aliquoted and stored at -80°C.

2.4.2 Terbium labelling of SNAP-tagged receptors

For Time-resolved fluorescence resonance energy transfer (TR FRET) based experiments (see 2.7.2) the SNAP-tagged receptors required labelling with Terbium (Tb^{3+}) cryptate.

HEK293T cells stably expressing SNAP-tagged CXCR2 receptors were grown in Poly-D-lysine coated T175 cm² flasks to 80-90% confluence. Cell culture medium was aspirated and after 2x PBS washes, cells were incubated with 10 ml/flask SNAP-Lumi4-Tb (Cisbio, Codolet, France; 100 nM final in LabMed media provided with kit) at 37°C for 60 minutes. Terbium was removed followed by another PBS wash. Cells were then detached from the plastic using a cell scraper (Thermo Fisher Scientific, Waltham, MA, USA) and 5-10 ml of PBS. The cell suspension was then centrifuged for 10 minutes at 2000 rpm and the supernatant discarded. Cell pellets were either immediately used to start a membrane preparation or frozen at -20°C.

Terbium labelling was also performed prior to whole cells experiments, using cells previously seeded onto white opaque 96-well plates. Cell media was aspirated and 2x PBS washes were performed. Cells were then treated with 50 µl/well SNAP-Lumi4-Tb (100 nM) in Tag-lite labelling medium (LABMED, Cisbio, Codolet, France) and incubated at 37° for 60 minutes. The terbium was aspirated and after a PBS wash, cells were immediately used for experiments.

2.5 Functional assays
2.5.1 Split luciferase complementation to detect CXCR2-effector interactions
2.5.1.1 Measuring the effect of negative allosteric modulators (NAMs) on CXCR2 activation

Receptor activation was measured as a function of its interaction with intracellular effectors using split luciferase complementation-based technology. The technology is based on tagging interacting proteins with fragments of the nanoluciferase enzyme (SmBiT, LgBiT; Dixon *et al.,* 2016). The complemented luciferase formed by fragment interaction oxidises its substrate (furimazine) to produce luminescence in the assay (see chapter 3). The luminescence produced can then be quantified and corresponds to the

extent of enzyme complementation resulting from activated receptor interaction with the tagged partner proteins. The luminescence was recorded repeatedly before and after the addition of an agonist to determine basal as well as agonist-stimulated complementation, for example to assess basal receptor activity and the presence of inverse agonism.

HEK293T cell lines stably co-transfected with the SNAP-CXCR2 receptor C terminally tagged with the LgBiT, and β-arrestin2 or mini Go N-terminally tagged with the SmBit fragment, were used for the split luciferase complementation assays. Cells were seeded into poly-D-lysine coated white 96-well while clear-bottom plates (Greiner Bio-One, Stonehouse, UK) at 30,000 cells/well density and incubated for 24 hours in a 37°C incubator at 5% CO_2. The following day, the media was aspirated, and cells were washed with 50 µl/well HEPES buffered salt solution HEPES Balanced Salt Solution (HepesBSS; 10mM HEPES, 2mM sodium pyruvate, 146mM NaCl, 5mM KCl, 1mM $MgSO_4$, 1.7mM $CaCl_2$, 1.5mM $NaHCO_3$, 5mM D-glucose; pH 7.45 with NaOH) containing 0.1% BSA. For agonist-mode assays, 40 µl/well buffer and 10 µl/well furimazine substrate (diluted to 1:1320 dilution from manufacturer's stock in assay buffer; Promega, Madison, US) were added and 3 cycles of basal luminescence were recorded at 2 min intervals using a PHERAstar plate reader (BMG, Offenburg, Germany), before adding a range of agonist concentrations. The agonist used was typically human CXCL8 (amino acids 28 – 99; SinoBio/Stratech Scientific (China/Cambridge, UK), The plate was then read for 16 more cycles at 2 min intervals, beginning 1 min after agonist addition.

Antagonist-mode assays (negative allosteric modulators (NAMs) in this work) were conducted in two alternative ways – by pre-treating cells with the NAM, followed by the agonist, or pre-treating cells with the agonist. In the first assay format, cells were pre-treated with the appropriate concentration of NAM in HBSS (40 µl/well) and incubated for 60 minutes prior to furimazine treatment (10 ml, concentration as above), and luminescence was measured before and after the addition of a range of concentrations of $CXCL8_{28-99}$ as described above.

In the second assay set-up, the effect of NAMs on pre-formed receptor-effector complexes was tested by pre-treating cells with 40 µl/well a fixed concentration of an agonist (60 minutes), then adding 10 µl/well vehicle or a range of NAM concentrations. The cells were incubated with the NAMs for 1,2, or 3 hours. Furimazine (10 µl/well) was then added (1:1320 from manufacturer's stock, 10 ml) and incubated for 5 min, after end point luminescence readings were taken using the PHERAstar. These assays were conducted in serum-reduced media (OptiMEM) with 0.1% BSA (with incubations in a 5 % CO_2 incubator) to sustain cell viability during the long incubations.

2.5.1.2 Wash-out assays to assess reversibility of NAM effects

HEK293T cells stably co-transfected with the SNAP-CXCR2-LgBiT receptor and SmBiT-β-arrestin2 were plated in 96-well while clear-bottom plates as described in 2.5.1.1 and incubated for 24 hours in a 37°C incubator at 5% CO2. The following day, the media was aspirated, and cells were washed with 50 µl/well HBSS-based buffer containing 0.1% BSA. Cells were pre-treated with the appropriate concentration of NAMs (40 µl/well in HBSS) and incubated for 60 minutes. Following the NAM pre-treatment, 2x HBSS/0.1%BSA washes were performed followed by a 15-minute incubation with HBSS/0.1%BSA (50 µl/well). The wash buffer was replaced with 40 µl/well HBSS/0.1%BSA/furimazine (1:1320 dilution) and luminescence was recorded (PHERAstar) for 3 cycles at 2 min intervals before the addition of a range of $CXCL8_{28-99}$ concentrations followed by reading 16 more cycles at 2 min intervals.

2.5.1.3 Estimating the presence of 'receptor reserve' using HiBiT peptide

The Split Luciferase complementation assay was also used to determine whether the concentration of CXCR2 receptors exceeded the SmBiT- effectors in the co-transfected cell lines. This would lead to potential 'receptor reserve' in the system, that is when a maximal effector complementation could occur without full occupancy of the CXCR2 receptor population. Cells stably

72

transfected with SNAP-CXCR2-LgBiT, and either SmBit- β-arrestin2 or SmBiT-mini Go, were plated into poly-D-lysine coated white Greiner 96-well plates at 30,000 cells/well density and incubated for 24 hours in a 37°C incubator. The following day, the media was aspirated, and cells were washed with 50 μl/well HBSS-based buffer containing 0.1% BSA. Cells were treated with 30 μl/well HBSS-based buffer only or HBSS-based buffer containing 100 μg/ml saponin or 50 μg/ml digitonin detergent for 15 minutes followed by the addition of 100 nM CXCL8$_{28-99}$ agonist (10 μl/well) or vehicle and 10 μl/well furimazine substrate (1:320 dilution) for 4-5 minutes. Two cycles of luminescence were recorded at 2 min intervals using a PHERAstar plate reader (BMG, Offenburg, Germany) prior to the addition of 10 μM purified HiBiT peptide (10 μl/well; peptide sequence VSGWRLFKKIS) or vehicle and the measurement of luminescence for 20-30 minutes. The HiBiT peptide has a very high affinity for the LgBiT fragment (Dixon et al., 2016), producing additional complementation in permeabilised cells with SNAP-CXCR2-LgBiT receptors that have not recruited effector proteins. The luminescent measurement immediately after chemokine/furimazine incubation and the one 10 minutes post HiBiT peptide addition were analysed in the results shown. The assay was conducted in triplicate.

2.6 Imaging cell surface expression of SNAP-tagged receptors

Fusing the CXCR2 receptor to a SNAP tag allows for visualising receptor expression and tracking its intracellular trafficking. The SNAP tag (20 kDa) is a mutant of the DNA repair protein O6-alkylguanine-DNA alkyltransferase which covalently reacts with benzyl guanine derivatives. To visualise the SNAP-tagged receptors (N-terminally) expressed on the surface of newly transfected cells, the SNAP tag was labelled with cell-impermeable fluorescently labelled benzyl guanine. The substrate of choice was SNAP-Surface® Alexa Fluor® 488 (496nm excitation – 520 nm emission) (New England Biolabs, Ipswich, USA) which is an impermeable reagent labelling receptor only at the plasma membrane. Basal and agonist-stimulated endocytosis of labelled receptors can be followed during subsequent incubations and imaging.

Stably transfected HEK293T cells were seeded at 30 000 cells/well density on poly-D-lysine coated black-bottomed 96-well plates (Greiner 655090) 24 hours prior to imaging them. On the following day cell media was aspirated and replaced with 0.2 µM SNAPsurface BG-AF488 in complete DMEM (60 µl/well) and cells were incubated for 30 minutes at 37°C, 5% CO_2. Next, cells were fixed in 3 % paraformaldehyde (PFA) in PBS for 15 minutes at room temperature followed by 2 x PBS washes and the labelling of cellular nuclei with 2 µg/ml Hoechst 33342 (100 µl/well) (Abcam, Cambridge, UK) in PBS for 15 minutes at room temperature. The PBS/Hoechst solution was replaced with 100 µl/well PBS and either stored at 4 °C or imaged straight away using an IX Ultra confocal plate reader and a Zeiss 40x ELWD air objective (Molecular Devices, San Diego, USA) using two emission filter sets: DAPI with 405 nm laser excitation (H33342; cell nuclei), FITC with 488 nm laser excitation (SNAP-Surface AF488 labelled SNAP-tagged receptor).

2.7 CXCL8-AF647 fluorescent ligand binding assays

Cells stably expressing SNAP-CXCR2-His constructs were used to characterise the binding of the fluorescent chemokine probe CXCL8-AF647 (labelled at C terminal lysine; Almac, NI,UK) and its modulation by unlabelled CXCL8 or a range of CXCR2 NAMs, using both imaging approaches in whole cells, and TR-FRET binding studies in either whole cells or membrane preparations.

2.7.1 Fluorescent chemokine binding measured using high-content imaging approaches in whole cells

The affinity and specificity of binding of CXCL8-AF647 to SNAP-CXCR2-His expressing cells was assessed using saturation binding assays. Stably transfected cells were seeded at 30 000 cells/well density on poly-D-lysine coated Greiner black-bottomed 96-well plates 24 hours prior to the assay. The receptor SNAP-tag was labelled with SNAPsurface BG-AF488 substrate using the protocol previously described (section 2.6.x). After labelling, cells were treated with 160 µl/well HBSS-based buffer containing 0.1% BSA and Hoechst nuclear stain (2 µg/ml) and incubated for 10 minutes at room temperature.

Following the incubation, 20 µl/well of unlabelled ligand or vehicle was added to the appropriate wells (to the final concentrations indicated in the results) and cells were incubated for 5 minutes at room temperature. Fluorescent CXCL8-AF488 tracer or vehicle (20 µl/well) were added to each well and its cellular labelling was recorded every 10 minutes for 60 minutes in total using an IX Ultra confocal plate reader (Molecular Devices) and the following three filter sets: DAPI using 405 nm laser excitation (H33342; cell nuclei) , FITC using 488 nm laser excitation (SNAP-Surface BG-AF488 labelled SNAP-tagged receptors), CY5 using 635 nm laser excitation (CXCL8-AF647, fluorescent chemokine).

2.7.2 CXCL8-AF647 binding measured using TR-FRET assays

Förster resonance energy transfer (FRET) is a technology based on the non-radiative energy transfer between a fluorescent donor and an acceptor of fluorescence, discussed in more detail in chapter 4. TR FRET was used to study the binding of CXCL8-AF647 in whole cells and membrane preparations and its modulation by a range of structurally distinct NAMs as well as unlabelled CXCL8 and GTP analogues. The TR FRET assays conducted in in this work used terbium cryptate (Tb^{3+} cryptate) as a donor molecule which interacts with the SNAP tag in a covalent manner. The energy transfer between the Tb^{3+} donor and the fluorescent probe was used as a measure of fluorescent ligand binding to the receptors.

2.7.2.1 Association binding kinetics of AF647CXCL8 in whole cells

Cells stably expressing SNAP-CXCR2-His receptors were seeded at 30 000 cells/well density on opaque 96-well plates 24 hours prior to conducting the assay. Receptor SNAP tags were labelled with Tb^{3+} cryptate as described earlier (section 2.4.2).

Immediately following the labelling procedure, the media was replaced with 30 µl/well LABMED (Cisbio, Codolet, France) and cells were treated with vehicle or 1 µM unlabelled $CXCL8_{28-99}$ (10 µl/well) for 10 minutes at room temperature to

set up total or non-specific binding (NSB) conditions for the fluorescent CXCL8-AF647 tracer. 10 µl CXCL8-AF647 was then added in the appropriate wells to give a range of final assay concentrations indicated in the results. TR-FRET measurements were made repeatedly on a PHERAstar plate reader at room temperature (337 nm excitation, 620 nm (donor) and 665 nm (acceptor) emission), using a read frequency of 6 s / min and a typical total read time of 40-60 min.

2.7.2.2 Equilibrium TR-FRET competition binding in whole cells

Cells stably expressing SNAP-CXCR2-His receptors were seeded at 30 000 cells/well density on opaque 96-well plates 24 hours prior to assay execution. Receptor SNAP tags were labelled with Tb^{3+} cryptate as described earlier (section 2.4.2).

Following the labelling procedure, 30 µl/well HBSS/0.1% BSA was added to each well and 10 µl/well of range of final concentrations of SB265610, R-navarixin, S-navarixin, AZD5069, AZ10397767, unlabelled $CXCL8_{28-99}$, GppNHp (Sigma Aldrich) or vehicle were added to the appropriate wells. Cells were incubated with the unlabelled compounds for 30 minutes at 37°C, 0% CO_2 followed by the addition of a fixed concentration (30 nM) CXCL8-AF647 tracer or buffer. Following tracer treatment cells were incubated at 37°C, 0% CO_2 for 150 minutes, during which end-point TR FRET measurements were collected on the PHERAstaras described above (from $30 - 150$ min). Non-specific binding in these experiments was defined by 1 µM cold $CXCL8_{28-99}$.

2.7.2.3 Fluorescent ligand TR-FRET binding in membrane preparations

TR FRET assays in membrane preparations were executed in a 384-well plate format. All assays were performed by thawing frozen terbium-labelled SNAP-CXCR2-His membrane stocks on ice and diluting them to the desired working concentrations (final assay concentration 3 µg/well). All binding experiments in membranes were carried out at room temperature (20-25 °C), in HBSS / 0.1 % BSA or low sodium (25 mM HEPES, 1 mM $MgCl_2$) / 0.1% BSA assay buffers (final

volume 30 µl) both containing 0.02% pluronic acid and 0.1 mg. mL^{-1} saponin as indicated in the relevant figures in the results.

2.7.2.3.1 Association binding kinetics of CXCL8-AF647

Membranes (3 µg/well, 10 µl/well) were pre-incubated with vehicle or 1 µM CXCL8$_{28-99}$ (10 µl/well) for 10 minutes at room temperature to define total or NSB binding. A range of fluorescent tracer concentrations or vehicle were then added to the appropriate wells (10 µl), and TR-FRET measurements on the PHERAstar were made using the settings described previously (read frequency of 6s/min and a typical total read time of 40-60 min).

2.7.2.3.2 Dissociation binding kinetics of CXCL8-AF647

All dissociation binding kinetics experiments were performed in the Na+ reduced buffer described in 2.7.2.3.

Membranes (3 µg/well, 10 µl/well) were pre-incubated with 1 µM unlabelled CXCL8$_{28-99}$ or vehicle (10 µl/well) for 10 minutes at room temperature to define NSB and total binding respectively. A single CXCL8-AF647 concentration (final 10 nM, 10 µl/well) was added to the appropriate wells and its association was recorded using TR-FRET measurements until the binding plateaued. The read was then paused, and fixed concentration of unlabelled compounds (10 µl/well) was added to the membrane/tracer mix to initiate dissociation. TR-FRET measurements were made on the PHERAstar for a further 30 – 60 min, using a typical read frequency of 6 s.

Alternatively, the membranes were pre-treated with unlabelled compounds at the concentrations indicated in the results for 40 minutes keeping them at 25°C on a shaking incubator at 225 rpm. 10 ml buffer (totals) or 1 mM CXCL8$_{28-99}$ (to define NSB) were then added to the appropriate wells and 10 ml membranes were incubated with them for 10 minutes at 25°C. A fixed concentration of fluorescent tracer (10 nM CXCL8-AF647, 10 µl) was added to the membranes and TR-FRET measurements were recorded until reaching equilibrium. The read was paused, and a fixed concentration of unlabelled 1

μM CXCL8$_{28-99}$ was added followed by a continuation of the PHERAstar TR-FRET readings for another 30-60 minutes, with a read frequency of 3-6 sec.

2.7.2.3.3 Equilibrium competition binding in membranes using the CXCL8-AF647 TR-FRET assay

Membranes (3 μg/well, 10 μl/well) were pre-incubated with a range of concentrations of unlabelled NAMs, GppNHp or CXCL8$_{28-99}$ for 30 minutes at room temperature. Next, a fixed concentration of a tracer (10 nM or 25 nM CXCL8-AF647, in low sodium and high sodium buffers respectively) was added. The binding of the tracer was recorded using PHERAstar TR-FRET measurements in an end-point manner for 1-5 hours incubation. 1 μM unlabelled CXCL8$_{28-99}$ was used to define NSB.

2.8 Signal detection and data analysis

2.8.1 Software

Experimental data were analysed and presented using GraphPad Prism 7.02/8/9 (GraphPad Software, La Jolla). The luminescence and fluorescence data from the PHERAstar were extracted through the integrated MARS software (BMG Labtech, Offenburg, Germany). Data from assays conducted using IX Ultra confocal plate reader were analysed and extracted using MetaExpress 2.0 software (Molecular Devices, San Diego, USA). DNA sequences were analysed using Chromas 2.66 software (Technelysium Pty Ltd, Australia). DNA vector maps were created using SnapGene Viewer 4.2.11 software (GSL Biotech LLC, USA). Molecular structures were drawn using ChemDraw Professional 16.0 (PerkinElmer, USA).

2.8.2 Split luciferase complementation analysis
2.8.2.1 Analysis of CXCL8-stimulated receptor activation
2.8.2.1.1 Nonlinear regression to analyse concentration-response relationships

The split luciferase complementation assays were conducted in duplicate unless otherwise stated. The luminescence was recorded in cycles of as short

as possible duration to cover all selected wells (e.g. for a whole 96-well plate the shortest cycle duration was 120 seconds). Raw luminescence counts in individual experiment replicates were normalised to the response produced by the highest agonist concentration (100 nM CXCL8$_{28-99}$ unless otherwise stated, 100%) and the baseline (vehicle) was set as 0%. The data represented in the kinetic timecourses were normalised to the response produced by the highest agonist concentration at the time point of the peak response (100%) and the baseline (vehicle) values were subtracted from the measurements for each condition, at each time point. Normalised data from individual cycles were plotted as concentration-response curves (Figure 2.3) using a non-linear regression function on GraphPad Prism (log (agonist) vs response, variable slope (4 parameters)'. This model estimates 4 parameters, being the agonist EC$_{50}$ (concentration of agonist to produce 50 % maximum response), minimum (Bottom), maximum (Top) and Hill slope of the curve. The agonist maximum response (R$_{max}$) is obtained as Top – Bottom.

Equation 3:

$$Response = Bottom + \frac{(Top - Bottom)}{(1 + 10^{((LogEC50 - X) \times Hill\ slope)})}$$
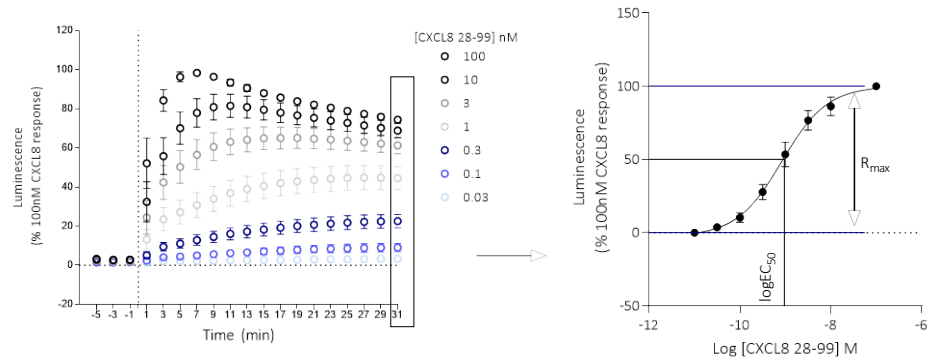
Figure 2.3 Analysis of Split luciferase complementation signal. The kinetic curves of CXCL8$_{28-99}$ at time points of choice were plotted as concentration-response curves. The concentration-response curve of CXCL8$_{28-99}$ on the right-hand side is constructed from the normalised luminescence counts at the last-time point of the kinetics curve; the blue lines and double arrow indicate the R$_{max}$ of the chemokine response (Top – Bottom); the point on the x-axis representing the log EC$_{50}$ of CXCL8$_{28-99}$ is also shown.

2.8.2.1.2 Area under the curve (AUC) analysis

The Split luciferase complementation assays introducing NAM pre-treatment followed by wash steps were alternatively analysed using area under the curve (AUC) analysis. Pooled data from the whole recruitment time course from 5 individual experiments for each NAM was analysed using AUC and numbers plotted against agonist concentration building CXCL8$_{28-99}$ concentration response curves of the whole time-course response. The span and potency of the chemokine were then quantified from the non-linear regression analysis described in 2.8.2.1.1.

2.8.2.2. Hemi-equilibrium operational model for antagonism

The hemi-equilibrium model for antagonism (Riddy et al., 2015; Kenakin, 2006) is based first on the Black and Leff operational model of agonism (Black and Leff, 1983). This empirical model fits concentration response curves to agonist data in terms of the agonist equilibrium dissociation constant (K$_A$, concentration of agonist that occupies 50 % of the receptor population at equilibrium) and an efficacy parameter *tau*, which is dependent both on

80

agonist intrinsic efficacy (ability to activate the receptor) and system factors such as amplification and the total number of receptors (Stott et al, 2016).

For the hemi-equilibrium model, pre-treatment with vehicle or antagonist to equilibrium is assumed. Following addition of agonist, concentration-response curves are then collected at various time points, over which a new equilibrium between agonist and antagonist receptor binding is re-established. The time to this equilibrium depends on the off rate (koff) of the antagonist, which can be extracted from the data along with an estimate of antagonist affinity Kb (Riddy et al., 2015; Kenakin, 2006):

$$Y = \frac{(Emax \times tau \times (10^{(x-logKA)} \times (1-H))}{((10^{(x-logKA)}) \times (I-H) \times tau + 1) + 1)}$$

$$D = \frac{\frac{B}{KB}}{\frac{B}{KB} + 10^{(x-logKA)}} + 1$$

$$F = \frac{\frac{B}{KB}}{(\frac{B}{KB} + 1)}$$

$$G = = \frac{(\frac{B}{KB} + 10^{(x-logKA)} + 1)}{(10^{(x-logKA)} + 1)} +$$

$$H = D \times \left(1 - e^{(-kxGxtime)}\right) + F \times e^{(-kxGxtime)}$$

Where logKA the log of the affinity (equilibrium dissociation constant) of the agonist, Emax - the maximal response of the agonist, and tau – the operational model measure of agonist; A – the agonist concentration, with x = log A; B – the antagonist concentration, KB – the antagonist affinity, k - the antagonist dissociation rate constant koff, and time – the agonist incubation time.

Pooled $CXCL8_{28-99}$ concentration response data at different times in the absence or presence of different NAMs were fitted to this model using a custom equation in Graphpad Prism, using global analysis that shared k_{off}, antagonist K_B, agonist K_A, tau and E_{max} parameters. As discussed in chapter 3, an assumption was made that the binding of NAMs and chemokine was mutually exclusive, and therefore effectively competitive.

2.8.3 Imaging analysis
2.8.3.1 Fluorescent ligand saturation binding

The saturation binding of CXCL8-AF647 was measured in duplicate, and in imaging studies was quantified using a granularity algorithm based on the identification of fluorescent puncta with a set diameter (1-2 µm) above a threshold set with reference to positive and negative controls (Figure 2.4). The analysis also identifies cellular nuclei through H33342 staining, allowing quantification of fluorescent ligand binding measured as integrated intensity per cell. Saturation data using these measurements was then analysed as described in 2.8.4.1.

10 nM AF647CXCL8   Vehicle

Image
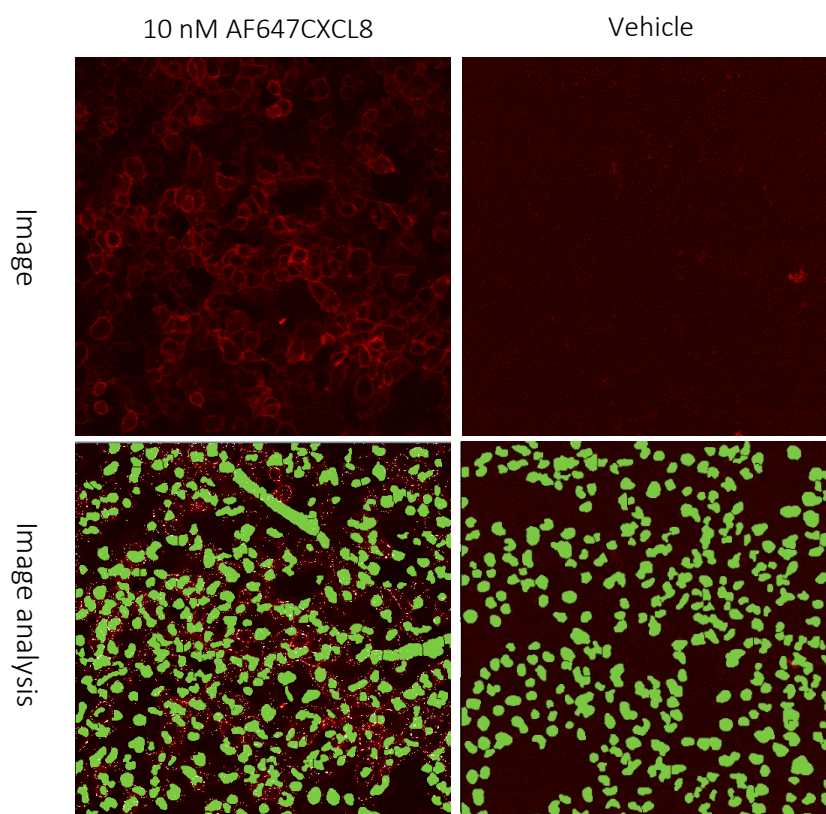
Image analysis

Figure 2.4 Granularity analysis of CXCL8-AF647 binding at CXCR2. The panel above shows images of 10 nM CXCL8-AF647 binding (left) or vehicle (right) detected through the Cy5 channel; in the lower panel there are images showing the detection of fluorescent ligand 1 – 2 μm diameter granules – the white dots in the 10 nM tracer treatment conditions detect fluorescence above the defined threshold, whereas in the vehicle treatment condition, no fluorescence is detected. Green spots indicate the nuclear detection in the images used to normalise granularity measurements to cell count. Analysis was carried out using MetaExpress 2.0 software (Molecular Devices, San Diego, USA).

2.8.4 Fitting of ligand binding data

Most models of ligand-target interactions are built on the mass action equation which in the context of pharmacology, defines the relationship between the free concentration of a drug ([D]) and the amount of drug-receptor complex that is formed ([DR]) where the receptor (R) is the drug target (Waage and Gulberg, 1986), (Kenakin, 2016).

Equation 4: Law of mass action:

$$D + R \leftrightarrow DR$$

The law of mass action states that the rates of drug association and dissociation defined by the forward and reverse rates of the reaction are in proportion to the concentration of the reactants. The point in the reaction where the forward and reverse rates become equal represents dynamic equilibrium. Under these conditions, the affinity of ligands (agonist, antagonist, inverse agonist) at GPCRs can be quantitatively assessed through the equilibrium dissociation constant (K_d). Kd is a widely used pharmacological parameter describing the free concentration of a drug that allows it to occupy 50% of its target receptors at equilibrium. The K_d of fluorescent ligands is often extracted from saturation ligand binding experiments at equilibrium where an increasing labelled ligand concentration is added, and its binding is recorded in an end-point manner. In this case scenario, K_d represents the ligand concentration producing half-maximum binding at the target when corrected for non-specific binding (NSB) effects. K_d can also be represented as the ratio (Equation 5) of the individual association rate constant (kon) and dissociation rate constant (koff) for a ligand. The koff (min^{-1}) is a unimolecular constant describing the dissociation of the ligand from the binding pocket independently of free-ligand concentration, and can be viewed as the proportion of ligand that dissociates from the receptor in unit time. The kon (M^{-1} min^{-1}), on the other hand, is bimolecular constant that describes the rate of formation of a complex between two molecules ligand and receptor. For a single site interaction between ligand and receptor, the observed association rate of the ligand to the target protein (kobs) is linearly related to the concentration of the labelled ligand, with the slope defining the association rate constant and the Y intercept, the dissociation rate constant (Equation 6).

Equation 5:

$$Kd = \frac{koff}{kon}$$

Equation 6:

$$Kobs = [Labelled\ drug]kon + koff$$

2.8.4.1 Saturation binding

Total and non-specific binding (NSB) of the fluorescent probe were plotted as integrated fluorescent intensity / cell (imaging experiments). Binding data were then normalised to the highest tracer concentration (100%). Total and non-specific binding data were globally fitted to a model showing the total and non-specific binding (equation 4, 5 respectively) to obtain the best-fit value for CXCL8-AF647 binding affinity (Kd) represented as pKd in results chapters (-logKd), as well as an estimate of total binding density B_{max} (Figure 2.5).

Equation 5:

$$Total\ binding = \frac{Bmax \times [Labelled\ drug]}{[Labelled\ drug]} + NS$$

Equation 6:

$$NS = Backrgound + m\,[Labelled\ drug]$$
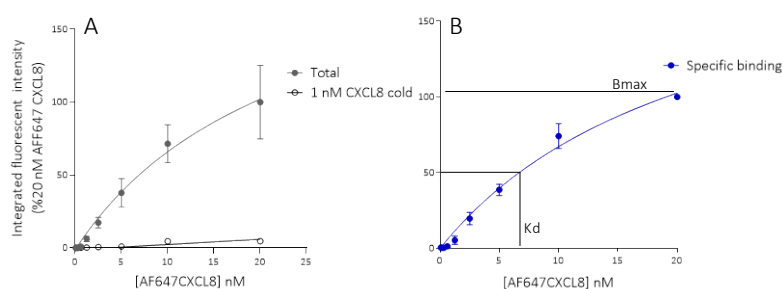
Figure 2.5 Analysis of saturation fluorescent ligand binding. The normalised integrated fluorescent intensity was plotted against CXCL8-AF647 concentration and analysed using a model considering both the total and non-specific binding (A), and one-site binding model of only the specific binding (B) The affinity (Kd) of the tracer and maximal binding (Bmax) could be extracted from B.

2.8.4.2. Ligand binding measured using TR-FRET

2.8.4.2.1 TR-FRET signal detection

The Tb^{3+} donor was always excited by a laser source at 6 flashes of 337 nm wavelength. A kinetic TR-FRET signal was collected at intervals which duration was determined by the number of wells read. The emission of the donor terbium was detected at 620 nm and the emission of the acceptor at 665 nm using HTRF PHERAstar settings. The ratio of acceptor and donor emission (665 nm/620 nm) was obtained for each data point and multiplied by 10, 000.

2.8.4.2.2. Association kinetics binding of CXCL8-AF647

Fluorescent ligand binding measured by TR-FRET was conducted in singlets in either a 96-well plate format (whole-cell assays) or 384-well plate format (membrane-preparation assays). The specific binding of CXCL8-AF647 was extracted from the raw TR FRET ratios by subtracting the NSB from the total measurements at each time point. The specific binding data for association kinetics at each fluorescent ligand concentration were then first globally fitted to a single-site model of association kinetics to obtain the association (kon) and dissociation (koff) rates and kinetically derived affinity (Kd, as koff / kon) of the fluorescent tracer. This analysis is based on the description of one site

86

association kinetics to determine kobs in equation 8, and the relationship between kobs, kon, koff and fluorescent ligand concentration described in equation 6.

Equation 8:

$$Specific\ binding = Plateau \times (1 - e^{kobs \times time})$$

As described in chapter 4, the association of CXCL8-AF647 was analysed with an alternative fit that considers more complex drug-receptor interactions composed of more than a single phase. This fit was used to extract fast and slow observed association rates (k_{fast}, k_{slow}), in component proportions defined by spanfast and spanslow (Equation 9).

Equation 9:

$$Specific\ bindin$$
$$= Basal + spanfast \times (1 - e^{(-kfast \times [time])}) + spanslow \times (1 - e^{(-kslow \times [time])})$$

2.8.4.2.3. Dissociation kinetics of CXCL8-AF647

The experiments measuring the dissociation kinetics of AF647 CXCL8 were conducted in singlets. The binding of the tracer was corrected for non-specific binding and expressed as a percentage of the binding of the tracer prior to the addition of unlabelled competitor for each condition (100%) and the maximum binding inhibition was set as a 0%. The data were then fitted to a model of two-phase decay to extract the fast and slow dissociation ligand rates (kfast, kslow), as well the fast fraction of tracer in each condition.

Equation 10:

$$Bound = Plateau + SpanFast \times (e^{-kFast \times t}) + SpanSlow \times (e^{-kSlow \times t})$$

The percentage of the fast dissociation component was then calculated as (SpanFast / (SpanFast+SpanSlow) x 100).

2.8.4.2.4. Equilibrium competition binding

The competition binding assays were conducted in a 384-well plate format, in duplicate. The specific binding counts from individual experiments were normalised to the highest cold $CXCL8_{28-99}$ concentration (NSB, 0%) and vehicle (totals 100%), and were fitted to a non-linear regression model assuming one-site binding to extract half-maximum inhibitory concentration of the unlabelled ligand (IC_{50}, Equation 11).

Equation 11:

$$Bound = \frac{(Top - Bottom)}{(1 + 10^{(log[Unlabelled\ ligand] - LogIC50)}) + Bottom}$$

Where competitive binding could be assumed (unlabelled $CXCL8_{28-99}$), the unlabelled ligand dissociation constant K_i was estimated from the IC_{50} estimates using the Cheng-Prusoff correction (Equation 12).

Equation 12:

$$Ki = IC50/(1 + [CXCL8AF647]/Kd(CXCL8AF647)$$

2.8.5 Statistical analysis

Where appropriate, parameter estimates from individual experiments were pooled as mean +/- s.e.m. Concentration measurements (e.g. EC_{50}, Kd) were pooled as log or -log (e.g. pEC_{50}) transforms. All statistical tests were performed using GraphPad Prism 7.02-8,9. Statistical significance was defined as $p < 0.05$ and expressed as * ($P \leq 0.05$), ** ($p \leq 0.01$) and *** ($p \leq 0.001$). Parametric one-way ANOVA tests were performed to compare pEC_{50}, R_{max} (NanoBiT assays), pKi (competition binding) or kinetic parameters such as ligand fast fraction (kinetics experiments), between more than 2 group

conditions, followed by Dunnett's multiple comparisons test. Student t-tests were used when comparing only two sets of data.

Chapter 3. Studying the Effects of Intracellular Negative Allosteric Modulators on CXCR2 Activation using the Split Luciferase Complementation Technology

3. Chapter three: Studying the Effects of Intracellular Negative Allosteric Modulators on CXCR2 Activation using Split Luciferase Complementation Technology

3.1 Introduction

GPCRs are activated by a vast range of extracellular ligands and canonically signal through the recruitment and activation of heterotrimeric G proteins (see chapter 1). This allows for the initiation of intracellular signalling cascades resulting in the appropriate physiological outcome. Signalling rapid turnoff is facilitated through receptor interaction with other effector proteins such as G protein kinases (GRKs) and arrestin proteins (see chapter 1). This chapter will discuss the molecular mechanism of GPCR-G protein and arrestin interactions and ways to measure these signalling events in vitro. This will then be discussed in the context of CXCR2-effector interactions and their modulation by intracellular negative allosteric modulators (NAMs).

3.1.2 GPCR-G protein interactions

Upon agonist stimulation, GPCRs canonically interact with and activate G protein effector proteins. While there are more than 350 genes encoding non-odorant human GPCRs, there are only 16 genes encoding the G protein $G\alpha$ subunits divided into 4 major families ($G\alpha_s$, $G\alpha_{i/o}$, $G\alpha_q$, $G\alpha_{12/13}$) (Takeda et al., 2002). The activation of GPCRs allowing G protein coupling is fairly conserved in terms of the structural rearrangements taking place in the GPCR and G protein interaction surfaces (see section 1.2).

The first structural data for the GPCR-G protein interaction interface came from the X-ray structure of the β2AR-$G\alpha$s complex complemented by

91

hydrogen-deuterium exchange mass spectrometry approach in parallel (Rasmussen, *et al.*, 2011), (Chung et al., 2011).The active β2AR structure is characterised by a large outward movement of TM6 and small outward movement and extension of TM5, and the formation of an α helix by ICL2 allowing for the opening of a crevice to accommodate G protein effectors. Early biochemical studies have elucidated that the C terminal helical domain of the G protein forms the GPCR interaction surface (Conklin et al., 1996), (Hamm et al., 1988), (Semack et al., 2016). The β2AR-Gαs structure complemented prior knowledge by showing that the $G\alpha_s$ inserts itself into the crevice formed within the receptor cytosolic surface with its α5-helix and forms further contacts with the receptor with the αN–β1 junction, the top of the β3-strand, and the α4-helix of the Gαs Ras-like domain (Chung et al., 2011) (Figure 3.1). The structural rearrangements allowing the insertion of the α5 helix destabilises the nucleotide binding pocket and the GαGTPase- GαAH domains (see 1.2) allowing for GDP to dissociate followed by the binding of GTP and dissociation of Gα both from the βγ dimer and from the activated receptor (Fung et al., 1981).

Interestingly, the position of the cytoplasmic end of TM6 and the extent of its movement is dependent not only on the nature of the stimulating ligand but also the effector the receptor couples to. For example, the movement of TM6 is larger for the β2AR bound to a $G\alpha_s$ compared to the receptor coupled to the nanobody Nb80 (Rasmussen, *et al.*, 2011b) despite Nb80 being a high-efficacy agonist for the receptor.

The release of the structures of other GPCR-G protein complexes (Liu et al., 2020), (Wang et al., 2021), (Koehl et al., 2018a), (Zhang et al., 2021), (Zhang et al., 2017), (Koehl et al., 2018b) has enabled the comparison of the structural rearrangements within receptors coupling to different Gα subunits and within the G proteins themselves. Differences in the extent of TM6 outward movement have been observed with a larger outward movement for the β2AR coupling to $G\alpha_s$ compared to the adenosine receptor A1R coupling to $G\alpha_i$ (Draper-Joyce *et al.*, 2018), (García-Nafría and Tate, 2019), (Ma *et al.*, 2020).

Furthermore, the binding of the Gαi to the receptor is not supported by the formation of an α helix by the receptor ICL2 (Ma *et al.*, 2020).

The GPCR-G protein interface of the β2AR and the adenosine receptor $A_{2A}R$ has also been compared to the serotonin receptor $5HT_{1B}R$ coupled to a Go protein (García-Nafría et al., 2018b). The interaction surface of the β2AR and the adenosine receptor $A_{2A}R$ both coupled to Gαs proteins (whole-length and minimal engineered Gαs) (García-Nafría, *et al.*, 2018) is larger (containing more amino acid contacts) compared to the $5HT_{1B}R$ coupled to a Go protein. Another difference is in the tilt of the α5 helix of the G protein when bound to the receptor likely arising from the different final C terminus amino acids, important in defining G protein specificity (Flock et al., 2015). In the case of comparing the β2AR-Gs to CXCR2-Gi complex, the α5 helix of the Gi protein contains less bulky residues than the Gs and required less of a TM6-mediated opening in the receptor cytosolic interface (Liu et al., 2020). The contribution of the β subunit of the heterotrimeric G protein in the binding to GPCRs also varies between receptors likely resulting from the positions and tilt of the α5 helix and its interaction with the β subunit (García-Nafría and Tate, 2019). Nevertheless, for all Class A GPCRs compared in various studies, the majority of contacts made with GPCRs are through the C terminal α5 helix of the Gα subunit.

The binding of an agonist to the family B representative Glucagon receptor (GCGR) coupled to a Gαs protein, on the contrary, is not associated with an outward movement of TM6. This rearrangement is only observed following the insertion of Gα5 helix of the Gαs protein (Hilger et al., 2020). This structural difference is likely associated with the activation kinetics of the GCGR and with the following sustained receptor signalling. Nevertheless, this is not a universal feature for all family B GPCRs demonstrated by the structure of the Corticotropin-releasing factor receptor (CRF1R)-G protein complex where the outward movement of TM6 is necessary for the binding of the Gα5 subunit (Ma *et al.*, 2020).
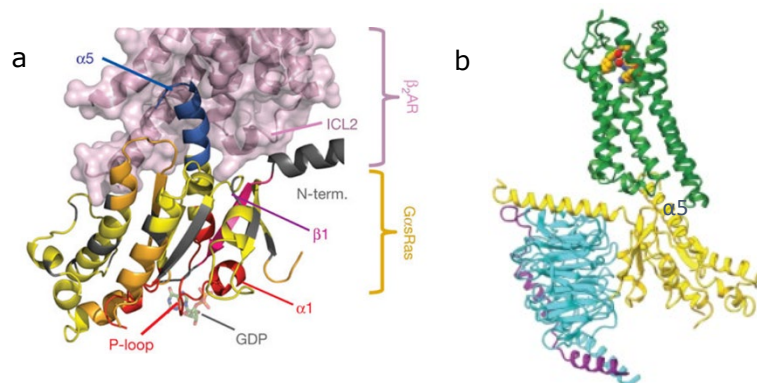
Figure 3.1. GPCR-G protein interaction surfaces. a) The interaction of Gαs with the cytosolic surface of β2AR revealed through X-ray crystallography and DXMS studies. b) The μ opioid receptor- Gαi complex structure obtained using cryo-EM. Images taken from (Chung *et al.,* 2011) and (Koehl *et al.,* 2018) respectively.

3.1.3 GPCR-arrestin interactions

Arrestin proteins preferentially bind activated and GRK-phosphorylated GPCRs and serve to terminate receptor signalling and execute other GPCR-independent functions (Gurevich and Gurevich, 2006). The arrestin molecule is composed of an N terminal and C terminal domain, each composed of antiparallel β sheets packed together forming 'sandwich'-like structures. The very carboxy terminal of the protein named 'C tail' connects to the C domain by a flexible linker and interacts with various parts of the C and N domains. A distinct feature of arrestin conformation is the functionally important 'polar core' comprised of conserved charged residues between the N and C domains in the very core of the molecule (Hirsch *et al.,* 1999) (Figure 3.2). The polar core allows for an easy reorganisation of the arrestin molecule upon activation through its function of a phosphate sensor that shifts the equilibrium of the arrestin molecule in favour of the active state upon interaction with the GPCR phosphates (Gurevich et al., 2018). The phosphate containing GPCR C terminus binds at the location of the arrestin C tail (across the N domain), displaces it

and causes structural rearrangements within the polar core allowing the rotation of the C terminus (Chen et al., 2018b).

Another important structural element in arrestin proteins is the 'finger loop' formed between β strand 5 and 6 in the N terminal domain (Figure 3.2). The finger loop of arrestins serves the 'active-receptor' sensor that engages with the cytosolic TM cavity opened upon GPCR activation (Kang et al., 2015), (Yin et al., 2019), (Staus et al., 2020). Upon activation, the finger loop forms an α helix and directly inserts itself into this pocket (Chen et al., 2018b).

These structural data have led to the formation of the 2-step model of arrestin interaction with GPCRs. In the first step, the GPCR phosphorylated C terminus engages with the N domain of arrestin based on high affinity charged interactions between the negative phosphates on the receptor and basic arrestin residues. This first interaction causes structural rearrangements within the arrestin molecule allowing for its second-step interaction with the GPCR core being the insertion of arrestin flinger loop into the binding pocket within TM5,6 and 3 (Shukla et al., 2014), (Huang et al., 2020).

The two-step interaction of arrestin with GPCRs and observations that arrestin can be activated only through the interaction with receptor phosphorylated C terminus have led to the idea of mutual binding of arrestins and G proteins at the GPCR (Kumari et al., 2017). The simultaneous binding of arrestin and G proteins at GPCRs has also been demonstrated with the formation of a megaplex between β2AR and V2R and arrestins and G proteins that exert signalling from intracellular compartments (Thomsen et al., 2016). The engagement of arrestin with GPCRs, however, is more common with both the phosphorylated C terminus and interhelical cavity shared with Gα5 which is the basis of homologous receptor desensitisation based on the occlusion of G protein binding (Gurevich and Gurevich, 2019).
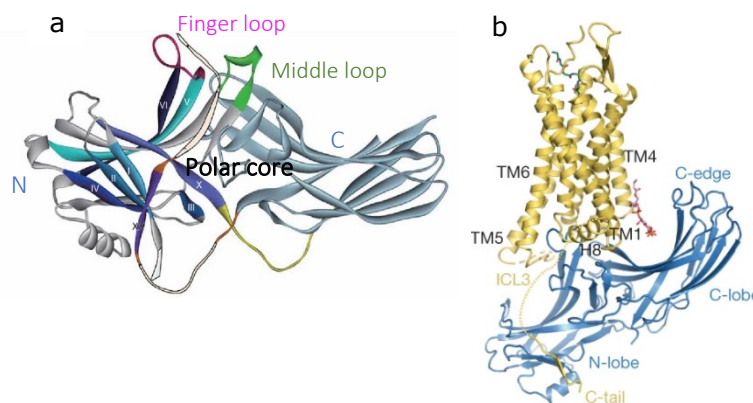
Figure 3.2 GPCR-arrestin interaction surfaces. a) Structure of the arrestin molecule showing the N and C domain shown with N and C respectively, finger loop in purple, middle loop in green and part of the C tail identified in yellow (Gurevich, Gurevich and Uversky, 2018) b) The complex between the neurotensin receptor (NTSR1) and β-arrestin 1 obtained using Cryo-EM (Huang *et al.*, 2020).

3.1.4 In vitro assays to measure GPCR-effector interactions

GPCR activation can be detected via a range of approaches that could measure second messenger signalling (eg. cAMP, calcium release), gene transcription or downstream function (eg. cell proliferation, cytokine release, cell migration) (Zhang and Xie, 2012). Measuring receptor activation at such downstream points, however, is associated with signal amplification which intervenes with the response generated and could mask differences between ligands with otherwise different efficacies (ability to activate the receptor), and 'biased' effects of ligands at different pathways (Kenakin, 2017). The kinetics of signalling events, which is often crucial for the signal outcome, is furthermore, often difficult to measure with a lot of commonly applied in vitro assay which are based on end-point reads. More recently, the use of biosensors that can detect conformational rearrangements in proteins, and the release of second messengers such as cAMP and calcium have allowed studying the spatio-temporal dynamics of GPCR signalling (Nikolaev et al., 2004), (Wright and Bouvier, 2021), (Matthees et al., 2021).

In vitro assays studying GPCR-effector interactions in real time and living cells have emerged as a direct way to detect GPCR activation and study how ligands affect distinct signalling pathways at very early stages unaffected by signal

96

amplification. The binding of arrestins to active, phosphorylated GPCRs makes them exploitable effector molecules to study as an indicator of GPCR activation and probe the effects of agonists, antagonists and allosteric modulators on this process. As arrestins bind phosphorylated, active GPCRs, assays measuring the GPCR-arrestin interaction has long been used as an indicator of receptor activation. These protein-protein interactions can be monitored by labelling the proteins of interest with either complementing β-galactosidase enzyme fragments or the Tango® assay, the latter based on the transcription of an enzyme producing fluorescent signal (Zhang and Xie, 2012). Whilst commonly implemented, neither assay can be used to monitor the recruitment of arrestin in real time, with either an irreversible end point measurement or the introduction of a significant delay between experimental treatments and taking the measurements. Another consideration is the extent to which the physiological system needs to be manipulated. The cellular distribution and binding of a fluorophore-labelled arrestin to unlabelled β2AR and V_2R has been monitored using imaging approaches providing the advantage of unmodified receptors (Oakley *et al.*, 2002). Furthermore, intramolecular arrestin Förster resonance energy transfer (FRET) sensors have also been used to monitor receptor-activation specific arrestin conformational rearrangements as well their kinetics (Nuber *et al.*, 2016), (Oishi et al., 2019). These approaches are advantageous for the lack of receptor modification and ability to monitor arrestin dynamics and arrestin-receptor interactions kinetically. Nevertheless, they require high-content imaging system and laborious protocols limiting their use in a high-throughput manner. Bioluminescence resonance energy transfer (BRET) allows for the multi-well plate format ratiometric recording of Luciferase-enzyme and a fluorophore of choice modified receptor/effector pair in real-time, living cells (Salahpour et al., 2012), (Spillmann et al., 2020).

GPCR-G protein interaction and GPCR driven G protein activation have also been exploited for the development of in vitro assays to probe GPCR ligands. One of the oldest and most common approaches is the GTPγS assay which utilises the radiolabelled non-hydrolysable analogue [^{35}S]GTPγS of GTP to measure the activation of the heterotrimeric G protein upon receptor

stimulation (Harrison and Traynor, 2003). The assay allows the extraction of classical pharmacological parameters such as ligand potencies and affinities without the issue of signal amplification. A major disadvantage, however, is the use of radiation, lack of kinetic resolution, as well the increased difficulty when studying GPCRs not coupling to $G\alpha_{i/o}$ effectors. Separation of the $G\alpha - G\beta\gamma$ subunits upon activation has been measured in real-time, living cells using intramolecular FRET sensors, which as previously discussed, are limited by the complex imaging instruments required and often low signal-to-noise ratio (Hein et al., 2005). The activation of G protein has also been studied by looking at the interaction of the separated dimer $\beta\gamma$ with the G protein coupled receptor kinase GRK3 (Bondar and Lazar, 2021).

BRET-based detection of GPCR-G protein interactions is another experimental approach that is challenging due to the existence of pre-formed receptor-heterotrimeric G protein complexes. BRET-based detection of GPCR-G protein interactions has also been designed (Galés et al., 2006), however, this approach is challenging due to the existence of GPCR-G protein pre-formed complexes and high background signal, as well as changes in the heterotrimeric G protein conformation as a result of nucleotide exchange and activation.

Measuring receptor-G protein interactions has been simplified through the development of minimal G proteins (mini G proteins) initially designed as solely the GαGTPase domain of $G\alpha_s$ (Carpenter and Tate, 2016). The design of the synthetic G protein probes involved truncation of the G protein N terminus and GαAH domain removing membrane anchor and $\beta\gamma$ binding interface, mutations to improve protein stability in vitro, and a mutation in the α5 helix preventing Gα dissociation from the GPCR upon GTP binding (Carpenter and Tate, 2016). These modifications allowed for the use of the probe in the crystallisation of receptor in their active conformation due to its reduced mobility, increased stability and smaller size, whilst preserving the GPCR binding interface (Carpenter et al., 2016). Later on, mini G protein probes representative of each Gα subfamilies were developed as follows mini Gsq, mini Gi1 (poorly expressing and unstable), mini Go1, mini Golf, for not only

structural but also functional studies (Nehmé et al., 2017b), (Wan *et al.*, 2018). The binding of some mini G proteins to βγ could be, however, preserved as shown in the structural 5HT$_{1B}$ receptor study (García-Nafría *et al.*, 2018). The small size of minimal G proteins and their recruitment from the cytosol upon GPCR activation makes then ideal sensors to robust receptor activation as a result of different ligand treatment.

3.1.5 Split Luciferase reporter system to study protein-protein interaction in real time

The Split Luciferase system utilises the small (19 kDa) and bright engineered luciferase enzyme NanoLuc (Nluc) originally derived from a deep-sea luminous shrimp (Hall et al., 2012). Nluc has been exploited for the development of a binary reporter by its separation into fragments used for tagging proteins of interest.

The Nluc binary reporter system developed by Promega (Madison, US) is based on splitting the Nluc enzyme into a 11-aa SmBiT fragment and 157-aa LgBit fragment. The LgBit fragment is optimised for stability through the introduction of point mutations, whereas the SmBit peptide sequence is varied for the development of alternative peptides with ~270000-fold range in LgBiT affinity (Dixon et al., 2016) (Figure 3.3).The low-affinity SmBit fragments allow for their use in detecting protein-protein interactions in robust reversible manner allowing for studying the kinetics of protein-protein interactions in live cells. The relatively small sizes of the tags, furthermore, aids preserving the actual protein affinities for one another. The HiBiT peptide (Promega, Madison, US) is another alternative peptide that forms a stable, slowly reversible interaction with the LgBiT fragment that is not appropriate for studying the dynamics of protein-protein interactions such as effector receptor recruitment have been exploited as tools to quantify protein expression or receptor internalisation (White *et al.*, 2020), (Reyes-Alcaraz et al., 2018), (Soave et al., 2019). The Nluc has been more recently split into two other unique fragments utilised for measuring β-arrestin recruitment to the plasma membrane

bringing the advantage of probing unmodified native receptors as an alternative to bystander BRET (Pedersen *et al.*, 2021).
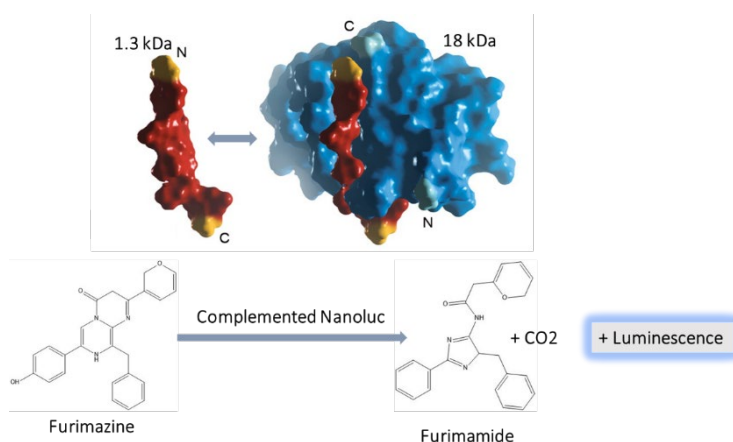
Figure 3.3 The Split luciferase complementation system principle. Nanoluciferase was split into LgBit (18 kDa) and SmBit (1.3 kDa) fragments which upon complementation form the active enzyme; Nanoluciferase (Nanoluc) oxidises the substrate furimazine into furimazine which is accompanied by the release of luminescence which is the assay output; image adapted from Dixon et al (2016).

3.1.6 Modulation of CXCR2 activation and intracellular signalling effector interactions

The crystallisation of the CXCR2 receptor in its inactive conformation bound by an intracellular NAM, 00767013 (structural match to navarixin) demonstrated the overlap of the NAM binding pocket with the hydrophobic canal accommodating the α5 helix of the Gαi subunit suggesting steric interference of the NAM with G protein binding (Liu et al., 2020). This is likely to underline at least partially the mechanism of action of the intracellular CXCR2 NAMs – inhibition of receptor activation and reduction in chemokine affinity due to the disturbed ternary complex. Nevertheless, there are still many unanswered questions such as if the structural diversity of these molecules underlines differences in their pharmacological profiles. Furthermore, the effect of NAMs on arrestin recruitment to CXCR2 has not been investigated so far and that could be different from that observed for G proteins, given the overlapping but not identical binding surface.

In addition, it has already been shown that NAMs like SB265610 bind in a fast reversible manner at CXCR2 (Bradley et al., 2009) whilst AZD5069 and R-

navarixin have small dissociation rate constants (k_{off}) making their binding at the receptor slowly reversible (Nicholls *et al.*, 2015), (Gonsiorek *et al.*, 2007). It is likely that such differences in NAMs binding kinetics would result in distinct pharmacological profiles that could be picked up in a functional assay measuring receptor activation in real time.

3.1.7 Chapter Aims

This work developed the Split Luciferase binary reporter system (NanoBiT) for studying the activation of CXCR2 in HEK293T cells expressing LgBiT tagged receptors and low-affinity SmBit tagged β-arrestin2 or mini Go proteins (Figure 3.4) with and without a range of structurally distinct intracellular NAMs – SB265610, AZ10307767, danirixin, S-navarixin, R-navarixin, and AZD5069 (see table 1.2 for structure) aimed at probing the effects of NAMs on CXCR2 activation and comparing them both between the two signalling systems and among each other. The goal of these studies was to extract information about the mechanism of action of the NAMs by analysing their effect of $CXCL8_{28-99}$ concentration-response relationships as well the kinetics of receptor-effector interactions. We aimed at extracting quantitative information of the NAMs affinity and binding kinetics at CXCR2 through the use of mathematical modelling and analysing these properties against their functional effects.

LgBit

Effector (arrestin/mini G protein)

SmBit

Substrate: furimazine
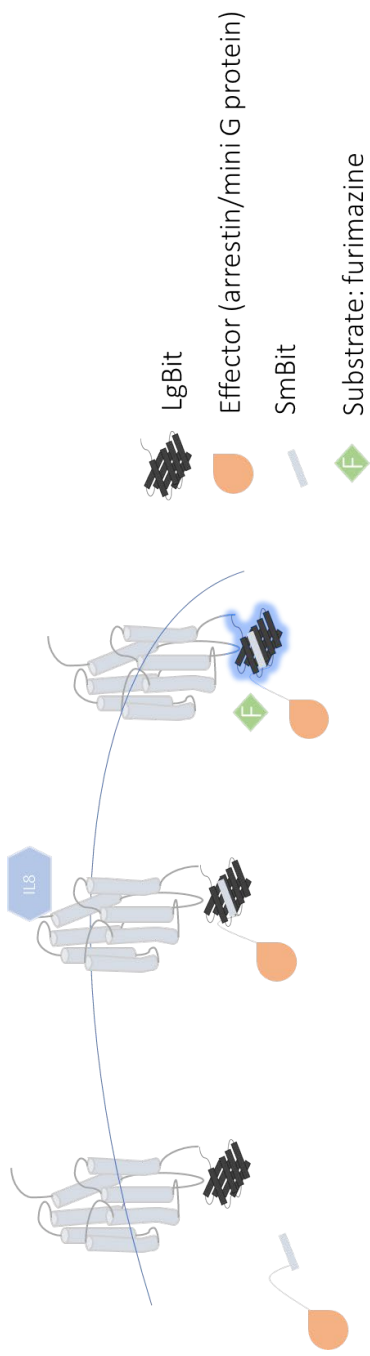
Figure 3.4 Principle of the Split Luciferase Complementation (NanoBiT) assay developed for the CXCR2 receptor. The receptor shown in grey, recruits effectors tagged with the SmBiT peptide basally or upon CXCL8 stimulation which leads to the complementation of the Nanoluciferase enzyme and the production of bring luminescence when the substrate furimazine is present.

3.2 Results

3.2.1 Characterisation and optimisation of the NanoBiT DNA constructs

The success of the Split luciferase complementation assay firstly depends on the appropriate DNA construct design. The tagging of the CXCR2 receptor with the LgBit fragment was based on previous investigations with other GPCRs in the laboratory (unpublished data). The addition of a linker between the receptor C terminus and the LgBiT peptide depends on the nature of the GPCR C terminus and the presence of an extended C terminus domain at CXCR2 did not require the introduction of an amino-acid linker prior to the LgBiT sequence, other than the two amino acids (LE) inserted as part of the XhoI restriction site (see chapter 2).

The position of the SmBiT fragment on the effector protein can be crucial to preserve receptor interaction, and appropriate complementation of the Split Luciferase. For example, the C terminus of the mini G constructs is critical for receptor engagement, so only N terminal mini G effector tagging with SmBiT was considered (Wan *et al.*, 2018). The location of the tag for the β-arrestin2 protein was optimised in transiently transfected HEK293T cells with either N- or C-terminally SmBiT tagged β-arrestin2 to determine which was the optimum orientation of the tag for the generation of a strong luminescence signal. The tagging of β-arrestin2 with SmBiT at the N terminus resulted in more efficient complementation with the LgBiT tagged CXCR2 manifesting in a higher luminescence signal (Figure 3.5). In addition, CXCL8 concentration-response relationship for the CXCR2-C-terminally tagged arrestin interaction, did not follow a sigmodal but a linear shape.

CXCL8$_{28-99}$ stimulated receptor activation with nanomolar affinity for both N-terminal and C-terminal arrestin effectors (pEC$_{50}$ = 9.7± 0.2;8.7±0.8 respectively; n =3).
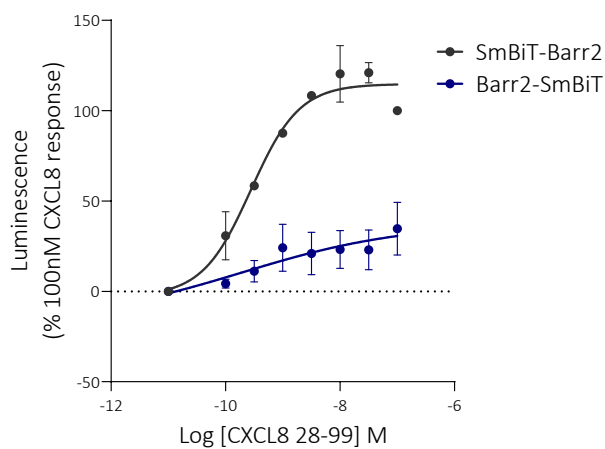
Figure 3.5 Interactions of CXCR2LgBit with N- or C-terminally SmBit tagged β-arrestin2. Cells were treated with furimazine substrate 5 minutes prior to recoding basal luminescence, followed by the addition of a range of concentrations of the agonists $CXCL8_{28-99}$. The recruitment of N-terminally (dark grey curve) or C-terminally (blue curve) SmBiT tagged β-arrestin2 is shown at 30 minutes post $CXCL8_{28-99}$ treatment. Graphs represent pooled data from 3 individual experiments, as mean ± S.E.M.

3.2.2 Generation of SNAPCXCR2Lg/ SmBit β-arrestin2 and SNAPCXCR2Lg / SmBit mini Go HEK293T cell lines

Following the determination of the optimum construct design, HEK293T cells were stably transfected with the LgBiT tagged CXCR2 receptor and either SmBiT-tagged β-arrestin2 or mini Go effectors (N-terminally tagged) and selected with the appropriate antibiotics. The SNAP-tag at the N terminus of CXCR2 was labelled with cell-impermeable SNAPsurface AF488 fluorophore and visualised using widefield microscopy and the appropriate detection filters. The receptors were expressed both on the plasma membrane and in intracellular compartments, reflecting a level of constitutive internalisation (Figure 3.6).
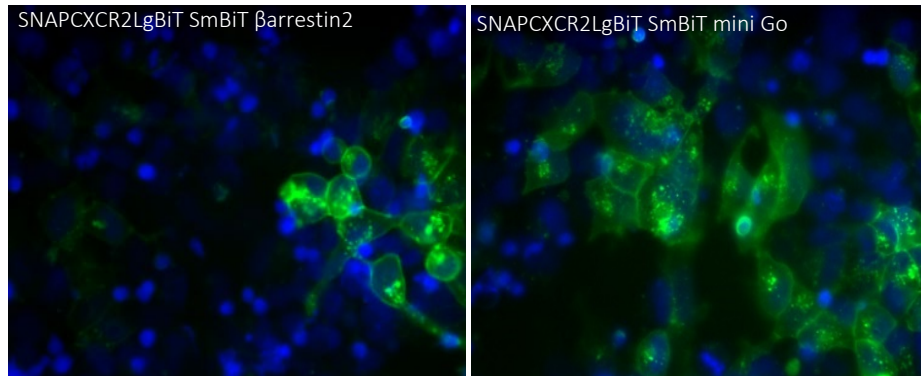
Figure 3.6 Expression of SNAP CXCR2LgBiT receptor in stably transfected HEK293T cells. Cells were stained with H33342 (blue) to identify nuclei and the SNAP-tag at CXCR2LgBiT labelled with cell impermeable SNAPsurface-AF488 fluorophore to identify receptors initially at the cell surface. The image in (A) shows SNAPCXCR2LgBiT receptors in cells dually transfected with SmBiT β-arrestin2 and the one in (B) SNAPCXCR2LgBit in cells transfected with SmBit mini Go. The images are representative of an individual experiment.

3.2.3 Recruitment of β-arrestin2 and mini Go proteins by CXCR2

Following the generation of the stable cell lines expressing NanoBiT-tagged CXCR2 receptors and effectors, cells were treated with furimazine and luminescence was recorded before and after stimulating with a range of $CXCL8_{28-99}$ concentrations. In both cell lines a basal level of luminescence was evident, suggesting a level of constitutive recruitment of each effector by CXCR2. Furthermore, chemokine stimulation produced a concentration-dependent increase of receptor-effector interactions that reached a peak between 5-7 minutes after highest agonist concentration addition (100 nM), followed by a broadly sustained response over the measurement period of 30 min (Figure 3.7).
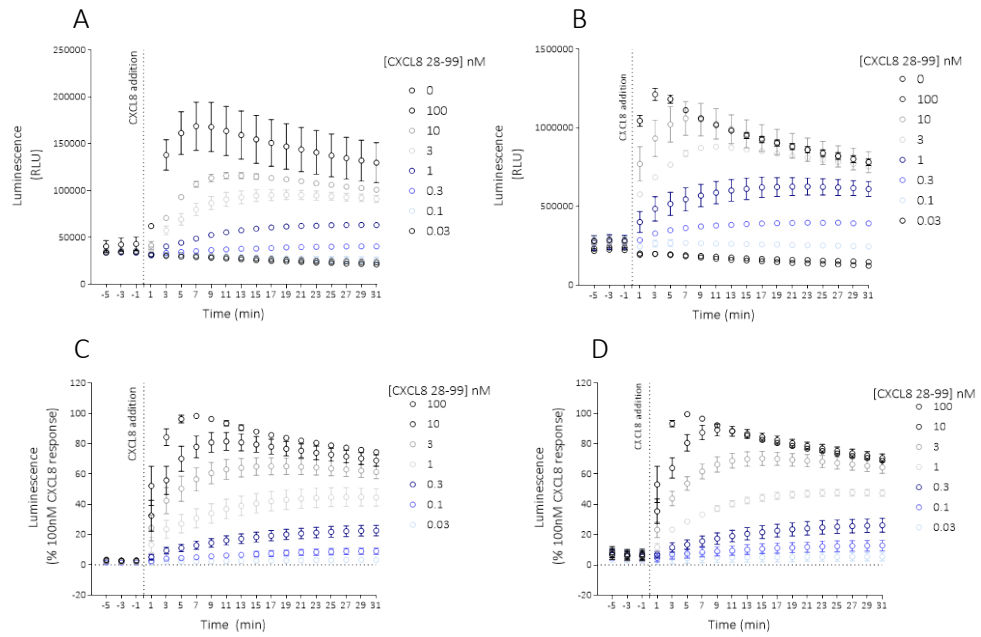
Figure 3.7 Kinetics of CXCR2-effector interactions. A) CXCR2-β-arrestin2 recruitment as raw luminescence counts upon $CXCL8_{28-99}$ treatment over 31 minutes. B) CXCR2-mini Go recruitment as raw luminescence counts upon $CXCL8_{28-99}$ treatment over 31 minutes. C) CXCR2-β-arrestin2 recruitment baseline-corrected and normalised to the 100 nM agonist at peak time. D) CXCR2-mini Go recruitment baseline corrected and normalised to 100 nM agonist at peak time. Data in A, B are representative from single experiments with error bars = S.D. and in C, D pooled from 5 individual experiments with error bars = S.E.M.

3.2.4 Optimisation of furimazine substrate concentration

The Split luciferase complementation assay utilises the oxidation of a substrate furimazine by the complemented luciferase enzyme to produce furimamide, CO_2 and luminescence as an output (Figure 3.8). Therefore, the concentration of the substrate needs to be optimised to avoid depletion across the timecourse of the read. It is also important to experimentally test that the concentration of furimazine does not influence the timecourse of the complementation response, so that it can be interpreted as the dynamics of the underlying protein-protein interactions. To probe this, the recruitment of β-arrestin2 by CXCR2 was monitored under 5 different dilution ratios of furimazine (diluted from the manufacturer's (undisclosed) top substrate concentration). The recruitment of β-arrestin2 stimulated by 100 nM CXCL8

was sustained with a peak at 5-7 minutes and a small drop observed from 15 minutes onwards. The difference in furimazine concentration only affected the absolute luminescence counts as expected but did not change the kinetics of the complementation response measurement stimulated by 100 nM $CXCL8_{28-99}$ agonist (Figure 3.6) – indicating that this was driven by the profile of the receptor-arrestin kinetics interactions.
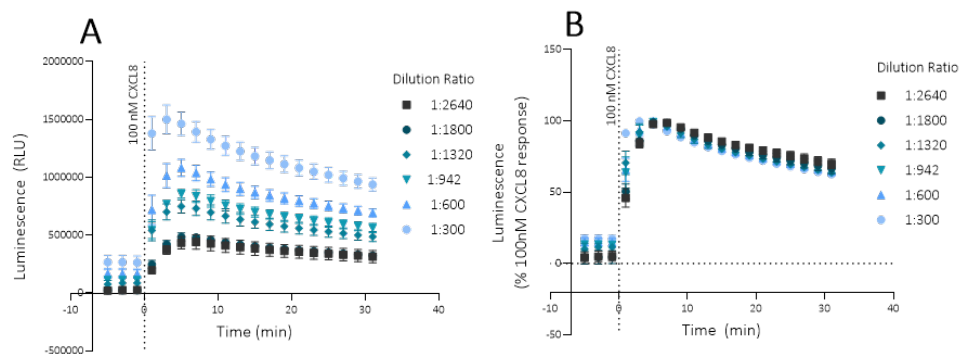
Figure 3.8 The interaction of CXCR2 with arrestin effectors stimulated by 100 nM CXCL8 with the addition of a range of concentrations of furimazine. (A) The recruitment of β-arrestin 2 by CXCR2 over time shown as raw luminescence counts. (B) The recruitment of β-arrestin 2 by CXCR2 over time normalised to the highest chemokine response time-point in each substrate concentration condition. Graphs represent pooled data from 3 individual experiments: error bars = S.E.M.

3.2.5 Characterisation of the effect of NAMs on CXCR2 activation

3.2.5.1 The effect of NAMs on $CXCL8_{28-99}$ pharmacology

Once the Split Luciferase assay conditions were optimised, we probed the ability of a range of structurally distinct intracellular NAMs of CXCR2 to inhibit receptor activation as a function of effector recruitment. This was approached by two experimental designs; HEK293T cells were either pre-treated with NAMs prior to agonist treatment, or NAMs were introduced post-chemokine agonist treatment. Each approach aimed at answering distinct questions concerning NAMs mechanism of action. NAM pre-treatment allowed the pre-formation of NAM-receptor complexes (using a NAM pretreatment time to allow this to approach equilibrium), followed by agonist ($CXCL8_{28-99}$) challenge.

Under these conditions, the agonist concentration response curves at different time points provide an indication of the mode of action of the antagonist (surmountable versus non-surmountable) at each time, and how this changes as the binding of agonist and NAM to the receptor re-approaches equilibrium after $CXCL8_{28-99}$ addition (Charlton and Vauquelin, 2010),(Riddy et al., 2015). These data also show the effect of NAMs on basal luminescence in the assay, and the potential for inverse agonism. In the second methodology, CXCL8-CXCR2-effector ternary complexes were preformed, and subsequent NAM addition was designed to discover how rapidly these were disrupted over time by the modulator, through the construction of IC_{50} curves at each timepoint.

$CXCL8_{28-99}$ stimulation of receptors led to the robust and sustained recruitment of both arrestin and mini Go proteins (pEC50 range 8.8 – 9.3; Figures 3.9, 3.10; Tables 3.1, 3.2) which was dose-dependently inhibited by the NAMs (SB265610 representative data Figure 3.9, A,B; Figure 3.10 A,B). Using the final time-point from the kinetic reads (30 minutes) concentration-response curves of $CXCL8_{28-99}$ were constructed and the effect of NAMs on the behaviour of the chemokine were analysed by fitting concentration response relations (Figure 3.9, B-G Figure 3.10, B-G). For each NAM, its concentration-dependent effects on the CXCL8 response profiles in the mini Go and arrestin assays were broadly similar. With the exception of AZ10397767, NAM pretreatment also reduced the basal luminescence measured in the receptor-arrestin or mini Go cell lines. AZ10397767, on the other hand, produced a slight increase in basal luminescence at higher concentrations, in both assays.

In each effector recruitment assay, the NAMs affected the 30 min concentration-response relationship of $CXCL8_{28-99}$ in distinct manners, which could be broadly classified in surmountable or non-surmountable terms. Pretreatment with SB265610, danirixin, and S-navarixin produced rightward shifts in $CXCL8_{28-99}$ curves indicating reduction in the chemokine potency without a clear change in agonist R_{max} (Tables 3.1, 3.2; Figures 3.9,3.10). In contrast, using the same pretreatment conditions, R-navarixin, AZ10397767, and AZD5069 primarily reduced the maximal response of the chemokine in a non-surmountable manner (Tables 3.1, 3.2; Figures 3.9, 3.10).

108
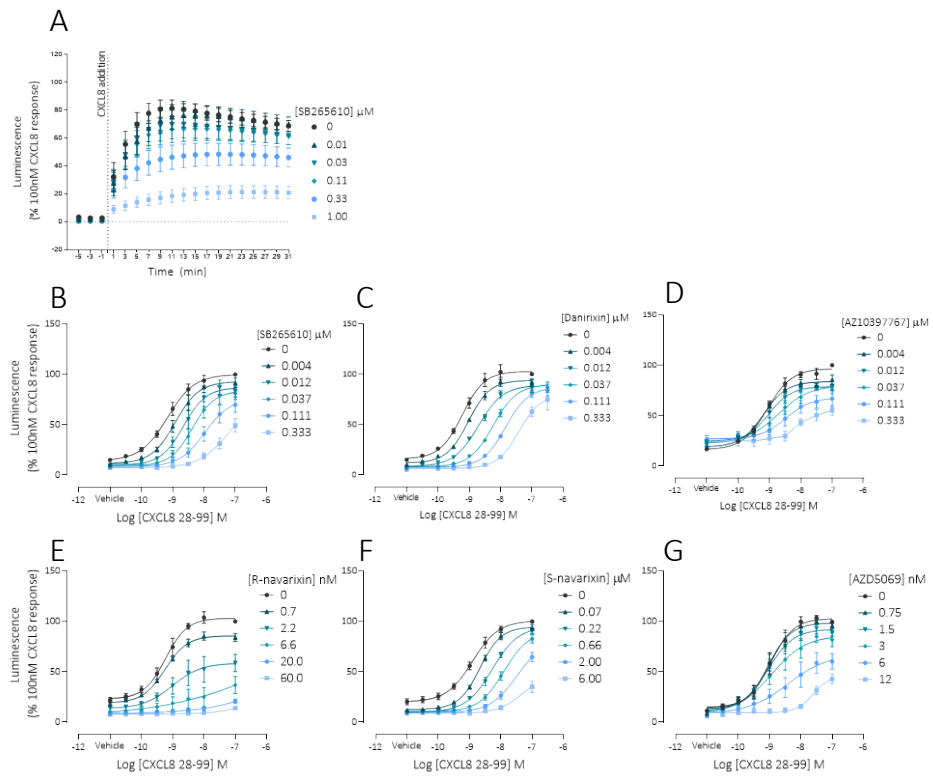
Figure 3.9 The effect of NAMs on CXCR2-β-arrestin2 interactions. Concentration-response curves for CXCL8$_{28-99}$ alone or with a range of concentration of the NAMs SB265610 (A,B), danirixin (C), AZ10397767(D), R-navarixin (E), S-navarixin (F), and AZD5069 (G) in its ability to stimulate β-arrestin2 recruitment by CXCR2. Cells pre-treated with each NAM for 60 minutes, furimazine substrate treatment as performed for 5 minutes and luminescence was recorded before and after the addition of CXCL8$_{28-99}$; the data in B-G show concentration-response curves of CXCR2-arrestin interactions 31 minutes post-agonist addition. Graphs represent pooled data from 5 individual experiments; error bars = S.E.M.
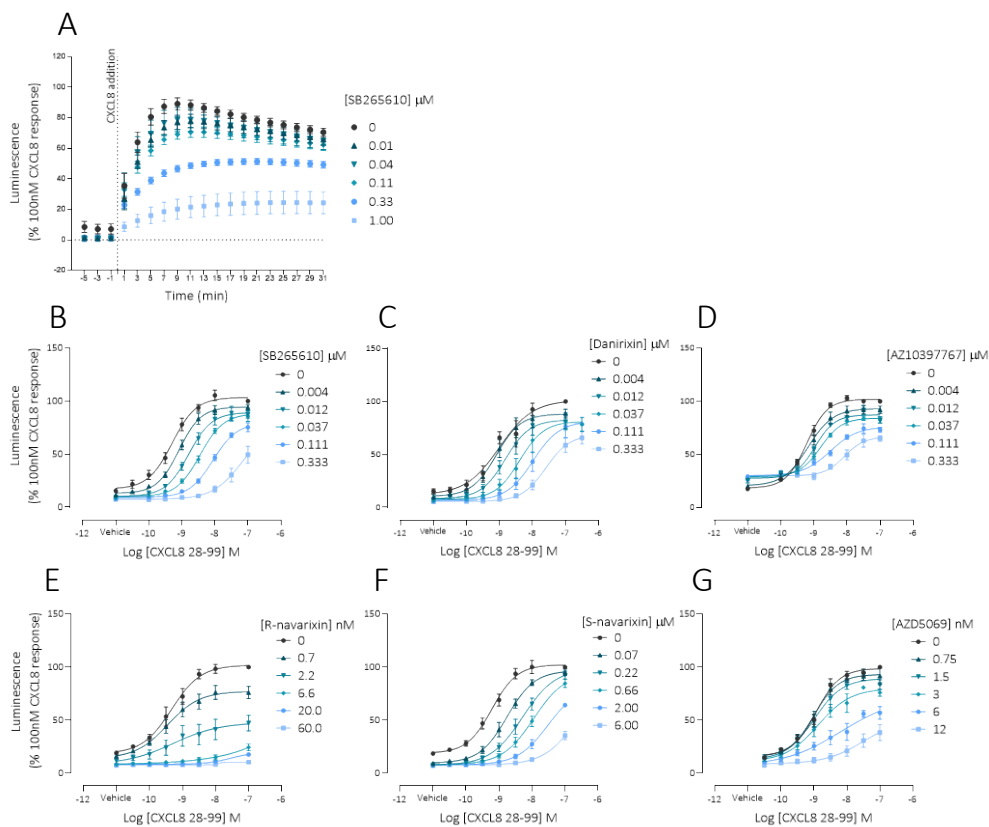
Figure 3.10 The effect of NAMs on CXCR2-mini Go interactions. Concentration-response curves for CXCL8$_{28-99}$ alone or with a range of concentration of the NAMs SB265610 (A,B), danirixin (C), AZ10397767(D),R-navarixin (E), S-navarixin (F), and AZD5069 (G) in its ability to stimulate mini Go recruitment by CXCR2. Cells pre-treated with each NAM for 60 minutes, furimazine substrate treatment as performed for 5 minutes and luminescence was recorded before and after the addition of CXCL8$_{28-99}$; the data in B-G show concentration-response curves of CXCR2-arrestin interactions 31 minutes post-agonist addition. Graphs represent pooled data from 5 individual experiments; error bars = S.E.M.

NAM	pEC_{50} control	pEC_{50} + NAM	R_{max} control	R_{max} + NAM
SB265610 (0.33 μM)	9.02 ± 0.14	7.77 ± 0.11*	89.07 ± 1.49	61.85 ± 3.03***
S-navarixin (0.22 μM)	8.89 ± 0.06	8.27 ± 0.062***	93.83 ± 6.11	89.75 ± 2.29
Danirixin (0.04 μM)	9.12 ± 0.12	8.13 ± 0.13***	88.64 ± 2.16	82.41 ± 5.50
R-navarixin (2.2 nM)	9.20 ± 0.09	8.47 ± 0.56	79.51 ± 2.24	61.38 ± 4.20**
AZ10397767 (0.11 μM)	9.04 ± 0.05	8.34 ± 0.09**	82.26 ± 2.23	43.93 ± 6.22***
AZD5069 (12 nM)	8.81 ± 0.20	7.26 ± 0.26	90.22 ± 4.06	43.86 ± 15.46**

Table 3.1 The effect of NAMs on CXCR2-arrestin interactions. The table shows the pEC_{50} values of $CXCL8_{28-99}$ alone or with SB265610, S-navarixin, danirixin, R-navarixin AZ10397767, AZD5069 (at the lowest concentration showing a significant effect (when any) from data in Figure 3.7 in the arrestin recruitment assay 31 minutes following agonist addition. Data represent mean values pooled from 5 individual experiments ± S.E.M. For each NAM, significant differences between the pEC_{50} values in the presence of NAM at differing concentrations, compared to the $CXCL8_{28-99}$ control, were assessed by One-way ANOVAS followed by Dunnett's multiple comparisons test. * $P < 0.05$, ** $P < 0.01$, *** $P < 0.001$

NAM	pEC_{50} control	pEC_{50} + NAM	R_{max} control (%)	R_{max} + NAM (%)
SB265610 (0.33 μM)	9.31 ± 0.08	8.05 ± 0.06***	87.03 ± 1.14	70.88 ± 5.90
S-navarixin (0.22 μM)	9.13 ± 0.04	8.20 ± 0.21**	84.16 ± 2.16	95.17 ± 10.79
Danirixin (0.04 μM)	9.03 ± 0.15	8.41 ± 0.11**	88.18 ± 3.98	76.09 ± 5.08
R-navarixin (2.2 nM)	9.28 ± 0.16	8.00 ± 0.50*	84.25 ± 2.68	51.57 ± 6.70**
AZ10397767 (0.11 μM)	9.20 ± 0.06	8.50 ± 0.06***	83.04 ± 1.24	46.28 ± 2.46***
AZD5069 (12 nM)	8.92 ± 0.11	7.80 ± 0.13***	83.07 ± 1.81	38.48 ± 14.21***

Table 3.2 The effect of NAMs on CXCR2-mini Go interactions. The table shows the pEC_{50} values of $CXCL8_{28-99}$ alone or with SB265610, S-navarixin, danirixin, R-navarixin AZ10397767, AZD5069 (at the lowest concentration showing a significant effect (when any) from data in Figure 3.7 in the mini Go recruitment assay 31 minutes following agonist addition. Data represent mean values pooled from 5 individual experiments ± S.E.M. For each NAM, significant differences between the pEC_{50} values in the presence of NAM at differing concentrations, compared to the $CXCL8_{28-99}$ control, were assessed by One-way ANOVAS followed by Dunnett's multiple comparisons test. * $P < 0.05$, ** $P < 0.01$, *** $P < 0.001$

To explore the kinetic signalling behaviour following NAM treatment in more depth, timecourses (Figure 3.11) and $CXCL8_{28-99}$ concentration response curves at 5 and 15 minutes (Figure 3.12) were constructed to compare the navarixin enantiomer variants. An increase in the control potency of $CXCL8_{28-99}$ was observed at 15 (pEC_{50} 8.94±0.12, n=5) and 30 min (pEC_{50} 9.20±0.09, n=5)

compared to the 5 min timepoint (8.07±0.24, n=5; Figure 3.12), reflecting the time to equilibrium for the agonist response (and shorter time to peak at high concentrations observed in Figure 3.11). The non-surmountable behaviour after R-navarixin pretreatment was evident throughout the timecourse, and equally the effects of S-navarixin / appeared surmountable even at 5 min post agonist addition.
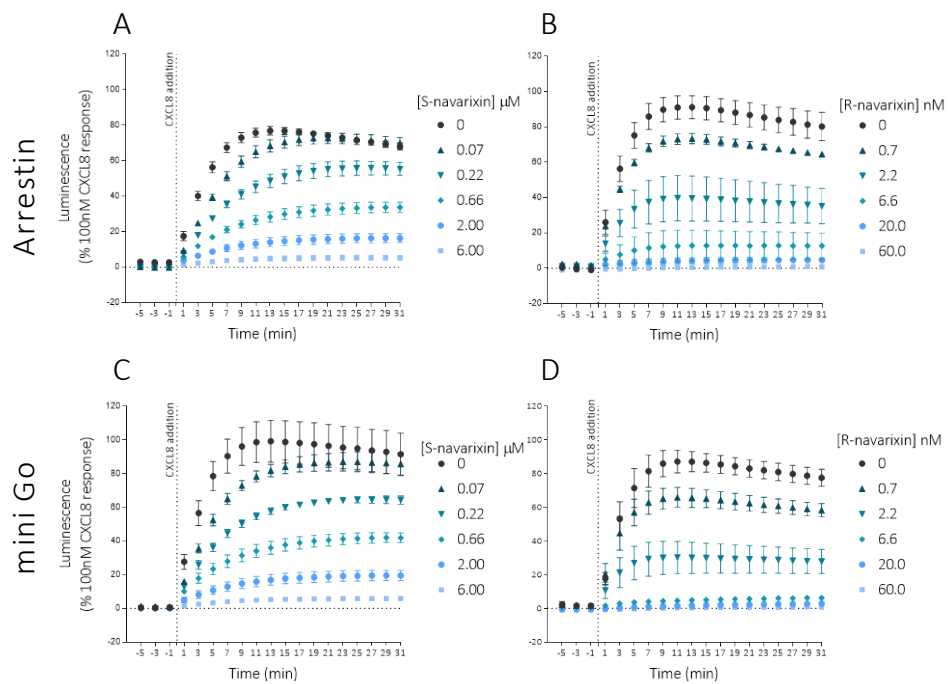
Figure 3.11 Effect of the navarixin enantiomers on the kinetics of CXCR2- effector interactions. The recruitment of β-arrestin2 (top panel) and mini Go (bottom panel) by CXCR2 over 31 minutes stimulated by 10 nM CXCL8 alone or a range of concentrations of S-navarixin (A,C) or R-navarixin (B,D). Cells pre-treated with each NAM for 60 minutes, furimazine substrate treatment was performed for 5 minutes and luminescence was recorded before and after the addition of $CXCL8_{28-99}$. Graphs represent pooled data from 5 individual experiments; error bars = S.E.M
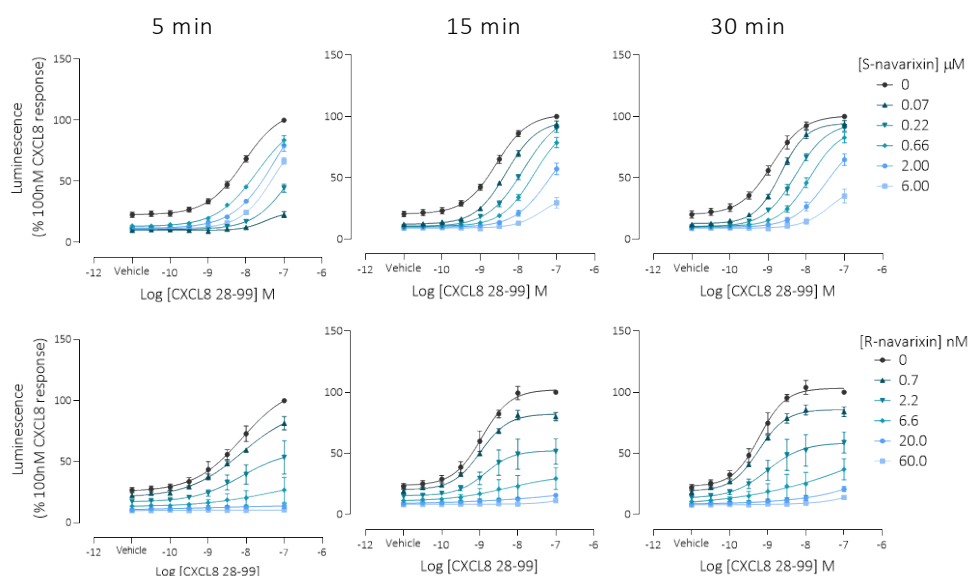
Figure 3.12 The effect of S-navarixin and R-navarixin on CXCL8 concentration-response curves at different time points. The enantiomer NAMs S-navarixin (top) and R-navarixin (bottom) inhibition on CXCR2-arrestin interactions at 5, 15, and 30 minutes post CXCL8 addition. Graphs represent pooled data from 5 individual experiments, error bars = S.E.M.

3.2.5.2 Quantifying NAM affinity and binding kinetic estimates using the hemi-equilibrium model

The effects of different NAMs on CXCL8 concentration response curve relationships (Figure 3.9, Figure 3.10) demonstrated concentration-dependent effects that were aligned with their reported affinities – for example, R navarixin and AZD5069 exerted inhibitory effects over a much lower concentration range than S navarixin or SB265610. However, extracting NAM functional affinity estimates from these data is problematic. Even when surmountable antagonism is observed, traditional Gaddum / Schild analysis requires that the interactions of agonist / antagonist with the receptor are competitive, and also that equilibrium conditions have been reached.

To test an alternative approach for analysis of the $CXCL8_{28-99}$ concentration response, data in the presence of different NAMs, we first made the assumption that although their CXCR2 binding sites are clearly different, binding of chemokine and NAM occurred in a mutually exclusive (and thereby

113

pharmacologically competitive) manner. The supporting evidence and rationale for this assumption will be discussed further in the binding studies described in Chapter 4. This then allowed the non-surmountable / surmountable behaviour of the different NAMs to be modelled kinetically, on the basis of differing dissociation rate constants (k_{off}). As antagonist k_{off} reduces, non-surmountable behaviour on the subsequent agonist concentration responses can be described on the basis of hemi-equilibrium conditions – i.e. when re-equilibration between NAM and agonist receptor binding has not been fully re-established at the measurement time point. The operational model of antagonism at hemi-equilibrium (Riddy et al., 2015), (Kenakin, 2006) (discussed in 2.8.2.2) was therefore fitted to the functional CXCR2 data. For the concentration response curve sets in the receptor-arrestin assay, this model produced estimates of SB265610, R-navarixin, and AZD5069 binding kinetics and affinity similar to what previously reported in the literature (Bradley et al., 2009), (Gonsiorek *et al.*, 2007), (Nicholls *et al.*, 2015). Furthermore, the model yielded negative values for the koff rate constants of R-navarixin and AZD5069 based on their very slow dissociation kinetics as previously reported (Gonsiorek *et al.*, 2007), (Nicholls *et al.*, 2015a). We, therefore, constrained the koff values to be ≥ 0. Faster dissociation kinetics were predicted for SB265610 and S-navarixin, with AZ10397767 characterised by an intermediate koff (Figure 3.14; table 3.4).
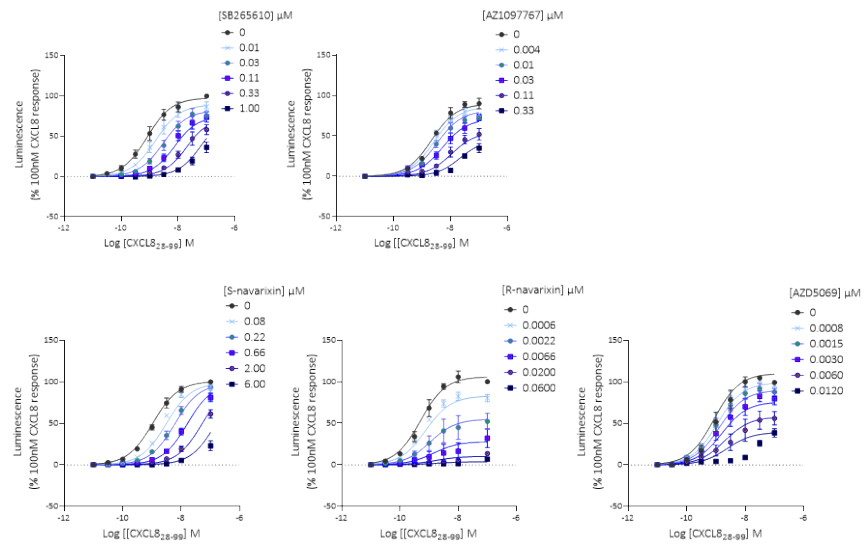
Figure 3.13. Operational model for antagonism at hemi-equilibrium. The data fitting shown for the effects of SB265610, S-navarixin, R-navarixin, and AZD5069 on CXCR2-arrestin recruitment stimulated by $CXCL8_{28-99}$ at 30 minutes (data are from Figures 3.9). Graphs represent pooled data from 5 individual experiments; error bars = S.E.M. The analysis is described in more detail in chapter 2.

NAM	SB265610	R-navarixin	S-navarixin	AZD5069	AZ10397767
Affinity (KB) nM	9	0.6	40	1.7	4
k_{off} (min^{-1})	0.01	9.6 e-027	0.08	2.5 e-032	0.005
Affinity (KB) nM Lit	1.2	0.1	N/A	9.1	19*
k_{off} (min^{-1}) Lit	0.3	0.0006	N/A	0.0019	N/A
Tau (CXCL8$_{28-99}$)	5.8	2.1	2.0	2.8	4.5
KA (CXCL8$_{28-99}$) nM	5.5	1.7	3	3	11

Table 3.3 Operational model for antagonism at hemi-equilibrium. Affinity (KB) and dissociation kinetics rate (k_{off}) for the unlabelled NAMs SB265610, R-navarixin, S-navarixin, AZDD5069, and AZ10397767 derived from fitting pooled data from 5 individual experiments to the operational model for hemi-equilibrium. The KB Lit and K_{off} Lit refer to the affinity and dissociation rate constant values derived elsewhere in the literature for these compounds taken from (Bradley *et al.,* 2009) for SB265610, (Gonsiorek *et al.*, 2007) for R-navarixin, (Nicholls *et al.,* 2016) for AZD5069, and *(De Kruijf *et al.,* 2009) for a structurally similar NAM to AZ10397767; N/A against S-navarixin refers to the lack of characterisation of this enantiomer in the literature. The parameters tau refers to the efficacy of the agonist CXCL8$_{28-99}$ and KA – to the affinity of CXCL8$_{28-99}$.

3.2.5.3 Probing the reversibility of NAM binding to CXCR2

The hemi-equilibrium analysis in 3.2.5.2 suggested that slower binding kinetics, rather than non-competitive allosteric behaviour alone, could underlie the distinction between non-surmountable and surmountable mode of action observed for the different NAMs in the CXCR2 assays. To test this hypothesis, wash out experiments were designed to remove unbound NAM prior to agonist treatment. NAMs characterised by slow dissociation kinetics would be expected to have an increased residence time with persistent receptor binding under wash out conditions, leading to maintained antagonism of the CXCL8$_{28-99}$ response. Figure 3.14 (and Table 3.5) show the results of this experiment comparing SB265610, S-navarixin and R-navarixin. Following the 60-minute NAM pre-incubation, 2x quick washes with buffer were performed, followed by a further 15-minute buffer incubation and wash. Next, the CXCR2-arrestin

NanoBiT luminescence response was recorded before and after CXCL8$_{28-99}$ additions. Whilst the chemokine response significantly recovered following the wash of S-navarixin and SB265610, R-navarixin retained its inhibitory effects unaffected by the washes. This was observed for the whole timecourse of the assay, shown by considering concentration response curves constructed on the basis of area under curve timecourse analysis (Figure 3.14) and supported statistically for the concentration-response curves taken at 30 minutes post chemokine addition (table 3.5).
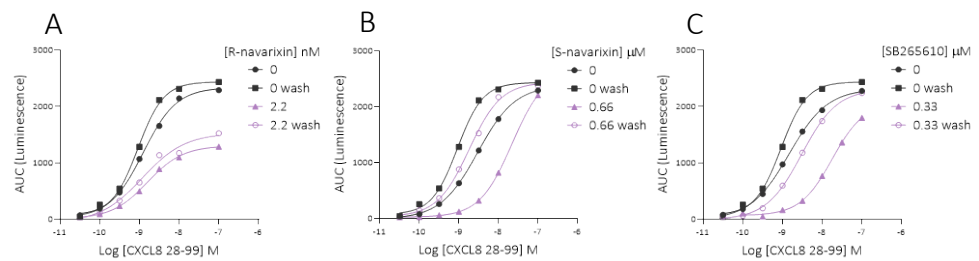
Figure 3.14 Effect of NAMs on CXCR2-arrestin interactions with and without wash steps. Concentration response curves of CXCL8$_{28-99}$ or CXCL8$_{28-99}$ with 60-minute R-navarixin (A), S-navarixin (B), and SB265610 (C) pre-treatment with and without wash steps following NAM treatment constructed using area-under-the curve analysis of the whole time-course of arrestin recruitment (31 minutes in total). The AUC analysis (mean only) was performed using pooled data from at least 3 individual experiments.

R-navarixin	pEC_{50}	Span (%)
0	9.20 ± 0.09	79.5 ± 2.2
0 wash	9.04 ± 0.04	82.0 ± 54.0
2.2 nM	8.46 ± 0.55	61.4 ± 4.2***
2.2 nM wash	9.9 ± 0.39	54.5 ± 8.5**
6.6 nM	N/A	N/A
6.6 nM wash	8.47 ± 0.78	49.5 ± 7.2***

S-navarixin	pEC_{50}	Span (%)
0	8.84 ± 0.06	93.8 ± 6.1
0 wash	9.04 ± 0.04	82.0 ± 1.3
0.66 µM	7.91 ± 0.08***	84.8 ± 3.6
0.66 µM wash	9.06 ± 0.06	77.5 ± 3.0
2 µM	7.41 ± 0.13***	83.6 ± 6.1
2 µM wash	8.92 ± 0.07	80.7 ± 3.9

SB265610	pEC_{50}	Span (%)
0	9.02 ± 0.14	89.07 ± 1.49
0 wash	9.04 ± 0.04	82.00 ± 1.3
0.33 µM	7.77 ± 0.11*	61.85 ± 3.03***
0.33 µM wash	8.52 ± 0.02	75.21 ± 2.83

Table 3.5. Reversibility of NAMs probed in wash assays. Unbound R-navarixin, S-navarixin, and SB265610 were washed off from the receptor binding pocket vicinity through wash steps introduced prior to $CXCL8_{28-99}$ agonist treatment and the effects of NAMs on agonist potency (pEC_{50}) and maximal response (span) were recorded. Data showing unwashed agonist control (0), washed agonist control (0 wash), NAM pretreatment unwashed (eg. R-navarixin 2.2 nM) or washed (eg. R-navarixin 2.2 nM wash) were pooled from at least 3 individual experiments were pooled and presented as means ± S.E.M. Experiments with wash steps included were run separately from ones without, therefore statistical analyses are performed between unwashed control and unwashed NAM treatment, and washed controls and washed NAM treatment. Statistical significance displayed as *p<0.05; *p<0.01; *p<0.001 is based on comparing NAM pretreated and washed wells to washed control wells (vehicle).

3.2.5.3 Effect of NAMs on pre-formed CXCR2-effector complexes

The experiments to date used a NAM pretreatment protocol to allow the modulator to bind CXCR2 prior to agonist stimulation. Conceivably, the preformation of a chemokine-CXCR2-effector complex might significantly alter the degree of inhibition afforded by NAMs in the assay – for example because a stable agonist-receptor-effector interaction then prevents access of the NAM to the intracellular binding site. To test this, R-navarixin and SB265610 were further compared by adding different concentrations of modulator to cells previously treated with 1 nM $CXCL8_{28-99}$ for 60 minutes to stimulate the CXCR2-mini Go interaction. Both NAMs inhibited the NanoBiT CXCR2-mini Go response, with a modest increase in inhibitory potency (~3 fold) and maximal inhibition for R-navarixin only with extended NAM incubation time. R-navarixin achieved receptor-effector complex formation inhibition with higher affinity compared to SB265610 (Figure 3.15, table 3.6). These data demonstrate the ability of the two NAMs to bind and inhibit activated CXCR2 responses in the assay under conditions of agonist pre-stimulation, and also support the reversibility of the LgBiT and SmBiT partner luciferase complementation as previously described (Dixon et al., 2016)

119
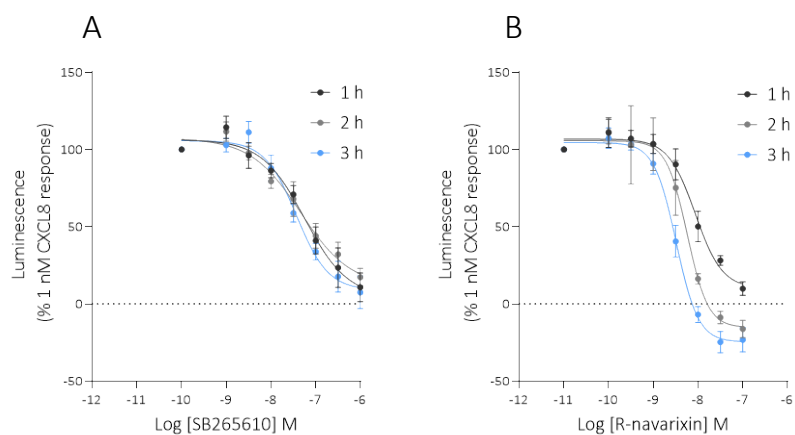
Figure 3.15 The effect of SB265610 and R-navarixin on pre-formed CXCR2-mini Go complexes. The NAMs R-navarixin (A) and SB265610 (B) were added 1-3 hours post 1 nM $CXCL8_{28-99}$ treatment for 60 minutes; graphs represent pooled data from 5 individual experiment; error bars = S.E.M.

	R-navarixin pIC50	R-navarixin maximal inhibition (%)	SB265610 pIC50	SB265610 maximal inhibition (%)
1 h	8.13 ± 0.10	93 ± 4	7.18 ± 0.11	100 ± 10
2 h	8.30 ± 0.10	129 ± 12	7.35 ± 0.17	97 ± 3
3 h	8.51 ± 0.09	133 ± 7	7.55 ± 0.15	109 ± 8

Table 3.6 Inhibition potency of SB265610 and R-navarixin to inhibit CXCR2-mini Go NanoBiT following chemokine pre-treatment. Pre-treated cells with 1 nM CXCL8/vehicle were treated with R-navarixin or SB2656510 for 1-3 hours. Data represents means ± S.E.M. pooled from 5 individual experiments.

3.2.6 Investigating the presence of receptor reserve in the CXCR2 NanoBiT assay system

It is possible that the consequences of a non-competitive mode of NAM action (or indeed, slow reversibility) might not translate to observed non-surmountable antagonist behaviour (Figure 3.9, 3.10), if there is a sufficiently high level of receptor reserve in the system. In the described NanoBiT assays, which directly measure receptor-effector interaction (a first step following receptor activation), receptor reserve could be created by the functional stoichiometry of receptor (R)/ effector (E) proteins (where concentrations of receptor are greater than that of the effector such as mini Go or arrestin). For example, with an R:E stoichiometry of 10:1, only 10 % of the receptors would need activation to fully engage the available effector proteins. Under these conditions, non-competitive or irreversible antagonists would first shift the agonist concentration response curve to the right (surmountable behaviour) prior to any reductions in maximal response.

The identification of actual receptor / effector concentrations in the assay NanoBiT cell lines would be challenging (not least given the nature of recruitment of effectors from a 3D pool of proteins to the 2D membrane environment). However, to assess the likelihood that a receptor reserve could exist, an assay method was designed to measure the availability of non-complemented LgBiT receptors following agonist stimulation.

This utilised the high-affinity SmBit peptide – HiBiT, to complement any unoccupied receptors post maximal chemokine stimulation. The HiBiT peptide (10 μM) was added to previously detergent-permeabilised cells to allow plasma membrane penetration. The addition of both saponin and digitonin detergents to cells decreased the luminescent signal likely due to an overall decrease in cell viability (Figure 3.16 A, B). Nevertheless, the addition of HiBiT peptide to the detergent treated cells significantly increased the net luminescent signal compared to wells stimulated with CXCL8 in both arrestin and mini Go cell lines indicating the presence of significant receptor reserve in

the system. Based on the signal increase following HiBiT addition, receptor reserve was more pronounced for the arrestin signalling system set-up (~100x increase vs. ~3x increase for arrestin and mini-Go cell line respectively).
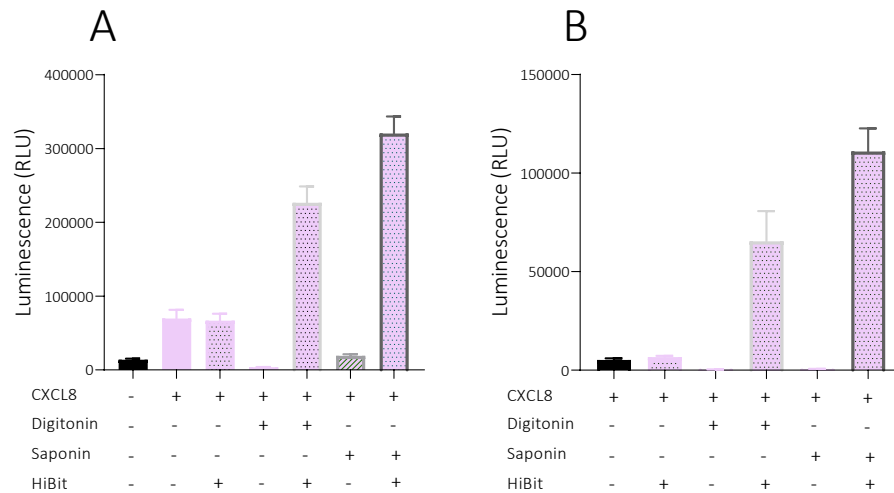
Figure 3.16 Detecting receptor reserve using LgBit-HiBiT complementation. Cells expressing SNAPCXCR2LgBiT/SmBiT mini Go (A) or SNAPCXCR2LgBiT/SmBiT arrestin (B) were treated with buffer/detergent (saponin or digitonin) followed by stimulation with 100 nM CXCL8$_{28-99}$ and the addition of 10 μM purified HiBiT peptide or buffer. The CXCR2-effector interaction is represented as the raw luminescence signal and the presence or absence of CXCL8, detergent, HiBiT is indicated as + or − under the corresponding bar on the graph. The graphs are representative experiments on n=2 and the error bars = S.D.

3.3 Discussion

3.3.1 NanoBiT mini Go and arrestin assays as a means to monitor CXCR2 activation

This work aimed at profiling CXCR2 NAMs on the receptor-effector interactions and evaluate if their pharmacology is effector dependent. We established the NanoBiT technology as a direct reporter of these interactions. For the set of NAMs tested, equivalent pharmacology was observed that wasn't effector dependent. Surprisingly, the ability of NAMs to generate non-surmountable versus surmountable antagonism in this assay appeared more closely related to duration of action than their common non-competitive allosteric mode of action. These data highlighted the importance of NAM binding kinetics, and a slow koff rate in generating the non-surmountable profile.

The Luciferase Complementation assay was successfully used to monitor kinetic recruitment of effectors to CXCR2 in a rapid and reversible fashion. The use of this sensor system has been broadly used to study protein-protein interactions in both non-GPCR (SARS-CoV-spike protein − ACE2 interaction (Azad et al., 2021); ELISA set-up Antibody-antigen recognition (Hwang et al., 2020) etc.) and GPCR (GPCR-arrestin recruitment (Spillmann et al., 2020), (Littmann *et al.*, 2019), GPCR-mini G protein recruitment (Wan *et al.*, 2018), (Laschet et al., 2019), G protein Gα/Gβγ subunit separation (Inoue et al., 2019), peptide binding at GPCRs (Hu *et al.*, 2018) and so on) systems.

The potency of the chemokine agonist $CXCL8_{28-99}$ at stimulating CXCR2-arrestin and CXCR2-mini Go interactions was in broad agreement with what previously measured through GTPγS G protein activation studies (Salchow et al., 2010), (Bradley et al., 2009), PathHunter detected arrestin recruitment (Kruijf et al., 2009), and other signalling assays such as neutrophil chemotaxis, calcium mobilisation, receptor desensitisation and internalisation (Nasser et al., 2009a).

CXCR2-arrestin interaction peaked earliest for the highest CXCL8$_{28-99}$ concentration used (100 nM) which is likely related to the association binding kinetics rate of the ligand which is concentration dependent (see 4.1.4, 4.1.5). Thus, 100 nM of a ligand will bind with a faster association rate compared to 30 nM and will likely produce a more rapid receptor-effector interaction.

The profile of CXCR2-β-arrestin2 interaction was sustained with a minor signal decay occurring around 10 minutes post ligand treatment. This indicates that there is either quick turnover of receptors due to fast internalisation and trafficking back to the plasma membrane for re-recruitment of arrestins, or alternatively, that the CXCR2-arrestin interaction is maintained both at the plasma membrane and in the cytosol and endosomal compartments following receptor internalisation. Past studies examining the desensitisation and trafficking of CXCR2 have demonstrated the rapid internalisation of CXCR2 upon agonist exposure that depends on receptor C tail phosphorylation, as well as β-arrestin, AP2-2 and dynamin protein interactions (Fan et al., 2001), (Su et al., 2005). The kinetics of CXCR2-arrestin interaction and stability of the complex, however, have not been previously studied. The sustained association of other chemokine receptor such as CXCR4, nevertheless, happens both at the plasma membrane and endosomal compartments (Orsini et al., 1999). Furthermore, prolonged arrestin interaction has been shown for other peptide-activated receptors such as the vasopressin receptor (Feinstein et al., 2013), somatostatin receptor type 2 (SSTR2), gastrin releasing peptide receptor (GRPR) (Spillmann et al., 2020), that are representatives of both the class A and class B GPCRs. In addition, previous work (Thomsen et al., 2016),(Nguyen et al., 2019) showed that GPCRs form sustained G protein/arrestin complexes that could signal from intracellular compartments. The latter is based on the partial arrestin interaction with the receptor C tail only and not the TM crevice (Shukla et al., 2014).

The basal and agonist-stimulated CXCR2-G protein interaction was monitored using a minimal G protein sensor – mini Go, instead of a full-length G protein. The mini G protein of choice was mini G$_o$ due to its improved stability and better expression in cells compared to mini G$_i$ and mini G$_{s/i}$ and the high

conservation between Gαi and Gαo subfamilies (Nehmé et al., 2017a), (Ueda et al., 1988).

Whilst not being identical to a full-length native G protein, the mini Go probe provided the necessary interface for receptor interaction (Gα-GTPase domain) (see 3.1). Furthermore, the recruitment of the mini G proteins from the cytoplasm as opposed to being receptor pre-coupled is a significant advantage of these probes as it allows for the generation of a sufficient assay window to measure both basal and agonist-stimulated effector recruitment.

Similarly to that reported by Wan et al (Wan *et al.*, 2018), with the opposite orientation of LgBiT/SmBiT fragments (Receptor-SmBiT/ Effector-LgBiT), the recruitment of the mini Go protein manifested as a rise in the luminescence in a concentration-dependent manner following agonist treatment, whereas the addition of NAMs reduced the luminescence signal both below basal and below agonist-stimulated levels. Agonist-stimulated and NAM inhibited G protein interactions for the CXCR2 receptor have been previously reported for the same or structural similar NAMs via the use of an alternative G protein activation detection assay (GTPγS) (Salchow et al., 2010).

The disadvantages of using minimal G proteins, however, are related to the lack of similarity to a native system where the Gα subunit interacts with βγ and the heterotrimeric protein associates with the plasma membrane and could pre-couple to the receptor. The lack of GTP/GDP exchange of the minimal G protein making its interaction with the receptor more stable, in addition, make the probe inappropriate for kinetic studies that require precise detail on the dynamics of receptor-G protein interactions.

Measuring the receptor-effector interactions as a means to profile ligands was largely chosen, because this assay detects very early stages of receptor signalling closer to ligand treatment and is unaffected by signal amplification which is often the case when measuring downstream signalling events such as cAMP/calcium release (Hill et al., 2010). What we observed, however, was a case of receptor reserve arising from the presence of more transfected receptor than effector proteins which led to the manifestation of

insurmountable antagonism as surmountable for NAMs with fast dissociation kinetic rates.

The Split Luciferase complementation assay was optimised by picking the right construct design for the optimum luminescence signal upon interaction of the LgBiT and SmBiT fragments whilst preserving the biological activity of the tagged proteins. The LgBiT fragment was placed at the receptor C terminal, close to the PDZ-binding domain (-STTL), important for the fate of internalised receptors as well as functional outcomes such as chemotaxis (Baugher and Richmond, 2008).

Mutations or deletions of the PDZ motif direct internalised receptor for lysosomal degradation shown for the CCR5 and CXCR2 receptor (Baugher and Richmond, 2008), (Delhaye et al., 2007) and are important for resensitisation following internalisation for the purinergic receptor $P2Y_{12}R$ (Nisar et al., 2011). The PDZ motif of the CXCR2 receptor has been argued by some to affect receptor fate at post-endocytic time-points without affecting the initial receptor internalisation (Baugher and Richmond, 2008) but also to bind AP2 adaptor proteins and be involved in the clathrin-mediated endocytosis and receptor sequestration from the plasma membrane (Fan *et al.*, 2001). The sustained receptor-effector interactions measured, however, do not suggest the presence of increased receptor lysosomal degradation as a result of potential PDZ inaccessibility due to the presence of the LgBit fragment.

The tagging of mini Go effectors with the SmBit fragment was only attempted at the N terminal site because of the insertion of the α5 helix into GPCR binding pocket (Hamm et al., 1988), (Oldham et al., 2006), (Liu et al., 2020). This emphasises the importance of careful construction design to avoid loss of functionality of the signalling proteins and it has been shown before for other proteins such as GRK proteins which amino terminus is essential for catalytic activity (Pao, Barker and Benovic, 2009). In the case of the β-arrestin2 effector proteins, the SmBit tag attachment was probed at both the N and C termini and the interaction with the LgBit tagged receptors was examined in transiently transfected cells prior to creating the stable cell lines. Our data demonstrated that the CXCR2LgBit receptors interact more readily with the N-

126

terminally SmBit tagged β-arrestin2 effectors. The reason for that could be the initial low affinity interactions between the arrestin and GPCR proteins that happen between the phosphorylated receptor C tail and the basal N-terminal residues in the arrestin molecule (Gurevich and Benovic, 1995).

In addition, CXCL8 stimulation only produced sigmoidal concentration-response relationship for the N-terminally tagged arrestin effector, whereas the interaction between CXCR2 and the C-terminally tagged effector increased in a linear-like fashion with increasing agonist concentration. The orientation of the tag and its molecular interaction with the receptor as explained above could underline this but also differences in effector expression despite identical transfection condition (eg. protein translation and expression following the DNA transfection).

3.3.2 Intracellular NAMs demonstrate equivalent inhibitory profiles for CXCR2 recruitment of mGo and arrestin effectors in the NanoBiT assay

Next, a range of structurally distinct intracellular NAMs were assessed in their ability to inhibit CXCR2-effector interactions. NAMs behaviour on the $CXCL8_{28-99}$ concentration-response curves were analysed by pre-treating cells with 5 fixed NAM concentrations, and then adding a concentration range of the chemokine agonist. The pre-treatment time with NAMs was set to 60 minutes aiming to allow plasma membrane penetration of the NAM and its equilibrium binding with the CXCR2 receptor. When each NAM was compared individually, its ability to inhibit CXCR2-βarrestin2 and mini Go effector was equivalent. This demonstrates, that for the range of structural pharmacophores under consideration, the binding of the NAM to the proposed CXCR2 intracellular pocket is unable to selectively modulate arrestin versus G protein engagement. This is not unexpected based on the similarities of the GPCR interaction surface for arrestins and G protein; the insertion of the of arrestins' finger loops into GPCRs cytoplasmic pocket partially mimics the insertion of the α5 helix of the Gα subunit, therefore they partly share the same GPCR binding interface (Szczepek et al., 2014b). Alternatively, situations of receptor-arrestin interaction dependent on preceding G protein coupling have been described

127

(Smith and Pack, 2021). It could be that NAMs block arrestin binding by simply limiting the earlier receptor-endogenous G proteins interactions. A further explanation is that by binding to the intracellular receptor pocket, NAMs may more generally stabilise the inactive CXCR2 receptor conformation (separate from steric hindrance of effector association), a concept that will be explored further in Chapter 4.

All NAMs except AZ10397767 acted as inverse agonists of CXCR2 as they reduced the receptor-effector interactions below basal. Such properties have been previously reported for the diarylurea SB265610 (Bradley et al., 2009) and the diarylsquaramide R-navarixin (Kredel et al., 2009). The increase of the basal receptor activity by AZ10397767 could be attributed to its partial agonistic properties previously reported for its structural analogue VUN10948 in a PathHunter arrestin recruitment assay (Kruijf et al., 2009). The differential effect of AZ10397767 cannot be attributed to its interaction with a distinct site as previous works showed it could be displaced by SB265610 and other intracellular NAMs (Kruijf et al., 2009), (Nicholls et al., 2008). The pre-treatment with AZ10397767 is likely to shift CXCR2 in a unique active conformation supporting effector recruitment, whilst preventing its full activation by reducing chemokine binding. That could be the case if the NAM occludes the effector binding pocket to a lesser extent compared to the other NAMs which is a possibility that could be explored through molecular dynamics computational simulations or structural studies.

The NAMs were able to inhibit CXCR2-mini Go interactions not only when applied prior to agonist stimulation but also following agonist treatment and the formation of receptor-effector complexes. The ability of NAMs to bind to their intracellular pocket suggest that either they have access to it within the ternary complex formed. Alternatively, and more likely, the periodic dissociation of the ligand-receptor-effector complex during the dynamic binding equilibrium allows for NAMs to access the intracellular binding pocket before rebinding of effector occurs. The ability of NAMs to inhibit pre-formed receptor-effector complexes may be also determined by the location of receptor especially following agonist stimulation. Internalised receptors in

128

endosomal compartments may switch conformation due to differences in the environment pH (Vogel and Siebert, 2001), (Ghanouni *et al.*, 2000). Such differences in receptor embraced conformations dependent on their cellular location may lead to a further layer of NAMs abilities to bind receptors and block their activation.

3.3.3 Slow NAM binding kinetics as a driver of insurmountability in the NanoBiT assays

All NAMs studied are allosteric and are (regarding binding) non-competitive, interacting with a separate site from the one of the chemokine ligand. Classical pharmacology dictates that these non-competitive binding interactions can be revealed as non-surmountable antagonism. However, we observed that while a number of NAMs displayed non-surmountable properties in the assays (R-navarixin, AZD5069, AZ10397767), others were surmountable (SB265610, danirixin, S-navarixin). While we identified the presence of receptor reserve in the assay, which might obscure non-surmountable effects, this appears insufficient to explain the difference in behaviour of closely related analogues such as R and S navarixin.

Instead, non-surmountable behaviour was closely correlated with reported slow koff rates, where known (Nicholls *et al.*, 2015), (Gonsiorek *et al.*, 2007) – indicating binding kinetics, and in particular long residence time and hemi-equilibrium conditions, was a key driver in generating this mode of action. This observation was supported by wash out assays demonstrating the persistence of antagonism for the slow off compounds such as R-navarixin that effectively reduced the chemokine maximal response.

Based on a presumption that kinetics and reversibility drove the nature of the NAM effects on CXCL8 CRCs, the hemi-equilibrium model was fitted to the data. This model estimated very slow dissociation rates and higher affinities for R-navarixin and AZD5069 compared to SB265610 and S-navarixin matching their functional insurmountable and surmountable-like profiles in the NanoBiT assay. Clearly, one drawback of using this model is that NAM and chemokine binding must be mutually exclusive to meet the assumptions of competitive

129

behaviours. This question will be revisited in chapter 4. Nevertheless, the data show that slow koff, as well as non-competitive mode of action, can be a key additional means to promote insurmountable behaviour as part of a desired CXCR2 NAM compound profile. Clinically an insurmountable mechanism can be beneficial in an anti-inflammatory therapeutic, in which inhibitory efficacy at CXCR2 may need to be maintained under conditions of high CXCL8 release and concentration (Mould et al., 2014a), (Vauquelin and Charlton, 2010). Thus, it is notable that two of the NAMs that have reached clinical study (R-navarixin, AZD5069) are slowly reversible.

Wash-off experiments further supported these observations by showing that R-navarixin retained its inhibitory effect on CXCR2-arrestin interactions following multiple buffer washes unlike SB265610 and S-navarixin. The semi-irreversible binding of R-navarixin likely didn't allow for its removal from the vicinity of the binding pocket unlike the quickly equilibrating compounds such as SB265610, and S-navarixin.

These observations taken together suggest that the surmountable profiles of SB265610, danirixin, and S-navarixin could result from negative binding cooperativity with the chemokine making the agonist and NAM interactions mutually exclusive (further explored in chapter 4) in combination with system factors such as receptor reserve. The insurmountable profiles of R-navarixin, AZD5069, and possibly AZ10397767 are on the contrary binding kinetics driven.

3.3.4 Critical evaluation and future directions

Whilst these data demonstrated that detecting the CXCR2-arrestin/mini Go interactions using the NanoBiT technology is a robust way to measure receptor activation and profile ligands, there are certain limitations in our system that could be addressed.

Concerns regarding the C-terminal modification of the receptor and its potential influence on receptor trafficking could be removed by using sensors that detect receptor activation as a function of the separation of the α and βγ subunits (Inoue et al., 2019) indicative of G protein activation. In a similar

fashion, there are intramolecular arrestin sensors (Charest et al., 2005), (Nuber *et al.*, 2016), allowing to study receptor-driven arrestin activation for native GPCRs. Furthermore, a stable version of an engineered minimal Gi protein such as the mini Gs/i chimera (Nehmé *et al.*, 2017) could be used instead of the mini Go protein for closer representative to the physiological CXCR2-G protein coupling.

Recombinant assay systems rely on transfecting the same amount of recombinant receptor and effector DNA which as we observed, does not necessarily correspond to equal expression of both proteins. In our case, this led to a case of 'receptor reserve' affecting the profiles of the examined ligands. The relative stoichiometry of interacting partners could affect the kinetic pattern of their interaction observed in the assay. This is particularly important for arrestin proteins where under/overexpression can influence the duration and sustainability of the signal because of their roles in receptor desensitisation, trafficking and potentially lysosomal degradation (Gurevich and Gurevich, 2019a). This has been elegantly demonstrated by White *et al.*, (White *et al.*, 2020) who showed that CXCR4 receptor overexpression relative to arrestin led to a slower peaking luminescence and vice versa - the overexpression of arrestin proteins led to a rapid peak followed by a rapid decline recruitment profile. The issue of protein overexpression has been overcome through the use of clustered regularly interspaced short palindromic repeats (CRISPR) technology for gene editing allows to modify proteins of interests with the desired tags whilst keeping their expression at native levels (White *et al.*, 2020).

3.3.5 Conclusions

In conclusion, NanoBiT based CXCR2-effector interaction assays demonstrated that intracellular CXCR2 NAMs provide equivalent inhibition of G protein and arrestin recruitment. We further demonstrated that the binding kinetic properties of the NAMs are likely to be a key driver of their observed insurmountable behaviour. Nevertheless, the functional data alone do not resolve direct effects of NAMs on effector recruitment, compared to the

extent they modulate chemokine binding directly. This may have a key impact on interpreting and modelling the functional data. To address this, Chapter 4 will look into the effect of unlabelled NAMs on the binding affinity and kinetics of a fluorescently labelled CXCL8 tracer in order to directly assess if their binding is mutually exclusive and if slowly-reversible NAMs differ in their effects compared to the fast off compounds.

Chapter 4. Studying the Effects of Intracellular Negative Allosteric Modulators on Fluorescent Chemokine Binding at CXCR2 Using High-Content Imaging Approaches and TR-FRET

4. Chapter four: Studying the Effects of Intracellular Negative Allosteric Modulators on Fluorescent Chemokine Binding at CXCR2 Using High-Content Imaging Approaches and TR-FRET

4.1 Introduction

4.1.1 Ligand induced conformational change in GPCR activation

The interaction of GPCRs with external stimuli is the basis for the modulation of a vast range of cellular events and ultimately – physiological responses. Ligands activating GPCRs cause the receptors to engage in an active conformation supporting their interaction with heterotrimeric G proteins and other signalling partners, allowing the initiation of downstream signalling events.

The simple two-state model (originally described for ion channels) (Del Castillo and Katz, 1957) was the first to relate ligand efficacy in the context of conformational change $(A \leftrightarrow AR \leftrightarrow AR*)$. At the heart of this model is the ability of agonists to stabilise an active conformation with higher affinity.

The binding of ligands and activation of GPCRs is more complex because of their allosteric nature and the formation of a ternary complex (TCM) between the agonist (A), receptor (R), and G protein (G) (De Lean et al., 1980). The TCM describes the transition of the receptor from a low to a high affinity conformation (R >>> R*) as a result of not only agonist (A) but also G protein (G) binding. Early binding studies demonstrated that uncoupling G proteins from the receptor by the addition of GTP or the non-hydrolysable GTP analogue GTPγS, led the agonist to revert to its low-affinity binding form (Hulme et al., 1978) supporting the positive allosteric modulation of GPCRs by G proteins.

Recognition of the agonist-independent constitutive GDP-GTP nucleotide exchange by GPCRs (Spalding et al., 1997) led to the extension of the ternary complex (extended ternary complex model / ETCM) model to accommodate this phenomenon (Samama et al., 1993). This model, such as the two-state model, proposes ligand biased affinities for different receptor species underlying a mechanism for ligand efficacy (Kenakin, 2004).

Nowadays, it is widely accepted that GPCRs exist in thermal equilibrium switching between a selection of conformations with various energy demands (Weis and Kobilka, 2018). Whilst agonists shift the thermal equilibrium in favour of a conformation supporting G protein binding and activation above the basal activity levels, inverse agonists lower the basal GPCR activation, and thus favour inactive conformation; neutral antagonists, on the other hand, do not affect the basal activity of receptors but inhibit agonist ability to promote GPCR activation through various mechanisms. The ability of different ligands to stabilise unique GPCR conformations upon binding could result in the initiation of different functional outcomes which is the basis of the phenomenon *biased signalling* (Wingler and Lefkowitz, 2020), (Goupil, Laporte and Hebert, 2012), (Peters et al., 2020).

The modulation of GPCR activity by ligands can be studied in the context of drug effects on receptor activation and signalling (discussed in chapter 3). Nevertheless, it is essential to understand the preceding steps in this process associated with the quantification of both drug affinity at its target in different conformations, and the lifetime of the drug-receptor complex. In fact, the lifetime of the ligand-receptor complex, and its conformational repertoire, largely dictates the effect of the drug in physiological context (Hoffmann et al., 2015), (Copeland et al., 2006), (Sykes et al., 2019a). The conformational rearrangements associated with ligand and G protein binding at the CXCR2 receptor, the subject of this study, are thoroughly described in Chapter 1.

4.1.2 Technologies used to study ligand binding at GPCRs

Ligand binding at GPCRs can be measured directly using radio- or fluorescently labelled ligand probes; both of these approaches allow for measuring the kinetics of ligand-receptor interactions (Sykes et al., 2019a). Traditional radioligand binding can be performed in whole cells and membranes and allows for quantifying the total amount of binding sites Bmax and ligand affinity (Kd) (Insel and Stoolman, 1978), (Buergisser et al., 1981), (Motulsky and Mahan, 1984).

A major limitation of radiolabelled ligand binding techniques, however, is the requirement for separation of the bound from free ligand, for example through a filtration step. Therefore, for kinetic studies, each time point is measured as a separate sample (Hulme and Trevethick, 2010).

Surface plasmon resonance (SPR) spectroscopy is another methodology used to study the affinity and kinetics of ligand-receptor interactions (Capelli et al., 2020). Whilst it offers the advantage of label free binding detection, it requires the presence of purified receptor proteins extracted from their native membrane environment (Olaru et al., 2015).

The development of fluorescence-based technologies has offered an alternative to radiolabelled ligand binding studies and the ability to measure ligand-receptor interactions in a homogenous, high throughput manner.

The design of fluorescent ligand probes is a multi-layered process involving the selection of an appropriate fluorophore and linker and the best area for their attachment at the pharmacophore of interest (Vernall et al., 2014).

For example, the N terminal and core domains of chemokine ligands are intimately involved in their interaction with cognate chemokine receptors, therefore modifying them with fluorophores N terminally is not the preferred strategy (Liu et al., 2020), (Burg et al., 2015b), (Qin et al., 2015). Fluorescent chemokine probes have been designed by labelling the ligands at C-terminal residues less important for binding such as the AF647 conjugate CXCL12 probe (CXCL12-af647) (Hatse et al., 2004), (White *et al.*, 2020) and the CXCL8- AF647 probe labelled at C terminal lysine residue. Despite the effort to label molecules at sites minimally involved in their interaction with targets, the addition of fluorophores increases the molecular weight of the molecule and alters its physiochemical properties which may manifest in changes in ligand affinity for their cognate GPCRs and also other molecules such as GAGs (discussed in chapter 1 and chapter 5), (Sykes et al., 2019a).

Nevertheless, modest changes in ligand properties are normally not a serious obstacle for using fluorescent ligands in probing receptor-ligand interactions effectively.

Fluorescent ligand binding can be monitored directly using microscopy-based technologies allowing the detection of the precise cellular localisation of the fluorescent probe and quantifying the fluorescence using the appropriate software and algorithm (Kilpatrick et al., 2015). Other techniques for studying the binding of fluorescent probes include florescence polarisation (Tota et al., 1994), and flow cytometry (Kozma et al., 2013), (Hatse et al., 2004). Resonance energy transfer (RET) based technologies, however, offer major advantages for studying fluorescently labelled ligand binding in both single cell and high throughput setups. They utilise the non-radiative energy transfer between a donor and an acceptor of fluorescence. The donor could be an enzyme catalysing a reaction that produces a bioluminescence output as in bioluminescence resonance energy transfer (BRET) technology (Stoddart et al., 2015a), or a fluorophore that upon a light source excitation emits and excites the fluorescent probe as in Förster resonance energy transfer (FRET). Their homogenous nature does not require the separation of bound from free ligand. Furthermore, multiple measurements taken from a single sample allow for kinetics to be recorded in a precise and high throughput fashion (Stoddart et al., 2016), (Lohse et al., 2012), (Sykes et al., 2017), (White *et al.*, 2020), (Peach et al., 2018). In order for RET to take place, the protein the fluorescent ligand binds to needs to also be modified either directly with a fluorophore or a sequence recognised by fluorophores (eg. SNAP tag) or in the case of BRET – a Nanoluc enzyme (Jones and Bradshaw, 2019). In a similar way to modifying ligands with fluorophores, a large tag at either the N or C terminal ends of the target protein could affect native function and ligand binding.

4.1.3 Förster resonance energy transfer (FRET) to study fluorescent ligand binding at GPCRs

FRET is used for monitoring interactions between biomolecules coupled to fluorescent tags provided there is sufficient overlap of the donor emission and acceptor excitation spectra, close proximity (<100 Å) between the donor and acceptor molecules and correct donor–acceptor orientation of dipole

137

moments (Stoddart et al., 2016). Under these conditions, the binding of fluorescently labelled ligand probes to GPCRs modified with fluorescent tags is readily adaptable in both single-cell and multi-well plate formats. Traditional FRET relies on the tagging of the GPCR of interest with fluorophores such as green fluorescent proteins (GFP), yellow fluorescent proteins (YFP), cyan fluorescent proteins (CFP) (Ilien et al., 2003), (Fernández-Dueñas et al., 2013) etc. which emissions are immediate and transient. These qualities of the fluorophores utilised in FRET lead to the detection of background fluorescence from the donor excitation and the ultimate reduction in the assay sensitivity and signal-to-noise ratio. Time resolved FRET (TR-FRET) overcomes these challenges through the use of rare earth lanthanide chelates such as europium or terbium as donors of fluorescence (Zwier et al., 2014) (Figure 4.1). Lanthanide ions do not absorb light efficiently, therefore terbium and europium used in the TR-FRET assays are in the form of cryptates meaning that they are embedded into macrocyclic motifs that serve as 'light collecting' devices. The long-lasting (1-2 ms) emission of lanthanide donors allows the collection of time-resolved measurements through the introduction of a delay between donor excitation and signal collection, ensuring the removal of any background short-lived fluorescence. Furthermore, the lanthanides emit fluorescence in several emission wavelengths which allows for good separation between the donor and acceptor spectra for a number of acceptor fluorophores, which further increases the signal-to-noise ratio (Zwier et al., 2014), (Stoddart et al., 2016), (Boute et al., 2002), (Degorce et al., 2009). GPCRs can be labelled with lanthanides conjugates to covalently binding antibodies; nevertheless, this methodology does not allow for adequate examination of the kinetics of ligand-receptor interactions due to the kinetics of binding of the antibody itself to the GPCR (Stoddart et al., 2016). GPCRs fused to N terminal extracellular SNAP-, CLIP- or Halo- tags (Kolberg et al., 2013) can form covalent bonds with terbium or europium cryptate (in the case of SNAP, conjugated to the benzyl guanine substrate) allowing for covalent labelling of receptors with the donor of fluorescence prior to conducting TR FRET assays. This methodology removes the issue of interference with the

138

kinetics of ligand-receptor interactions measured in the assay. Importantly, the cryptate substrates do not cross cellular plasma membrane, and this means that intracellular labelling of tagged GPCRs (e.g. for studying intracellular fluorescent ligand binding) must be carried out in membrane preparations or purified receptor systems. TR FRET has been successfully utilised for studying the kinetics of fluorescent ligand binding at GPCRs such as the binding of fast and slow ligands at the dopamine receptor 2 and its implications in antipsychotic drugs side effects (Sykes et al., 2017), as well as the binding of ligands at the parathyroid hormone receptor (PTHR) (Emami-Nemini et al., 2013), vasopressin and oxytocin receptors (Albizu et al., 2007), neurotensin receptor (Mazor et al., 2002) and so on.
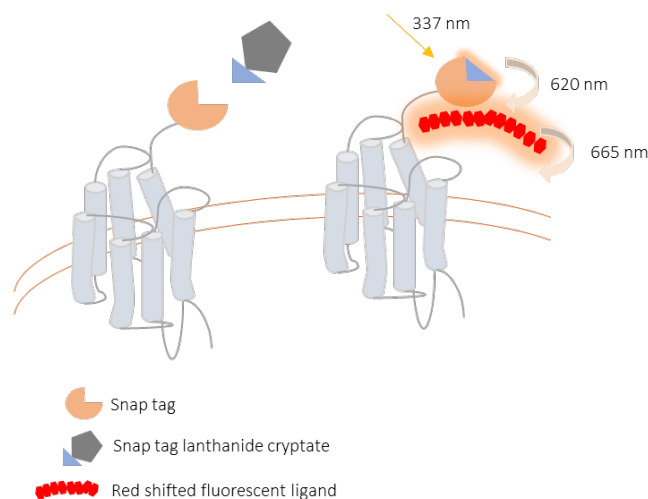
Figure 4.1. TR FRET for studying fluorescent ligand binding at SNAP-tagged GPCRs. SNAP tags are labelled with lanthanide cryptate benzyl guanine substrates (e.g. terbium) that serve the donor of fluorescence. The terbium donor is excited by a laser light source at 337 nm; one of its emission peaks at 620 nm is appropriate for the excitation of a far-red fluorescent ligand (e.g. AF647 conjugate) that in turn emits fluorescence picked at 665 nm. The ratio of acceptor emission over donor emission (620/665 nm) is taken as FRET ratio representing specific ligand binding.

4.1.4 Equilibrium and kinetics assays for the study of ligand binding at GPCRs

There are several types of experiments designed to study the binding of ligands at GPCRs. The analysis of each of these methods is described in more

detail in chapter 2 and thoroughly discussed in some published reviews (Hulme and Trevethick, 2010b), (Sykes et al., 2019a), (Hoffmann *et al.*, 2015).

The binding properties of labelled ligands (for example a fluorescent tracer), can be analysed in two main types of experiment. In saturation binding experiments, the binding of an increasing concentration of a labelled ligand is measured at equilibrium and analysed to extract its equilibrium dissociation constant (Kd) as well as the maximum binding of the tracer Bmax, which represents the density of receptor sites. When using homogeneous fluorescent binding methods, the association kinetics of different concentrations of fluorescent tracer can be recorded over time. From the family of association kinetic curves, association, and dissociation rates (kon, kon) and the kinetically derived affinity (Kd) can be obtained, where the binding mode is to a single site receptor population (since under these conditions the observed association rate kobs = kon [FL] + koff). Finally, dissociation of the tracer-receptor complex can be initiated by limiting dilution or the addition of an excess unlabelled competitor (Sykes and Charlton, 2018). The analysis of this type of assay yields the dissociation rate of the tracer and demonstrates the reversibility of tracer binding.

The affinity of unlabelled ligands can be quantified using competition binding assays where the binding of a single concentration of a labelled ligand is measured in the presence of increasing concentration of unlabelled competitor at equilibrium. The analysis of equilibrium competition binding data yields the half-maximum inhibitory concentration IC50 which can be corrected for tracer concentration and affinity through the Cheng-Prusoff equation to yield the unlabelled ligand equilibrium dissociation constant Ki. This conversion assumes labelled and competing ligands bind at the same receptor site. The kinetics of unlabelled ligands can also be determined in experiments where the labelled and unlabelled compounds are added simultaneously, and association of the fluorescent tracer is recorded over time. The profiles of these association curves depend on the relative kinetic properties of the tracer and competing ligand. These types of assay could be performed when the labelled and unlabelled compounds interact with the

140

same target site and when the labelled ligand kinetic parameters have been previously quantified (Motulsky and Mahan, 1984).

4.1.5 Importance of studying the kinetics of drug binding at GPCRs

The rate of drug-receptor complex formation and its lifetime dictate the duration and efficiency of signal transduction by GPCRs. Therefore, studying the kinetics of ligand-receptor interactions has emerged as an important concept in pharmacodynamics and drug discovery (Hoffmann *et al.*, 2015).

Whilst pharmacokinetics (rates of drug absorption, distribution, metabolism and excretion) largely contributes to drug duration of action and target (Derendorf et al., 2000), the success of certain ligands as therapeutics can be attributed to their slow rate of target dissociation. One of these drugs is tiotropium, the leading drug for the treatment of chronic airway obstructive conditions (Tashkin, 2005). Tiotropium is a muscarinic M3 receptor antagonist with a very similar structure and pharmacokinetics to a previous leading bronchodilating drug - ipratropium. Tiotropium, nevertheless, is characterised by a >24h duration of action, compared to the <6 h for ipratropium based on its much slower dissociation from the M3 compared to ipratropium (Disse et al., 1993). The long duration of action of tiotropium correlates with its slow receptor dissociation kinetics (k_{off} = 0.01 min^{-1}) compared to the one of ipratropium (k_{off} = 2.66 min^{-1}) (Barnes, 2000), (Sykes et al., 2009).

Another wide-known example of a slow-off rate antagonist with long duration of action (136 h) in the clinic is the CCR5 NAM maraviroc used for the treatment of HIV infection (k_{off} = 0.042 min^{-1}) (Lieberman-Blum et al., 2008), (Watson et al., 2005), (Swinney et al., 2014).

The prolonged duration of action for both tiotropium and maraviroc, underlined by the slow kinetics of drug-receptor interactions, is essential in their use for the treatment of chronic conditions such as COPD and AIDS.

Other drugs with correlated slow dissociation and long duration of action are the neurokinin receptor antagonist aprepitant (Lindström et al., 2007), the histamine H1 receptor antagonist desloratadine (Slack et al., 2011), and μ opioid receptor antagonist alvimopan (Cassel et al., 2005).

Another advantage associated with long residence time of drug-receptor complex is the so called 'kinetic selectivity' provided that the drug of interest exerts long-residence time at the target receptor, whilst it binds transiently at collateral proteins that may produce off target effects (Tummino and Copeland, 2008). Tiotropium mentioned above for example dissociates much more slowly from M3 receptors compared M1 and M2 making it kinetically selective compared to Ipratropium (Barnes, 2000). The mechanism of kinetic selectivity of muscarinic antagonists, however, has been challenged with further work showing that NVA237, an M3 receptor antagonist, is more selective than tiotropium based on its faster onset of action (faster k_{on}) and faster k_{off} (Sykes et al., 2012).

Although there are relatively limited examples of ligand koff extending duration of action, beyond that dictated by pharmacokinetic properties, slow koff can also have a crucial impact in determining the efficacy of inhibitors and receptor antagonists through insurmountability (as discussed in chapter 3). Under conditions where the stimulating agonist varies dynamically in concentration (e.g. neurotransmitter at synapse, cytokine burst during inflammation), slow koff antagonists do not rapidly re-equilibrate, leading to insurmountability (depression of the maximal response). This helps maintain target inhibition even under conditions of transiently higher concentrations of the stimulating messenger, which may be beneficial therapeutically (Sykes et al., 2016), (Mould et al., 2014b), (Vanderheyden et al., 2000).

The kinetic effects of drugs on duration of action and efficacy are not solely attributed to the dissociation rates of ligands. For example, recent data have challenged a previous notion that typical antipsychotic extrapyramidal on-target side effects are related to slow D2 koff (Kapur and Seeman, 2001). In fact it is the association rate of antipsychotics that is most clearly correlated with their extrapyramidal adverse-effect profile (Sykes et al., 2017). The study suggested that the fast association of D2R antagonists within the confined environment of synapses, leads to the rebinding of these drugs to the same or nearby receptors. The effect of this rebinding is predicted to increase the local concentration of the antipsychotic within diffusion restricted reservoir of the

142

synapse – thereby enhancing inhibition. Notably the clinical side effect of hyperprolactaemia is still associated with slow koff and proposed insurmountability at pituitary D2 receptors, because in this environment free drug exchange with plasma should occur.

The examples above demonstrate that long duration of action in vivo could be desirable or adverse depending on the effect of the ligand on the biological system, and the physiological context. In the case of receptor antagonism, the mechanism underlying this process would be of importance.

The time agonists need to achieve binding equilibrium is also governed by their koff rates and defines the onset and kinetics of different signalling pathways mediated by them (Klein Herenbrink et al., 2016). This has led to the notion that 'biased' signalling observed for some agonist ligands, could be dependent on the timescale of the assay and change over time (Grundmann and Kostenis, 2017).

4.1.5 Factors influencing ligand binding at GPCRs

The mathematical equations utilised for the analysis of binding data are based on certain assumptions that are not always met in the experimental set-ups or physiological context. One of these assumptions is that the association and dissociation of the drug happens in a single step. The binding of chemokines to chemokine ligands, however, is an example of a multi-step process associated with the sequel interaction of the chemokine ligand first with the N-terminus, and then - the TM pocket of CKRs (see chapter 1) (Perpina-Viciano et al., 2020), (Liu et al., 2020). The ability of chemokine (and other) ligands to dimerise is another factor in making the binding more complex than a single-step matter (Liu et al., 2020), (Kufareva et al., 2015a).

Another example of binding more complex than a single-step process is the interaction of lipophilic ligands with the membrane lipid bilayer prior to reaching the receptor binding pocket. This has been shown for example for the cannabinoid CB2 receptor (Hurst et al., 2010), sphingosine-1-phosphate (S1P) receptor (Hanson et al., 2012) and for the binding of vorapaxar at the protease-activated-receptor-1 (PAR1) (Bokoch et al., 2018).

The interaction of lipophilic ligands with the plasma membrane shown for example for certain β2AR such as salmeterol, creates depots of high concentration of the ligand around the vicinity of the plasma membrane and the receptor (Sykes et al., 2014b), (Gherbi et al., 2018). This influences the measured association rates and kinetically-derived affinity of ligands (Sykes et al., 2014b). Ligands able to rebind the receptors could also contribute to the preservation of the drug in the local receptor environment (Vauquelin and Charlton, 2010a).

As discussed earlier, GPCRs sample multiple conformations and whilst the simple ligand-receptor binding models assume single-site, homogenous receptor population binding, this is more often not the case (Latorraca et al., 2017). The measured on and off rates, and kinetically derived affinities, therefore, reflect a multi-component process that could be to a limited extend explored in binding assays. In addition, the 'induced-fit' mechanism whereupon an initial loose bimolecular interaction between ligand and receptor followed by isomerisation of the complex to a tighter conformation, is suggested relevant for the maintenance of long residence time (Vauquelin, 2015).

Models fitting the binding of ligands to a two-phase process may provide some extra insights into the binding of drugs to different receptor conformations, nevertheless they may be insufficient to account for all possible states and binding modes of ligands (Tummino and Copeland, 2008).

The conformational-driven receptor activation is the basis of the presence of low- and high-affinity agonist binding states of receptors (Hoffmann et al., 2008) and as mentioned in 4.1.1. the formation of the ternary complex upon agonist stimulation or simultaneously, shifts the receptor to a high-affinity agonist binding state (De Lean et al., 1980). The addition of synthetic GTP analogues such as GppNHp in the assay buffer when studying ligand binding especially in isolated membrane preparations (GTP levels in whole cells vs. membranes explained below) is commonly implemented for attempting to study ligand binding at low-affinity receptor conformation as a single receptor population system (Hulme and Trevethick, 2010a), (Sykes et al., 2019b).

144

The presence of a sodium binding pocket which is fairly conserved among class A GPCRS (see chapter 1) underlines the common allosteric modulation of GPCR conformation by sodium cations (Gutié Rrez-De-Terá et al., 2013), (White et al., 2018), (Draper-Joyce et al., 2018), (Friedman et al., 2020)

(Katritch et al., 2014). Molecular dynamics studies at the $A_{2A}R$ show the preference of sodium ions for the inactive receptor conformation which they stabilise upon binding leading to the loss of important agonist-receptor interactions (Gutié Rrez-De-Terá et al., 2013). Another example of many is the reduction of acetylcholine (Ach) potency for the muscarinic receptor M2 (M2R) by sodium ions (Friedman et al., 2020).

The presence or absence of sodium in the assay buffer is another consideration in binding assays and could affect the population of receptor conformations.

Finally, to adequately characterise the binding of labelled and unlabelled ligands at GPCRs, it is important to consider the system in which the assays are conducted. The use of intact cells as opposed to membrane preparations is beneficial due to the fact it mimics the physiological environment closer. Nevertheless, one of the assumptions of the law of mass underlining all equations used to quantify ligand binding, is the equal accessibility of receptors by the ligand which is easily violated when working with whole cells (Kenakin, 2016). This is particularly true when studying the binding of ligands interacting with intracellular binding pockets (Ortiz Zacarías et al., 2018) that may not be able to interact with its target within the timeframe of the assay due to accessibility issues. Furthermore, studying the binding of labelled or unlabelled probes that act as agonists at the receptor becomes challenging if the ligand stimulates receptor trafficking and internalisation leading to changes in receptor number at the plasma membrane and possibly receptor driven ligand intracellular accumulation. Another important difference between intact cells and membrane preparations is that in whole cells the GPCR-G protein complexes are short lived due to the high concentrations of GTP in the cytosol, whereas in membrane preparations the concentration of GTP can be modulated to promote prolonged GPCR-G protein interactions.

4.1.6 Considerations in measuring the effects of allosteric ligands on orthosteric ligand binding kinetics

GPCRs can be modulated by ligands that interacts with sites distinct from the endogenous ligand binding pocket (see chapter 1). As described in chapter 1, allosteric ligand (both NAMs and PAMs) bind could alter the orthosteric ligand affinity, efficacy, or both (May *et al.*, 2007).

The effect of allosteric ligands on ligand binding is attributed to their ability to evoke additional receptor conformations. This could alter the association, dissociation or both rates of the orthosteric ligand which may or may not result in changes in orthosteric ligand binding affinity (Kostenis et al., 1996), (Molderings et al., 2000). Furthermore, allosteric ligands are characterised by probe dependence, therefore they may increase or decrease the residence time of one orthosteric ligand compared to another (May et al., 2007b). The ability of allosteric molecules to alter the binding kinetics of an orthosteric ligand is an important consideration when incorporating unlabelled allosteric ligands in kinetics competition assays and applying the Motulsky-Mahan equation to analyse the data (Motulsky and Mahan, 1984). Allosteric effects on the binding kinetics of endogenous labelled ligands has been demonstrated for many GPCRs. PAMs and NAMs of the adenosine receptor A1 and A3 decreased of increase the dissociation and association rates (k_{on} and k_{off}) of a fluorescent adenosine derivative which had varying effects on agonist affinity and was receptor dependent (May *et al.*, 2010). PAMs of the glutamate receptor mGlu2 decreased the dissociation rates of glutamate and other synthetic receptor agonists, increasing their association rates and increased orthosteric affinities for mGlu2. The NAMs of the receptor altered orthosteric ligand binding kinetics at the receptor but in a probe-dependent way unlike the PAMs (Doornbos et al., 2018). For the CCR1 receptor activated by CCL3 chemokine, PAMs increased the agonist affinity by increased the association rates with little effect on the k_{off} rates of the orthosteric ligand (Jensen et al., 2008).

There are more complex examples such as the modulation of the muscarinic receptor M_2 (mAChR) by the NAM gallamine (Clark and Mitcheson, 1976), (Stockton et al., 1983). Whilst gallamine retards the dissociation of the orthosteric ligand, it also decreases the association rates at lower concentration ranges than those required to increase the orthosteric ligand residence time at receptors, thus decreasing binding affinity as a net effect (Lane et al., 2017).

Naturally, the mode of drug action, relative to the endogenous ligand binding site, should also be considered. As outlined earlier, full inhibition of dopamine action in the striatum is associated with severe adverse effects (Sykes et al., 2017). The ability of allosteric drugs to modulate receptor function without fully inhibiting the action of the endogenous ligand is an alternative mechanism heavily researched in the field of drug discovery and its applications in combination with 'infinite residence time' has been recently explored with the design of covalent negative allosteric modulators (NAMs) of the chemokine receptor CCR2 (Ortiz Zacarías et al., 2021).

4.1.7 Aims of the chapter

In this chapter, we characterised the binding of CXCL8 - AF647, a fluorescent CXCL8 probe labelled with AF647 fluorophore at a C-terminal lysine residue, to the CXCR2 receptor using confocal imaging and TR-FRET binding approaches. We demonstrated high affinity binding of the tracer to the CXCR2 receptor and quantified its kinetic properties in both whole cells and membrane preparations. We then used these fluorescent ligand binding systems to further investigate the mechanism of action of different CXCR2 NAMs, focussed on their influence on the labelled chemokine affinity and kinetics.

4.2 Results

All ligand binding experiments were performed in whole cells or membrane preparations containing N-terminally SNAP-tagged human CXCR2 receptors modified with double 6xHistidine tag at the C terminus. The N-terminal SNAP tag allowed for visualising the receptors and performing ligand-binding experiments using imaging approaches; furthermore, the SNAP-tag was utilised was for the TR-FRET binding experiments for terbium labelling acting as a donor of fluorescence. The histidine tag was added to allow for future purification of solubilised receptor preparations.

4.2.1 High-content imaging approaches to monitor fluorescent ligand binding

The binding of CXCL8-AF647 was first probed in whole HEK293T cells expressing SNAPCXCR2His receptor using high-content imaging approaches. Cells were treated with a range of concentrations of the tracer with or without the addition of 20 nM unlabelled CXCL8 (28-99) and 2 µM SB265610 to define non-specific binding and the binding was recorded for 60 minutes at 5 different time points (10, 20, 30, 50, and 60 minutes) at room temperature. At 20 minutes the binding of CXCL8-AF647 was detected at the cell surface overlapping with the location of the receptor, and at 50 minutes – the tracer was detected intracellularly (figures 4.2, 4.3, 4.4). The binding of CXCL8-AF647 was fully displaced by 20 nM cold CXCL8 (28-99) (Figures 4.3, 4.4). The fluorescent intensity of the images was quantified using a granularity algorithm allowing the identification of fluorescent granules (fluorescent ligand) primarily on the cell membrane but also intracellularly (Kilpatrick et al., 2010), and plotted as saturation binding curves (figure 4.4) to extract the affinity of CXCL8-AF647 at each recorded time-point – this was 26.9 nM (20 minutes) and 4.16 nM (50 minutes) (table 4.1; figure 4.4.).

4.2.3 Functional characterisation of CXCL8-AF647 in Split Luciferase complementation assay

A range of concentrations of CXCL8-AF647 were tested in their ability to stimulate CXCR2-arrestin interactions in whole HEK293T cells. The tracer was functional as it stimulated receptor-arrestin interactions with potency (pEC50) of 7.35 ± 0.03 (n=2) which was lower than that previously found for the unlabelled CXCL8$_{28-99}$ (see chapter 3) (figure 4.5).
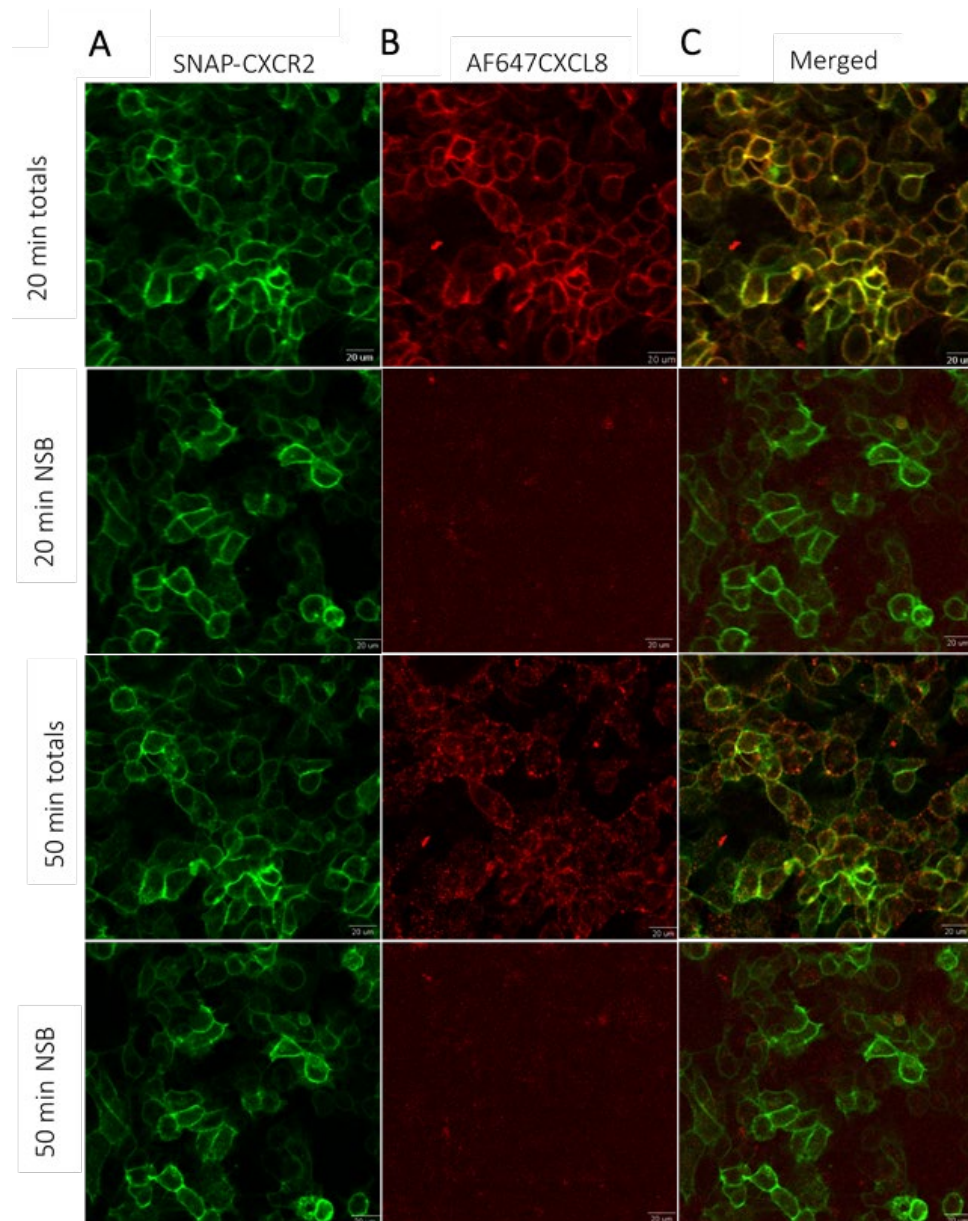
Figure 4.2 The binding of AF647CXCL8 in whole HEK293T cells expressing SNAP-CXCR2-His. (A) SNAP tags were labelled with cell impermeable SnapSurface AF488 (green) to visualise the CXCR2 receptors (B) The binding of 10 nM AF647CXCL8 alone (totals) or pre-treated with 20 nM cold CXCL8 (28-99) (NSB) is shown in red. (C) Merged images of AF488-labelled SNAPCXCR2His receptors and AF647CXCL8 in wells pre-treated with vehicle (totals) or 20 nM cold CXCL8 (28-99) to define non-specific binding (NSB) at 20- and 50 minutes post-tracer addition. Images were acquired using the IX Ultra confocal plate reader (Molecular Devices).

20	10	5	2.5	1.3	0.7	0.4	0.2	0.1	0

A

B
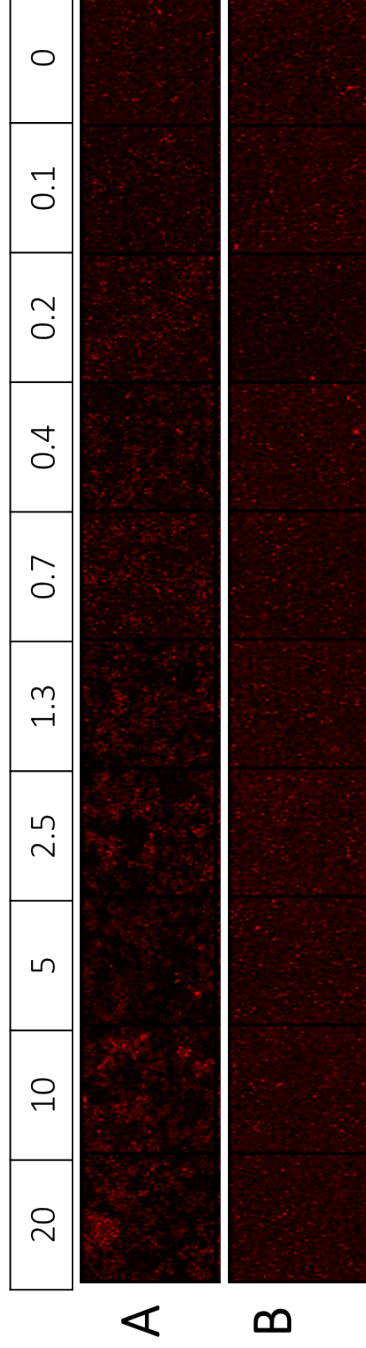
Figure 4.3 The binding of CXCL8-AF647 in whole HEK293T cells. Montage thumbnail images of CXCL8-AF647 saturation binding in cells expressing SNAP-CXCR2-His receptors, at the indicated concentrations (nM) (A) Total binding of tracer (B) Binding in wells treated with 20 nM cold CXCL8 (28-99) to define non-specific binding. Images were taken at 20 minutes post tracer addition and room temperature incubation.

Time (minutes)	CXCL8-AF647 pKd
20	7.57 ± 0.31
30	8.12 ± 0.05
50	8.38 ± 0.09
60	8.44 ± 0.12

Table 4.1 Binding affinity of CXCL8-AF647 at SNAPCXCR2His receptors measured using high-content imaging approaches. The affinity of CXCL8-AF647 (pKd) obtained quantifying the fluorescence intensity of images at different time points using granularity algorithm (MetaXpress); data represent mean ± S.E.M. pooled from 3 individual experiments.
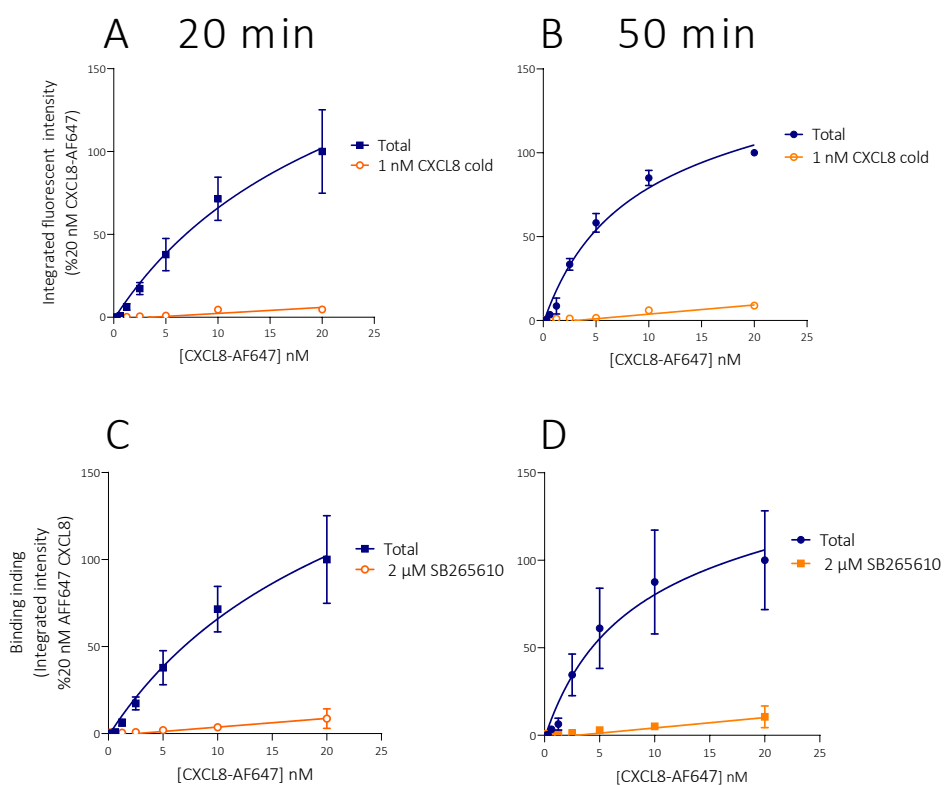
Figure 4.4 Saturation binding of CXCL8-AF647 in whole-cells measured using high-content imaging approaches. A range of tracer concentrations were added with or without pre-treating the cells with cold $CXCL8_{28-99}$ or SB265610 to define non-specific binding (NSB). The blue curves show the total binding of the tracer including specific + non-specific and the orange lines – the non-specific binding of the tracer defined by the unlabelled compounds. The graphs represent pooled data from 3 experiments; error bars = S.E.M.
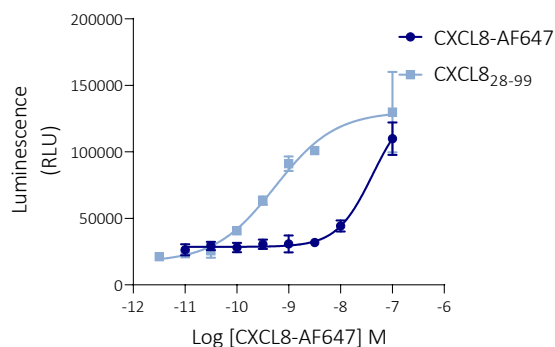
Figure 4.5 Functional characterisation of CXCL8-AF647. The fluorescent tracer was probed in the NanoBiT CXCR2-arrestin recruitment assay to test its potency and compare it to cold CXCL8$_{28-99}$ chemokine. The graph is combined data from two separate experiments for the sake of comparing the fluorescent and cold chemokines; both concentration-response curves are taken 30 minutes following agonist addition. Data represent a single experiment perfumed in duplicate; error bars = S.D.

4.2.4 CXCL8-AF647 binding to SNAP-CXCR2-His receptors in whole cells detected by TR FRET

The binding of CXCL8-AF647 was further characterised in whole HEK293T cells using TR-FRET technology. The tracer was run under room temperature conditions and in this whole-cell kinetics set up – under LabMed (CisBio) buffer conditions. A range of tracer concentrations with or without 1 μM cold CXCL8$_{28-99}$ added to cells and the binding was recorded kinetically. The binding of the tracer did not reach a plateau but instead increased over the 70 minutes of the kinetic reads, with potentially two phases of association. To explore this in more detail, the data from 0 to 20 minutes post-tracer addition were globally fitted to a model of association kinetics (figure 4.6, B), or each tracer concentration individually fitted to a one- (figure 4.6, C) or two-phase (figure 4. 6 D) association and quantified. Using a single phase globally fitted association model, the following estimates for CXCL8-AF647 were obtained at CXCR2 - k_{on} 1.03 ± 0.32 x 10^7 $M^{-1}min^{-1}$, k_{off} 0.35 ± 0.18 min^{-1}, and kinetically derived affinity (pK_d) 7.53 ± 0.21 (n = 3). However, this single phase fit poorly

modelled the data, and fitting was improved by including two kinetic components (Figure 4.6 D). The decision to fit the data using two kinetic components was also supported by conducting F tests that supported using the more-complex two-phase association fit (F ratios >>> 1, p << 0.05). Similar conclusions were made by considering individual fits to each tracer concentration and exploring the relationship between k_{obs} and [CXCL8-AF647] (Figure 4.7, Table 4.2). The association parameter data for each tracer concentration were individually plotted to a single-phase association model (figure 4.6, A) or a two-phase association model (figure 4.6, B, C, D; table 4.2). The fast and slow observed rates broadly increased with increasing ligand concentration, nevertheless, more data points are necessary to fully define their increase pattern (figure 4.7, B, C). Similarly, the ligand fast fraction was higher for higher ligand concentrations without following a strict linear increase (figure 4.7, D)
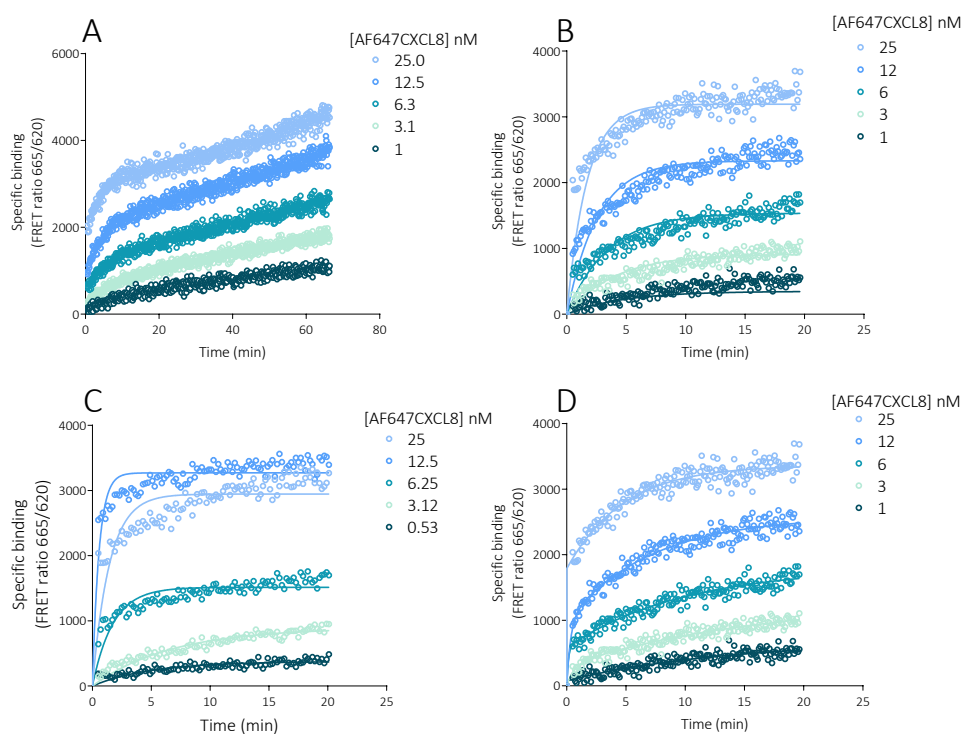
Figure 4.6 Association kinetics binding of CXCL8-AF647 at SNAPCXCR2His receptor in whole HEK293T cells measured using TR FRET. (A) Concentration range of AF647CXCL8 binding at Tb-labelled SNAPCXCR2His cells over 70 minutes. (B) Data globally fitted to a model of association kinetics binding. (C) Data fitted to a model of one-phase association model; (D) Data fitted to a model of two-phase association model representative data from a single experiment. The graphs contain representative data from single experiments.

	25 nM	12.5 nM	6.25 nM	3.13 nM
Fast fraction (%)	56.81 ± 7.01	52.78 ± 8.18	32.14 ± 8.30	20.69 ±5.68
kob_{fast} (min^{-1})	3.00 ± 0.57	4.66 ± 1.56	3.30 ± 0.70	3.03 ± 0.75
kob_{slow} (min^{-1})	0.35 ± 0.14	0.14 ± 0.03	0.07 ± 0.02	0.05 ± 0.01

Table 4.2 Pseudo first-order association kinetics of CXCL8-AF647 in whole cells extracted from two-phase association kinetics binding model. Pseudo first-order association constant kob (min^{-1}) represents the association kinetics of the tracer for each individual concentration. In two-phase association model, the association is composed of a fast and a slow phase each characterised by association rate constants per individual ligand concentration kob_{fast} (min^{-1}) and kob_{slow} (min^{-1}). Data represents means ± S.E.M. pooled from 3 individual experiments.
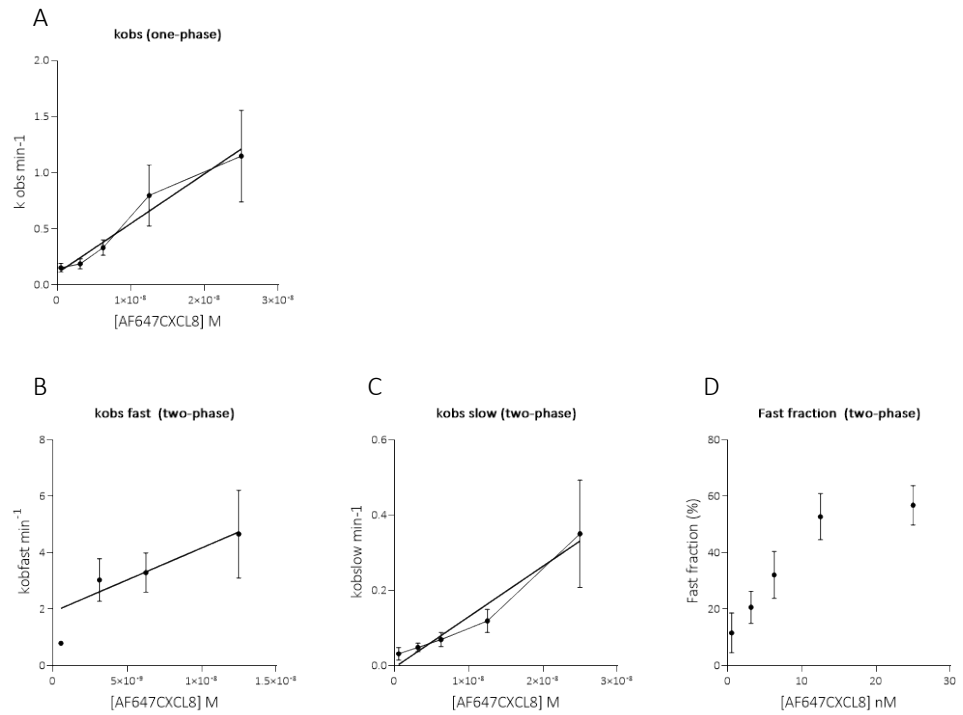
Figure 4.7 The relationship between observed kinetic components and CXCL8-AF647 concentration, estimated by two phase (B – D) or one phase (A) association fitting in whole cell kinetics experiments. (A) K_{ob} plot against tracer concentration extracted from a single-phase association fit; (B) The fast k_{ob} plot against tracer concentration extracted from a two-phase association fit; (C) The slow k_{ob} plot against tracer concentration extracted from a two-phase association fit; (D) The fraction of ligand accounting for the fast association phase (percentage fast) against tracer concentration; Graphs represent mean values from 3 individual experiments; error bars = S.E.M.

155

4.2.5 CXCL8-AF647 binding in membrane preparations detected by TR-FRET

4.2.5.1 Association kinetic binding measurements using CXCL8-AF647 in membranes

To avoid receptor driven internalisation of the tracer, that might be a confounding factor in whole cell measurements, the binding of CXCL8-AF647 was further probed in membrane preparations from terbium labelled HEK293T cells expressing SNAPCXCR2His receptors, initially using HBSS based assay buffer. Measuring binding of CXCL8-AF647 in membrane preparations should also remove the issue of intracellular ligand accumulation and bystander TR-FRET in endosomes. Indeed, under these conditions a specific binding plateau was rapidly (< 20 min) reached at each tracer concentration (Figure 4.8). However, the overall level of specific binding in membranes in HBSS-based buffer conditions was low, limiting the degree to which reliable estimates of binding kinetics could be obtained (Figure 4.8).

As a consequence, CXCL8-AF647 binding to SNAP-CXCR2 membrane preparations was explored in an alternative binding buffer (25 mM HEPES, 1 mM $MgCl_2$, 0.1% BSA, 0.1 mg/ml saponin, 0.02% Pluronic acid), also at RT– in particular to investigate whether the reduced Na^+ concentration within this buffer improved the level of specific binding of the agonist fluorescent ligand (Katritch et al., 2014). The removal of sodium ions from the buffer led to higher levels of CXCL8-AF647 specific binding over time in the TR-FRET membrane assay, and an improved assay window to allow study of the influence of unlabelled ligands on tracer binding in further experiments. Therefore, the low Na^+ binding buffer was selected for all membrane-based TR FRET binding assays.

Under low Na^+ buffer conditions the association binding of a range of tracer concentrations was examined kinetically and data were both globally fitted to a model of single-phase association (figure 4.9, A) as well as individually to one- (figure 4.9, B) and two-phase (figure 4.9, C, table 4.3) association kinetics

fits. The association kinetics constant (kon), dissociation kinetics constant (koff), and kinetically derived affinity (pKd) of the tracer derived from the global single-phase association fit were $1.65 \times 10^7 \pm 0.24$ $M^{-1}min^{-1}$, 0.20 ± 0.03 min^{-1}, and 7.90 ± 0.07 respectively. The tracer did not bind to receptor with k_{obs} proportional to is concentration but similarly to whole cells, the fast proportion of the ligand was higher at higher concentrations (figure 4.9).

The on and off rates, and kinetically derived affinity of the tracer were generally similar to that found in whole cells (p = ns for each parameter mentioned tested by unpaired Student's t test). The percentage of fast ligand at 25 and 20 nM and 10 and 12.5 nM in whole cell and membranes was also similar (p = ns; tested by unpaired Student's t test).

The binding of CXCL8-AF647 fitted better to a two-phase association model suggesting the existence of multiphasic binding of the tracer. To investigate this further a high concentration of a non-hydrolysable GTP analogue that uncouples receptors from G proteins (100 μM GppNHp) was incorporated in the assay by pre-treating membranes with it for 60 minutes prior to tracer addition (figure 4.11). The rationale for this experiment was that the presence of GppNHp would help disrupt a high affinity CXCL8-AF647 – CXCR2 – G protein ternary complex (De Lean et al., 1980). However, the presence of 100 μM GppNHp didn't significantly alter the profile of CXCL8-AF647 association kinetics observed in low sodium buffer, nor change the overall level of tracer specific binding observed (Figure 4.11; table 4.4); (p=ns; tested by unpaired Student's t test).
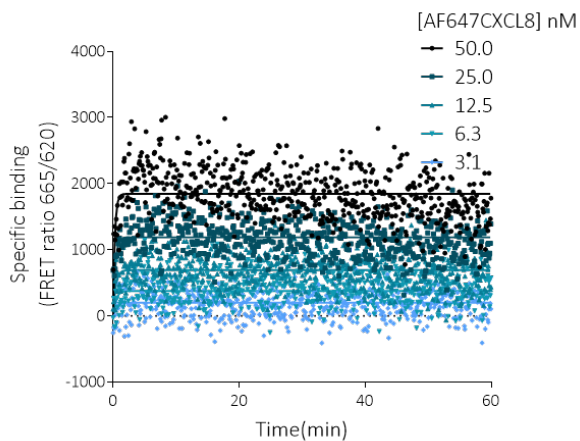
Figure 4.8 Association kinetics binding of CXCL8-AF647 at SNAPCXCR2His receptor in membrane preparations measured using TR FRET in HBSS-based buffer. (A) Concentration range of CXCL8-AF647 binding at Tb-labelled SNAPCXCR2His expressing membranes over time. The graph is a representative from a single experiment.
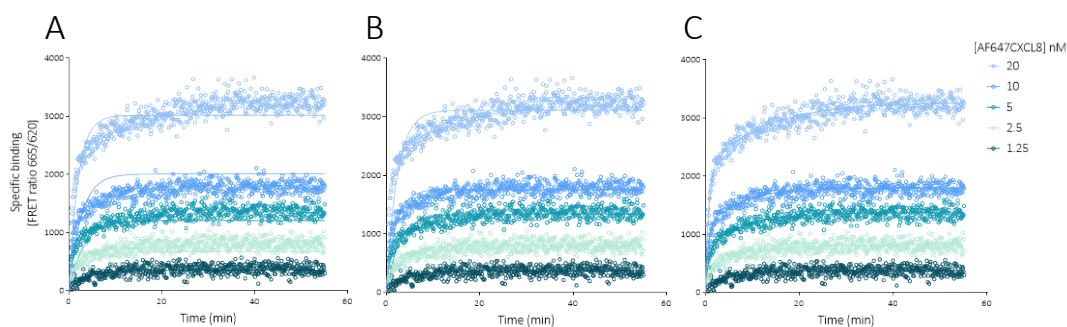
Figure 4.9 Association kinetics binding of CXCL8-AF647 at SNAPCXCR2His receptor in membrane preparations measured using TR FRET in low Na⁺ - assay buffer. (A) CXCL8-AF647 binding globally fitted to a model of single-phase association kinetics (B) CXCL8-AF647 binding curves individually fitted to a single-phase association kinetics model (C) CXCL8-AF647 binding fitted to a two-phase association kinetics model; Graphs show the same representative individual experiment, from n>3.

	20 nM	10 nM	5 nM	2.5 nM	1.25 nM
Fast fraction (%)	59.31 ± 4.16	55.02 ± 6.10	51.82 ± 2.30	45.81 ± 6.53	35.30 ± 8.58
Kob_{fast} (min^{-1})	1.70 ± 0.22	1.70 ± 0.22	1.09 ± 0.29	2.20 ± 0.43	2.24 ± 0.56
Kob_{slow} (min^{-1})	0.06 ± 0.01	0.09 ± 0.02	0.09 ± 0.03	0.11± 0.02	0.12 ± 0.02

Table 4.3 Association kinetics of AF647CXCL8 in membranes using a a two-phase binding model independently for each tracer concentration In the two-phase association model, the association is composed of a fast and a slow phase each characterised by individual association rate constants $k_{obsfast}$ (min-1) and $k_{obsslow}$ (min-1), with the proportions for each component estimated by (% fast) Data represent mean ± S.E.M. pooled from >3 individual experiments.
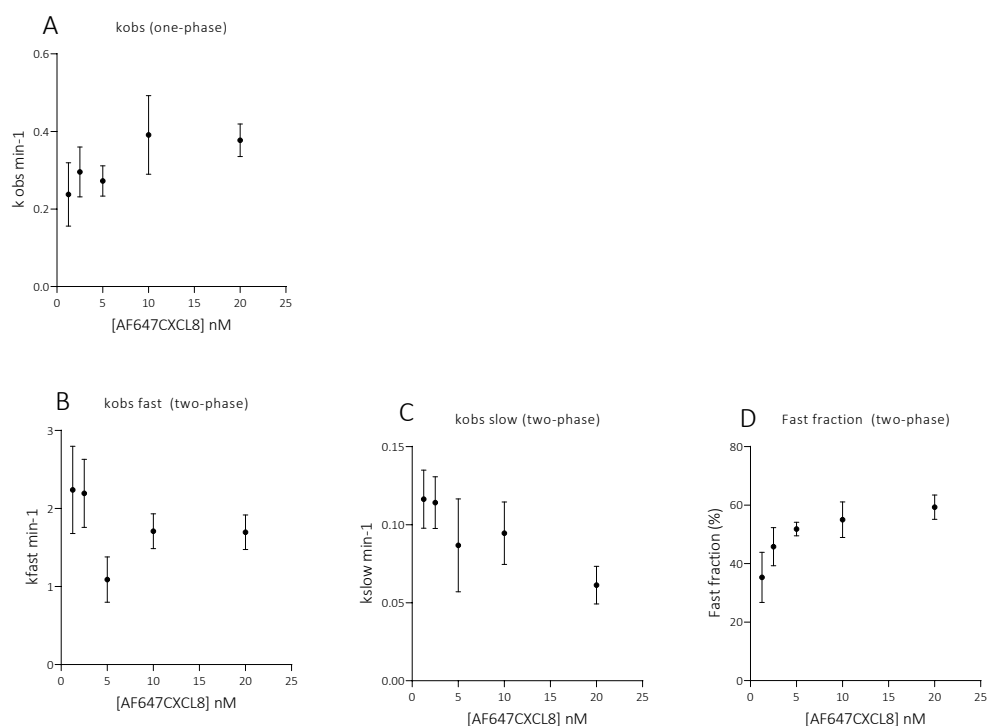
Figure 4.10 The relationship between observed kinetic components and AF647CXCL8 concentration, estimated by two phase (B – D) or one phase (A) association fitting in whole cell kinetics experiments. (A) K_{obs} plot against tracer concentration extracted from a single-phase association fit; (B) The fast k_{ob} plot against tracer concentration extracted from a two-phase association fit; (C) The slow k_{obs} plot against tracer concentration extracted from a two-phase association fit; (D) The fraction of ligand accounting for the fast association phase (percentage fast) against tracer concentration; Graphs represent mean values from 3 individual experiments; error bars = S.E.M.

Figure 4.11 Association kinetic binding of AF647CXCL8 alone or with GppNHp, in low sodium buffer. Membranes were pre-treated with vehicle or 100 µM GTP non-hydrolysable analogue (GppNHp) for 60 minutes prior to tracer (10 nM) addition, prior to recording tracer association kinetics. The graph is a representative experiment, from n = 3.

	Control	100 uM GppNHp
Fast fraction (%)	35.88 ± 2.08	33.96 ± 2.81
Kob_{fast} (min^{-1})	1.67 ± 0.16	1.90 ± 0.19
Kob_{slow} (min^{-1})	0.02 ± 0.01	0.01 ± 0.003

Table 4.4 Association kinetics of AF647CXCL8 in membranes with or without GppNHp addition using a a two-phase binding model. In the two-phase association model, the association is composed of a fast and a slow phase each characterised by individual association rate constants k_{obfast} (min^{-1}) and k_{obslow} (min^{-1}), with the proportions for each component estimated by the fast fraction (% fast) Data represent mean ± S.E.M. pooled from =3 individual experiments.

4.2.3.2 Estimates of CXCL8-AF647 kinetic binding parameters from TR-FRET dissociation kinetics experiments in membranes

To further explore the multi-component nature of CXCL8-AF647 binding to the SNAP-CXCR2-His receptor and validate kinetic parameter estimates, we developed a protocol to measure the dissociation of the tracer directly in low sodium buffer at room temperature. CXCL8-AF647 dissociation was measured by recording the association of a single tracer concentration (10 nM, to plateau

160

at 20-40 min) followed by the addition of a high concentration of unlabelled competitor – 1 µM CXCL8$_{28-99}$– to prevent re-binding of the tracer (figure 4.12, A). As before, a single-phase model provided a limited goodness of fit to the data and so the dissociation component of the data was modelled using a two-phase decay– providing estimates of fast and slow dissociation rate constants for the tracer (figure 4.12, B). The decision to fit the data using two kinetic components was also supported by conducting F tests that supported using the more-complex two-phase association fit (F ratios >>> 1, p << 0.05). The two-phase decay model yielded $k_{offslow}$= 2.07 ± 1.04 min^{-1}, $k_{offslow}$= 0.04 ± 0.01 min^{-1}, and 56.8 ± 6.5 % fast fraction of the ligand (figure 4.12, B) which agrees with the kinetics data derived from association kinetics experiments. The addition of GppNHp (1 mM) did not shift the dissociation of CXCL8-AF647 from CXCR2 to a single-phase, nor significantly affected the dissociation kinetics of the tracer with the two-phase decay fit providing similar values for the slow and fast components of the dissociation figure 4.12; table 4.5).
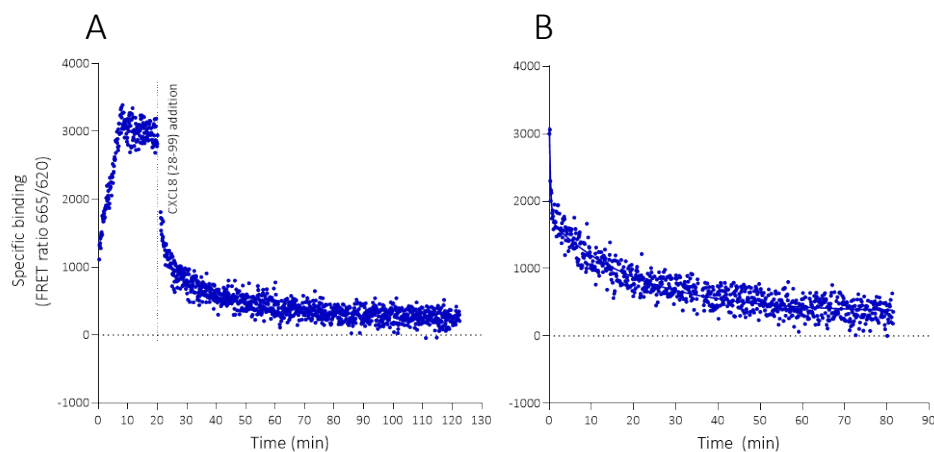
Table 4.12 Dissociation kinetics of AF647CXCL8 at SNAPCXCR2His in membrane preparations measured using TR FRET in low Na$^+$ buffer. (A) The binding of 10 nM AF647CXCL8 before and after the addition of 1 µM unlabelled CXCL8$_{28-99}$ (B) The binding of 10 nM CXCL8-AF647 after the addition of 1 µM unlabelled CXCL8 fitted to a two-phase decay model; graphs are representative of one individual experiment of 5.
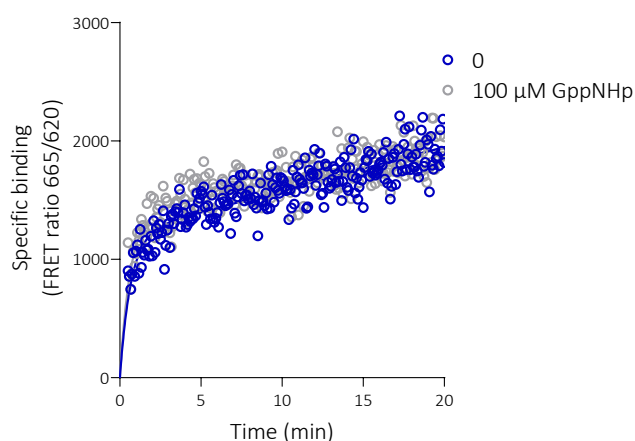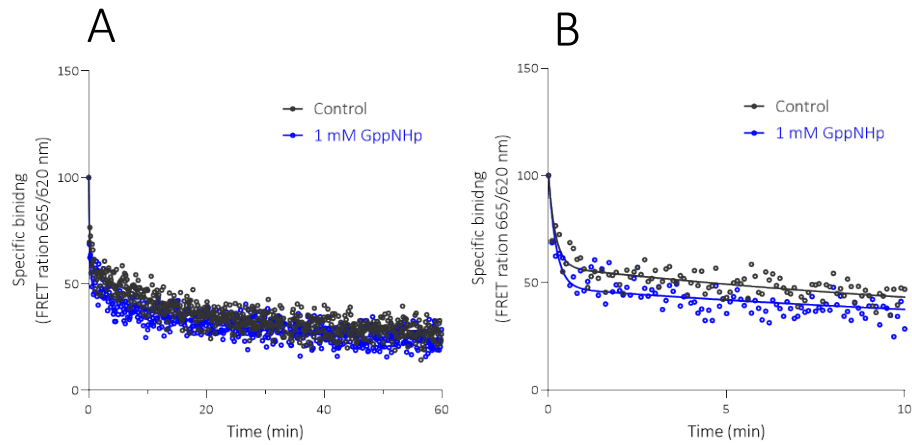
Figure 4.12 Dissociation kinetics of AF647CXCL8 at SNAPCXCR2His receptor in membrane preparations measured using TR FRET in low Na+ buffer. The binding of 10 nM AF647CXCL8 after the addition of 1 μM unlabelled CXCL8$_{28-99}$ was measured kinetically in membranes pre-treated for 60 minutes with 1 mM GppNHp or buffer. A) shows the full timecourse of AF647CXCL8 dissociation (normalised as % of binding counts prior to CXCL8 (28-99) addition and B) the fast phase up to 10 minutes post competitor addition. Graphs are representative of a single experiment, from n = 5.

	Control	1 mM GppNHp
Fast fraction (%)	56.8 ± 6.48	65.53 ± 2.17
$k_{offfast}$ (min^{-1})	6.50 ± 2.15	5.19 ± 1.05
$k_{offslow}$ (min^{-1})	0.058 ± 0.005	0.053 ± 0.006

Table 4.5 Dissociation kinetic parameters for 10 nM AF647CXCL8, measured in membranes with or without 1 mM GppNHp pre-treatment for 60 min. Data represent means ± S.E.M. from 5 individual experiments. Values in the presence of 1 mM GppNHp were not significantly different from control (Student's t test).

4.2.3.3 Tracer competition binding with cold CXCL8$_{28-99}$

Next, the ability of cold CXCL8$_{28-99}$ to compete for binding with CXCL8-AF647 was measured in equilibrium competition binding assay. CXCL8$_{28-99}$ fully displaced 10 nM CXCL8-AF647 binding from CXCR2 receptors with high affinity, with estimates stable from $1-5$ h indicating equilibrium had been reached (figure 4.13, table 4.6). In line with the lack of effect of GppNHp on kinetic tracer measurements, this nucleotide analogue had no concentration-dependent effect on CXCL8-AF647 chemokine binding in low sodium buffer, over time periods up to 5 h (figure 4.13).
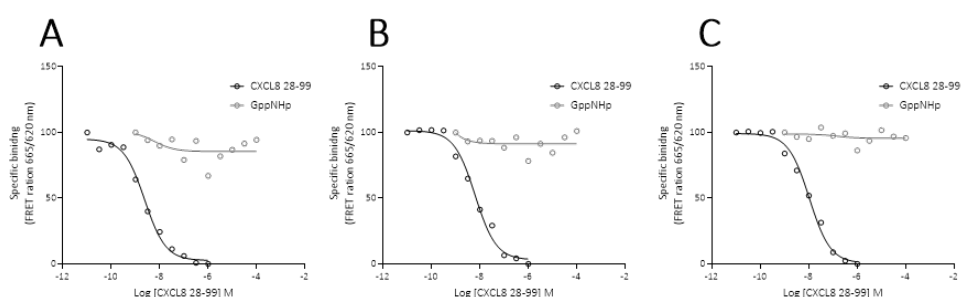
Figure 4.13 Competition binding assay using CXCL8-AF647, comparing unlabelled CXCL8$_{28-99}$ and GppNHp in low-sodium buffer. Membranes were pre-treated for 30 minutes with a concentration range of cold CXCL8$_{28-99}$ (black circles) of GppNHp (grey circles) and 10 nM of CXCL8-AF647 and end-point binding reads were taken at 1 (A), 3 (B), and (C) 5 hours. Graphs are representative single experiments performed without replicates from n > 4.

Time point (hour)	1	2	3	4	5
CXCL8$_{28-99}$ pKi	8.61 ± 0.09	8.36 ± 0.10	8.44 ± 0.28	8.13 ± 0.28	7.91 ± 0.10

Table 4.6 Affinity (pKi) of CXCL8$_{28-99}$ estimated from 10 nM CXCL8-AF647 competition binding studies in SNAP-CXCR2-His membranes and low sodium buffer. Data represent mean values ± S.E.M. from n > 4 experiments at each time point post tracer addition. The pKi values were derived from IC50 estimates using Cheng-Prusoff correction.

4.2.4 Effect of CXCR2 NAMs on CXCL8-AF647 binding in whole cells and membrane preparations

4.2.4.1 Equilibrium competition binding studies in membrane preparations

Following the characterisation of the fluorescent chemokine tracer and its competition by orthosteric ligands and GppNHp, the representative intracellular NAMs of CXCR2 used in Chapter 3 (SB265610, AZ10397767, R-navarixin, S-navarixin, and AZD5069) were probed for their ability to directly influence AF647 chemokine tracer binding. The effect of NAMs on CXCL8-AF647 binding was first investigated through the use of equilibrium and kinetic TR-FRET based assays in membrane preparations containing SNAPCXCR2His receptors and in the low sodium buffer conditions.

Tb-labelled CXCR2 membranes were pre-treated with a concentration range of unlabelled CXCL8$_{28-99}$ or SB265610, AZ10397767, R-navarixin, S-navarixin, AZD5069 NAMs and the binding of 10 nM CXCL8-AF647 was recorded in an end-point manner between 1 to 5 hour time points. None of the NAMs tested caused full inhibition of the tracer binding. Furthermore, measures of affinity (as Ki) could not be directly estimated from the IC$_{50}$s Cheng-Prusoff correction which assumes competitive interactions (figure 4.14). The order of maximal inhibition of tracer binding each NAM achieved relative to (CXCL8$_{28-99}$) is as follows AZD5069, AZ10397767, R-navarixin and SB265610, S-navarixin (from high to low) (table 4.7).

To investigate whether the low sodium conditions reduced the effect of the NAMs, the ability of NAMs and also GppNHp to compete for binding with CXCL8-AF647 was also assessed in high sodium HBSS-based buffer (figure 4.15). The NAMs still did not achieve full displacement of the tracer binding. Nevertheless, both SB265610 and R-navarixin produced higher maximal inhibition of tracer binding in Na$^+$ - rich compared to Na$^+$ - low conditions (p ≤ 0.01 and p ≤ 0.05 respectively; measured by unpaired Student's t test for each NAM pair).

Notably, GppNHp produced an increased level of displacement of CXCL8-AF647 in the Na^+- rich HBSS assay environment compared to low Na^+ buffer conditions (figure 4.14).
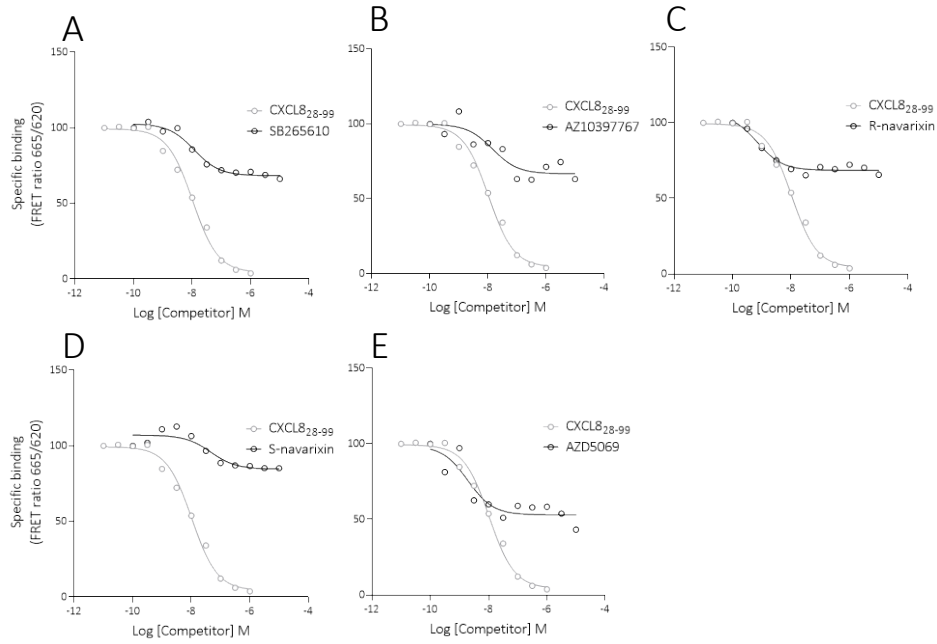
Figure 4.14 Equilibrium competition binding of NAMs and CXCL8-AF647 in low Na⁺ buffer. The inhibition by A) SB265610, B) AZ10397767, C) R-navarixin, D) S-navarixin, and E) AZD5069 of 10 nM CXCL8-AF647 binding relative to unlabelled CXCL8$_{28-99}$ (black curves) at 5 hours post tracer addition. Graphs are a representative single experiment (from n > 4) without replicates, normalising the data to 10 nM CXCL8-AF647 binding without inhibitor.
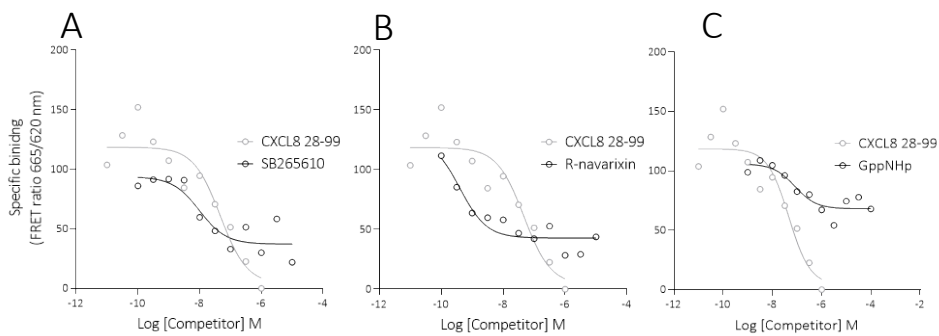
Figure 4.15 Equilibrium competition binding of NAMs, GppNHp and CXCL8-AF647 in HBSS-based buffer. The competition of A) SB265610, B) R-navarixin, C) GppNHp, relative to cold CXCL8$_{28-99}$ (black curves) at 5 hours post tracer (25 nM) addition. Graphs are representative from a single experiment (from n = 2).

CXCL8	SB265610	AZ10397767	R-navarixin	S-navarixin	AZD5069	GppNHp
Low Na$^+$ pIC$_{50}$						
7.65 ± 0.09	7.91 ± 0.32	8.01 ± 0.40	8.60 ± 0.60	6.72 ± 0.29	8.59 ± 0.13	6.50 ± 0.50
Low Na$^+$ Maximal inhibition (% CXCL8$_{28-99}$)						
100.0	32.20 ± 1.56	41.75 ± 9.86	32.75 ± 5.92	28.20 ± 6.61	46.00 ± 3.79	14.50 ± 11.50
High Na$^+$ pIC$_{50}$						
7.33 ± 0.17	7.65 ± 0.18		9.40 ± 1.01			5.91 ± 0.59
High Na$^+$ Maximal inhibition (% CXCL8$_{28-99}$)						
100.0	61.50 ± 6.5		74.00 ± 16.00			30.50 ± 5.50

Table 4.7 Inhibitory potencies (pIC$_{50}$) of CXCL8$_{28-99}$, NAMs and GppNHp and maximal tracer binding inhibition of NAMs and GppNHP relative to CXCL8$_{28-99}$ in membrane preparations under low and high Na+ buffer conditions. Inhibitory potencies of cold CXCL8$_{28-99}$, NAMs and GppNHp with 10 nM CXCL8-AF647 in Na$^+$ reduced buffer at 5 hours post tracer addition and maximal inhibition of tracer binding relative to CXCL8$_{28-99}$Data represent mean values ± S.E.M from n > 4 experiments.

Inhibitory potencies of cold CXCL8 (28-99), NAMs and GppNHp with 10 nM CXCL8-AF647 in Na$^+$ rich (HBSS) buffer at 5 hours post tracer addition and maximal inhibition of tracer binding relative to CXCL8$_{28-99.}$ Data represent mean values ± S.E.M from n > 2 experiments.

4.2.4.2 Equilibrium binding studies in the presence of CXCR2 NAMs in whole cells

Whole HEK293T cells stably expressing SNAP-CXCR2-His labelled were labelled with Tb prior to their pre-treatment with unlabelled CXCL8$_{28-99}$ or SB265610, AZ10397767, R-navarixin, S-navarixin, and AZD5069 NAMs and the binding of 30 nM CXCL8-AF647 was recorded in an end-point manner between 30 and 150 minutes. Cold CXCL8$_{28-99}$ and all NAMs fully displaced the binding of the tracer with nanomolar inhibitory potency. Of the NAMs, R-navarixin inhibited tracer binding with the highest, and S-navarixin – lowest inhibitory potencies (pIC50) at most time-points following tracer addition (figure, 4.16; table 4.8). The affinity of CXCL8-AF647 tracer in whole-cell at 60 minutes was estimated to be 5.7 nM (n=1) (saturation binding data not shown) and this estimate was used to derive the affinity of cold CXCL8$_{28-99}$ at 60 minutes following tracer addition using the Cheng-Prusoff correction – pKi = 8.33 ± 0.07 (n = 5). This is a similar to that found for the cold CXCL8$_{28-99}$ in membranes, in low Na$^+$ buffer (table 4.7).
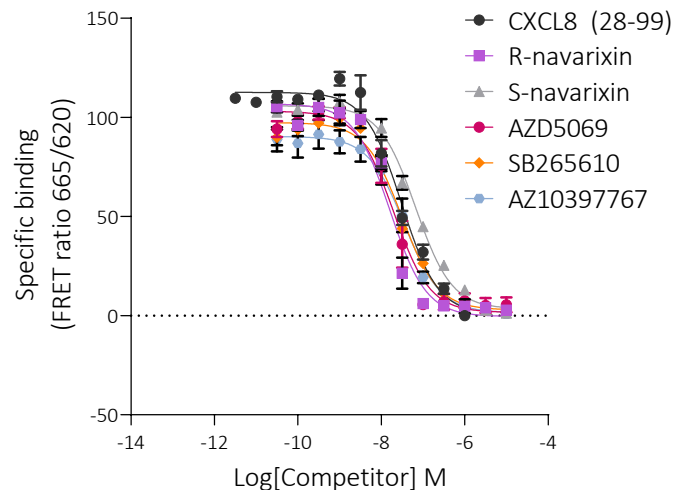
Figure 4.16 Equilibrium competition binding of NAMs and AF647CXCL8 in whole cells, in HBSS-based buffer. The competition and NAMs relative to cold CXCL8 (28-99) (black curve) at 60 minutes post tracer (30 nM) addition. The graph represents pooled data from n = 5 experiments.

pIC50						
Time (h)	CXCL8$_{28-99}$	R-navarixin	S-navarixin	AZD5069	SB265610	AZ10397767
0.5	8.08 ± 0.11	7.90 ± 0.04	7.25 ± 0.09	7.61 ± 0.13	7.82 ± 0.20	7.59 ± 0.13
1	7.63 ± 0.03	7.86 ± 0.01	7.24 ± 0.71	7.70 ± 0.20	7.88 ± 0.40	7.76 ± 0.31
1.5	7.10 ± 0.05	7.91 ± 0.07	7.04 ± 0.10	7.74 ± 0.22	7.61 ± 0.19	7.61 ± 0.15
2.0	6.82 ± 0.03	7.78 ± 0.04	7.09 ± 0.08	7.63 ± 0.20	7.53 ± 0.27	7.49 ± 0.22
2.5	6.05 ± 0.26	7.30 ± 0.52	6.77 ± 0.12	7.47 ± 0.18	7.08 ± 0.09	7.34 ± 0.25

Table 4.8 Inhibitory potencies (pIC50) of CXCL8 (28-99) and NAMs on 30 nM tracer binding in whole cells. Data represent mean values from n = 5 experiments at each time point.

4.2.4.3 Dissociation kinetics of CXCL8-AF647 in CXCR2 membranes, in the absence and presence of unlabelled NAMs

The effect of NAMs on tracer binding to CXCR2 was also assessed kinetically in low dissociation buffer by looking at NAMs effect on the rate of CXCL8-AF647 dissociation. Membranes were pre-equilibrated with a fixed CXCL8-AF647 concentration (10 nM) and dissociation then initiated by the addition of a high concentration (10 µM) of the NAMs - SB265610 (figure 4.17 A), AZ10397767 (figure 4.17, B), R-navarixin (figure 4.17, C) or S-navarixin (figure 14.7 D), compared to unlabelled CXCL8$_{28-99}$ at 1 µM. Each NAM initiated only partial dissociation (to an approximately equivalent level) in contrast to unlabelled CXCL8$_{28-99}$.

169
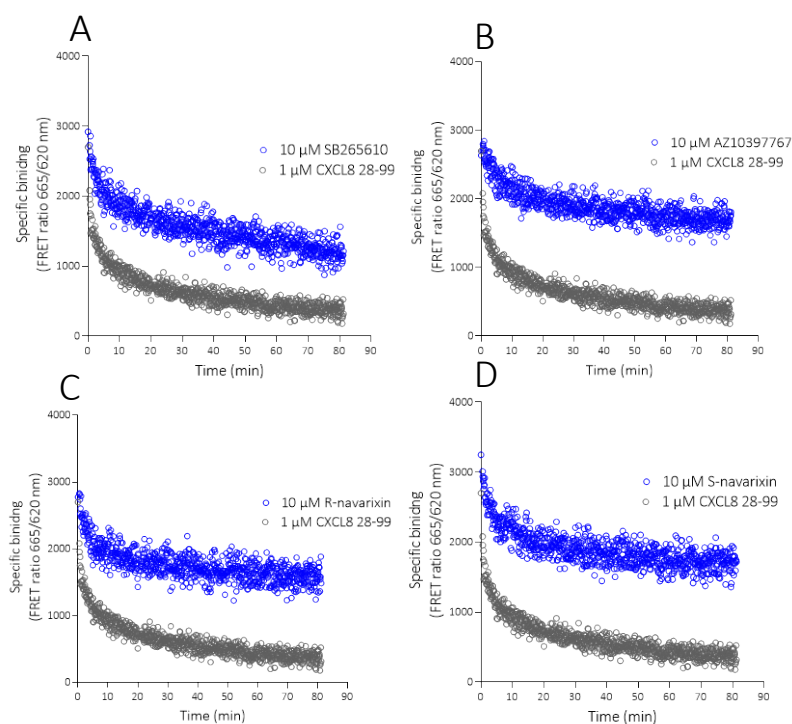
Figure 4.17 Dissociation kinetics of AF647CXCL8 following NAMs or cold CXCL828-99 **addition.** Membranes in low sodium buffer were treated with 10 nM AF647CXCL8 and its specific binding was recorded following the addition of 10 µM A) SB265610, B) AZ10397767, C) R-navarixin, and D) S-navarixin (blue circles) or 1 µM cold CXCL8$_{28-99}$ (grey circles). Data represent a single experiment, from n = 4.

Following these findings, new experiments were designed to test whether NAMs (R-navarixin, SB265610, AZD5069) are able to instead accelerate the rate of tracer dissociation in the presence of 1 µM unlabelled CXCL8$_{28-99}$.

Membranes were pre-treated with the different NAMs at approximately equipotent concentrations in the binding assay (for 60 min) or vehicle, prior to CXCL8-AF647 addition. After equilibrium binding was established (plateau at 20 – 40 min), dissociation was initiated by addition of the unlabelled CXCL8$_{28-99}$. The kinetics of dissociation were then analysed using a model of two-phase decay (figure 4.18, table 4.9). The kinetic constants describing the rate of the fast and slow components were equivalent across conditions, however the proportion of the fast component was significantly increased compared to control in the presence of AZD5069 or R-navarixin, but not SB265610 (Table 4.9).
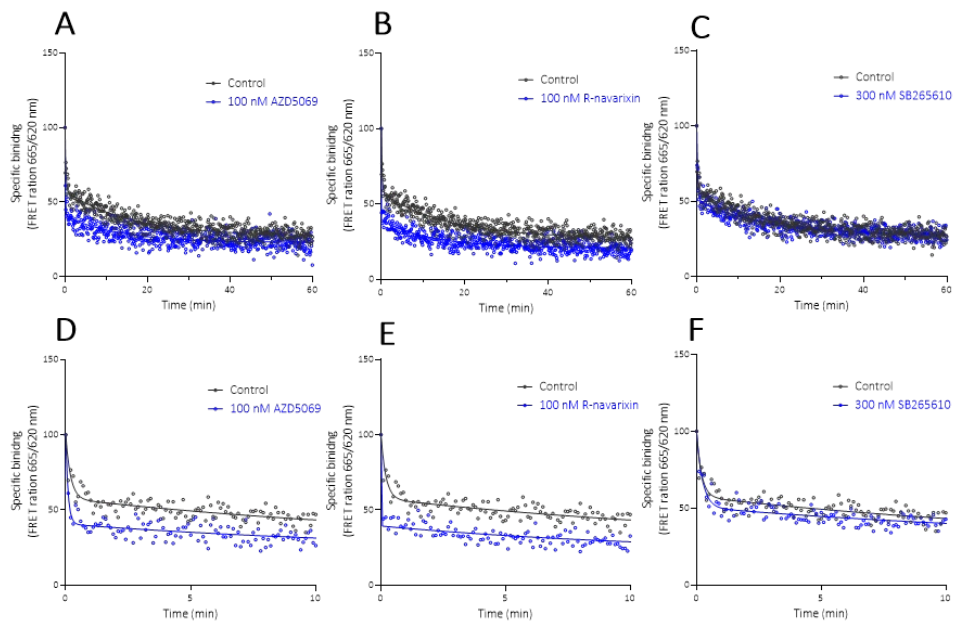
Figure 4.18 Dissociation kinetics of CXCL8-AF647CXCL8 following CXCL8 addition with or without NAM pre-treatment. Membranes were pre-treated with A,D) AZD5069, B,E) R-navarixin, C,F) SB265610 or vehicle 60 minutes prior to 10 nM AF647CXCL8 addition and binding was recorded following the addition of 1µM cold CXCL8. Data were fitted to a two-phase decay model and shown for the whole timecourse or up to 10 minutes post cold CXCL8$_{28-99}$ addition. Graphs are representative for a single experiment, from n=5.

Control	100 nM AZD5069	100 nM R-navarixin	300 nM SB265610
Fast fraction (%)			
56.8 ± 6.48	72.87 ± 4.35*	77.45 ± 3.50**	62.59 ± 1.83
$koff_{fast}$ (min^{-1})			
6.50 ± 2.15	7.02 ± 1.31	11.07 ± 3.42	4.13 ± 1.11
$koff_{slow}$ (min^{-1})			
0.058 ± 0.005	0.056 ± 0.008	0.065 ± 0.009	0.054 ± 0.006

Table 4.9 The dissociation kinetics of CXCL8-AF647 following CXCL8$_{28-99}$ addition with and without NAM pre-treatment. Membranes were pre-treated with 100 nM AZD5069, 100 nM R-navarixin, 300 nM SB265610, or vehicle and 10 nM AF647CXCL8 binding was recorded post 1 µM CXCL8$_{28-99}$ addition. Data were fitted to a model of two-phase decay and the fast and slow dissociation kinetics constants ($k_{offfast}$ and $k_{offslow}$) extracted, as well as the fraction of CXCR2 supporting fast CXCL8 dissociation (fast fraction). Data represent mean values ± S.E.M. from 5 individual experiments. Statistical significance is indicated as * ($p \leq 0.05$) or ** ($p \leq 0.01$) and derived using one-way ANOVA followed by Dunnett's multiple comparison test.

4.3 Discussion

In this work a TR-FRET based CXCR2 binding assay was established for the first time, using fluorescently labelled CXCR2 agonist CXCL8-AF647, suitable for both equilibrium and kinetic based measurements in membranes and whole cells.

Kinetic measurements using the fluorescent tracer indicated a complex multi-component nature to its binding – explanations include the effects of receptor trafficking (whole cells), multi-step binding to receptor complexes, and the presence of multiple receptor conformations of differing affinities within the assay system. In contrast to orthosteric ligand competition experiments, only partial inhibition of the tracer binding was observed in the presence of intracellular NAMs, under conditions predicted to support high affinity agonist binding. This supports an allosteric mechanism, as does (for high affinity, slow koff NAMs) an acceleration of the ligand dissociation rate. The extent of inhibition was increased under conditions in which the inactive R conformation population might be promoted (high sodium, whole cells) – consistent with stabilisation of the inactive CXCR2 conformation by the NAMs to allosterically modulate CXCL8 binding affinity.

Under whole cell conditions, almost full inhibition of tracer binding was observed in the presence of NAMs – supporting a high degree of negative co-operative in functional experiments – and the "effectively competitive" assumptions made in interpreting functional data in Chapter 3.

4.3.1 The use of CXCL8-AF647 to develop a TR-FRET binding assay

The binding of the fluorescent chemokine tracer CXCL8-AF647 at human SNAPCXCR2His receptors was probed in both whole cells and membrane preparations using high-content imaging approaches and TR FRET. Each method detected high-affinity, specific binding of the tracer indicating that the C-terminal lysine-attached AF647 fluorophore did not disturb the ligand-receptor interactions. This was expected for the CXCL8 probe as its binding to

173

CXCR2 has been shown to be primarily through its core and N-terminal residues (Liu et al., 2020). In addition, there are examples of other C-terminal fluorescently labelled chemokines with preserved biological activity (Hatse et al., 2004), (Kawamura et al., 2014a).

In addition to preserved binding ability, CXCL8-AF647 was a functional agonist at CXCR2 as it stimulated receptor-arrestin interaction measured in the Split Luciferase complementation assay and caused receptor internalisation detected in the high-content imaging assays. The potency of the tracer in the NanoBiT assay was lower compared to the unlabelled $CXCL8_{28-99}$. This difference is likely underpinned not only by the fluorophore modification, but also the longer length of the peptide prior to labelling (78 AA) compared to CXCL8 $CXCL8_{28-99}$ (73 AA). As described in chapter 1, posttranslational truncations of chemokines typically define their biological activities (Mortier et al., 2008). Nevertheless, more assays are necessary to fully characterise the efficacy of the tracer relative to unlabelled CXCL8 chemokines.

CXCL8-AF647 potency was lower compared to its binding affinity in assays conducted in both whole-cells and membranes, low- and high-sodium buffer conditions. This is an unexpected observation and could be attributed to the inability of the ligand to induce efficient active conformation of the receptor supporting effector coupling despite its high-affinity binding.

Following from the high-content imaging-based ligand binding assays, we picked a resonance energy transfer (RET) technology to detect CXCL8-AF647 binding. TR-FRET allowed for the homogenous detection of chemokine binding at CXCR2 in both real-time and end-point setups. The binding of chemokine ligands to other CKRs has not been extensively studied by RET technologies in the past, nevertheless the binding of chemokine ligands at ACKR3 and CXCR2 has been detected by BRET (Gustavsson et al., 2019), (Sakyiamah et al., 2019), (White et al., 2017).

In general, the TR-FRET counts detected for CXCL8-AF647-SNAPCXCR2His interactions with CXCR2 were lower compared to what observed for other GPCRs studied in house (eg. adrenoceptors, dopamine receptors). The efficient energy transfer in RET is as described in chapter 1, dependent on the distance

of the interacting molecules and orientation of the tags. The relatively long N-terminal domain of CXCR2 could increase the distance between the Tb donor at the far N terminus (at SNAP tag) and the AF647 acceptor when bound at the receptor TM pocket. The relatively small agonist ligands and short N termini of adrenergic and dopamine receptors, on the other hand, could be the underlying factors for a high FRET signal (Katritch et al., 2012), (Schiöth and Lagerström, 2008).

The affinity of the fluorescent tracer estimated in the TR FRET assay, as well as the one of the unlabelled $CXCL8_{28-99}$ were in the nanomolar range and in line with what reported previously in the literature (Salchow et al., 2010), (Joseph et al., 2010).

4.3.2 The multi-component nature of CXCL8-AF647 binding to CXCR2

In all TR FRET kinetics assay formats (whole cells, membranes under different buffer conditions), there was strong evidence for a complex multi-component interaction as CXCL8-AF647 associated and dissociated from its receptor – illustrated by fast and slow phases of both association and dissociation.

The binding of the tracer in whole cells failed to reach an equilibrium plateau but instead, the ratios increased over the course of the assay. That could be a consequence of receptor-driven ligand internalisation and accumulation in the confined intracellular locations (eg. endosomes) leading to the generation of high bystander FRET signal. The ability of the ligand to cause receptor internalisation and to remain in the intracellular spaces was observed in the high-content imaging experiments. Therefore, whilst fluorescent agonist probes represent a good tool to explore ligand-receptor co-internalisation for example (Stoddart *et al.*, 2015), (Arttamangkul et al., 2000), they impose a challenge in characterising ligand binding affinity and kinetics in isolation from other cellular events. Therefore, a goal of this work was to set up CXCL8-AF647 TR FRET-detected binding in membrane preparations containing SNAPCXCR2His receptors.

The binding of the tracer in membranes, unlike in whole cells, reached binding equilibrium characterised by a plateau phase, supporting the effect of agonist-driven receptor trafficking in the ligand binding kinetics profile in cells. The binding of the tracer was defined better by both two-phase association and dissociation fits indicating a more complex than a single-step binding relationship. This was also supported by the lack of concentration-dependent increase in the observed binding rates (k_{obs}).

As discussed in 4.1, the binding of ligands to GPCRs could be a multi-step process underpinned by for example, two-separate orthosteric binding sites seen for CXCR2 and other chemokine receptors (Kleist et al., 2016), and initial interaction of certain lipophilic ligands with membrane lipids prior to binding the receptor (Vauquelin and Packeu, 2009). The multi-component association and dissociation of CXCL8-AF647 tracer from the target, is nevertheless, more likely attributed to the presence of heterogenous population of CXCR2 receptors in the membranes, with different affinities or/and kinetic properties for the fluorescent tracer.

According to the ternary complex model, uncoupled GPCRs are their low-affinity agonist binding conformation (R) and vice versa – G protein binding shifts R to R* which is the active state, supporting high-affinity agonist binding (Hulme et al., 1978), (De Lean et al., 1980). What we identified was indeed, a lower and higher affinity conformations of CXCR2 by decreasing the presence of sodium ions in the assay buffer. Tracer binding was greatly increased in the absence of Na^+ confirming the role of these ions as negative allosteric modulators of receptor conformation removing the high-affinity binding sites of CXCR2 when present. The addition of GppNHp which disrupts GPCR-G protein complexes reduced some of the binding of the tracer in Na^+-rich but, not in Na^+- deprived conditions. This suggests that whilst G protein coupling supports the transition to active, high-affinity receptor state, its net effect is negligible when the receptor population is already transitioned to a certain high-affinity conformation due to the lack of sodium ions. Alternatively, CXCR2 receptors in the sodium free buffer could be in an intermediate dynamic state represented by a free G protein pocket, in which case they would not be

176

affected by the addition of GppNHp (Abdulaev *et al.,* 2006), (Park, Lodowski and Palczewski, 2008).

Na$^+$ modulates the constitutive activity and conformation of other chemokine receptors such as CXCR4 and CCR5 whilst exhibiting distinct binding modes as each receptor (Taddese et al., 2018). For CXCR4 specifically, sodium stabilises the residue interactions that keep the receptor in an inactive conformation (Cong and Golebiowski, 2018). The evolution of the sodium pocket has been proposed important in the functional division of CKRs into pro- and anti-inflammatory (Taddese et al., 2018). Nevertheless, there is less information of the precise effects of these ions on ligand-receptor interactions. The presence of more than one CXCR2 conformation bound by chemokine agonist with different affinities has also been identified before through uncoupling G proteins using non-hydrolysable GTP analogue in sodium rich buffer conditions (Salchow et al., 2010).

The binding of ligands to GPCRs is often heterogeneous due to the ability of receptors to form homo or heterodimers both prior to and as a result of the labelled ligand binding. Such dimer/oligomer formation could alter the donor:acceptor ratio recoded in TR FRET and lead to a multi-component binding kinetic curves (Gherbi et al., 2015), (May et al., 2011). There is some evidence for the ability of CXCR2 to both form homodimers and to dimerise with other GPCRs such as CXCR1 and the DOP opioid receptors (Trettel et al., 2003), (Papers et al., 2005), (Parenty et al., 2008). The formation of CXCR2 homodimers would be relevant in this study and could underpin the multi-phase ligand-receptor kinetic interactions.

The formation of receptor dimeric complexes has been shown for other chemokine receptors such as the agonist-induced dimerization of CCR2 (Rodríguez-Frade et al., 1999), CCL5-induced CCR2 homodimerisation (Vila-Coro et al., 2000), ACKR3 constitutive homodimerization with subunit rearrangements observed upon agonist and antagonist binding (Kalatskaya et al., 2009). Furthermore, the rearrangement of the CXCR4 subunits in the dimer following agonist activation has been shown to contribute to the slower kinetics of receptor activation of the receptor compared to monomeric GPCRs

177

(Perpina-Viciano et al., 2020). Such propensity of CXCR4 to dimerise is likely reflected in the multiphasic binding of ligands observed (Soave et al., 2020).

4.3.3 The effect of NAMs in the TR-FRET assay supports a negative allosteric effect on chemokine affinity, potentially by stabilising the inactive CXCR2 conformation.

The effects of NAMs on CXCL8-AF647 binding was examined in both whole cells and membrane preparation under low- and high- Na^+ buffer conditions. We investigated if NAMs primary mechanism of action is to disrupt receptor-effector coupling as suggested by structural and mutagenesis data (see chapters 1, 3) or additionally, to alter the affinity of CXCR2 for its chemokine agonist. There is limited amount of studies that have demonstrated the direct impact of CXCR2 intracellular NAMs on the binding of labelled chemokines (Salchow et al., 2010), (Salchow et al., 2010). This work, however, demonstrated a direct inhibitory effect of NAMs on CXCL8-AF647 binding both in the confocal imaging studies and the TR FRET assays.

The partial effect of NAMs on tracer binding in low sodium buffer is consistent with a non-competitive, negative allosteric effect on fluorescent chemokine binding affinity. A notable observation in these conditions was that the effect of NAMs was greater than that of GppNHp. This suggests a direct effect of NAMs in stabilising a low agonist affinity conformation of the CXCR2 receptor, rather than simply disrupting the R*-G interaction as part of the CXCL8-CXCR2*-G protein high affinity ternary complex. Under low sodium conditions, accelerated dissociation of CXCL8-AF647 (in the presence of excess unlabelled CXCL8) could be detected, but only in the presence of the high-affinity / slow-koff NAMs AZD5069 and R-navarixin. The limited effects of NAMs on CXCR2 binding and binding kinetics in low-Na^+ environment could be a conformational selectivity effect underlined by the preference of ligands behaving as 'inverse agonists' for the inactive receptor conformation. The conformational differences in CXCR2 bound by a chemokine agonist / Gi protein or a NAM (active and inactive conformation) in the cryo-EM receptor structure study support this idea (Liu et al., 2020). Therefore, the inclusion of sodium in the

assay buffer (HBSS) in both membranes and whole cells enhanced the effect of NAMs due to shift in the assay equilibrium populations of CXCR2 receptors towards R from R*.

In whole-cell environment and sodium-rich conditions, the TR-FRET binding data demonstrated the capability of NAMs to fully inhibit labelled tracer binding – indicating strong negative co-operativity and likely, mutually exclusive binding with the agonist. This supports the interpretation of functional data (chapter 3), and the use of 'competitive' antagonism models in estimating the effect of NAM dissociation kinetics on the insurmountability profiles observed.

4.3.4 Conclusions and future directions

To conclude, the binding of the fluorescent chemokine derivative CXCL8-AF647 at CXCR2 receptors was probed using a combination of imaging and non-radiative energy transfer approaches. The specific binding of the tracer was demonstrated in both whole cells and in membrane preparations and the presence of heterogenous receptor populations with different affinities for chemokine agonist binding were identified. A range of structurally distinct intracellular NAMs were compared in their ability impact CXCL8-AF647 binding and binding kinetics under different assay conditions. It was demonstrated that the NAMs inhibit CXCR2 function at least partly through an allosteric effect on the receptor conformation that limits the binding of the chemokine and increases its dissociation kinetics to a certain extent. The extent of which NAMs affected chemokine binding was dependent on the receptor conformation as suggested by their differential effects in low or high sodium buffer conditions. The findings in this chapter supported the negative cooperativity mechanism of actions and kinetics-driven insurmountability suggested in chapter 3.

There are more assay formats that could be utilised in order to collect further information of the effects of NAMs on the CXCL8-AF647 fluorescent tracer binding. Saturation tracer binding assays with or without each NAM pre-

treatment could be conducted to further assess the effect of NAMs of CXCL8 tracer affinity. This assay format, if conducted in membrane preparations, would again reflect the ability of NAMs to impact agonist binding in buffer conditions shifting the conformational equilibrium to the R* receptor conformation.

The binding assays could further incorporate the addition of purified mini G proteins which would directly assess the effect of ternary complex formation on NAM binding and impact, or vice versa – removing the R-G interactions with pertussis toxin and not only GppNHp.

Another important characteristic of allosteric modulators – probe dependence – could be explored by working with other chemokine fluorescent tracers such as CXCL1 which would be possible for the promiscuous CXCR2 receptor. This way it could be investigated if NAM profiles are orthosteric-ligand selective.

In addition, the whole cell binding kinetic assays could be investigated in the presence of receptor internalisation inhibitors in order to isolate the binding of the agonist tracer from the otherwise observed trafficking events. This would allow for more accurate estimates of tracer affinity and kinetics.

Chapter Five: General Discussion

5. Chapter five: General Discussion

5.1 Summary of this project

The signalling of the chemokine CXCL8 / CXCR2 axis mediates immune cell trafficking both during normal homeostasis and in states of acute and chronic inflammation. CXCR2 expression and signalling is also associated with cancer progression (chapter 1). Because of these functions of the receptor, there have been efforts in the field of drug discovery to block CXCR2 signalling through the use of small-molecule negative allosteric modulators (NAMs), which interact with CXCR2 at an intracellular binding pocket (chapter 1; chapter 3). Some of these molecules are currently in clinical trials as part of combination cancer therapies but have failed for the treatment of inflammatory conditions due to lack of efficacy, and others – due to on target unwanted effects such as neutropenia (chapter 1). Therefore, as of yet, there has not been a clinically approved NAM (and any other drug) targeted at CXCR2. There remains potential to tailor the effects of NAMs to obtain better in vitro compound profiles, with the ultimate aim to improve therapeutic efficacy and reduce on target side effects. These opportunities exist due to the complex ability of allosteric ligands to regulate different aspects of chemokine signalling at CXCR2 (affinity, efficacy modulation) and to different magnitudes. Moreover, the contribution of NAM binding kinetics to allosteric regulation and effects over time is yet to be fully explored.

This work increased understanding of the mechanism of action of a range of structurally distinct and enantiomeric intracellular CXCR2 NAMs, particularly considering the potential impact of ligand binding kinetics in regulating CXCL8 binding and signalling through novel pharmacological assays. As part of the assay development process, CXCR2 was genetically modified N terminally with a relatively large tag (SNAP tag; 19.4 kDa) which still allowed for chemokine binding and receptor activation. Similarly, the modification of CXCR2 C terminally with a LgBiT tag (18 kDa) preserved interaction with effectors and internalisation to take place as expected. These modifications importantly allowed us to measure ligand binding at the receptor and receptor activation

182

in real-time, living cells, and membrane preparations, using TR FRET and Split luciferase complementation technologies.

Chapter three characterised the effects of NAMs on CXCR2 activation detected through the Split luciferase complementation (NanoBiT) technology as a function of receptor-effector interactions. A range of structurally distinct NAMs, as well as enantiomers, were compared in their ability to inhibit receptor activation. All NAMs showed equivalent inhibition of CXCR2 – arrestin and mini Go interactions. NAMs were different in the way they affected the basal receptor-effector interactions, and importantly – in their effect on CXCL8 concentration-response relationships. NAMs (R-navarixin and AZDD5069) that supressed CXCR2 activation insurmountably were also the ones with slow dissociation kinetics at CXCR2 supported both with previous studies in the literature and by means of mathematical modelling in this study. On the contrary, fast koff NAMs (S-navarixin, SB265610) were surmountable in their CXCR2-effector recruitment inhibition. Therefore, the functional effects of NAMs were linked to their binding kinetics properties at the receptor.

Chapter four explored the binding of a fluorescently labelled chemokine tracer AF647CXCL8 in both whole cells and membrane preparations and under different buffer compositions. NAMs were then compared in their ability to compete for binding with the tracer, prevent tracer rebinding, and alter the agonist binding kinetics in the different experimental set-ups. Our results demonstrated that intracellular NAM binding negatively modulates chemokine binding in addition to blockade of effector interaction, indicating that NAMs such as navarixin may actively stabilise the lower affinity inactive receptor conformation leading to negative co-operativity.

Specific data were discussed in depth at the end of each chapter and here, the significance of this work, its place in the field of chemokine drug discovery, as well as its limitations, have been outlined.

5.2 Importance of this work and the potential of CXCR2 as a clinical target

The current work successfully evaluated intracellular CXCR2 NAMs in their ability to affect receptor activation and fluorescent chemokine binding at the

target. This is the first work that has used kinetically resolved and non-radiation-based technologies to study CXCR2 and chemokine binding of the receptor. In addition, it is the first work which aims to decipher the contributions of chemokine affinity modulation and effector blockade to the mechanism of intracellular NAMs, as well as the impact of the binding kinetics of CXCR2 NAM molecules (even though indirectly as discussed below) and on their functional profiles.

As discussed in previous chapters, the kinetics of drug-receptor interactions, and not only the pharmacokinetics properties of drug candidates should be considered in drug development (Vauquelin and Charlton, 2010b). It is dependent on the clinical context whether fast or slow binding drugs could be advantageous or unfavourable. For example, the slow dissociating kinetics of antagonists of the orexin receptor used for the treatment of sleep disorders is likely linked to drowsiness and other unwanted effects, whereas the slow-binding kinetics of the CCR5 NAM maraviroc used in the management of AIDs is suitable for the dosing regimen and management of a chronic disease (Mould *et al.*, 2014), (Swinney et al., 2014). In the context of the chemokine signalling system, identifying molecules with slow binding kinetics could be a strategy to surmount the large chemokine concentration gradients released in the inflammatory response (Stone et al., 2017b). Alternatively, slow, semi-irreversible binding, also underlying high-affinity receptor interactions, may be attributed to unwanted on-target effects such as neutropenia in the case of the slow-off CXCR2 NAM - navarixin (Holz et al., 2010) likely caused by bone marrow neutrophil trafficking suppression. It may be therefore challenging to find the balance between supressing pathological inflammation and normal immune defence when blocking CKRs involved in these processes. The approaches described in this thesis provide a validated means to quantify the relationship between off rate and insurmountable effects, potentially to find an optimal kinetic profile balancing the benefits of insurmountability during inflammation with the risks of neutropenia.

Slowly dissociating compounds can also lead to kinetic receptor selectivity, in which slower off rates at the target receptor than related receptors contribute to enhanced target coverage compared to off target receptors responsible for side effects (Tautermann et al., 2013), (Sykes *et al.*, 2021). In the case of treating chronic inflammatory conditions where the signalling of more than 1 chemokine and CKR pair is involved, a specific receptor inhibition may not be considered. For example, a dual CXCR1 / CXCR2 NAM may be a preferred strategy given the function of both receptors in mediating neutrophil trafficking (Ha et al., 2017). One such molecule is reparixin which likely interacts with a different allosteric pocket at CXCR1 and CXCR2 which is yet to be structurally identified (Bertini et al., 2004) (Moriconi et al., 2007), (Kruijf et al., 2009).

It would be useful to extend the kinetic investigations we have performed with CXCR2 to other chemokine receptors which NAMs may interact with such as CXCR1, CCR7, CCR2, CCR9 (Zheng et al., 2016), (Jaeger et al., 2019), (Oswald et al., 2016). Understanding the kinetic profiles if NAMs (eg. for R-navarixin, AZD5069) for multiple receptors would help provide data in support of binding-kinetics underlined target selectivity. Navarixin, for example has been shown to interact with an intracellular pocket at CCR7 and supress CCL19 stimulated receptor-arrestin interactions with low affinity (Jaeger et al., 2019). The addition of the less active at CXCR2 navarixin enantiomer (S-navarixin) would be a useful comparison at CXCR7.

Pursuing the CXCR2 receptor as a target for the treatment of different types of cancer has been the more recent strategy in drug discovery and currently, both slow koff NAMs tested in this work – navarixin and AZD5069, are in trials as combination therapies for the inhibiting tumour progression (Che et al., 2019). Navarixin is given in combination with a checkpoint inhibitor antibody pembrolizumab that stimulates the cytotoxic activity of T cells (Adamaki and Zoumpourlis, 2021). Given the dual pro- and anti-inflammatory functions of CXCR2 in the cancer environment, an immunostimulant treatment along with CXCR2 blockage could compensate for the reduced immune response as a result of the latter in addition to the desirable cancer growth inhibition.

The use of biologics to target CXCR2 itself, could generally be an exciting avenue for the treatment of cancer. A recent study has identified an antibody interacting with the chemokine orthosteric binding pocket of CXCR2 with picomolar affinity (Shi et al., 2021). Interestingly, the antibody showed selective inhibition of some CXCR2-mediated signalling pathways, whilst enhanced others, which is the first evidence for a functionally selective CXCR2 'ligand'.

CXCR2 has been previously targeted with biparatopic nanobodies that bind epitopes across one or two CXCR2 receptors and inhibit their function (Bradley et al., 2015). The advantage of these nanobodies is their ability to bind various CXCR2 conformations including the ones supported by the monomeric, hetero or homo – dimeric receptor structures. The use of nanobodies has been recognised for their advantages of smaller size and better pharmacokinetic properties compared to antibodies (Heukers et al., 2019), (Cromie et al., 2015). A CXCR4-interacting nanobody for example, differentially blocked HIV viral entry, whilst preserving CXCL12-mediated receptor activation and functionality (Van Hout et al., 2018).

The use of nanobodies in targeting chemokine receptors is an exciting avenue for targeting specific and different epitopes at the large orthosteric binding pocket and probe-dependently modulate receptor function. Taken the dual roles of immune cells expressing CKRs in cancer, such as N1 and N2 pro- and anti- inflammatory neutrophils respectively (Galdiero *et al.*, 2018), a tool recognising specific malignancy-associated patterns on the cells or receptors themselves, could be of great therapeutic benefit. The nanobodies, indeed, may be a promising candidate for such targeted drugging strategy. Despite the therapeutic potential of biologics, the use of small molecules to target the receptor is a key strategy for CXCR2 inhibition due to a range of advantages they offer. The small size of the molecules underlines the potential for better oral bioavailability (Veber et al., 2002). In addition, small molecules have improved access to sites of action that may be difficult to target with large biologic molecules such as solid tumours and any CNS BBB enclosed areas. In fact, lipophilicity driven cellular plasma membrane penetration (logP

186

= 2.5 for navarixin, provided by Bianca Casella, Shailesh Mistry group, data not shown) required for intracellular receptor pocket interaction increases the likelihood of BBB penetration (Bellettato and Scarpa, 2018).

This work importantly demonstrated along with the CXCR2 structure with a small-molecule NAM (Liu et al., 2020) that intracellular CXCR2 NAMs modulate orthosteric agonist binding affinity as well as sterically block effector coupling. The recognition that this is part of the mechanism of action opens up a broader range of allosteric effects possible with intracellular NAMs (Kenakin, 2013). This study and general chemokine intracellular allosteric modulation data at Gi coupled CKRs, suggests commonality in intracellular transducer binding blockage and stabilisation of inactive conformation (Jaeger et al., 2019), (Oswald et al., 2016), (Zheng et al., 2016). A more recent work pharmacologically explored the prostaglandin receptor EP2 modulation by a compound predicted to bind at an intracellular pocket and inhibit receptor signalling whilst enhancing agonist binding affinity (positive cooperativity between agonist and allosteric compound binding) (Jiang et al., 2020). It would be beneficial to compare the structures and intracellular pocket fitting of such 'PAM antagonists' to NAMs such as the CXCR2 ones that reduce agonist binding affinity for additional insights into the possibility of fine receptor tuning. One such 'use dependent' property may be of interest in the context of chemokine signalling in which blockage is enhanced at highly active receptors during for example the event of 'chemokine / cytokine storm' (Lazennec and Richmond, 2010).

The ligand binding and functional systems developed in this project could provide means to detect both the functional antagonism and use dependent effects on chemokine binding and further aid the better search for these types of ligands.

5.3 Limitations and future directions

With the available tools, we provided indirect evidence for the connection between NAMs binding kinetics and their functional properties. It was, nevertheless, not possible to measure directly the binding kinetics of NAMs at the intracellular site, other than with reference to previous studies using tritiated radioligands (Gonsiorek *et al.*, 2007), (Nicholls *et al.*, 2015),(Bradley et al., 2009), (de Kruijf et al., 2009). One avenue being pursued, in progress at the time of submission, is the synthesis of suitable fluorescent labelled molecular probes targeting the CXCR2 IAM site. The synthesis of fluorescently labelled NAM probes would be a logical next step to confirm NAMs binding affinities and kinetics. The medicinal chemistry side of this work (Bianca Casella, Shailesh Mistry group) has provided the unlabelled navarixin enantiomers (Dwyer et al., 2006) and has successfully generated a navarixin derivative attached to different linker congeners to allow for a fluorophore attachment, with preserved CXCR2 inhibition properties and cell permeability (figure 5.1).
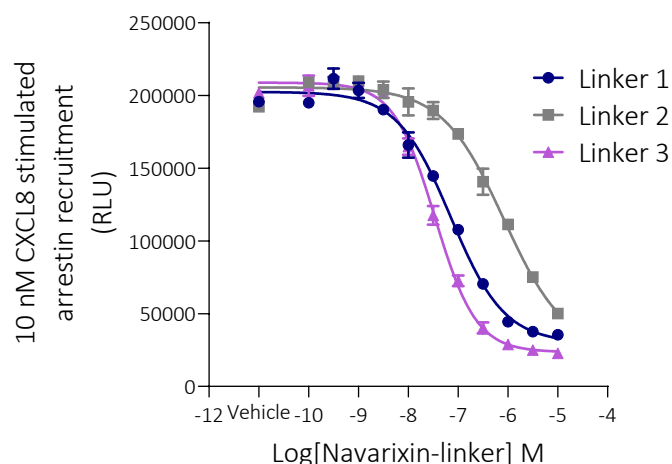
Figure 5.1 CXCR2-arrestin interactions inhibited by navarixin NAM derivative attached to different linkers. HEK293 cells stably expressing SNAPCXCR2LgBit and SmBit β-arrestin 2 were pre-treated with a range of a range of navarixin derivatives linked to 3 different linkers (Linker 1, Linker 2, Linker 3) or buffer (-10 point) for 60 minutes at 37°C This was followed by the addition of 10 nM $CXCL8_{28-99}$ and the detection of luminescence on furimazine addition 30 minutes later in an end-point manner. The graph represents a single experiment from n =3. Error bars = S.D between replicates. The inhibitory potencies (pIC50) of the NAMs linked to Linker 1,2,3 respectively were 7.18 ± 0.03, 6.12 ± 0.04, and 7.40 ± 0.05 respectively representing means from n=3 individual experiments ± S.E.M.

The synthesis of fluorescent NAM probes via fluorophore attachment to the linker congeners from figure 5.1 would be a valuable tool to expand the current work by establishing a binding assay that directly measures the binding of the probes to the intracellular allosteric pocket.

One way to do that is by setting up a NanoBRET assay with a C-terminal Nanoluciferase receptor tag that serves as a donor to excite the fluorescent intracellular probe which has been recently established for the CCR2 receptor (Huber et al., 2021). The binding of fluorescent IAMs could be detected via TR-FRET too provided the successful labelling of intracellular SNAP tags with lanthanide cryptates. Similarly to the homogenous real-time detection labelled chemokine binding at CXCR2, the use of TR-FRET would allow for the precise characterisation of the intracellular probe binding kinetics properties. Unlike the binding studies in chapter 4 however, a fluorescent IAM probe assay would allow the direct measure and Ki calculation of the unlabelled NAMs as their

189

interactions will be competitive with the labelled probe. This importantly allows a form of analysis known as Motulsky-Mahan (MM) method (Motulsky and Mahan, 1984) successfully applied to characterise the kinetics of unlabelled ligands at GPCRs relative to the one of a labelled probe based on same binding site interaction (Sykes *et al.*, 2021), (Sykes *et al.*, 2014), (Bosma et al., 2019), (Bosma et al., 2018). In the MM approach different concentrations of unlabelled ligand are added simultaneously to the preparation and the association kinetics of the probe is monitored over time. The profiles of the time courses of tracer association vary depending on the relative kinetics of the tracer and unlabelled ligand. They can be analysed using a model assuming competitive binding site interaction to extract the kon and koff estimates of the unlabelled compound.

To directly address effector occlusion as a mechanism of action of NAM CXCR2 inhibition a more direct assay in a controlled system could be developed. This could utilise purified effector proteins such as mini G proteins, arrestin, full-length $G\alpha$ / $G\alpha\beta\gamma$, GRKs (Carpenter and Tate, 2017), (Vishnivetskiy et al., 2014), (Loudon and Benovics, 1994). The NanoBiT complementation system would allow for studying how unlabelled NAMs compete with SmBit-tagged effectors for LgBit tagged receptor interactions. The advantages of such system would be the ability to control precisely the effector concentration – or for example to quantify the effects of NAMs on affinity. Alternatively, fluorescent NAM probes and unlabelled purified effectors could be competed for receptor binding in a NanoBRET or TR-FRET based assays. These experiments could be established using CXCR2-LgBit/CXCR2-Nanoluc/CXCR2-SNAP-Tb^{3+} membrane preparations where the receptor concentration and organisation is not precisely controlled, and native G proteins in the preparation may influence the behaviour of all species involved in the interaction (receptor, effector, ligands). An alternative is to therefore, isolate receptors from the plasma membrane whilst keeping some of their native lipid environment using styrene maleic-acid lipid particles (SMALPs) ~ 20 nm in diameter providing 1 / 2 receptor proteins per particle (Postis et al., 2015), (Wheatley et al., 2016), (Grime et al., 2020).

In a longer timeframe, this work could be expanded to equivalent mechanism of action studies on the CXCR2 NAMs in native human cell types, such as pro versus anti-inflammatory neutrophils, as well as other myeloid-derived suppressor cells (MDSCs). A recent study, for example purified CD8+ T cells (cytotoxic) and B cells from murine tissue of tumour bearing mice with myeloid targeted CXCR2 deletion and compared the migration patterns of these cells via chemotaxis assays, the release of cytokines and killing capacity (for the cytotoxic T cells) (Yang et al., 2021). The study also compared the metastatic tumour progression in mice treated with a dual CXCR1/CXCR2 antagonist SX-682 and the effects were similar of what observed in genetic myeloid CXCR2 deletion. It would be useful to conduct more experiments in such systems where cells from tumour tissue in myeloid cell manipulated animals could be probed with a range of CXCR2 selective or CXCR1 / CXCR2 dual acting NAMs. It will be however, much more challenging to interpret NAMs molecular mechanism in of action in more complex primary systems.

The gap between assays development in vivo / primary cell systems and recombinant cells could be reduced by applying technologies such as CRISPR/Cas9-genome editing which has been utilised for transfecting cells with tagged or untagged proteins of interest allowing for studying them at endogenous expression levels (Carl White et al., 2020), (Oh-hashi et al., 2017). The tagging of the chemokine receptor CXCR4 and arrestin with NanoBit fragments using this approach has allowed the monitoring of arrestin recruitment kinetics by the NanoBiT method with native receptor expression (White *et al.*, 2020). Indeed, this study indicated differences in the recruitment kinetics between overexpressed and natively expressed protein levels.

The NanoBiT system has been further exploited to characterise the binding of high affinity SmBiT (HiBiT) tagged nanobodies at CXCR4 relative to orthosteric and allosteric receptor ligands in natively expressing Jurkat T cells (Soave et al., 2020). Having validated the functionality of various constructs in this study, CXCR2-effector interactions could be detected in CRISPR/Cas9 mediated endogenous level effector expression for example as shown for CXCR4 (White *et al.*, 2020). The transfection of such CXCR2 constructs could be done in more

191

physiologically relevant in vitro systems such as cancer cell lines including mammary, ovarian, colorectal tumour, glioblastoma cell lines etc. (Nannuru et al., 2011), (Yang et al., 2010), (Ning et al., 2012), (Diao et al., 2019). Regardless of receptor expression levels, studying the receptor in a disease relevant context is beneficial due to presence of modulatory proteins for example that could alter receptor behaviour such as ligand-receptor interactions, receptor-effector interactions etc. For example, GPCR behaviour such as trafficking could be affected by Receptor-activity modifying proteins (RAMPs) and their expression could be cell-type dependent (Hay and Pioszak, 2016). Similarly, the expression of Gαo G protein subtypes is most abundant in the CNS (De Oliveira et al., 2019).

Modified receptor / effector constructs, however, cannot be transfected in all relevant cell types and neutrophils are one example of primary cells difficult to transfect due to their short lifespan (Blanter et al., 2021). In such cases, native receptor studies could be designed following the CXCR4 study showing HiBit native receptor labelling and LgBit-nanobody/ligand competition studies (Soave et al., 2020).

In the context of cancer, it would be valuable to explore CXCR2 function in tumour-derived anti-inflammatory versus pro-inflammatory neutrophils (Shaul et al., 2016). The identification of distinct neutrophil populations within tumours, however, could be technically challenging due to the lack of knowledge of distinct cellular markers.

5.4 Challenges and new avenues in targeting the chemokine signalling system

Currently there are only three approved drugs targeting chemokine receptors. These are the antibody against CCR4 – mogamulizumab used for cutaneous T-cell lymphomas, the CXCR4 partial agonist plerixafor used to mobilise hematopoietic stem cells from the bone marrow in cancer, and maraviroc – a negative allosteric modulator of CCR5 used for preventing the entry of HIV into cells (Zhao et al., 2019).

The difficulties associated with drugging chemokine receptor, despite their likely therapeutic potential could be attributed to a few reasons. One of these

is the species differences in chemokine / CKR expression and function which imposes issues when studying CKR drugs in in vitro vs. in vivo systems and predicting drug selectivity and associated unwanted effects (Bajoghli, 2013). For example, despite the recent identification of a CXCR2 murine homologue, it has long been unclear if murine neutrophils express both CXCR2 and CXCR2 receptors or CXCR2 only which questions the relevance of CXCR2 knock-down / knock out studies for instance, performed in mice (Stadtmann et al., 2012), (Fu et al., 2005).

5.4.1 Is there redundant or selective signalling of the chemokine signalling system?

Another major point of discussion in the field that makes studying the chemokine signalling system challenging, is its ability to manifest redundancy because of the promiscuity of some chemokine receptors, as well as the ability of a single chemokine to agonise multiple receptors (Dyer *et al.*, 2019). For further complexity, immune cells simultaneously express multiple inflammatory CKRs. The chemokine CXCL8 for example binds and activates both CXCR1 and CXCR2 receptors but whilst CXCR1, is only activated by CXCL8, CXCR2 is promiscuous and also responds to CXCL1,2,3,4,5,6,7 (Rajagopalan and Rajarathnam, 2004). The actual presence of such 'redundancy' *in vivo*, has nevertheless, been challenged (Dyer, 2020a). Potential mechanisms leading to greater selectivity in vivo have been suggested, including chemokine – glycosaminoglycan (GAG) interactions that are often neglected due to the difficulty of examining them in in vitro assays

GAGs are sulphated, negatively charged polysaccharides found on the surface of various cell types and in the extracellular matrix (Johnson et al., 2005), and their interaction with chemokines is necessary for the formation of chemokine gradients as discussed in chapter 1. The GAG binding sites at chemokines (primarily at the C terminal residues) are not, as originally proposed, completely separated from the CKR binding motifs. CXCL1, for example, is unable to bind its cognate CKRs when bound by the GAG heparin (Sepuru and

Rajarathnam, 2016). In addition, a CXCL7-monomer bound to heparin cannot bind CXCR2 (Brown et al., 2017a).

The literature suggests that GAGs may regulate the availability of chemokines, and their ability to bind CKRs by mediating chemokine ligand oligomerisation. The ability of the chemokine ligand to then bind receptors could be both hindered and promoted depending on the situation (Lau et al., 2004), (Hoogewerf et al., 1997). For example, GAGs are suggested to control the CXCL8 monomer – dimer equilibrium differentially in different tissues and microenvironment and that in turn, regulates neutrophil recruitment between tissues (Gangavarapu et al., 2012).

The roles of GAGs in regulating the chemokine signalling system seem crucial, however, are challenging to be explored in vitro. These molecules are extremely diverse in their structure and sizes, and difficult to produce synthetically and characterise (Proudfoot et al., 2017). Their ability to modulate the availability of chemokines for receptor binding, in a tissue-specific way, also makes predicting chemokine receptor interactions in vitro likely inaccurate in terms of affinity and selectivity. In addition, the control of chemokine oligomerisation and competition for ligand binding with receptors by GAGs could really change the concept of 'redundancy' to a strictly spatially and temporally controlled signalling system (Handel and Dyer, 2021).

The ability of CXCL8-AF647 and unlabelled CXCL8$_{28-99}$ as well as ligands that lack GAG binding sites (Proudfoot et al., 2003) to bind and activate CXCR2 receptors could be characterised in the systems set up in this work in the presence or absence of commercially available GAGs such as heparin or heparan sulphate (Xu and Esko, 2014). It should be noted, however, that C-terminal lysine labelling of chemokines with fluorophores may already affect their ability to interact with GAGs (Kawamura et al., 2014b), (Tanino et al., 2010).

The ability of the chemokine fluorescent probes to dimerise upon the presence or absence of GAGs using fluorescence correlation spectroscopy (FCS) for example could be explored (Nederveen-Schippers et al., 2021). Alternatively, trapped chemokine monomers or dimers could be compared in their binding

194

affinities to CXCR2 and abilities to activate receptor signalling (Nasser *et al.*, 2009), (Brown et al., 2017b). In addition, it would be interesting to explore if NAMs show any probe dependence by screening them against monomeric vs. dimeric chemokine molecules applying the synthetic trapped ligand techniques.

Other mechanisms suggested to confer specificity in the chemokine signalling system are the differential ligand and receptor expression in different tissues, which as discussed above, may also correlate to the distribution of GAGs. In addition, the potential for biased signalling has bene proposed as a driver of specific signalling outcomes (Dyer, 2020b), (Handel and Dyer, 2021).

The concept of biased signalling has been studied more thoroughly for the chemokine receptor CXCR3 which may be activated by different interferon (IFN) inducible chemokines interacting with different pocket residues leading to differential intracellular responses (Metzemaekers et al., 2017). Small-molecule biased agonists for CXCR3 have also been identified (Smith et al., 2018).

The concept of biased signalling would indeed explain the observed redundancy in the system, nevertheless, it requires good experimental design and tools for obtaining reliable results that are not biased for different expression levels in the system studied, or the lack of kinetic resolution of the signalling assays (Herenbrink et al., 2016).

The techniques developed in this work – ligand-receptor interactions and receptor activation provide assays that can in principle measure the kinetics of ligand binding and responses in a single homogeneous format. The current study investigated NAM CXCR2 receptor activation inhibition by looking at two signalling pathways – arrestin and G protein coupling, which is a typical framework for biased signalling to be explored in. There were no differences detected, however, in the ability of NAMs to reduce interactions of CXCR2 with one effector over the other. It is perhaps more feasible to design AMs that bind to more effector specific residues if a biased arrestin or G protein signalling is desired. The overexpression of intracellular transducers, however, could generally affect the overall propensity of the receptor to interact with

195

different downstream signalling partners ("bias") affecting the qualitative nature of the functional response (Gundry et al., 2017). The endogenous expression of receptor / effector molecules as discussed earlier in term of CRSPR / Cas9 technologies could be an essential tool to overcoming this hurdle The regulation of chemokine availability and other mechanisms that make individual chemokine signalling systems selective rather than redundant is therefore important for further exploration. The knowledge of individual chemokines and receptor activation in different tissues and environments could focus on the right CXR targets when looking for druggable receptors for treating inflammatory diseases (Schall and Proudfoot, 2011).

5.5. Summary and conclusions

This work profiled a range of CXCR2 intracellular NAMs using real-time receptor activation and fluorescent ligand binding assays. The data demonstrated that whilst NAMs interact with the same allosteric pocket, they could differentially affect the pharmacology of endogenous chemokine ligands and that this is influenced by their binding kinetic properties. This work, in line with others, demonstrated complexity in chemokine-chemokine receptor-NAM interactions and showed in detail how these allosteric ligands of CXCR2 can negative modulate both chemokine binding and receptor coupling to both G protein and arrestin effectors. We demonstrated that the key property of antagonist insurmountability, a useful feature to combat dynamically high levels of chemokine release during inflammation, was enhanced in the in vitro systems by NAMs with slow binding kinetics, and not solely the result of the noncompetitive nature of the ligands. The project introduced the real-time NanoBiT complementation and TR-FRET as techniques to study CXCR2 activation and signalling in real-time for the first time, showing how the kinetic pharmacology of intracellular NAMs can be conveniently assayed in a homogenous assay format. These methods will in general be useful to optimise *in vitro* compound mechanistic profiles in the future, as a better balance between sufficient therapeutic efficacy of CXCR2 drugs in

inflammation and cancer, and side effects such as neutropenia, is sought to be addressed.

iii. References

Abrams, P., Andersson, K.E., Buccafusco, J.J., Chapple, C., Groat, W.C. De, Fryer, A.D., et al. (2006). Muscarinic receptors: their distribution and function in body systems, and the implications for treating overactive bladder. Br. J. Pharmacol. *148*: 565-578.

Adamaki, M., and Zoumpourlis, V. (2021). Immunotherapy as a Precision Medicine Tool for the Treatment of Prostate Cancer. Cancers (Basel). *13*: 1–23.

Addison, C.L., Daniel, T.O., Burdick, M.D., Liu, H., Ehlert, J.E., Xue, Y.Y., et al. (2000). The CXC Chemokine Receptor 2, CXCR2, Is the Putative Receptor for ELR + CXC Chemokine-Induced Angiogenic Activity. J. Immunol. *165*: 5269–5277.

Ahn, S., Kahsai, A.W., Pani, B., Wang, Q.T., Zhao, S., Wall, A.L., et al. (2017). Allosteric 'beta-blocker' isolated from a DNA-encoded small molecule library. Proc. Natl. Acad. Sci. U. S. A. *114*: 1708–1713.

Albizu, L., Teppaz, G., Seyer, R., Bazin, H., Ansanay, H., Manning, M., et al. (2007). Toward efficient drug screening by homogeneous assays based on the development of new fluorescent vasopressin and oxytocin receptor ligands. J. Med. Chem. *50*: 4976–4985.

Alexander, S.P.H., Christopoulos, A., Davenport, A.P., Kelly, E., Mathie, A., Peters, J.A., et al. (2019). THE CONCISE GUIDE TO PHARMACOLOGY 2019/20: G protein-coupled receptors. Br. J. Pharmacol. *176*: S21–S141.

Allegretti, M., Bertini, R., Cesta, M.C., Bizzarri, C., Bitondo, R. Di, Cioccio, V. Di, et al. (2005). 2-Arylpropionic CXC chemokine receptor 1 (CXCR1) ligands as novel noncompetitive CXCL8 inhibitors. J. Med. Chem. *48*: 4312–4331.

Allen, S.J., Crown, S.E., and Handel, T.M. (2007). Chemokine:Receptor Structure, Interactions, and Antagonism. Annurev.Immunol.*25*: 787–820.

Ariens, E.J. (1954). Affinity and intrinsic activity in the theory of competitive inhibition. 1. Problems and theory. Arch. Int. Pharmacodyn. Ther. *99*: 32–49.

Arttamangkul, S., Alvarez-Maubecin, V., Thomas, G., Williams, J.T., and Grandy, D.K. (2000). Binding and Internalization of Fluorescent Opioid Peptide Conjugates in Living Cells. Mol. Pharmacol. *58*: 1570–1580.

Azad, T., Singaravelu, R., Brown, E.E.F., Taha, Z., Rezaei, R., Arulanandam, R., et al. (2021). SARS-CoV-2 S1 NanoBiT: A nanoluciferase complementation-based biosensor to rapidly probe SARS-CoV-2 receptor recognition. Biosens. Bioelectron. *180*: 113122.

Bachelerie, F., Ben-Baruch, A., Burkhardt, A.M., Combadiere, C., Farber, J.M., Graham, G.J., et al. (2014). International Union of Basic and Clinical Pharmacology. Update on the extended family of chemokine receptors and

introducing a new nomenclature for atypical chemokine receptors. Pharmacol. Rev. *66*: 1–79.

Baeriswyl, V., and Christofori, G. (2009). The angiogenic switch in carcinogenesis. Semin. Cancer Biol. *19*: 329–337.

Bajoghli, B. (2013). Evolution and function of chemokine receptors in the immune system of lower vertebrates. Eur. J. Immunol. *43*: 1686–1692.

Baldwin, J.M. (1993). The probable arrangement of the helices in G protein-coupled receptors. EMBO J. *12*: 1693–1703.

Barak, L.S., Ménard, L., Ferguson, S.S.G., Colapietro, A.M., and Caron, M.G. (1995). The Conserved Seven-Transmembrane Sequence NP(X)2,3Y of the G-Protein-Coupled Receptor Superfamily Regulates Multiple Properties of the β2-Adrenergic Receptor. Biochemistry *34*: 15407–15414.

Barnes, P.J. (2000). The Pharmacological Properties of Tiotropium. Chest *117*: 63S-66S.

Baugher, P.J., and Richmond, A. (2008). The carboxyl-terminal PDZ ligand motif of chemokine receptor CXCR2 modulates post-endocytic sorting and cellular chemotaxis. J. Biol. Chem. *283*: 30868–78.

Bellettato, C.M., and Scarpa, M. (2018). Possible strategies to cross the blood-brain barrier. 11 Medical and Health Sciences 1109 Neurosciences. Ital. J. Pediatr. *44*: 131.

Bender, A.M., Jones, C.K., and Lindsley, C.W. (2017). Classics in Chemical Neuroscience: Xanomeline. ACS Chem. Neurosci. *8*: 435–443.

Benovic, J.L. (2021). Historical Perspective of the G Protein-Coupled Receptor Kinase Family. Cells *10*:555.

Benovic, J.L., DeBlasi, A., Stone, W.C., Caron, M.G., and Lefkowitz, R.J. (1989). B-adrenergic receptor kinase: Primary structure delineates a multigene family. Science. *246*: 235–240.

Benovic, J.L., Kuhn, H., Weyand, I., Codina, J., Caron, M.G., and Lefkowitz, R.J. (1987). Functional desensitization of the isolated beta-adrenergic receptor by the beta-adrenergic receptor kinase: potential role of an analog of the retinal protein arrestin (48-kDa protein). Proc. Natl. Acad. Sci. *84*: 8879–8882.

Bernhagen, J., Krohn, R., Lue, H., Gregory, J.L., Zernecke, A., Koenen, R.R., et al. (2007). MIF is a noncognate ligand of CXC chemokine receptors in inflammatory and atherogenic cell recruitment. Nat. Med. *13*: 587–596.

Bertini, R., Allegretti, M., Bizzarri, C., Moriconi, A., Locati, M., Zampella, G., et al. (2004). Noncompetitive allosteric inhibitors of the inflammatory chemokine receptors CXCR1 and CXCR2: Prevention of reperfusion injury. Proc. Natl. Acad. Sci. *101*: 11791–11796.

Bertini, R., Barcelos, L.S., Beccari, A.R., Cavalieri, B., and Moriconi, A. (2012).

Receptor binding mode and pharmacological characterization of a potent and selective dual CXCR1/CXCR2 non-competitive allosteric inhibitor. Br. J. Pharmacology.165:436-454.

Bertram, A., and Ley, K. (2011). Protein Kinase C Isoforms in Neutrophil Adhesion and Activation. Arch. Immunol. Ther. Exp. *59*: 79–87.

Besnard, A.-G., Struyf, S., Guabiraba, R., Fauconnier, L., Rouxel, N., Proost, P., et al. (2013). CXCL6 antibody neutralization prevents lung inflammation and fibrosis in mice in the bleomycin model. J. Leukoc. Biol. *94*: 1317–1323.

Bhat, K., Sarkissyan, M., Wu, Y., and Vadgama, J. V. (2017). GRO-overexpression drives cell migration and invasion in triple negative breast cancer cells. Oncol. Rep. *38*: 21–30.

Black, J.W., Leff, P., Shankley, N.P., and Wood, J. (1985). An operational model of pharmacological agonism: the effect of E/[A] curve shape on agonist dissociation constant estimation. Br. J. Pharmacol. *84*: 561–571.

Blanter, M., Gouwy, M., and Struyf, S. (2021). Studying Neutrophil Function in vitro: Cell Models and Environmental Factors. J. Inflamm. Res. *14*: 141.

Bokoch, M.P., Jo, H., Valcourt, J.R., Srinivasan, Y., Pan, A.C., Capponi, S., et al. (2018). Entry from the Lipid Bilayer: A Possible Pathway for Inhibition of a Peptide G Protein-Coupled Receptor by a Lipophilic Small Molecule. Biochemistry *57*: 5748–5758.

Bolitho, C., Hahn, M.A., Baxter, R.C., and Marsh, D.J. (2010). The chemokine CXCL1 induces proliferation in epithelial ovarian cancer cells by transactivation of the epidermal growth factor receptor. Endocr. Relat. Cancer *17*: 929–940.

Bondar, A., and Lazar, J. (2021). Optical sensors of heterotrimeric G protein signaling. FEBS J. *288*: 2570–2584.

Booth, V., Clark-Lewis, I., and Sykes, B.D. (2004). NMR structure of CXCR3 binding chemokine CXCL11 (ITAC). Protein Sci. *13*: 2022.

Bos, J.L., Rehmann, H., and Wittinghofer, A. (2007). GEFs and GAPs: Critical Elements in the Control of Small G Proteins. Cell *129*: 865–877.

Bosma, R., Bor, J. van den, Vischer, H.F., Labeaga, L., and Leurs, R. (2018). The long duration of action of the second generation antihistamine bilastine coincides with its long residence time at the histamine H1 receptor. Eur. J. Pharmacol. *838*: 107–111.

Bosma, R., Stoddart, L.A., Georgi, V., Bouzo-Lorenzo, M., Bushby, N., Inkoom, L., et al. (2019). Probe dependency in the determination of ligand binding kinetics at a prototypical G protein-coupled receptor. Sci. Reports. *9*: 1–13.

Boute, N., Jockers, R., and Issad, T. (2002). The use of resonance energy transfer in high-throughput screening: BRET versus FRET. Trends Pharmacol. Sci. *23*: 351–354.

Bradley, M., Bond, M., Manini, J., Brown, Z., and Charlton, S. (2009). SB265610 is an allosteric, inverse agonist at the human CXCR2 receptor. Br. J. Pharmacol. *158*: 328–338.

Bradley, M.E., Manini, J., Willis, J., Vlerick, D., Taeye, S. De, Heede, K. Van Den, et al. (2015). Potent and Efficacious Inhibition of CXCR2 Signaling by Biparatopic Nanobodies Combining Two Distinct Modes of Action s. Mol. Pharmacol. Mol Pharmacol *87*: 251–262.

Bremnes, T., Paasche, J.D., Mehlum, A., Sandberg, C., Bremnes, B., and Attramadal, H. (2000). Regulation and intracellular trafficking pathways of the endothelin receptors. J. Biol. Chem. *275*: 17596–604.

Brown, A.J., Sepuru, K.M., and Rajarathnam, K. (2017a). Structural Basis of Native CXCL7 Monomer Binding to CXCR2 Receptor N-Domain and Glycosaminoglycan Heparin. Int. J. Mol. Sci. *18*: 508.

Broxmeyer, H.E., Orschell, C.M., Clapp, D.W., Hangoc, G., Cooper, S., Plett, P.A., et al. (2005). Rapid mobilization of murine and human hematopoietic stem and progenitor cells with AMD3100, a CXCR4 antagonist. J. Exp. Med. *201*: 1307–1318.

Buanne, P., Carlo, E. Di, Caputi, L., Brandolini, L., Mosca, M., Cattani, F., et al. (2007). Crucial pathophysiological role of CXCR2 in experimental ulcerative colitis in mice. J. Leukoc. Biol. *82*: 1239–1246.

Buergisser, E., Lefkowitz, R.J., and DeLean, A. (1981). Alternative explanation for the apparent 'two-step' binding kinetics of high-affinity racemic antagonist radioligands. Mol. Pharmacol. *19*: 509–512.

Bünemann, M., Bücheler, M.M., Philipp, M., Lohse, M.J., and Hein, L. (2001). Activation and deactivation kinetics of alpha 2A- and alpha 2C-adrenergic receptor-activated G protein-activated inwardly rectifying K+ channel currents. J. Biol. Chem. *276*: 47512–47517.

Burg, J.S., Ingram, J.R., Venkatakrishnan, A.J., Jude, K.M., Dukkipati, A., Feinberg, E.N., et al. (2015a). Structural basis for chemokine recognition and activation of a viral G protein-coupled receptor. Science *347*: 1113–1117.

Cahill, T.J., Thomsen, A.R.B., Tarrasch, J.T., Plouffe, B., Nguyen, A.H., Yang, F., et al. (2017). Distinct conformations of GPCR-β-arrestin complexes mediate desensitization, signaling, and endocytosis. Proc. Natl. Acad. Sci. U. S. A. *114*: 2562–2567.

Capelli, D., Parravicini, C., Pochetti, G., Montanari, R., Temporini, C., Rabuffetti, M., et al. (2020). Surface Plasmon Resonance as a Tool for Ligand Binding Investigation of Engineered GPR17 Receptor, a G Protein Coupled Receptor Involved in Myelination. Front. Chem. *0*: 910.

Carman, C. V., and Benovic, J.L. (1998). G-protein-coupled receptors: turn-ons and turn-offs. Curr. Opin. Neurobiol. *8*: 335–344.

Carpenter, B., Nehmé, R., Warne, T., Leslie, A.G.W., and Tate, C.G. (2016).

Structure of the adenosine A2A receptor bound to an engineered G protein. Nature *536*: 104–107.

Carpenter, B., and Tate, C. (2017). Expression and Purification of Mini G Proteins from Escherichia coli. Bio-protocol *7*:2235.

Carpenter, B., and Tate, C.G. (2016). Engineering a minimal G protein to facilitate crystallisation of G protein-coupled receptors in their active conformation. Protein Eng. Des. Sel. *29*: 583–594.

Cassel, J.A., Daubert, J.D., and DeHaven, R.N. (2005). [3H]Alvimopan binding to the μ opioid receptor: Comparative binding kinetics of opioid antagonists. Eur. J. Pharmacol. *520*: 29–36.

Castillo, J. del, and Katz B. (1957). Interaction at end-plate receptors between different choline derivatives. Proc. R. Soc. Lond. B. Biol. Sci. *146*: 369–381.

Chao, T., Furth, E.E., and Vonderheide, R.H. (2016). CXCR2-dependent accumulation of tumor-associated neutrophils regulates T-cell immunity in pancreatic ductal adenocarcinoma. Cancer Immunol. Res. *4*: 968–982.

Charest, P.G., Terrillon, S., and Bouvier, M. (2005). Monitoring agonist-promoted conformational changes of β-arrestin in living cells by intramolecular BRET. EMBO Rep. *6*: 334–340.

Charlton, S.J., and Vauquelin, G. (2010). Elusive equilibrium: The challenge of interpreting receptor pharmacology using calcium assays. Br. J. Pharmacol. *161*: 1250–1265.

Che, J., Song, R., Chen, B., and Dong, X. (2019). Targeting CXCR1/2: The medicinal potential as cancer immunotherapy agents, antagonists research highlights and challenges ahead. Eur. J. Med. Chem. *185*: 1118-53.

Chen, L., Deng, H., Cui, H., Fang, J., Zuo, Z., Deng, J., et al. (2018a). Inflammatory responses and inflammation-associated diseases in organs. Oncotarget *9*: 7204–7218.

Chen, Q., Iverson, T.M., and Gurevich, V. V. (2018b). Structural basis of arrestin-dependent signal transduction. Trends Biochem. Sci. *43*: 412.

Cheng, Y., Ma, X. lei, Wei, Y. quan, and Wei, X.W. (2019a). Potential roles and targeted therapy of the CXCLs/CXCR2 axis in cancer and inflammatory diseases. Biochim. Biophys. Acta - Rev. Cancer *1871*: 289–312.

Christopoulos, A. (2002). Allosteric binding sites on cell-surface receptors: Novel targets for drug discovery. Nat. Rev. Drug Discov. *1*: 198–210.

Christopoulos, A., and Kenakin, T. (2002). G protein-coupled receptor allosterism and complexing. Pharmacol. Rev. *54*: 323–374.

cChristopoulos, A., and Mitchelson, F. (1997). Application of an Allosteric Ternary Complex Model to the Technique of Pharmacological Resultant Analysis. J. Pharm. Pharmacol. *49*: 781–786.

Chung, K.Y., Rasmussen, S.G.F., Liu, T., Li, S., DeVree, B.T., Chae, P.S., et al. (2011). Conformational changes in the G protein Gs induced by the β2 adrenergic receptor. Nature *477*: 611–5.

Citro, A., Cantarelli, E., and Piemonti, L. (2013). Anti-inflammatory strategies to enhance islet engraftment and survival. Curr. Diab. Rep. *13*: 733–744.

Clark, A.L., and Mitcheson, F. (1976). The inhibitory effect of gallamine on muscarinic receptors. Br. J. Pharmacol. *58*: 323–331.

Clore, G.M., Appella, E., Yamada, M., Matsushima, K., and Gronenborn, A.M. (2002). Three-dimensional structure of interleukin 8 in solution. Biochemistry *29*: 1689–1696.

Cong, X., and Golebiowski, J. (2018). Allosteric Na+-binding site modulates CXCR4 activation. Phys. Chem. Chem. Phys. *20*: 24915–24920.

Conklin, B.R., Herzmark, P., Ishida, S., Voyno-Yasenetskaya, T.A., Sun, Y., Farfel, Z., et al. (1996). Carboxyl-terminal mutations of Gq alpha and Gs alpha that alter the fidelity of receptor activation. Mol. Pharmacol. *50*:885-890.

Conn, P.J., Jones, C.K., and Lindsley, C.W. (2009). Subtype-selective allosteric modulators of muscarinic receptors for the treatment of CNS disorders. Trends Pharmacol. Sci. *30*: 148–155.

Copeland, R.A., Pompliano, D.L., and Meek, T.D. (2006). Drug-target residence time and its implications for lead optimization. Nat. Rev. Drug Discov. *5*: 730–739.

Cromie, K., Heeke, G., and Boutton, C. (2015). Nanobodies and their Use in GPCR Drug Discovery. Curr. Top. Med. Chem. *15*: 2543–2557.

Das, S.T., Rajagopalan, L., Guerrero-Plata, A., Sai, J., Richmond, A., Garofalo, R.P., et al. (2010). Monomeric and Dimeric CXCL8 Are Both Essential for In Vivo Neutrophil Recruitment. PLoS One *5*: 117-154.

Degorce, F., Card, A., Soh, S., Trinquet, E., Knapik, G.P., and Xie, B. (2009). HTRF: A technology tailored for drug discovery - a review of theoretical aspects and recent applications. Curr. Chem. Genomics *3*: 22–32.

Delhaye, M., Gravot, A., Ayinde, D., Niedergang, F., Alizon, M., and Brelot, A. (2007). Identification of a Postendocytic Sorting Sequence in CCR5. Mol. Pharmacol. *72*: 1497–1507.

Derendorf, H., Lesko, L.J., Chaikin, P., Colburn, W.A., Lee, P., Miller, R., et al. (2000). Pharmacokinetic/pharmacodynamic modeling in drug research and development. J. Clin. Pharmacol. *40*: 1399–1418.

Devalaraja, R.M., Nanney, L.B., Qian, Q., Du, J., Yu, Y., Devalaraja, M.N., et al. (2000). Delayed Wound Healing in CXCR2 Knockout Mice. J. Invest. Dermatol. *115*: 234.

Diao, W., Tong, X., Yang, C., Zhang, F., Bao, C., Chen, H., et al. (2019). Behaviors

of Glioblastoma Cells in in Vitro Microenvironments. Sci. Reports 2019 91 *9*: 1–9.

Disse, B., Reichl, R., Speck, G., Traunecker, W., Rominger, K.L., and Hammer, R. (1993). Ba 679 BR, A novel long-acting anticholinergic bronchodilator. Life Sci. *52*: 537–544.

Dixon, A.S., Schwinn, M.K., Hall, M.P., Zimmerman, K., Otto, P., Lubben, T.H., et al. (2016). NanoLuc Complementation Reporter Optimized for Accurate Measurement of Protein Interactions in Cells. ACS Chem. Biol. *11*: 400–408.

Doornbos, M.L.J., Vermond, S.C., Lavreysen, H., Tresadern, G., IJzerman, A.P., and Heitman, L.H. (2018). Impact of allosteric modulation: Exploring the binding kinetics of glutamate and other orthosteric ligands of the metabotropic glutamate receptor 2. Biochem. Pharmacol. *155*: 356–365.

Downes, G.B., and Gautam, N. (1999). The G protein subunit gene families. Genomics *62*: 544–552.

Draper-Joyce, CJ. Khoshouei,M., Thal, DM., Liang, YL., Nguyen, ATN., Furness SGB. et al. (2018). Structure of the adenosine-bound human adenosine A 1 receptor-G i complex. Nature *558*: 559–565.

Draper-Joyce, C.J., Verma, R.K., Michino, M., Shonberg, J., Kopinathan, A., Klein Herenbrink, C., et al. (2018). The action of a negative allosteric modulator at the dopamine D2 receptor is dependent upon sodium ions. Sci. Rep. *8*: 1208.

Drury, L.J., Ziarek, J.J., Gravel, S., Veldkamp, C.T., Takekoshi, T., Hwang, S.T., et al. (2011). Monomeric and dimeric CXCL12 inhibit metastasis through distinct CXCR4 interactions and signaling pathways. Proc. Natl. Acad. Sci. *108*: 17655–17660.

Dwyer, M.P., Yu, Y., Chao, J., Aki, C., Chao, J., Biju, P., et al. (2006). Discovery of 2-hydroxy-N,N-dimethyl-3-{2-[[(R)-1-(5-methylfuran-2-yl) propyl]amino]-3,4-dioxocyclobut-1-enylamino}benzamide (SCH 527123): A potent, orally bioavailable CXCR2/CXCR1 receptor antagonist. J. Med. Chem. *49*: 7603–7606.

Dyer, D.P. (2020a). Understanding the mechanisms that facilitate specificity, not redundancy, of chemokine-mediated leukocyte recruitment. Immunology *160*: 336–344.

Dyer, D.P., Medina-Ruiz, L., Bartolini, R., Schuette, F., Hughes, C.E., Pallas, K., et al. (2019a). Chemokine Receptor Redundancy and Specificity Are Context Dependent. Immunity *50*: 378-389.

Eash, K.J., Greenbaum, A.M., Gopalan, P.K., and Link, D.C. (2010). CXCR2 and CXCR4 antagonistically regulate neutrophil trafficking from murine bone marrow. J. Clin. Invest. *120*: 2423–2431.

Eckhard, U., Huesgen, P.F., Schilling, O., Bellac, C.L., Butler, G.S., Cox, J.H., et al. (2016). Active site specificity profiling of the matrix metalloproteinase family: Proteomic identification of 4300 cleavage sites by nine MMPs explored with structural and synthetic peptide cleavage analyses. Matrix Biol. *49*: 37–60.

Ehlert, F.J. (1988). Estimation of the affinities of allosteric ligands using radioligand binding and pharmacological null methods. Mol. Pharmacol. *33*:187-194.

Emami-Nemini, A., Roux, T., Leblay, M., Bourrier, E., Lamarque, L., Trinquet, E., et al. (2013). Time-resolved fluorescence ligand binding for G protein–coupled receptors. Nat. Protoc. *8*: 1307–1320.

Fan, G.H., Yang, W., Wang, X.J., Qian, Q., and Richmond, A. (2001). Identification of a motif in the carboxyl terminus of CXCR2 that is involved in adaptin 2 binding and receptor internalization. Biochemistry *40*: 791–800.

Feinstein, T.N., Yui, N., Webber, M.J., Wehbi, V.L., Stevenson, H.P., King, J.D., et al. (2013). Noncanonical control of vasopressin receptor type 2 signaling by retromer and arrestin. J. Biol. Chem. *288*: 27849–27860.

Felder, C.C., Goldsmith, P.J., Jackson, K., Sanger, H.E., Evans, D.A., Mogg, A.J., et al. (2018). Current status of muscarinic M1 and M4 receptors as drug targets for neurodegenerative diseases. Neuropharmacology *136*: 449–458.

Fernández-Dueñas, V., Gómez-Soler, M., Morató, X., Núñez, F., Das, A., Kumar, T.S., et al. (2013). Dopamine D2 receptor-mediated modulation of adenosine A 2A receptor agonist binding within the A2AR/D2R oligomer framework. Neurochem. Int. *63*: 42–46.

Filipek, S. (2019). Molecular switches in GPCRs. Curr. Opin. Struct. Biol. *55*: 114–120.

Flock, T., Hauser, A.S., Lund, N., Gloriam, D.E., Balaji, S., and Babu, M.M. (2017). Selectivity determinants of GPCR–G-protein binding. Nat. *545*: 317–322.

Flock, T., Ravarani, C.N.J., Sun, D., Venkatakrishnan, A.J., Kayikci, M., Tate, C.G., et al. (2015). Universal allosteric mechanism for Gα activation by GPCRs. Nat. *524*: 173–179.

Foster, D.J., and Conn, P.J. (2017). Allosteric Modulation of GPCRs: New Insights and Potential Utility for Treatment of Schizophrenia and Other CNS Disorders. Neuron *94*: 431–446.

Fredriksson, R. (2003). The G-Protein-Coupled Receptors in the Human Genome Form Five Main Families. Phylogenetic Analysis, Paralogon Groups, and Fingerprints. Mol. Pharmacol. *63*: 1256–1272.

Fredriksson, R., Lagerström, M.C., Lundin, L.G., and Schiöth, H.B. (2003). The G-protein-coupled receptors in the human genome form five main families. Phylogenetic analysis, paralogon groups, and fingerprints. Mol. Pharmacol. *63*: 1256–1272.

Frendéus, B., Godaly, G., Hang, L., Karpman, D., Lundstedt, A.C., and Svanborg, C. (2000). Interleukin 8 receptor deficiency confers susceptibility to acute experimental pyelonephritis and may have a human counterpart. J. Exp. Med. *192*: 881–90.

Friedman, S., Tauber, M., and Ben-Chaim, Y. (2020). Sodium ions allosterically modulate the M2 muscarinic receptor. Sci. Reports *10*: 1–10.

Fu, W., Zhang, Y., Zhang, J., and Chen, W.F. (2005). Cloning and characterization of mouse homolog of the CXC chemokine receptor CXCR1. Cytokine *31*: 9–17.

Fung, B.K., Hurley, J.B., and Stryer, L. (1981). Flow of information in the light-triggered cyclic nucleotide cascade of vision. Proc. Natl. Acad. Sci. U. S. A. *78*: 152.

Galdiero, M.R., Varricchi, G., Loffredo, S., Mantovani, A., and Marone, G. (2018). Roles of neutrophils in cancer growth and progression. J. Leukoc. Biol. *103*: 457–464.

Galés, C., Durm, J.J.J. Van, Schaak, S., Pontier, S., Percherancier, Y., Audet, M., et al. (2006). Probing the activation-promoted structural rearrangements in preassembled receptor–G protein complexes. Nat. Struct. Mol. Biol. *13*: 778–786.

Gangavarapu, P., Rajagopalan, L., Kolli, D., Guerrero-Plata, A., Garofalo, R.P., and Rajarathnam, K. (2012). The monomer-dimer equilibrium and glycosaminoglycan interactions of chemokine CXCL8 regulate tissue-specific neutrophil recruitment. J. Leukoc. Biol. *91*: 259.

García-Nafría, J., Lee, Y., Bai, X., Carpenter, B., and Tate, C.G. (2018a). Cryo-EM structure of the adenosine A2A receptor coupled to an engineered heterotrimeric G protein. Elife *7*: 359-46.

García-Nafría, J., Nehmé, R., Edwards, P.C., and Tate, C.G. (2018b). Cryo-EM structure of the serotonin 5-HT1B receptor coupled to heterotrimeric Go. Nature *558*: 620.

García-Nafría, J., and Tate, C.G. (2019). Cryo-EM structures of GPCRs coupled to Gs, Gi and Go. Mol. Cell. Endocrinol. *488*: 1–13.

Gherbi, K., Briddon, S.J., and Charlton, S.J. (2018). Micro-pharmacokinetics: Quantifying local drug concentration at live cell membranes. Sci. Rep. *8*: 1–8.

Gherbi, K., May, L.T., Baker, J.G., Briddon, S.J., and Hill, S.J. (2015). Negative cooperativity across β1-adrenoceptor homodimers provides insights into the nature of the secondary low-affinity CGP 12177 β1-adrenoceptor binding conformation. FASEB J. *29*: 2859–2871.

Gonsiorek, W., Fan, X., Hesk, D., Fossetta, J., Qiu, H., Jakway, J., et al. (2007a). Pharmacological characterization of Sch527123, a potent allosteric CXCR1/CXCR2 antagonist. J. Pharmacol. Exp. Ther. *322*: 477–85.

Goupil, E., A. Laporte, S., and E. Hebert, T. (2012). Functional Selectivity in GPCR Signaling: Understanding the Full Spectrum of Receptor Conformations. Mini-Reviews Med. Chem. *12*: 817–830.

Griffith, J.W., Sokol, C.L., and Luster, A.D. (2014a). Chemokines and Chemokine

Receptors: Positioning Cells for Host Defense and Immunity. Annu. Rev. Immunol. *32*: 659–702.

Grime, R.L., Goulding, J., Uddin, R., Stoddart, L.A., Hill, S.J., Poyner, D.R., et al. (2020). Single molecule binding of a ligand to a G-protein-coupled receptor in real time using fluorescence correlation spectroscopy, rendered possible by nano-encapsulation in styrene maleic acid lipid particles. Nanoscale *12*: 11518–11525.

Grundmann, M., and Kostenis, E. (2017). Temporal Bias: Time-Encoded Dynamic GPCR Signaling. Trends Pharmacol. Sci. *38*: 1110–1124.

Gundry, J., Glenn, R., Alagesan, P., and Rajagopal, S. (2017). A practical guide to approaching biased agonism at G protein coupled receptors. Front. Neurosci. *11*: 17.

Gurevich, E. V., Tesmer, J.J.G., Mushegian, A., and Gurevich, V. V. (2012). G protein-coupled receptor kinases: more than just kinases and not only for GPCRs. Pharmacol. Ther. *133*: 40.

Gurevich, E. V, and Gurevich, V. V (2006). Arrestins: ubiquitous regulators of cellular signaling pathways. Genome Biol. *7*: 236.

Gurevich, V. V., and Gurevich, E. V. (2019). GPCR signaling regulation: The role of GRKs and arrestins. Front. Pharmacol. *10*: 125.

Gurevich, V. V., Gurevich, E. V., and Uversky, V.N. (2018). Arrestins: structural disorder creates rich functionality. Protein Cell 2018 912 *9*: 986–1003.

Gustavsson, M., Dyer, D.P., Zhao, C., and Handel, T.M. (2019). Kinetics of CXCL12 binding to atypical chemokine receptor 3 reveal a role for the receptor N-terminus in chemokine binding. Sci. Signal. *12*:.

Gutié Rrez-De-Terá, H., Massink, A., Rodríguez, D., Liu, W., Han, G.W., Joseph, J.S., et al. (2013). The Role of a Sodium Ion Binding Site in the Allosteric Modulation of the A 2A Adenosine G Protein-Coupled Receptor. Struct. Des. *21*: 2175–2185.

Ha, H., Debnath, B., and Neamati, N. (2017). Theranostics. Role of the CXCL8-CXCR1 / 2 Axis in Cancer and Inflammatory Diseases. *7*: 1543-1588.

Hall, D.A. (2000). Modeling the functional effects of allosteric modulators at pharmacological receptors: An extension of the two-state model of receptor activation. Mol. Pharmacol. *58*: 1412–1423.

Hall, M.P., Unch, J., Binkowski, B.F., Valley, M.P., Butler, B.L., Wood, M.G., et al. (2012). Engineered luciferase reporter from a deep sea shrimp utilizing a novel imidazopyrazinone substrate. ACS Chem. Biol. *7*: 1848–1857.

Hamm, H.E., Deretic, D., Arendt, A., Hargrave, P.A., Koenig, B., and Hofmann, K.P. (1988). Site of G protein binding to rhodopsin mapped with synthetic peptides from the α subunit. Science *241*: 832–835.

Handel, T.M., and Dyer, D.P. (2021). Perspectives on the Biological Role of Chemokine:Glycosaminoglycan Interactions. J. Histochem. Cytochem. *69*: 87–91.

Hansen C., Nichols, B. (2003). Molecular mechnaisms of clathrin-independnet endocytosis. J. Cell Sci. *116*: 4707–4714.

Hanson, M.A., Roth, C.B., Jo, E., Griffith, M.T., Scott, F.L., Reinhart, G., et al. (2012). Crystal structure of a lipid G protein-coupled receptor. Science *335*: 851–855.

Harrison, C., and Traynor, J.R. (2003). The [35S]GTPγS binding assay: Approaches and applications in pharmacology. Life Sci. *74*: 489–508.

Hatse, S., Princen, K., Liekens, S., Vermeire, K., Clercq, E. De, and Schols, D. (2004). Fluorescent CXCL12AF647 as a novel probe for nonradioactive CXCL12/CXCR4 cellular interaction studies. Cytom. Part A *61*: 178–188.

Hay, D.L., and Pioszak, A.A. (2016). Receptor Activity-Modifying Proteins (RAMPs): New Insights and Roles. Annu. Rev. Pharmacol. Toxicol. *56*: 469–487.

Hein, P., Frank, M., Hoffmann, C., Lohse, M.J., and Bünemann, M. (2005). Dynamics of receptor/G protein coupling in living cells. EMBO J. *24*: 4106.

Hein, P., Rochais, F., Hoffmann, C., Dorsch, S., Nikolaev, V.O., Engelhardt, S., et al. (2006). Gs activation is time-limiting in initiating receptor-mediated signaling. J. Biol. Chem. *281*: 33345–51.

Herenbrink, C.K., Sykes, D.A., Donthamsetti, P., Canals, M., Coudrat, T., Shonberg, J., et al. (2016). The role of kinetic context in apparent biased agonism at GPCRs. Nat. Commun. *7*: 108-42.

Heukers, R., Groof, T.W.M. De, and Smit, M.J. (2019). Nanobodies detecting and modulating GPCRs outside in and inside out. Curr. Opin. Cell Biol. *57*: 115–122.

Higashijima, T., Ferguson, K.M., and Sternweis, P.C. (1987). Effects of Mg2+ and the βγ-subunit complex on the interactions of guanine nucleotides with G proteins. J. Biol. Chem. *262*: 762–766.

Hilger, D., Kumar, K.K., Hu, H., Pedersen, M.F., O'Brien, E.S., Giehm, L., et al. (2020). Structural insights into differences in G protein activation by family A and family B GPCRs. Science. *369*:.

Hill, S.J., Williams, C., and May, L.T. (2010). Insights into GPCR pharmacology from the measurement of changes in intracellular cyclic AMP; advantages and pitfalls of differing methodologies. Br. J. Pharmacol. *161*: 1266.

Hirsch, J.A., Schubert, C., Gurevich, V. V., and Sigler, P.B. (1999). A Model for Arrestin's Regulation: The 2.8 Å Crystal Structure of Visual Arrestin. Cell *97*: 257–269.

Hoffmann, C., Castro, M., Rinken, A., Leurs, R., Hill, S.J., and Vischer, H.F.

(2015a). Ligand Residence Time at G-protein–Coupled Receptors—Why We Should Take Our Time To Study It. Mol. Pharmacol. *88*: 552–560.

Hoffmann, C., Zürn, A., Bünemann, M., and Lohse, M.J. (2008). Conformational changes in G-protein-coupled receptors - The quest for functionally selective conformations is open. Br. J. Pharmacol. *153*: 358–366.

Holz, O., Khalilieh, S., Ludwig-Sengpiel, A., Watz, H., Stryszak, P., Soni, P., et al. (2010). SCH527123, a novel CXCR2 antagonist, inhibits ozone-induced neutrophilia in healthy subjects. Eur. Respir. J. *35*: 564–570.

Hoogewerf, A.J., Kuschert, G.S.V., Proudfoot, A.E.I., Borlat, F., Clark-Lewis, I., Power, C.A., et al. (1997). Glycosaminoglycans mediate cell surface oligomerization of chemokines. Biochemistry *36*: 13570–13578.

Hout, A. Van, Klarenbeek, A., Bobkov, V., Doijen, J., Arimont, M., Zhao, C., et al. (2018). CXCR4-targeting nanobodies differentially inhibit CXCR4 function and HIV entry. Biochem. Pharmacol. *158*: 402–412.

Hsu, Y.L., Hou, M.F., Kuo, P.L., Huang, Y.F., and Tsai, E.M. (2013). Breast tumor-associated osteoblast-derived CXCL5 increases cancer progression by ERK/MSK1/Elk-1/Snail signaling pathway. Oncogene *32*: 4436–4447.

Hu, MJ.,Shao XX., Li HZ., Nie WH., Wang JH., Liu YL., et al. (2018). Development of a novel ligand binding assay for relaxin family peptide receptor 3 and 4 using NanoLuc complementation. Amino Acids *50*: 1111–1119.

Huang, W., Masureel, M., Qu, Q., Janetzko, J., Inoue, A., Kato, H.E., et al. (2020). Structure of the neurotensin receptor 1 in complex with β-arrestin 1. Nat. 2020 5797798 *579*: 303–308.

Hubbell, W.L., Altenbach, C., Hubbell, C.M., and Khorana, H.G. (2003). Rhodopsin structure, dynamics, and activation: A perspective from crystallography, site-directed spin labeling, sulfhydryl reactivity, and disulfide cross-linking. Adv. Protein Chem. *63*: 243–290.

Huber, M.E., Toy, L., Schmidt, M.F., Vogt, H., Budzinski, J., Wiefhoff, M.F.J., et al. (2021). A Chemical Biology Toolbox Targeting the Intracellular Binding Site of CCR9: Fluorescent Ligands, New Drug Leads and PROTACs. Angew. Chemie Int. Ed.

Hughes, C.E., and Nibbs, R.J.B. (2018). A guide to chemokines and their receptors. Febs J. *285*: 2944.

Hulme, E.C., Birdsall, N.J.M., Burgen, A.S.V., and Mehta, P. (1978). The binding of antagonists to brain muscarinic receptors. Mol. Pharmacol. *14*: 737–750.

Hulme, E.C., and Trevethick, M.A. (2010a). Ligand binding assays at equilibrium: Validation and interpretation. Br. J. Pharmacol. *161*: 1219–1237.

Hurst, D.P., Grossfield, A., Lynch, D.L., Feller, S., Romo, T.D., Gawrisch, K., et al. (2010). A Lipid Pathway for Ligand Binding Is Necessary for a Cannabinoid G Protein-coupled Receptor. J. Biol. Chem. *285*: 17954.

Hwang, B. (Brian), Engel, L., Goueli, S.A., and Zegzouti, H. (2020). A homogeneous bioluminescent immunoassay to probe cellular signaling pathway regulation. Commun. Biol. *3*: 1–12.

Ilien, B., Franchet, C., Bernard, P., Morisset, S., Weill, C.O., Bourguignon, J.J., et al. (2003). Fluorescence resonance energy transfer to probe human M1 muscarinic receptor structure and drug binding properties. J. Neurochem. *85*: 768–778.

Im, S.-Y., Wiedmeier, S.E., Cho, B.-H., Lee, D.G., Beigi, M., and Daynes, R.A. (1989). Dual effects of pertussis toxin on murine neutrophils in vivo. Inflamm. *13*: 707–726.

Innamorati, G., Gouill, C. Le, Balamotis, M., and Birnbaumer, M. (2001). The long and the short cycle. Alternative intracellular routes for trafficking of G-protein-coupled receptors. J. Biol. Chem. *276*: 13096–103.

Inoue, A., Raimondi, F., Kadji, F.M.N., Singh, G., Kishi, T., Uwamizu, A., et al. (2019). Illuminating G-Protein-Coupling Selectivity of GPCRs. Cell *177*: 1933.

Insel, P.A., and Stoolman, L.M. (1978). Radioligand binding to beta adrenergic receptors of intact cultured S49 cells. Mol. Pharmacol. *14*: 549–561.

Işbilir, A., Möller, J., Arimont, M., Bobkov, V., Perpiñá-Viciano, C., Hoffmann, C., et al. (2020). Advanced fluorescence microscopy reveals disruption of dynamic CXCR4 dimerization by subpocket-specific inverse agonists. Proc. Natl. Acad. Sci. U. S. A. *117*: 29144–29154.

Issafras, H., Angers, S., Bulenger, S., Blanpain, C., Parmentier, M., Labbé-Jullié, C., et al. (2002). Constitutive Agonist-independent CCR5 Oligomerization and Antibody-mediated Clustering Occurring at Physiological Levels of Receptors. J. iol. Chem. *277*: 34666–34673.

Jaeger, K., Bruenle, S., Weinert, T., Guba, W., Muehle, J., Miyazaki, T., et al. (2019). Structural Basis for Allosteric Ligand Recognition in the Human CC Chemokine Receptor 7. Cell *178*: 1222-1230.

Jensen, P.C., Thiele, S., Ulven, T., Schwartz, T.W., and Rosenkilde, M.M. (2008). Positive Versus Negative Modulation of Different Endogenous Chemokines for CC-chemokine Receptor 1 by Small Molecule Agonists through Allosteric Versus Orthosteric Binding . J. Biol. Chem. *283*: 23121–23128.

Jiang, C., Amaradhi, R., Ganesh, T., and Dingledine, R. (2020). An Agonist Dependent Allosteric Antagonist of Prostaglandin EP2 Receptors. ACS Chem. Neurosci. *11*: 1436–1446.

Jin, H., Shen, X., Baggett, B.R., Kong, X., and LiWang, P.J. (2007). The human CC chemokine MIP-1β dimer is not competent to bind to the CCR5 receptor. J. Biol. Chem. *282*: 27976–27983.

Jin, T., Xu, X., and Hereld, D. (2008). Chemotaxis, chemokine receptors and human disease. Cytokine *44*: 1.

Johnson, Z., Proudfoot, A., and Handel, T. (2005). Interaction of chemokines and glycosaminoglycans: a new twist in the regulation of chemokine function with opportunities for therapeutic intervention. Cytokine Growth Factor Rev. *16*: 625–636.

Jones, G.A., and Bradshaw, D.S. (2019). Resonance Energy Transfer: From Fundamental Theory to Recent Applications. Front. Phys. *0*: 100.

Joseph, P.R.B., Sarmiento, J.M., Mishra, A.K., Das, S.T., Garofalo, R.P., Navarro, J., et al. (2010). Probing the role of CXC motif in chemokine CXCL8 for high affinity binding and activation of CXCR1 and CXCR2 receptors. J. Biol. Chem. *285*: 29262–29269.

Jurcevic, S., Humfrey, C., Uddin, M., Warrington, S., Larsson, B., and Keen, C. (2015). The effect of a selective CXCR2 antagonist (AZD5069) on human blood neutrophil count and innate immune functions. Br. J. Clin. Pharmacol. *80*: 1324–1336.

Kalatskaya, I., Berchiche, Y.A., Gravel, S., Limberg, B.J., Rosenbaum, J.S., and Heveker, N. (2009). AMD3100 Is a CXCR7 Ligand with Allosteric Agonist Properties. Mol. Pharmacol. *75*: 1240–1247.

Kaneider, N.C., Agarwal, A., Leger, A.J., and Kuliopulos, A. (2005). Reversing systemic inflammatory response syndrome with chemokine receptor pepducins. Nat. Med. *11*: 661–665.

Kang, Y., Zhou, X.E., Gao, X., He, Y., Liu, W., Ishchenko, A., et al. (2015). Crystal structure of rhodopsin bound to arrestin by femtosecond X-ray laser. Nature *523*: 561–7.

Kapur, S., and Seeman, P. (2001). Does fast dissociation from the dopamine D2 receptor explain the action of atypical antipsychotics?: A new hypothesis. Am. J. Psychiatry *158*: 360–369.

Katoh, H., Wang, D., Daikoku, T., Sun, H., Dey, S.K., and DuBois, R.N. (2013). CXCR2-expressing myeloid-derived suppressor cells are essential to promote colitis-associated tumorigenesis. Cancer Cell *24*: 631.

Katritch, V., Cherezov, V., and Stevens, R.C. (2012). Diversity and Modularity of G Protein-Coupled Receptor Structures. Trends Pharmacol. Sci. *33*: 17.

Katritch, V., Fenalti, G., Abola, E.E., Roth, B.L., Cherezov, V., and Stevens, R.C. (2014). Allosteric sodium in class A GPCR signaling. Trends Biochem. Sci. *39*: 233–244.

Kawamura, T., Stephens, B., Qin, L., Yin, X., Dores, M.R., Smith, T.H., et al. (2014a). A General Method for Site Specific Fluorescent Labeling of Recombinant Chemokines. PLoS One *9*:.

Kenakin, T. (2004). Principles: Receptor theory in pharmacology. Trends Pharmacol. Sci. *25*: 186–192.

Kenakin, T. (2006). Orthosteric Drug Antagonism. A Pharmacology Primer,

(Elsevier), pp 99–126.

Kenakin, T. (2013). Allosteric Drugs and Seven Transmembrane Receptors. Curr. Top. Med. Chem. *13*: 5–13.

Kenakin, T. (2016). The mass action equation in pharmacology. Br. J. Clin. Pharmacol. *81*: 41–51.

Kenakin, T. (2017). Theoretical aspects of GPCR-ligand complex pharmacology. Chem. Rev. *117*: 4–20.

Kenakin, T., Jenkinson, S., and Watson, C. (2006). Determining the potency and molecular mechanism of action of insurmountable antagonists. J. Pharmacol. Exp. Ther. *319*: 710–723.

Kiefer, F., and Siekmann, A.F. (2011). The role of chemokines and their receptors in angiogenesis. Cell. Mol. Life Sci. *68*: 2811–2830.

Kilpatrick, L.E., Briddon, S.J., Hill, S.J., and Holliday, N.D. (2010). Quantitative analysis of neuropeptide Y receptor association with β-arrestin2 measured by bimolecular fluorescence complementation. Br. J. Pharmacol. *160*: 892.

Kilpatrick, L.E., Briddon, S.J., and Holliday, N.D. (2012). Fluorescence correlation spectroscopy, combined with bimolecular fluorescence complementation, reveals the effects of β-arrestin complexes and endocytic targeting on the membrane mobility of neuropeptide Y receptors. Biochim. Biophys. Acta *1823*: 1068–1081.

Kilpatrick, L.E., Humphrys, L.J., and Holliday, N.D. (2015). A G protein-coupled receptor dimer imaging assay reveals selectively modified pharmacology of neuropeptide y Y1/Y5 receptor heterodimers. Mol. Pharmacol. *87*: 718–732.

Klein Herenbrink, C., Sykes, D.A., Donthamsetti, P., Canals, M., Coudrat, T., Shonberg, J., et al. (2016). The role of kinetic context in apparent biased agonism at GPCRs. Nat. Commun. *7*: 1–14.

Kleist, A.B., Getschman, A.E., Ziarek, J.J., Nevins, A.M., Gauthier, P.-A., Chevigné, A., et al. (2016). New paradigms in chemokine receptor signal transduction: Moving beyond the two-site model. Biochem. Pharmacol. *114*: 53–68.

Koch, W.J., Inglese, J., Stone, W.C., and Lefkowitz, R.J. (1993). The binding site for the βγ subunits of heterotrimeric G proteins on the β-adrenergic receptor kinase. J. Biol. Chem. *268*: 8256–8260.

Koehl, A., Hu, H., Maeda, S., Zhang, Y., Qu, Q., Paggi, J.M., et al. (2018a). Structure of the μ-opioid receptor–Gi protein complex. Nat. *558*: 547–552.

Kolberg, K., Puettmann, C., Pardo, A., Fitting, J., and Barth, S. (2013). SNAP-Tag Technology: A General Introduction. Curr. Pharm. Des. *19*: 5406–5413.

Kollmar, O., Junker, B., Rupertus, K., Scheuer, C., Menger, M.D., and Schilling, M.K. (2008). Liver Resection-Associated Macrophage Inflammatory Protein-2

Stimulates Engraftment but not Growth of Colorectal Metastasis at Extrahepatic Sites. J. Surg. Res. *145*: 295–302.

Komolov, K.E., and Benovic, J.L. (2018). G protein-coupled receptor kinases: Past, present and future. Cell. Signal. *41*: 17–24.

Koppen, C.J. Van, and Jakobs, K.H. (2004). Arrestin-independent internalization of G protein-coupled receptors. Mol. Pharmacol. *66*: 365–367.

Korczynska, M., Clark, M.J., Valant, C., Xu, J., Moo, E. Von, Albold, S., et al. (2018). Structure-based discovery of selective positive allosteric modulators of antagonists for the M2 muscarinic acetylcholine receptor. Proc. Natl. Acad. Sci. U. S. A. *115*: 2419–2428.

Kozma, E., Gizewski, E.T., Tosh, D.K., Squarcialupi, L., Auchampach, J.A., and Jacobson, K.A. (2013). Characterization by flow cytometry of fluorescent, selective agonist probes of the A3 adenosine receptor. Biochem. Pharmacol. *85*: 1171–1181.

Kruijf, P. de, Heteren, J. van, Lim, H.D., Conti, P.G.M., Lee, M.M.C. van der, Bosch, L., et al. (2009). Nonpeptidergic Allosteric Antagonists Differentially Bind to the CXCR2 Chemokine Receptor. J. Pharmacol. Exp. Ther. *329*: 783–790.

Kruijf, P. De, Lim, H.D., Roumen, L., Zhao, J., Webb, M.L., Auld, D.S., et al. (2011). Identification of a Novel Allosteric Binding Site in the CXCR2 Chemokine Receptor *80*: 1108–1118.

Kufareva, I., Salanga, C.L., and Handel, T.M. (2015b). Chemokine and chemokine receptor structure and interactions: Implications for therapeutic strategies. Immunol. Cell Biol. *93*: 372–383.

Kufareva, I., Stephens, B.S., Holden, L.G., Qin, L., Zhao, C., Kawamura, T., et al. (2014). Stoichiometry and geometry of the CXC Chemokine receptor 4 complex with CXC ligand 12: Molecular modeling and experimental validation. Proc. Natl. Acad. Sci. U. S. A. *111*: 5363–5372.

Kumari, P., Srivastava, A., Ghosh, E., Ranjan, R., Dogra, S., Yadav, P.N., et al. (2017). Core engagement with β-arrestin is dispensable for agonist-induced vasopressin receptor endocytosis and ERK activation. Mol. Biol. Cell *28*: 1003.

Lane, J.R., May, L.T., Parton, R.G., Sexton, P.M., and Christopoulos, A. (2017). A kinetic view of GPCR allostery and biased agonism. Nat. Chem. Biol. *13*: 929–937.

Laschet, C., Dupuis, N., and Hanson, J. (2019). A dynamic and screening-compatible nanoluciferase-based complementation assay enables profiling of individual GPCR–G protein interactions. J. Biol. Chem. *294*: 4079.

Latorraca, N.R., Venkatakrishnan, A.J., and Dror, R.O. (2017). GPCR dynamics: Structures in motion. Chem. Rev. *117*: 139–155.

Lau, E.K., Paavola, C.D., Johnson, Z., Gaudry, J.P., Geretti, E., Borlat, F., et al. (2004). Identification of the glycosaminoglycan binding site of the CC chemokine, MCP-1: implications for structure and function in vivo. J. Biol. Chem. *279*: 22294–22305.

Lazaar, A.L., Miller, B.E., Donald, A.C., Keeley, T., Ambery, C., Russell, J., et al. (2020). CXCR2 antagonist for patients with chronic obstructive pulmonary disease with chronic mucus hypersecretion: A phase 2b trial. Respir. Res. *21*:.

Lazaar, A.L., Sweeney, L.E., Macdonald, A.J., Alexis, N.E., Chen, C., and Tal-Singer, R. (2011). SB-656933, a novel CXCR2 selective antagonist, inhibits ex vivo neutrophil activation and ozone-induced airway inflammation in humans. Br. J. Clin. Pharmacol. *72*: 282–293.

Lazennec, G., and Richmond, A. (2010). Chemokines and chemokine receptors: new insights into cancer-related inflammation. Trends Mol. Med. *16*: 133–144.

Lean, A. De, Stadel, J.M., and Lefkowitz, R.J. (1980). A ternary complex model explains the agonist-specific binding properties of the adenylate cyclase-coupled beta-adrenergic receptor. J. Biol. Chem. *255*: 7108–17.

Lefkowitz, R.J. (1993). G protein-coupled receptor kinases. Cell *74*: 409–412.

Li, A., Dubey, S., Varney, M.L., Dave, B.J., and Singh, R.K. (2003). IL-8 Directly Enhanced Endothelial Cell Survival, Proliferation, and Matrix Metalloproteinases Production and Regulated Angiogenesis. J. Immunol. *170*: 3369–3376.

Lieberman-Blum, S.S., Fung, H.B., and Bandres, J.C. (2008). Maraviroc: A CCR5-receptor antagonist for the treatment of HIV-1 infection. Clin. Ther. *30*: 1228–1250.

Lindström, E., Mentzer, B. Von, Påhlman, I., Ahlstedt, I., Uvebrant, A., Kristensson, E., et al. (2007). Neurokinin 1 receptor antagonists: Correlation between in vitro receptor interaction and in vivo efficacy. J. Pharmacol. Exp. Ther. *322*: 1286–1293.

Litschig, S., Gasparini, F., Rueegg, D., Stoehr, N., Josef Flor, P., Vranesic, I., et al. (1993). CPCCOEt, a Noncompetitive Metabotropic Glutamate Receptor 1 Antagonist, Inhibits Receptor Signaling Without Affecting Glutamate Binding. Mol. Pharmacol. *55*:453-61.

Littmann, T., Ozawa, T., Hoffmann, C., Buschauer, A., and Bernhardt, G. (2018). A split luciferase-based probe for quantitative proximal determination of Gαq signalling in live cells. Sci. Rep. *8*: 17179.

Liu, K., Wu, L., Yuan, S., Wu, M., Xu, Y., Sun, Q., et al. (2020). Structural basis of CXC chemokine receptor 2 activation and signalling. Nature *585*: 135–140.

Lodowski, D.T., Tesmer, V.M., Benovic, J.L., and Tesmer, J.J.G. (2006). The Structure of G Protein-coupled Receptor Kinase (GRK)-6 Defines a Second Lineage of GRKs. J. Biol. Chem. *281*: 16785–16793.

Loetscher, P., Pellegrino, A., Gong, J.H., Mattioli, I., Loetscher, M., Bardi, G., et al. (2001). The Ligands of CXC Chemokine Receptor 3, I-TAC, Mig, and IP10, Are Natural Antagonists for CCR3. J. Biol. Chem. *276*: 2986–2991.

Lohse, M.J., Nuber, S., and Hoffmann, C. (2012).Fluorescence/bioluminescence resonance energy transfer techniques to study g-protein-coupled receptor activation and signaling. Pharmacol. Rev. *64*: 299–336.

Loktionov, A. (2019). Eosinophils in the gastrointestinal tract and their role in the pathogenesis of major colorectal disorders. World J. Gastroenterol. *25*: 3503.

Loudon, R.P., and Benovics, J.L. (1994). Expression, Purification, and Characterization of the G Protein-coupled Receptor Kinase GRK6. J. Biol. Chem. *269*: 22691–22697.

Love, P.E., and Bhandoola, A. (2011). Signal integration and cross-talk during thymocyte migration and emigration. Nat. Rev. Immunol. *11*: 469.

M, S., and SD, M. (2009). Olfactory receptors: G protein-coupled receptors and beyond. J. Neurochem. *109*: 1570–1583.

Ma, S., Shen, Q., Zhao, L.-H., Mao, C., Zhou, X.E., Shen, D.-D., et al. (2020a). Molecular Basis for Hormone Recognition and Activation of Corticotropin-Releasing Factor Receptors. Mol. Cell *77*: 669-680.

Ma, X., Hu, Y., Batebi, H., Heng, J., Xu, J., Liu, X., et al. (2020b). Analysis of β2AR-Gs and β2AR-Gi complex formation by NMR spectroscopy. Proc. Natl. Acad. Sci. U. S. A. *117*: 23096.

Manglik, A., Kim, T.H., Masureel, M., Altenbach, C., Yang, Z., Hilger, D., et al. (2015). Structural insights into the dynamic process of β2-adrenergic receptor signaling. Cell *161*: 1101.

Martin, C., Burdon, P.C.., Bridger, G., Gutierrez-Ramos, J.-C., Williams, T.J., and Rankin, S.M. (2003). Chemokines Acting via CXCR2 and CXCR4 Control the Release of Neutrophils from the Bone Marrow and Their Return following Senescence. Immunity *19*: 583–593.

Masuho, I., Skamangas, N.K., Muntean, B.S., and Martemyanov, K.A. (2021). Diversity of the Gβγ complexes defines spatial and temporal bias of GPCR signaling. Cell Syst. *12*: 324-337.

Matsuo, Y., Raimondo, M., Woodward, T.A., Wallace, M.B., Gill, K.R., Tong, Z., et al. (2009). CXC-chemokine/CXCR2 biological axis promotes angiogenesis in vitro and in vivo in pancreatic cancer. Int. J. Cancer *125*: 1027–1037.

Matthees, E.S.F., Haider, R.S., and Hoffmann, C. (2021). β-arrestin–based biosensors: Tools to explore structural determinants of metabolic functions? Curr. Opin. Endocr. Metab. Res. *16*: 66–74.

May, L.T., Bridge, L.J., Stoddart, L.A., Briddon, S.J., and Hill, S.J. (2011). Allosteric interactions across native adenosine-A3 receptor homodimers:

quantification using single-cell ligand-binding kinetics. FASEB J. *25*: 3465.

May, L.T., Leach, K., Sexton, P.M., and Christopoulos, A. (2007). Allosteric Modulation of G Protein–Coupled Receptors. Annu. Rev. Pharmacol. Toxicol. *47*: 1–51.

May, L.T., Self, T.J., Briddon, S.J., and Hill, S.J. (2010). The effect of allosteric modulators on the kinetics of agonist-G protein-coupled receptor interactions in single living cells. Mol. Pharmacol. *78*: 511–23.

Mazor, O., Hillairet De Boisferon, M., Lombet, A., Gruaz-Guyon, A., Gayer, B., Skrzydelsky, D., et al. (2002). Europium-Labeled Epidermal Growth Factor and Neurotensin: Novel Probes for Receptor-Binding Studies. Anal. Biochem. *301*: 75–81.

Mcheik, S., Eeckhout, N. Van, Poorter, C. De, Galés, C., Parmentier, M., and Springael, J.-Y. (2019). Coexpression of CCR7 and CXCR4 During B Cell Development Controls CXCR4 Responsiveness and Bone Marrow Homing. Front. Immunol. *0*: 2970.

Metzemaekers, M., Vanheule, V., Janssens, R., Struyf, S., and Proost, P. (2017). Overview of the Mechanisms that May Contribute to the Non-Redundant Activities of Interferon-Inducible CXC Chemokine Receptor 3 Ligands. Front. Immunol. *8*:.

Miao, Y., Nichols, S.E., and McCammon, J.A. (2014). Mapping of allosteric druggable sites in activation-associated conformers of the M2 muscarinic receptor. Chem. Biol. Drug Des. *83*: 237–246.

Miller, B.E., Mistry, S., Smart, K., Connolly, P., Carpenter, D.C., Cooray, H., et al. (2015). The pharmacokinetics and pharmacodynamics of danirixin (GSK1325756) - a selective CXCR2 antagonist - in healthy adult subjects. BMC Pharmacol. Toxicol. *16*:.

Miller, M.C., and Mayo, K.H. (2017). Chemokines from a structural perspective. Int. J. Mol. Sci. *18*: 2088.

Moran, S.P., Maksymetz, J., and Conn, P.J. (2019). Targeting Muscarinic Acetylcholine Receptors for the Treatment of Psychiatric and Neurological Disorders. Trends Pharmacol. Sci. *40*: 1006.

Moriconi, A., Cesta, M.C., Cervellera, M.N., Aramini, A., Coniglio, S., Colagioia, S., et al. (2007). Design of noncompetitive interleukin-8 inhibitors acting on CXCR1 and CXCR2. J. Med. Chem. *50*: 3984–4002.

Morrison, K.J., Moore, R.H., Carsrud, N.D., Trial, J., Millman, E.E., Tuvim, M., et al. (1996). Repetitive endocytosis and recycling of the beta 2-adrenergic receptor during agonist-induced steady state redistribution. Mol. Pharmacol. *50*: 692–9.

Mortier, A., Berghmans, N., Ronsse, I., Grauwen, K., S, S., Damme, J. Van, et al. (2011). Biological activity of CXCL8 forms generated by alternative cleavage of the signal peptide or by aminopeptidase-mediated truncation. PLoS One *6*:.

Mortier, A., Damme, J. Van, and Proost, P. (2008). Regulation of chemokine activity by posttranslational modification. Pharmacol. Ther. *120*: 197–217.

Motulsky, H.J., and Mahan, L.C. (1984). The kinetics of competitive radioligand binding predicted by the law of mass action. Mol. Pharmacol. *25*:.

Mould, R., Brown, J., Marshall, F.H., and Langmead, C.J. (2014a). Binding kinetics differentiates functional antagonism of orexin-2 receptor ligands. Br. J. Pharmacol. *171*: 351–363.

Mozaffari, S., Nikfar, S., and Abdollahi, M. (2015). Inflammatory bowel disease therapies discontinued between 2009 and 2014. Expert Opin. Investig. Drugs *24*: 949–956.

Munk, C., Mutt, E., Isberg, V., Nikolajsen, L.F., Bibbe, J.M., Flock, T., et al. (2019). An online resource for GPCR structure determination and analysis. Nat. Methods *16*: 151–162.

Murphy, C., McGurk, M., Pettigrew, J., Santinelli, A., Mazzucchelli, R., Johnston, P.G., et al. (2005). Nonapical and cytoplasmic expression of interleukin-8, CXCR1, and CXCR2 correlates with cell proliferation and microvessel density in prostate cancer. Clin. Cancer Res. *11*: 4117–4127.

Nagarsheth, N., Wicha, M.S., and Zou, W. (2017). Chemokines in the cancer microenvironment and their relevance in cancer immunotherapy. Nat. Rev. Immunol. *17*: 559–572.

Nannuru, K., Sharma, B., Varney, M., and Singh, R. (2011). Role of chemokine receptor CXCR2 expression in mammary tumor growth, angiogenesis and metastasis. J. Carcinog. *10*:.

Nasser, M.W., Raghuwanshi, S.K., Grant, D.J., Jala, V.R., Rajarathnam, K., and Richardson, R.M. (2009a). Differential activation and regulation of CXCR1 and CXCR2 by CXCL8 monomer and dimer. J. Immunol. *183*: 3425–32.

Nathan, C. (2006). Neutrophils and immunity: challenges and opportunities. Nat. Rev. Immunol. 2006 63 *6*: 173–182.

Nederveen-Schippers, L.M., Pathak, P., Keizer-Gunnink, I., Westphal, A.H., Haastert, P.J.M. van, Borst, J.W., et al. (2021). Combined FCS and PCH Analysis to Quantify Protein Dimerization in Living Cells. Int. J. Mol. Sci. *22*:.

Nehmé, R., Carpenter, B., Singhal, A., Strege, A., Edwards, P.C., White, C.F., et al. (2017a). Mini-G proteins: Novel tools for studying GPCRs in their active conformation. PLoS One *12*: 175642.

Neptune, E.R., and Bourne, H.R. (1997). Receptors induce chemotaxis by releasing the βγ subunit of Gi, not by activating Gq or Gs. Proc. Natl. Acad. Sci. U. S. A. *94*: 14489–14494.

Neptune, E.R., Iiri, T., and Bourne, H.R. (1999). Gαi Is Not Required for Chemotaxis Mediated by Gi-coupled Receptors *. J. Biol. Chem. *274*: 2824–2828.

Ness, T.L., Hogaboam, C.M., Strieter, R.M., and Kunkel, S.L. (2003). Immunomodulatory role of CXCR2 during experimental septic peritonitis. J. Immunol. *171*: 3775–84.

Nguyen, A.H., Thomsen, A.R.B., Cahill, T.J., III, Huang, R., Huang, L.-Y., et al. (2019). Structure of an Endosomal Signaling GPCR–G Protein–β-arrestin Mega-Complex. Nat. Struct. Mol. Biol. *26*: 1123.

Nicholls, D.J., Tomkinson, N.P., Wiley, K.E., Brammall, A., Bowers, L., Grahames, C., et al. (2008). Identification of a Putative Intracellular Allosteric Antagonist Binding-Site in the CXC Chemokine Receptors 1 and 2. Mol. Pharmacol. *74*: 1193–1202.

Nicholls, D.J., Wiley, K., Dainty, I., Macintosh, F., Phillips, C., Gaw, A., et al. (2015). Pharmacological Characterization of AZD5069, a Slowly Reversible CXC Chemokine Receptor 2 Antagonist s. J. Pharmacol. Exp. Ther. J Pharmacol Exp Ther *353*: 340–350.

Favre, N., Fanelli, F., Missotten, M., Nichols, A., Wilson ,J., di Tiani M., et al. (2005). The DRY Motif as a Molecular Switch of the Human Oxytocin Receptor. Biochemistry *44*: 9990–10008.

Nikolaev, V.O., Bünemann, M., Hein, L., Hannawacker, A., and Lohse, M.J. (2004). Novel single chain cAMP sensors for receptor-induced signal propagation. J. Biol. Chem. *279*: 37215–8.

Ning, Y., Labonte, M.J., Zhang, W., Bohanes, P.O., Gerger, A., Yang, D., et al. (2012). The CXCR2 Antagonist, SCH-527123, Shows Antitumor Activity and Sensitizes Cells to Oxaliplatin in Preclinical Colon Cancer Models. Mol. Cancer Ther. *11*: 1353–1364.

Nisar, S., Daly, M.E., Federici, A.B., Artoni, A., Mumford, A.D., Watson, S.P., et al. (2011). An intact PDZ motif is essential for correct P2Y12 purinoceptor traffic in human platelets. Blood *118*: 5641.

Nuber, S., Zabel, U., Lorenz, K., Nuber, A., Milligan, G., Tobin, A.B., et al. (2016). β-Arrestin biosensors reveal a rapid, receptor-dependent activation/deactivation cycle. Nature *531*: 661–4.

Oakley, R.H., Laporte, S.A., Holt, J.A., Barak, L.S., Caron, M.G., and § (1999). Association of beta-arrestin with G protein-coupled receptors during clathrin-mediated endocytosis dictates the profile of receptor resensitization. J. Biol. Chem. *274*: 32248–57.

Oh-hashi, K., Furuta, E., Fujimura, K., and Hirata, Y. (2017). Application of a novel HiBiT peptide tag for monitoring ATF4 protein expression in Neuro2a cells. Biochem. Biophys. Reports *12*: 40–45.

Oishi, A., Dam, J., and Jockers, R. (2019). β-Arrestin-2 BRET Biosensors Detect Different β-Arrestin-2 Conformations in Interaction with GPCRs. ACS Sensors *5*: 57–64.

Olaru, A., Bala, C., Jaffrezic-Renault, N., and Aboul-Enein, H.Y. (2015). Surface

Plasmon Resonance (SPR) Biosensors in Pharmaceutical Analysis. Crit. Rev. Anal. Chem. *45*: 97–105.

Oliveira, P.G. De, Ramos, M.L.S., Amaro, A.J., Dias, R.A., and Vieira, S.I. (2019). Gi/O-protein coupled receptors in the aging brain. Front. Aging Neurosci. *11*: 89.

Oliveira, S. de, Reyes-Aldasoro, C.C., Candel, S., Renshaw, S.A., Mulero, V., and Calado, Â. (2013). Cxcl8 (Interleukin-8) mediates neutrophil recruitment and behavior in the zebrafish inflammatory response. J. Immunol. *190*: 4349.

Olszyna, D.P., Florquin, S., Sewnath, M., Branger, J., Speelman, P., van Deventer, S.J.H., et al. (2001). CXC Chemokine Receptor 2 Contributes to Host Defense in Murine Urinary Tract Infection. J. Infect. Dis. *184*: 301–307.

Orsini, M.J., Parent, J.-L., Mundell, S.J., and Benovic, J.L. (1999). Trafficking of the HIV Coreceptor CXCR4: Role of arrestins and identification of residues in the c-terminal tail that mediate receptor internalization. J. Biol. Chem. *274*: 31076–31086.

Oswald, C., Rappas, M., Kean, J., Doré, A.S., Errey, J.C., Bennett, K., et al. (2016). Intracellular allosteric antagonism of the CCR9 receptor. Nature *540*: 462–465.

Palczewski, K., Kumasaka, T., Hori, T., Behnke, C.A., Motoshima, H., Fox, B.A., et al. (2000). Crystal structure of rhodopsin: A G protein-coupled receptor. Science *289*: 739–745.

Palczewski, K., McDowell, J.H., Jakes, S., Ingebritsen, T.S., and Hargrave, P.A. (1989). Regulation of rhodopsin dephosphorylation by arrestin. J. Biol. Chem. *264*: 15770–3.

Papers, J.B.C., Doi, M., Wilson, S., Wilkinson, G., Milligan, G., Trettel, C., et al. (2005). The CXCR1 and CXCR2 Receptors Form Constitutive Homo- and Heterodimers Selectively and with Equal Apparent Affinities * CXCR1 receptor to homodimerize or to interact with the. *280*: 28663–28674.

Parenty, G., Appelbe, S., and Milligan, G. (2008). CXCR2 chemokine receptor antagonism enhances DOP opioid receptor function via allosteric regulation of the CXCR2–DOP receptor heterodimer. Biochem. J. *412*: 245.

Park, S.H., Das, B.B., Casagrande, F., Tian, Y., Nothnagel, H.J., Chu, M., et al. (2012). Structure of the chemokine receptor CXCR1 in phospholipid bilayers. Nature *491*: 779–783.

Patel, D.F., and Snelgrove, R.J. (2018). The multifaceted roles of the matrikine Pro-Gly-Pro in pulmonary health and disease. Eur. Respir. Rev. *27*:.

Peach, C.J., Mignone, V.W., Arruda, M.A., Hill, S.J., Kilpatrick, L.E., and Woolard, J. (2018). Molecular Pharmacology of VEGF-A Isoforms : Binding and Signalling at VEGFR2. Int. J. Mol. Sci. 19:1264.

Pededrsen, M.H., Pham J., Mancebo, H., Inoue, A., Ashe,r WB., and Javtich, J.

219

(2021). A novel luminescence-based β-arrestin recruitment assay for unmodified receptors. J. Biol. Chem. *296*:.

Perpina-Viciano, C., Isbilir, A., Zarca, A., Caspar, B., Kilpatrick, L.E., Hill, S.J., et al. (2020). Kinetic analysis of the early signaling steps of the human chemokine receptor CXCR4. Mol. Pharmacol. *98*:72-87.

Peters, B.L., Deng, J., and Ferguson, A.L. (2020). Free energy calculations of the functional selectivity of 5-HT2B G protein-coupled receptor. PLoS One *15*: e0243313.

Pippig, S., Andexinger, S., and Lohse, M.J. (1995). Sequestration and recycling of beta 2-adrenergic receptors permit receptor resensitization. Mol. Pharmacol. *47*: 666–76.

Pitcher, J.A., Freedman, N.J., and Lefkowitz, R.J. (2003). G protein–coupled receptor kinases. Annurev.Biochem. *67*: 653–692.

Postis, V., Rawson, S., Mitchell, J.K., Lee, S.C., Parslow, R.A., Dafforn, T.R., et al. (2015). The use of SMALPs as a novel membrane protein scaffold for structure study by negative stain electron microscopy. Biochim. Biophys. Acta - Biomembr. *1848*: 496–501.

Powell, D.R., and Huttenlocher, A. (2016). Neutrophils in the Tumor Microenvironment. Trends Immunol. *37*: 41–52.

Price, M.R., Baillie, G.L., Thomas, A., Stevenson, L.A., Easson, M., Goodwin, R., et al. (2005). Allosteric modulation of the Cannabinoid CB1 receptor. Mol. Pharmacol. *68*: 1484–1495.

Proudfoot, A.E.I., Handel, T.M., Johnson, Z., Lau, E.K., LiWang, P., Clark-Lewis, I., et al. (2003). Glycosaminoglycan binding and oligomerization are essential for the in vivo activity of certain chemokines. Proc. Natl. Acad. Sci. *100*: 1885–1890.

Proudfoot, A.E.I., Johnson, Z., Bonvin, P., and Handel, T.M. (2017). Glycosaminoglycan Interactions with Chemokines Add Complexity to a Complex System. Pharmaceuticals *10*: 70.

Qin, L., Kufareva, I., Holden, L.G., Wang, C., Zheng, Y., Zhao, C., et al. (2015). Crystal structure of the chemokine receptor CXCR4 in complex with a viral chemokine. Science *347*: 1117.

Qiu, Y., Zhu, J., Bandi, V., Atmar, R.L., Hattotuwa, K., Guntupalli, K.K., et al. (2003). Biopsy Neutrophilia, Neutrophil Chemokine and Receptor Gene Expression in Severe Exacerbations of Chronic Obstructive Pulmonary Disease. Am. J. Respir. Crit. Care Med. *168*: 968–975.

Rajagopalan, L., and Rajarathnam, K. (2004). Ligand selectivity and affinity of chemokine receptor CXCR1. Role of N-terminal domain. J. Biol. Chem. *279*: 30000–30008.

Rajagopalan, L., and Rajarathnam, K. (2006). Structural basis of chemokine

receptor function - A model for binding affinity and ligand selectivity. Biosci. Rep. *26*: 325–339.

Raport, C.J., and Gray, P.W. (2010). Chemokines and chemokine receptors. structure and function. Handbook of Cell Signaling, 2/E, (Elsevier Inc.),157–161.

Rasmussen, S.G.F., Choi, H.-J., Fung, J.J., Pardon, E., Casarosa, P., Chae, P.S., et al. (2011). Structure of a nanobody-stabilized active state of the β2 adrenoceptor. Nature. *469*: 175–180.

Rasmussen, S.G.F., Choi, H.-J., Rosenbaum, D.M., Kobilka, T.S., Thian, F.S., Edwards, P.C., et al. (2007). Crystal structure of the human β2 adrenergic G-protein-coupled receptor. Nature *450*: 383–387.

Rasmussen, S.G.F., Devree, B.T., Zou, Y., Kruse, A.C., Chung, K.Y., Kobilka, T.S., et al. (2011). Crystal structure of the β 2 adrenergic receptor-Gs protein complex. Nature *477*: 549–557.

Reyes-Alcaraz, A., Lee, Y.-N., Yun, S., Hwang, J.-I., and Seong, J.Y. (2018). Conformational signatures in β-arrestin2 reveal natural biased agonism at a G-protein-coupled receptor. Commun. Biol. *1*: 128.

RH, O., CC, H., RD, C., DM, M., RE, P., SM, R., et al. (2002). The cellular distribution of fluorescently labeled arrestins provides a robust, sensitive, and universal assay for screening G protein-coupled receptors. Assay Drug Dev. Technol. *1*: 21–30.

Riddy, D.M., Valant, C., Rueda, P., Charman, W.N., Sexton, P.M., Summers, R.J., et al. (2015). Label-free kinetics: Exploiting functional hemi-equilibrium to derive rate constants for muscarinic receptor antagonists. Mol. Pharmacol. *88*: 779–790.

Rio, L. Del, Bennouna, S., Salinas, J., and Denkers, E.Y. (2001). CXCR2 Deficiency Confers Impaired Neutrophil Recruitment and Increased Susceptibility During Toxoplasma gondii Infection. J. Immunol. *167*: 6503–6509.

Rodríguez-Frade, J.M., Vila-Coro, A.J., Ana, A.M. De, Albar, J.P., Martínez-A., C., and Mellado, M. (1999). The chemokine monocyte chemoattractant protein-1 induces functional responses through dimerization of its receptor CCR2. Proc. Natl. Acad. Sci. U. S. A. *96*: 3628.

Roland, C.L., Lynn, K.D., Toombs, J.E., Dineen, S.P., Udugamasooriya, D.G., and Brekken, R.A. (2009). Cytokine Levels Correlate with Immune Cell Infiltration after Anti-VEGF Therapy in Preclinical Mouse Models of Breast Cancer. PLoS One *4*: 7669.

Rosenbaum, D.M., Rasmussen, S.G.F., and Kobilka, B.K. (2014). The Structure and Function of G-Protein-Coupled Receptors. Nature *459*: 356–363.

Rotondo, R., Barisione, G., Mastracci, L., Grossi, F., Orengo, A.M., Costa, R., et al. (2009). IL-8 induces exocytosis of arginase 1 by neutrophil polymorphonuclears in nonsmall cell lung cancer. Int. J. Cancer *125*: 887–893.

221

Saini, V., Marchese, A., and Majetschak, M. (2010). CXC chemokine receptor 4 is a cell surface receptor for extracellular ubiquitin. J. Biol. Chem. *285*: 15566–15576.

Sakyiamah, M.M., Nomura, W., Kobayakawa, T., and Tamamura, H. (2019). Development of a NanoBRET-based sensitive screening method for CXCR4 ligands. Bioconjug. Chem. *30*: 1442–1450.

Salahpour, A., Espinoza, S., Masri, B., Lam, V., Barak, L.S., and Gainetdinov, R.R. (2012). BRET biosensors to study GPCR biology, pharmacology, and signal transduction. Front. Endocrinol. *3*:.

Salchow, K., Bond, M., Evans, S., Press, N., Charlton, S., Hunt, P., et al. (2010). A common intracellular allosteric binding site for antagonists of the CXCR2 receptor: Research paper. Br. J. Pharmacol. *159*: 1429–1439.

Samama, P., Cotecchia, S., Costa, T., and Lefkowitz, R.J. (1993). A mutation-induced activated state of the β2-adrenergic receptor. Extending the ternary complex model. J. Biol. Chem. *268*: 4625–4636.

Sánchez-Sánchez, N., Riol-Blanco, L., and Rodríguez-Fernández, J.L. (2006). The Multiple Personalities of the Chemokine Receptor CCR7 in Dendritic Cells. J. Immunol. *176*: 5153–5159.

Sanchez, J., Huma, Z. e., Robert Lane, J., Liu, X., Bridgford, J.L., Payne, R.J., et al. (2019). Evaluation and extension of the two-site, two-step model for binding and activation of the chemokine receptor CCR1. J. Biol. Chem. *294*: 3464–3475.

Sawant, K. V., Poluri, K.M., Dutta, A.K., Sepuru, K.M., Troshkina, A., Garofalo, R.P., et al. (2016). Chemokine CXCL1 mediated neutrophil recruitment: Role of glycosaminoglycan interactions. Sci. Reports *6*: 1–8.

Schall, T.J., and Proudfoot, A.E.I. (2011). Overcoming hurdles in developing successful drugs targeting chemokine receptors. Nat. Rev. Immunol. *11*: 355–363.

Schertler, G.F.X. (1998). Structure of rhodopsin. Eye *12*: 504–510.

Schiöth, H.B., and Lagerström, M.C. (2008). Structural diversity of G protein-coupled receptors and significance for drug discovery. Nat. Rev. Drug Discov. *7*: 339–357.

Scholten, D.J., Canals, M., Maussang, D., Roumen, L., Smit, M.J., Wijtmans, M., et al. (2012). Pharmacological modulation of chemokine receptor function. Br. J. Pharmacol. *165*: 1617–1643.

Schwindinger, W.F., Giger, K.E., Betz, K.S., Stauffer, A.M., Sunderlin, E.M., Sim-Selley, L.J., et al. (2004). Mice with Deficiency of G Protein γ 3 Are Lean and Have Seizures . Mol. Cell. Biol. *24*: 7758–7768.

Semack, A., Sandhu, M., Malik, R.U., Vaidehi, N., and Sivaramakrishnan, S. (2016). Structural Elements in the Gαs and Gαq C Termini That Mediate

Selective G Protein-coupled Receptor (GPCR) Signaling. J. Biol. Chem. *291*: 17929–17940.

Semple, B.D., Kossmann, T., and Morganti-Kossmann, M.C. (2010). Role of chemokines in CNS health and pathology: a focus on the CCL2/CCR2 and CXCL8/CXCR2 networks. J. Cereb. Blood Flow Metab. *30*: 459–73.

Sepuru, K.M., and Rajarathnam, K. (2016). CXCL1/MGSA is a novel Glycosaminoglycan (GAG)-binding chemokine: structural evidence for two distinct non-overlapping binding domains. J. Biol. Chem. *291*: 4247–4255.

Servant, G., Weiner, O.D., Herzmark, P., Balla, T., Sedat, J.W., and Bourne, H.R. (2000). Polarization of chemoattractant receptor signaling during neutrophil chemotaxis. Science *287*: 1037–1040.

SG, R., and YS, B. (1997). Regulation of phosphoinositide-specific phospholipase C isozymes. J. Biol. Chem. *272*: 15045–15048.

Sharma, B., Nawandar, D.M., Nannuru, K.C., Varney, M.L., and Singh, R.K. (2013). Targeting CXCR2 enhances chemotherapeutic response, inhibits mammary tumor growth, angiogenesis, and lung metastasis. Mol. Cancer Ther. *12*: 799–808.

Shaul, M.E., Levy, L., Sun, J., Mishalian, I., Singhal, S., Kapoor, V., et al. (2016). Tumor-associated neutrophils display a distinct N1 profile following TGFβ modulation: A transcriptomics analysis of pro- vs. antitumor TANs. Oncoimmunology *5*:.

Shenoy, S.K., and Lefkowitz, R.J. (2011). B-Arrestin-Mediated Receptor Trafficking and Signal Transduction. Trends Pharmacol. Sci. *32*: 521–533.

Shi, X., Wan, Y., Wang, N., Xiang, J., Wang, T., Yang, X., et al. (2021). Selection of a picomolar antibody that targets CXCR2-mediated neutrophil activation and alleviates EAE symptoms. Nat. Commun. *12*: 1–14.

Shichi, H., and Somers, R.L. (1978). Light-dependent phosphorylation of rhodopsin. Purification and properties of rhodopsin kinase. *253:* 7040-6.

Shukla, A.K., Westfield, G.H., Xiao, K., Reis, R.I., Huang, L.-Y., Tripathi-Shukla, P., et al. (2014). Visualization of arrestin recruitment by a G-protein-coupled receptor. Nature *512*: 218–222.

Slack, RJ., Russel, LJ., Hall, DA., Luttmann, MA., Ford, AJ., Saunders KA. et al. (2011). Pharmacological characterization of GSK1004723, a novel, long-acting antagonist at histamine H(1) and H(3) receptors. Br. J. Pharm. *164*: 1627-41.

Smith, J.S., Nicholson, L.T., Suwanpradid, J., Glenn, R.A., Knape, N.M., Alagesan, P., et al. (2018). Biased agonists of the chemokine receptor CXCR3 differentially control chemotaxis and inflammation. Sci. Signal. *11*:.

Soave, M., Heukers, R., Kellam, B., Woolard, J., Smit, M.J., Briddon, S.J., et al. (2020). Monitoring Allosteric Interactions with CXCR4 Using NanoBiT Conjugated Nanobodies. Cell Chem. Biol. *27*: 1250-1261.

Soave, M., Kellam, B., Woolard, J., Briddon, S.J., and Hill, S.J. (2019). NanoBiT Complementation to Monitor Agonist-Induced Adenosine A1 Receptor Internalization. SLAS Discov. *25*: 186–194.

Spalding, T.A., Burstein, E.S., Wells, J.W., and Brann, M.R. (1997). Constitutive activation of the m5 muscarinic receptor by a series of mutations at the extracellular end of transmembrane 6. Biochemistry *36*: 10109–10116.

Spillmann, M., Thurner, L., Romantini, N., Zimmermann, M., Meger, B., Behe, M., et al. (2020). New Insights into Arrestin Recruitment to GPCRs. Int. J. Mol. Sci. *21*: 1–14.

Sprang, S.R. (2003). G PROTEIN MECHANISMS: Insights from Structural Analysis. Annualrev. Biochem. *66*: 639–678.

Springael, J.Y., Urizar, E., and Parmentier, M. (2005). Dimerization of chemokine receptors and its functional consequences. Cytokine Growth Factor Rev. *16*: 611–623.

Sriram, K., and Insel, P.A. (2018a). G protein-coupled receptors as targets for approved drugs: How many targets and how many drugs? Molecular Pharmacology, (American Society for Pharmacology and Experimental Therapy), pp 251–258.

Stadtmann, A., Zarbock, A., Ley, K., and Hickey, M. (2012). CXCR2: from bench to bedside. Front. Immunol. *3*:.

Staus, D.P., Hu, H., Robertson, M.J., Kleinhenz, A.L.W., Wingler, L.M., Capel, W.D., et al. (2020). Structure of the M2 muscarinic receptor–β-arrestin complex in a lipid nanodisc. Nature. *579*: 297–302.

Stein, J. V, and Nombela-Arrieta, C. (2005). Chemokine control of lymphocyte trafficking: a general overview. Immunology *116*: 1.

Stockton, J.M., Birdsall, N.J.M., Burgen, A.S.V., and Hulme, E.C. (1983). Modification of the binding properties of muscarinic receptors by gallamine. Mol. Pharmacol. *23*: 551–557.

Stoddart, L.A., Johnstone, E.K.M., Wheal, A.J., Goulding, J., Robers, M.B., MacHleidt, T., et al. (2015a). Application of BRET to monitor ligand binding to GPCRs. Nat. Methods *12*: 661–663.

Stoddart, L.A., Vernall, A.J., Briddon, S.J., Kellam, B., and Hill, S.J. (2015b). Direct visualisation of internalization of the adenosine A3 receptor and localization with arrestin3 using a fluorescent agonist. Neuropharmacology *98*: 68–77.

Stoddart, L.A., White, C.W., Nguyen, K., Hill, S.J., and Pfleger, K.D.G. (2016). Fluorescence- and bioluminescence-based approaches to study GPCR ligand binding. Br. J. Pharmacol. *173*: 3028.

Stone, M.J., Hayward, J.A., Huang, C., Huma, Z.E., and Sanchez, J. (2017a). Mechanisms of regulation of the chemokine-receptor network. Int. J. Mol. Sci.

18:.

Stott, L.A., Hall, D.A., and Holliday, N.D. (2016). Unravelling intrinsic efficacy and ligand bias at G protein coupled receptors: A practical guide to assessing functional data. Biochem. Pharmacol. *101*: 1–12.

Stumpf, A.D., and Hoffmann, C. (2016). Optical probes based on G protein-coupled receptors - Added work or added value? Br. J. Pharmacol. *173*: 255–266.

Su, Y., Raghuwanshi, S.K., Yu, Y., Nanney, L.B., Richardson, R.M., and Richmond, A. (2005). Altered CXCR2 Signaling in β-Arrestin-2-Deficient Mouse Models. J. Immunol. *175*: 5396–5402.

Sum, C.S., Murphy, B.J., Li, Z., Wang, T., Zhang, L., and Cvijic, M.E. (2004). Pharmacological Characterization of GPCR Agonists, Antagonists, Allosteric Modulators and Biased Ligands from HTS Hits to Lead Optimization (Eli Lilly & Company and the National Center for Advancing Translational Sciences).

Suzuki, N., Hajicek, N., and Kozasa, T. (2009). Regulation and Physiological Functions of G12/13-Mediated Signaling Pathways. Neurosignals. *17*: 55.

Swinney, D.C., Beavis, P., Chuang, K.-T., Zheng, Y., Lee, I., Gee, P., et al. (2014). A study of the molecular mechanism of binding kinetics and long residence times of human CCR5 receptor small molecule allosteric ligands. Br. J. Pharmacol. *171*: 3364.

Sykes, D.A., Bradley, M.E., Riddy, D.M., Willard, E., Reilly, J., Miah, A., et al. (2016). Fevipiprant (QAW039), a Slowly Dissociating CRTh2 Antagonist with the Potential for Improved Clinical Efficacy. Mol. Pharmacol. *89*: 593–605.

Sykes, D.A., Dowling, M.R., and Charlton, S.J. (2009). Exploring the Mechanism of Agonist Efficacy: A Relationship between Efficacy and Agonist Dissociation Rate at the Muscarinic M3 Receptor. Mol. Pharmacol. *76*: 543–551.

Sykes, D.A., Dowling, M.R., Leighton-Davies, J., Kent, T.C., Fawcett, L., Renard, E., et al. (2012). The Influence of Receptor Kinetics on the Onset and Duration of Action and the Therapeutic Index of NVA237 and Tiotropium. J. Pharmacol. Exp. Ther. *343*: 520–528.

Sykes, D.A., Jiménez-Rosés, M., Reilly, J., Fairhurst, R.A., Charlton, S.J., and Veprintsev, D.B. (2021). Exploring the kinetic selectivity of drugs targeting the β1-adrenoceptor. BioRxiv 2021.08.31.458064.

Sykes, D.A., Lochray, J., Comfort, H.M.F., Jain, P., and Charlton, S.J. (2021b). Exploring the kinetic selectivity of antipsychotics for dopamine D2 and 5-HT2A receptors: implications for the prevalence of EPS and receptor occupancy. BioRxiv 2021.11.14.468520.

Sykes, D.A., Moore, H., Stott, L., Holliday, N., Javitch, J.A., Robert Lane, J., et al. (2017). Extrapyramidal side effects of antipsychotics are linked to their association kinetics at dopamine D2 receptors. Nat. Commun. *8*: 1–11.

Sykes, D.A., Parry, C., Reilly, J., Wright, P., Fairhurst, R.A., and Charlton, S.J. (2014). Observed Drug-Receptor Association Rates Are Governed by Membrane Affinity: The Importance of Establishing 'Micro-Pharmacokinetic/Pharmacodynamic Relationships' at the b 2-Adrenoceptor s. Mol. Pharmacol. Mol Pharmacol *85*: 608–617.

Sykes, D.A., Stoddart, L.A., Kilpatrick, L.E., and Hill, S.J. (2019a). Binding kinetics of ligands acting at GPCRs. Mol. Cell. Endocrinol. *485*: 9–19.

Syrovatkina, V., Alegre, K.O., Dey, R., and Huang, X.-Y. (2016). Regulation, Signaling and Physiological Functions of G-proteins. J. Mol. Biol. *428*: 3850.

Szczepek, M., Beyrière, F., Hofmann, K.P., Elgeti, M., Kazmin, R., Rose, A., et al. (2014a). Crystal structure of a common GPCR-binding interface for G protein and arrestin. Nat. Commun. *5*: 1–8.

Szczepek, M., Beyrière, F., Hofmann, K.P., Elgeti, M., Kazmin, R., Rose, A., et al. (2014b). Crystal structure of a common GPCR-binding interface for G protein and arrestin. Nat. Commun. *5*: 4801.

Taddese, B., Deniaud, M., Garnier, A., Tiss, A., Guissouma, H., Abdi, H., et al. (2018). Evolution of chemokine receptors is driven by mutations in the sodium binding site. PLoS Comput. Biol. *14*:.

Takeda, S., Kadowaki, S., Haga, T., Takaesu, H., and Mitaku, S. (2002). Identification of G protein-coupled receptor genes from the human genome sequence. FEBS Lett. *520*: 97–101.

Tanino, Y., Coombe, D.R., Gill, S.E., Kett, W.C., Kajikawa, O., Proudfoot, A.E.I., et al. (2010). Kinetics of Chemokine-Glycosaminoglycan Interactions Control Neutrophil Migration into the Airspaces of the Lungs. J. Immunol. *184*: 2677.

Tashkin, D.P. (2005). Is a long-acting inhaled bronchodilator the first agent to use in stable chronic obstructive pulmonary disease? Curr. Opin. Pulm. Med. *11*: 121–128.

Tautermann, C.S., Kiechle, T., Seeliger, D., Diehl, S., Wex, E., Banholzer, R., et al. (2013). Molecular basis for the long duration of action and kinetic selectivity of tiotropium for the muscarinic M3 receptor. J. Med. Chem. *56*: 8746–8756.

Thal, D.M., Sun, B., Feng, D., Nawaratne, V., Leach, K., Felder, C.C., et al. (2016). Crystal structures of the M1 and M4 muscarinic acetylcholine receptors. Nature *531*: 335–340.

Thelen, M. (2001). Dancing to the tune of chemokines Structure insights for receptor coupling Hooks or active coreceptors? Nat. Immunol. *2*: 129–134.

Thomsen, A.R.B., Plouffe, B., Cahill, T.J., Shukla, A.K., Tarrasch, J.T., Dosey, A.M., et al. (2016). GPCR-G Protein-β-Arrestin Super-Complex Mediates Sustained G Protein Signaling. Cell *166*: 907–919.

Tota, M.R., Daniel, S., Sirotina, A., Mazina, K.E., Fong, T.M., Longmore, J., et al. (1994). Characterization of a Fluorescent Substance P Analog. Biochemistry *33*:

13079–13086.

Trettel, F., Bartolomeo, S. Di, Lauro, C., Catalano, M., Ciotti, M.T., and Limatola, C. (2003). Ligand-independent CXCR2 Dimerization. J. Biol. Chem. *278*: 40980–40988.

Tummino, P.J., and Copeland, R.A. (2008). Residence time of receptor - Ligand complexes and its effect on biological function. Biochemistry *47*: 5481–5492.

Ueda, H., Harada, H., Nozaki, M., Katada, T., Ui, M., Satoh, M., et al. (1988). Reconstitution of rat brain mu opioid receptors with purified guanine nucleotide-binding regulatory proteins, Gi and Go. Proc. Natl. Acad. Sci. *85*: 7013–7017.

Ulvmar, M.H., Hub, E., and Rot, A. (2011). Atypical chemokine receptors. Exp. Cell Res. *317*: 556–568.

Underwood, J.G., Bragg, A.E., Neumark, D.M., Zgierski, M.Z., Seideman, T., Stolow, A., et al. (2008). The 2.6 Angstrom Crystal Structure of a Human A2A Adenosine Receptor Bound to an Antagonist. *322*: 1211–1218.

Urwyler, S., Mosbacher, J., Lingenhoehl, K., Heid, J., Hofstetter, K., Froestl, W., et al. (2001). Positive allosteric modulation of native and recombinant γ-aminobutyric acidb receptors by 2,6-Di-tert-butyl-4-(3-hydroxy-2,2-dimethyl-propyl)-phenol (CGP7930) and its aldehyde analog CGP13501. Mol. Pharmacol. *60*: 963–971.

Vanderheyden, P.M.L., Fierens, F.L.P., and Vauquelin, G. (2000). Angiotensin II type 1 receptor antagonists: Why do some of them produce insurmountable inhibition? Biochem. Pharmacol. *60*: 1557–1563.

Vauquelin, G. (2015). On the 'micro'-pharmacodynamic and pharmacokinetic mechanisms that contribute to long-lasting drug action. Expert Opinion on Drug Discovery *10*: 1085–1098.

Vauquelin, G., and Charlton, S.J. (2010a). Long-lasting target binding and rebinding as mechanisms to prolong in vivo drug action. Br. J. Pharmacol. *161*: 488.

Vauquelin, G., and Packeu, A. (2009). Ligands, their receptors and … plasma membranes. Mol. Cell. Endocrinol. *311*: 1–10.

Veber, D.F., Johnson, S.R., Cheng, H.Y., Smith, B.R., Ward, K.W., and Kopple, K.D. (2002). Molecular properties that influence the oral bioavailability of drug candidates. J. Med. Chem. *45*: 2615–2623.

Veglia, F., Sanseviero, E., and Gabrilovich, D.I. (2021). Myeloid-derived suppressor cells in the era of increasing myeloid cell diversity. Nat. Rev. Immunol. 2021 218 *21*: 485–498.

Venkatakrishnan, A.J., Deupi, X., Lebon, G., Tate, C.G., Schertler, G.F., and Madan Babu, M. (2013). Molecular signatures of G-protein-coupled receptors. Nature *494*: 185–194.

Venkatakrishnan, A.J., Ma, A.K., Fonseca, R., Latorraca, N.R., Kelly, B., Betz, R.M., et al. (2019). Diverse GPCRs exhibit conserved water networks for stabilization and activation. Proc. Natl. Acad. Sci. *116*: 3288–3293.

Vernall, A.J., Hill, S.J., and Kellam, B. (2014). The evolving small-molecule fluorescent-conjugate toolbox for Class A GPCRs. Br. J. Pharmacol. *171*: 1073–1084.

Vila-Coro, A.J., Mellado, M., Ana, A.M. de, Lucas, P., Real, G. del, Martínez-A., C., et al. (2000). HIV-1 infection through the CCR5 receptor is blocked by receptor dimerization. Proc. Natl. Acad. Sci. U. S. A. *97*: 3388.

Vilardaga, J.P., Bünemann, M., Krasell, C., Castro, M., and Lohse, M.J. (2003). Measurement of the millisecond activation switch of G protein-coupled receptors in living cells. Nat. Biotechnol. *21*: 807–812.

Vishnivetskiy, S.A., Zhan, X., Chen, Q., Iverson, T.M., and Gurevich, V. V. (2014). Arrestin Expression in E. coli and Purification. Curr. Protoc. Pharmacol. *67*: 2.11.1.

Waage, P., and Gulberg, C.M. (1986). Studies concerning affinity. J. Chem. Educ. *63*: 1044–1047.

Wan, Q., Okashah, N., Inoue, A., Nehmé, R., Carpenter, B., Tate, C.G., et al. (2018a). Mini G protein probes for active G protein-coupled receptors (GPCRs) in live cells. J. Biol. Chem. *293*: 7466–7473.

Wang, L.-H., Cheng, G., Park, S., Shu, S., He, L., Kong, W., et al. (2008). Advances of AKT Pathway in Human Oncogenesis and as a Target for Anti-Cancer Drug Discovery. Curr. Cancer Drug Targets *8*: 2–6.

Wang, L., Xu, J., Cao, S., Sun, D., Liu, H., Lu, Q., et al. (2021). Cryo-EM structure of the AVP–vasopressin receptor 2–Gs signaling complex. Cell Res. *31*: 932–934.

Watson, C., Jenkinson, S., Kazmierski, W., and Kenakin, T. (2005). The CCR5 receptor-based mechanism of action of 873140, a potent allosteric noncompetitive HIV entry inhibitor. Mol. Pharmacol. *67*: 1268–1282.

Weis, W.I., and Kobilka, B.K. (2018). The Molecular Basis of G Protein-Coupled Receptor Activation. Annu. Rev. Biochem. *87*: 897–919.

Wente, M.N., Keane, M.P., Burdick, M.D., Friess, H., Büchler, M.W., Ceyhan, G.O., et al. (2006). Blockade of the chemokine receptor CXCR2 inhibits pancreatic cancer cell-induced angiogenesis. Cancer Lett. *241*: 221–227.

Wheatley, M., Charlton, J., Jamshad, M., Routledge, S.J., Bailey, S., La-Borde, P.J., et al. (2016). GPCR–styrene maleic acid lipid particles (GPCR–SMALPs): their nature and potential. Biochem. Soc. Trans. *44*: 619–623.

White, C.W., Caspar, B., Vanyai, H.K., Pfleger, K.D.G., Correspondence, S.J.H., and Hill, S.J. (2020a). CRISPR-Mediated Protein Tagging with Nanoluciferase to Investigate Native Chemokine Receptor Function and Conformational Changes.

Cell Chem. Biol. *27*: 499–510.

White, C.W., Caspar, B., Vanyai, H.K., Pfleger, K.D.G., and Hill, S.J. (2020b). CRISPR-Mediated Protein Tagging with Nanoluciferase to Investigate Native Chemokine Receptor Function and Conformational Changes. Cell Chem. Biol. *27*: 499-510.

White, C.W., Vanyai, H.K., See, H.B., Johnstone, E.K.M., and Pfleger, K.D.G. (2017). Using nanoBRET and CRISPR/Cas9 to monitor proximity to a genome-edited protein in real-time. Sci. Reports *7*: 1–14.

White, J.R., Lee, J.M., Young, P.R., Hertzberg, R.P., Jurewicz, A.J., Chaikin, M.A., et al. (1998). Identification of a potent, selective non-peptide CXCR2 antagonist that inhibits interleukin-8-induced neutrophil migration. J. Biol. Chem. *273*: 10095–10098.

White, K.L., Eddy, M.T., Gao, Z.G., Han, G.W., Lian, T., Deary, A., et al. (2018). Structural Connection between Activation Microswitch and Allosteric Sodium Site in GPCR Signaling. Structure *26*: 259-269.

Widdowson, K.L., Elliott, J.D., Veber, D.F., Nie, H., Rutledge, M.C., McCleland, B.W., et al. (2004). Evaluation of Potent and Selective Small-Molecule Antagonists for the CXCR2 Chemokine Receptor. J. Med. Chem. *47*: 1319–1321.

Wilden, U., Hall, S.W., and Kühn, H. (1986). Phosphodiesterase activation by photoexcited rhodopsin is quenched when rhodopsin is phosphorylated and binds the intrinsic 48-kDa protein of rod outer segments. Proc. Natl. Acad. Sci. U. S. A. *83*: 1174.

Wingler, L.M., and Lefkowitz, R.J. (2020). Conformational Basis of G Protein-Coupled Receptor Signaling Versatility. Trends Cell Biol. *30*: 736–747.

Wright, P.T., Schobesberger, S., and Gorelik, J. (2015). Studying GPCR/cAMP pharmacology from the perspective of cellular structure. Front. Pharmacol. *6*:.

Wright, S.C., and Bouvier, M. (2021). Illuminating the complexity of GPCR pathway selectivity – advances in biosensor development. Curr. Opin. Struct. Biol. *69*: 142–149.

Wu, B., Chien, E.Y.T., Mol, C.D., Fenalti, G., Liu, W., Katritch, V., et al. (2010). Structures of the CXCR4 chemokine GPCR with small-molecule and cyclic peptide antagonists. Science *330*: 1066–1071.

Xiao, Z., Zhang, N., Murphy, D.B., and Devreotes, P.N. (1997). Dynamic Distribution of Chemoattractant Receptors in Living Cells During Chemotaxis and Persistent Stimulation. J. Cell Biol. *139*: 365–374.

Xu, D., and Esko, J.D. (2014). Demystifying heparan sulfate-protein interactions. Annu. Rev. Biochem. *83*: 129–157.

Xu, G., Guo, J., and Wu, Y. (2014). Chemokine Receptor CCR5 Antagonist Maraviroc: Medicinal Chemistry and Clinical Applications. Curr. Top. Med.

Chem. *14*: 1504–1514.

Xu, H., Lin, F., Wang, Z., Yang, L., Meng, J., Ou, Z., et al. (2018). CXCR2 promotes breast cancer metastasis and chemoresistance via suppression of AKT1 and activation of COX2. Cancer Lett. *412*: 69–80.

Yang, G., Rosen, D.G., Liu, G., Yang, F., Guo, X., Xiao, X., et al. (2010). CXCR2 Promotes Ovarian Cancer Growth through Dysregulated Cell Cycle, Diminished Apoptosis, and Enhanced Angiogenesis. Clin. Cancer Res. *16*: 3875–3886.

Yang, J., Yan, C., Vilgelm, A.E., Chen, S.C., Ayers, G.D., Johnson, C.A., et al. (2021). Targeted Deletion of CXCR2 in Myeloid Cells Alters the Tumor ImmuneEnvironment to Improve Antitumor Immunity. Cancer Immunol. Res. *9*: 200.

Yang, X.D., Corvalan, J.R.F., Wang, P., Roy, C.M.N., and Davis, C.G. (1999). Fully human anti-interleukin-8 monoclonal antibodies: Potential therapeutics for the treatment of inflammatory disease states. J. Leukoc. Biol. *66*: 401–410.

Yin, W., Li, Z., Jin, M., Yin, Y.-L., Waal, P.W. de, Pal, K., et al. (2019). A complex structure of arrestin-2 bound to a G protein-coupled receptor. Cell Res. 2019 2912 *29*: 971–983.

Yohn, S.E., and Conn, P.J. (2018). Positive allosteric modulation of M 1 and M 4 muscarinic receptors as potential therapeutic treatments for schizophrenia. Neuropharmacology *136*: 438–448.

Zhang, M., Gui, M., Wang, Z.-F., Gorgulla, C., Yu, J.J., Wu, H., et al. (2021). Cryo-EM structure of an activated GPCR–G protein complex in lipid nanodiscs. Nat. Struct. Mol. Biol. *28*: 258–267.

Zhang, R., and Xie, X. (2012). Tools for GPCR drug discovery. Acta Pharmacol. Sin. *33*: 372.

Zhang, Y., Ma, K.L., Gong, Y.X., Wang, G.H., Hu, Z.B., Liu, L., et al. (2018). Platelet microparticles mediate glomerular endothelial injury in early diabetic nephropathy. J. Am. Soc. Nephrol. *29*: 2671–2695.

Zhang, Y., Sun, B., Feng, D., Hu, H., Chu, M., Qu, Q., et al. (2017). Cryo-EM structure of the activated GLP-1 receptor in complex with a G protein. Nature *546*: 248–253.

Zhao, S., Wu, B., and Stevens, R.C. (2019). Advancing Chemokine GPCR Structure Based Drug Discovery. Structure *27*: 405–408.

Zheng, Y., Han, G.W., Abagyan, R., Wu, B., Stevens, R.C., Cherezov, V., et al. (2017). Structure of CC Chemokine Receptor 5 with a Potent Chemokine Antagonist Reveals Mechanisms of Chemokine Recognition and Molecular Mimicry by HIV. Immunity *46*: 1005-1017.e5.

Zheng, Y., Qin, L., Zacarías, N.V.O., Vries, H. De, Han, G.W., Gustavsson, M., et al. (2016). Structure of CC chemokine receptor 2 with orthosteric and allosteric antagonists. Nature *540*: 458–461.

Zhou, Q., Yang, D., Wu, M., Guo, Y., Guo, W., Zhong, L., et al. (2019a). Common activation mechanism of class a GPCRs. Elife *8*:.

Zhou, Z., Xia, G., Xiang, Z., Liu, M., Wei, Z., Yan, J., et al. (2019b). A C-X-C Chemokine Receptor Type 2–Dominated Cross-talk between Tumor Cells and Macrophages Drives Gastric Cancer Metastasis. Clin. Cancer Res. *25*: 3317–3328.

Zlotnik, A., and Yoshie, O. (2000). Chemokines: A New Classification System and Their Role in Immunity. Immunity *12*: 121–127.

Zweemer, A.J.M., Bunnik, J., Veenhuizen, M., Miraglia, F., Lenselink, E.B., Vilums, M., et al. (2014). Discovery and mapping of an intracellular antagonist binding site at the chemokine receptor CCR2. Mol. Pharmacol. *86*: 358–368.

Zwier, J.M., Bazin, H., Lamarque, L., and Mathis, G. (2014). Luminescent lanthanide cryptates: From the bench to the bedside. Inorg. Chem. *53*: 1854–1866.

iv. Appendix 1

Professional internship for PhD Students

Note to examiners

This statement is included as an appendix to the thesis in order that the thesis accurately captures the PhD training experienced by the candidate as a BBSRC Doctoral Training Partnership student. The Professional Internship for PhD Students is a compulsory 3-mont placement which must e undertaken by DTP students. It is usually cantered on a specific project and must not be related to the PhD project. The reflective statement is designed to capture the skills development which has taken place during the student's placement and the impact on their career plans it has had.

Reflective statement

As a student enrolled to the Nottingham – BBSRC Doctoral training partnership I undertook a 3-month Professional Internship for PhD Students (PIP) during the course of the PhD. The PIP is designed to encourage PhD students to broaden their sets of skills by working in a different set-up from their research group. Ultimately, PIPs aim at helping students make a decision on their career progression following the completion of their PhD.

I undertook a placement in Sosei Heptares, Cambridge, which is an international biopharmaceutical group focused on the discovery and early development of new therapeutics based on structure-activity relationship (SAR) exploring platforms. Sosei Heptares work to develop medicines across a broad range of therapeutic areas including neurology, immunology, gastroenterology and inflammatory diseases.

My decision to apply for a PIP in Sosei Heptares was based on my aspiration to build a career in drug discovery and compare this process in an academic versus an industrial set-up. I was eager to work on different form my PhD drug targets, learn new laboratory techniques and explore ways to make research higher throughput. In addition, I wanted to expand my scientific network and build up on my soft skills.

The project I worked on in Sosei Heptares, Pharmacology explored a GPCR target with functions in the immune system. I aimed at setting-up receptor signalling assays that could help the team decipher the pattern of target signalling and its modulation by a range of ligands with different structures. In addition, I worked on other projects on the side looking into more targets in the immune system in native set-ups such as in freshly isolated neutrophils and T cells from donors' blood.

In terms of laboratory techniques, my PIP allowed me to expand the ones I was already familiar with but apply them in a larger scale and in higher throughput manner. I learned about what additional controls experiments need to include in order for the data to be validated and taken forward which was something completely new to me. I received additional training on techniques such as blood cell extraction, Dynamic Mass Redistribution (DMR), radiation work, and Flow Cytometry.

Projects in the company were a collaborative effort of the Pharmacology, Protein Engineering, Biochemistry, Molecular modelling, and Translational teams. That meant that whilst I worked in the Pharmacology group, I had ongoing communication with the other teams learning more about the collaborative nature of drug discovery. In addition, I attended multiple internal meetings that allowed me to learn about the projects all other scientists worked on.

The friendly environment in the company also meant that I could openly communicate with scientists from different departments, discuss science with them, and expand my knowledge.

In addition to all the lab-based and soft skills I gained by working in Sosei Heptares, the PIP gave me the opportunity to spend 3 months in the vibrant town of Cambridge. This was truly amazing and allowed me to meet students from one the best academic institutions in the world which is an opportunity I am extremely grateful for.

The benefits of the PIP I undertook were enormous. I gained additional laboratory lab skills that I added to my CV and that I am confident helped me with interviewing for and securing a postdoctoral position in drug discovery. I

233

expanded my scientific network and I am happy to say I have managed to stay in touch with scientists I met at the company. Most importantly, I gained confidence as a scientist due to the positive feedback I received on completion of the placement and decided that I am certainly eager to stay in the field of drug discovery and that I enjoy working both in academic and industrial laboratories.